
THE UNIVERSITY
*of* EDINBURGH

# The role of TET1 in adipose tissue


Bonnie M Nicholson

Submitted for the degree of Doctor of Philosophy

The University of Edinburgh

2019

**Declaration**

I declare that the work presented in this thesis is entirely my own work, except where stated in the text. This work has not been submitted for any other degree, and to the best of my knowledge contains no material published or written by any other person, except where stated in the text.

Bonnie Nicholson
February 2019

**Acknowledgements**

A number of people have made this work possible. Firstly, many people have willingly offered their time and expertise. Thank you to Dr John Thompson for sharing his technical expertise in bioinformatics, and to Lynne Ramage for sharing her skills and knowledge in primary adipose culture, and for always being willing to drop what she was doing to offer guidance. Likewise, thank you to Dr Rod Carter for his technical help with adipose tissue culture and use of the Seahorse, and to Clare McFadden for helping with dissections. My gratitude goes to Dr Roland Stimson for being available for brainstorming PhD ideas and providing new inspiration. Thank you to our collaborators at the University of Birmingham, Dr Daniel Tenant, Dr Alpesh Thakker, Dr Christian Ludwig and Prof Gareth Lavery, for carrying out and providing expertise in GC-MS. I'd also like to thank the staff at the Wellcome Trust Clinical Research Facility for carrying out the sequencing and being patient when experiments took longer than planned. Further thanks to Dr Jimi Wills and Dr Andrew Finch of the mass spectrometry facility, Institute for Genetic and Molecular Medicine, University of Edinburgh, for carrying out the UPLC.

I have been lucky enough to share my time with a wonderful group of CVS students. Thanks to all the students in the centre who have made the QMRI a friendly and enjoyable place to spend each day. I must also thank Amy Sandison, who joined Team Drake for her undergraduate project and contributed to some of the phenotyping analyses, and Eamon Fitzgerald for teaching me how to do pyrosequencing. A huge thanks must go to all past and present members of Team Drake, especially Dr Jessy Cartier and Dr Marcus Lyall for training me technically, for sharing with me protocols they had spent months optimising, and for allowing me to pester them constantly with questions.

Thanks to Dr Will Cawthorn and members of his group who guided me in my bone-related studies; and thank you to my second supervisor, Prof Nik Morton, who always made time to offer specialist metabolism knowledge and technical advice and provide feedback on my reports, as well as spending hours calibrating the PhenoMaster so that it was just right.

Finally and most importantly, I am hugely grateful to my primary supervisor, Dr Mandy Drake. Her positive attitude motivated me to get back in the lab when science 'wouldn't work'; her supportive nature encouraged me to progress scientifically and professionally; and her baking kept me suitably sugared up during lab meetings.

**Abstract**

The global obesity epidemic is associated with 2.8 million deaths per year and contributes to the prevalence of numerous cardiometabolic disease risk factors, including non-alcoholic fatty liver disease (NAFLD), hypertension, type 2 diabetes, hyperlipidaemia and stroke.

The Ten-Eleven-Translocation enzymes (TET1-3) modify DNA by adding a methyl group to generate 5-hydroxymethylcytosine (5hmC) from 5-methylcytosine (5mC). This DNA methylation mark can alter the nature of the information conveyed by DNA; for example by modulating access of transcription factors. TET1 plays an important role in promoting adipocyte differentiation. I hypothesised that *Tet1* gene deficiency impairs adipocyte development and function, thereby counteracting the development of obesity. TET enzymatic activity requires the TCA cycle metabolite α-ketoglutarate (α-KG) as a substrate, and is allosterically inhibited by TCA cycle metabolites succinate and fumarate. Obesity is associated with a number of key metabolic changes including increased levels of glutamate and many constitutive metabolites of the tricarboxylic acid (TCA) cycle (such as α-ketoglutarate, succinate, fumarate, and malate). I therefore additionally hypothesised that TET activity is altered as a consequence of the metabolic perturbations that accompany obesity.

To test these hypotheses, male *Tet1* gene knockout ($Tet1^{-/-}$) mice and littermate mice wildtype for the *Tet1* allele ($Tet1^{+/+}$) were fed a high-fat diet (HFD) for 11 weeks. Food intake, adiposity (TD-NMR), energy expenditure (indirect calorimetry) and fat depot mass, including bone marrow adipose tissue (MAT) were measured. RNA-sequencing of adipose tissue gene expression and analysis of 5hmC in adipose tissue DNA was performed.

Fat mass of $Tet1^{-/-}$ mice was 50% lower than that of $Tet1^{+/+}$ littermates after 11 weeks HFD. No changes in MAT were observed. $Tet1^{-/-}$ mice showed a relative reduction in food intake over 11 weeks and a reduction in energy expenditure in the absence of changes in activity levels. RNA-sequencing of mesenteric adipose tissue revealed changes in gene expression related to muscle organ development, synaptic vesicle exocytosis and acyl-coA metabolic processes in $Tet1^{-/-}$ mice. Notably, leptin mRNA and circulating leptin levels were lower in $Tet1^{-/-}$ mice compared to $Tet1^{+/+}$. $Tet1^{-/-}$ mice challenged with exogenous leptin had a greater reduction in food intake, indicating higher leptin sensitivity. Hydroxymethylated DNA immunoprecipitation-sequencing (hMeDIP-seq) was performed to analyse 5hmC patterns: however, no global differences in 5hmC levels were identified between $Tet1^{-/-}$ and $Tet1^{+/+}$

mice. Specifically, despite the marked change in leptin mRNA expression, no changes in 5hmC or 5mC were observed within the leptin promoter to indicate causality of DNA methylation changes in altered leptin expression.

Brown adipose tissue (BAT) is the main organ of thermogenesis in rodents and has a high energy demand when activated. The recent discovery of active BAT, or an intermediate thermogenic fat called "beige", in human adults has prompted research into the potential of therapeutic BAT activation for the treatment of obesity. A number of epigenetic marks, of which DNA methylation is one, have been associated with activation of thermogenesis in BAT including histone acetylation. However, the potential role of 5mC and 5hmC in BAT function has not been investigated.

While histone modifications – most notably histone acetylation in the enhancer regions of *Pparg* and *Ucp1*, and putative regulatory regions of *Ppara* – have been shown to play a role in the transcriptional activation of the thermogenic gene programme, the role of 5mC and 5hmC has not been investigated. I hypothesised that TET1 activity would be altered by changes in metabolite levels in cold-induced thermogenesis, resulting in altered 5hmC.

To test this hypothesis, C57BL/6J mice were maintained at 30°C or 4°C for 48 hours, after which adipose tissue was collected. RNA and DNA were extracted from white (WAT), brown (BAT) and beige adipose tissue for RNA-seq and hMeDIP-seq, and the polar phase metabolites were extracted for gas chromatography mass-spectrometry. In mice exposed to 4°C, all metabolites of the tricarboxylic acid (TCA) cycle were significantly increased in WAT and BAT compared to mice housed at 30°C, with the exception of α-KG and succinate in BAT. TET activity was decreased in WAT at 4°C but not in BAT or beige adipose tissue. No global changes in 5hmC were observed in WAT or BAT between the 4°C and 30°C conditions. However, there is a decrease in 5hmC in BAT at 30°C and 4°C, and in WAT at 4°C, at 10% of gene length in a select subset of genes involved in neuromuscular synaptic transmission and perception of chemical stimuli. Many gene pathways were upregulated transcriptionally in all three adipose depots, including mitochondrial function, oxidative phosphorylation and the TCA cycle, but these transcriptional changes are not associated with changes in 5hmC.

In summary**,** this data supports my original hypothesis by showing that *Tet1*$^{-/-}$ mice have decreased susceptibility to diet-induced obesity due to a reduction in food intake, in

association with higher leptin sensitivity. However, in contrast to published data, 5hmC or 5mC modification was not altered at the leptin promoter in adipocytes, and therefore the hypothesis that DNA methylation at the leptin promoter accounts for the observed *Tet1*$^{-/-}$ phenotype must be rejected. Finally, numerous changes occur in the TCA cycle metabolites in BAT and WAT with cold exposure, which may contribute to the selective decrease in TET activity in WAT. However, no changes are observed in 5hmC in WAT, rejecting the hypothesis that altered TET1 activity in cold exposure results in altered 5hmC. In conclusion, this thesis contends that TET enzymes and 5hmC are not primary drivers of gene expression changes in obesity or cold-induced thermogenesis. However, TET enzymes may act in synergy with other epigenetic changes to alter gene expression in this context, and may remain important contributors to altered adiposity and its metabolic consequences.

**Lay summary**

Obesity is associated with 2.8 million deaths per year and contributes to the development of other related diseases, including fatty liver disease, high blood pressure, type 2 diabetes and stroke. The development of obesity is known to be partly controlled by our DNA.

DNA is made up of smaller units, known as genes. Genes are responsible for all biological processes, by coding for proteins – molecules that have a vast array of functions within all organisms. The function of genes can be changed by adding or removing chemical groups to or from DNA; for example, the addition of a chemical group known as 5-methylcytosine (5mC), which causes genes to switch off. Three proteins, known as the Ten-Eleven-Translocation enzymes (TET1-3), can convert 5mC into another chemical group: 5-hydroxymethylcytosine (5hmC). In contrast to 5mC, 5hmC is thought to switch genes on.

TET1 is important for fat cell development. I predicted that without the *Tet1* gene, fat cell development and function would be impaired, thereby counteracting the development of obesity.

To test this, mice lacking the *Tet1* gene (termed 'knockout' or 'KO' mice) and animals with a normal *Tet1* gene (termed 'wildtype' or 'WT' mice) were fed a high-fat diet for 11 weeks. I measured food intake, body composition and calorie expenditure of the mice. I then analysed how obesity affected the genes in fat tissue.

KO mice lacking the *Tet1* gene gained less fat than WT mice after 11 weeks high-fat diet. KO mice ate less and burned fewer calories than normal WT mice, but their levels of activity and movement were not different. I saw many differences in the genes in the fat tissue between KO and WT mice, including in genes important for the function of fat. In particular, the gene for the 'satiety hormone', leptin – the hormone that signals a feeling of fullness to the brain – was much lower in KO mice, which could explain why the KO mice eat less than the WT mice. Surprisingly, despite the lack of *Tet1*, no differences were seen in the levels of 5hmC between KO and WT mice.

Brown fat is responsible for producing body heat in rodents, and is turned on in the cold. Recently, brown fat has also been found in adult humans. Because it is a very energy-demanding organ when turned on, many researchers believe that it can be 'turned on' to treat obesity. The role of 5hmC in brown fat has not been studied. I predicted that TET activity

would be altered when brown fat is turned on in the cold, and that there would be changes in 5hmC levels and gene function.

To test this, mice were kept in cages at either 30°C or 4°C for 48 hours. In mice kept in the cold, some of the molecules involved in generating energy were increased in brown fat compared to mice kept in the warm. Some of these molecules are also known to change the function of the TET proteins. Although I saw many differences in the genes of mice kept in the cold, I saw no changes in 5hmC levels in brown fat.

In summary**,** these findings support my original prediction, by showing that *Tet1* KO mice are less likely to become obese. However, this seems to be because they are eating less, rather than an effect specifically in the fat. Finally, in brown fat in the cold, I saw an increase in molecules that could possibly change the activity of the TET proteins. However, there were no changes 5hmC. In conclusion, this thesis finds that the TET proteins and 5hmC are not responsible for changes in fat cell gene function in obesity or in the cold.

**Abbreviations**

| | |
|---|---|
| α-KG | Alpha-ketoglutarate |
| α-MSH | Alpha-melanocortin stimulating hormone |
| β3-AR | Beta 3-adrenoreceptor |
| $^{18}$FDG | $^{18}$F-fluorodeoxyglucose |
| $^{18}$FTHA | $^{18}$F-fluoro-thiaheptadecanoic acid |
| 2HG | 2-hydroxyglutarate |
| 2OG | 2-oxoglutarate |
| 3-PG | Glycerol-3-phosphate |
| 5caC | 5-carboxylcytosine |
| 5fC | 5-formylcytosine |
| 5hmC | 5-hydroxymethylcytosine |
| 5mC | 5-methylcytosine |
| Acaa1b | Acetyl-coenzyme A acyltransferase 1B |
| Acadm | Acyl-CoA dehydrogenase medium chain |
| Acss2 | Acyl-CoA synthetase short chain family member 2 |
| Actb | Actin beta |
| ACTH | Adrenocorticotropic hormone |
| ADIPOQ | Adiponectin |
| ADP | Adenosine diphosphate |
| Adrb1 | Adrenoceptor beta 1 |
| ADSF | Resistin |
| ANCOVA | Analysis of covariance |
| Angptl4 | Angiopoietin like 4 |
| Anxa2 | Annexin A2 |
| Apoa1/4 | Apolipoprotein A1/A4 |
| Apoe | Apolipoprotein E |
| Aqp7 | Aquaporin 7 |
| ATF2 | Activating transcription factor 2 |
| Atgl (Pnpla2) | Patatin-like phospholipase domain containing 2 |
| ATP | Adenosine triphosphate |
| B3gnt3 | UDP-GlcNAc:betaGal beta-1,3-N-acetylglucosaminyltransferase 3 |
| BAIBA | Beta-aminoisobutyric acid |
| BAT | Brown adipose tissue |
| BBB | Blood brain barrier |
| Bcap31 | B-cell receptor associated protein 31 |
| BDNF | Brain-derived neurotrophic factor |
| BER | Base-excision repair |
| BMAL1 | Aryl hydrocarbon receptor nuclear translocator-like |
| BMI | Body mass index |
| Bmp4 | Bone morphogenetic protein 4 |
| BRG1 | Brahma-related-gene-1 |

| | |
|---|---|
| Cacnb2 | Calcium voltage-gated channel auxiliary subunit beta 2 |
| cAMP | Cyclic adenosyl monophosphate |
| CCL2 | C-C motif chemokine ligand 2 |
| CD | Control diet |
| CD24/29/31/34/45 | Cluster of differentiation 24/29/31/34/45 |
| CDF | Common data format |
| CEBPB | CCAAT enhancer binding protein beta |
| CEBPA | CCAAT enhancer binding protein alpha |
| CFD | Complement factor D |
| CGL | Congenital lipodystrophy |
| Chrnb1 | Acetylcholine receptor subunit beta-1 |
| Chrnb3 | Acetylcholine receptor subunit beta-3 |
| Cox8b | Cytochrome c oxidase subunit 8B |
| CpG | Cytosine-phosphate-Guanine |
| CPT1b | Carnitine palmitoyltransferase 1B |
| CR | Calorie restriction |
| CS | Citrate synthase |
| CSF | Cerebrospinal fluid |
| CTCF | CCCTC-binding factor |
| Cyb5b | Cytochrome b5 type B |
| Cyp3a13 | Cytochrome P450, family 3, subfamily a, polypeptide 13 |
| Cyp4a10 | Cytochrome P450, family 4, subfamily a, polypeptide 10 |
| Cyp4a14 | Cytochrome P450, family 4, subfamily a, polypeptide 14 |
| Cyp4f14 | Cytochrome P450, family 4, subfamily f, polypeptide 14 |
| DAG | Diacylglyceride |
| DBI | Diazepam binding inhibitor |
| DIO | Diet-induced obesity |
| DIO2 | Iodothyronine deiodinase 2 |
| DNA | Deoxyribonucleic acid |
| DNMT | DNA methyltransferase enzymes |
| DPF3 | Double PHD fingers 3 |
| DUSP1 | Dual specificity phosphatase 1 |
| EBF1/ 2 | Early B cell factor 1/ 2 |
| EDTA | Ethylenediaminetetraacetic acid |
| EE | Energy expenditure |
| Egfr | Epidermal growth factor receptor |
| EHMT1 | Euchromatic histone lysine methyltransferase 1 |
| ELISA | Enzyme-linked immunosorbent assay |
| ERRα | Estrogen related receptor alpha |
| ESC | Embryonic stem cell |
| FA | Fatty acid |
| FABP4 | Fatty acid binding protein 4 |

| | |
|---|---|
| Fasn | Fatty acid synthase |
| Fbp2 | Fructose-bisphosphatase 2 |
| FDG PET | Fluorodeoxyglucose positron emission tomography |
| FDR | False discovery rate |
| FGF21 | Fibroblast growth factor 21 |
| FLI | Free leptin index |
| Foxc1/ 2 | Forkhead box C1/ 2 |
| FPKM | Fragments Per Kilobase of transcript per Million mapped reads |
| FTO | Fat mass and obesity associated |
| G6pdx | Glucose-6-phosphate dehydrogenase X-linked |
| Gabrg2 | Gamma-aminobutyric acid receptor subunit gamma-2 |
| Gata4/6 | GATA binding protein 4/6 |
| GC-MS | Gas chromatography-mass spectrometry |
| GDH | Glutamate dehydrogenase |
| GI | Glycemic index |
| Gk | Glycerol kinase |
| GLAST | Glutamate aspartate transporter |
| Glra4 | Glycine receptor subunit alpha-4 |
| GLUT1/4 | Glucose transporter 1/4 |
| GPR109A (HCAR2) | Hydroxycarboxylic acid receptor 2 |
| G-proteins | Guanine nucleotide-binding proteins |
| Gpt | Glutamic-pyruvic transaminase |
| GWAS | Genome-wide association study |
| Gys2 | Glycogen synthase 2 |
| H2-4 | Histone proteins 2-4 |
| $H_2O_2$ | Hydrogen peroxide |
| H3K27me3 | Histone 3 lysine 27 trimethylation |
| H3K39me3 | Histone 3 lysine 36 trimethylation |
| H3K4me3 | Histone 3 lysine 4 trimethylation |
| H3K9me2/3 | Histone 3 lysine 9 di-and tri-methylation |
| Hacd2 | 3-hydroxyacyl-coa dehydratase 2 |
| HAT | Histone acetyltransferase |
| HDAC1/2/3 | Histone deacetylase 1/2/3 |
| HFD | High fat diet |
| hMeDIP-seq | Hydroxymethyl DNA immunoprecipitation-sequencing |
| Hnf4a/g | Hepatocyte nuclear factor 4 alpha/gamma |
| HOXC9 | Homeobox C9 |
| HPLC | High-performance liquid chromatography |
| HSC | Haematopoietic stem cell |
| Hsd-1 | Hydroxysteroid dehydrogenase homolog |
| HSL | Hormone sensitive lipase |

| | |
|---|---|
| Htr3b | 5-hydroxytryptamine receptor 3B |
| IDH1/ 2 | Isocitrate dehydrogenases 1/ 2 |
| IGF-1 | Insulin-like growth factor 1 |
| IL-6 | Interleukin-6 |
| Insig1 | Insulin induced gene 1 |
| IRF4 | Interferon regulatory factor 4 |
| JAK | Janus kinase |
| JBP1 & 2 | J-binding protein 1 & 2 |
| JmjC | Jumonji C |
| JMJD | Jumonji C-domain-containing demethylase |
| KD | Knockdown |
| Klf5 | Kruppel like factor 5 |
| KO | Knockout |
| LDL | Low density lipid |
| LEP | Leptin |
| LepR | Leptin receptor |
| LH | Luteinising hormone |
| LHX8 | LIM homeobox protein 8 |
| Lpl | Lipoprotein lipase |
| LSD1 | Lysine-specific histone methylase 1 |
| LXR (NR1H3) | Nuclear receptor subfamily 1, group H, member 3 |
| MAG | Monoacylglyceride |
| MAPK | Mitogen-activated protein kinase |
| MAT | Marrow adipose tissue |
| MBD | Methyl-CpG-binding domain |
| MC4R | Melanocortin 4 receptor |
| Me1 | Malic enzyme 1 |
| MECP2 | Methyl-CpG binding protein 2 |
| MED1 | Mediator complex subunit 1 |
| MEOX2 | Mesenchyme homeobox 2 |
| Mgam | Maltase-glucoamylase |
| MLL | Mixed lineage leukaemia |
| mNF-H | Mouse neurofilament-H |
| MPC1 | Mitochondrial pyruvate carrier 1 |
| mRNA | Messenger ribonucleic acid |
| Mttp | Microsomal triglyceride transfer protein |
| Mup3/20 | Major urinary protein 3/20 |
| Myf5 | Myogenic factor 5 |
| Myom1 | Myomesin 1 |
| NAD+ | Nicotinamide adenine dinucleotide |
| NAFLD | Non-alcoholic fatty liver disease |
| Napb | N-ethylmaleimide sensitive fusion protein attachment protein beta |

| | |
|---|---|
| Ng2 (Cspg4) | Chondroitin sulfate proteoglycan 4 |
| Nsdhl | NAD(P) dependent steroid dehydrogenase-like |
| Ntsr2 | Neurotensin receptor 2 |
| Ob | Obese gene (leptin) |
| OB-R | Leptin receptor |
| Olfr | Olfactory receptor |
| Olr1 | Oxidized low density lipoprotein receptor 1 |
| p107 | Retinoblastoma-like protein 1 |
| p38MAPK | P38 mitogen-activated protein kinases |
| PC | Pyruvate carboxylase |
| PCR | Polymerase chain reaction |
| PCSK1 | Proprotein convertase subtilisin/kexin type 1 |
| Pdgfra | Platelet derived growth factor receptor alpha |
| PDHA1 | Pyruvate dehydrogenase |
| Pdk3/4 | Pyruvate dehydrogenase kinase 3/4 |
| PET/CT | Positron emission tomography–computed tomography |
| PF | Paired feeding |
| PGC1a | Peroxisome proliferator-activated receptor gamma coactivator 1-alpha |
| Pgd | Phosphogluconate dehydrogenase |
| PKA | Protein kinase |
| PLIN1 | Perilipin 1 |
| PLXND1 | Plexin D1 |
| Pnpla3 | Patatin-like phospholipase domain containing 3 |
| POMC | Proopiomelanocortin |
| Ppara/g | Peroxisome proliferator activated receptor alpha/gamma |
| Ppargc1a | Peroxisome proliferative activated receptor, gamma, coactivator 1 alpha |
| PPRE | Peroxisome proliferator activated receptor response element |
| PRC2 | Polycomb repression complex 2 |
| PRDM16 | PR domain containing 16 |
| Pref1 (Dlk1) | Preadipocyte factor 1 |
| Prkag3 | Protein kinase AMP-activated non-catalytic subunit gamma 3 |
| Prx1 | Paired related homeobox 1 |
| Ptchd4 | Patched domain containing 4 |
| PTP1B | Phosphotyrosine phosphatase |
| Ranbp3l | RAN binding protein 3 like |
| Rb | RB transcriptional corepressor 1 |
| Rbp2/7 | Retinol binding protein 2/7 |
| RER | Respiratory exchange ratio |
| Rgn | Regucalcin |
| RGS2 | Regulator of G protein signaling 2 |
| Rims2 | Regulating synaptic membrane exocytosis 2 |
| RNA | Ribonucleic acid |

| | |
|---|---|
| RNA-seq | Ribonucleic acid-sequencing |
| RT-qPCR | Reverse transcriptase-quantatative polymerase chain reaction |
| SAM | S-adenosyl methionine |
| Sca-1 | Stem cells antigen-1 |
| SFRP4 | Secreted frizzled related protein 4 |
| Sim1 | Single-minded family bHLH transcription factor 1 |
| siRNA | Small interfering ribonucleic acid |
| SIRTs | Sirtuin demethylases |
| Sis | Sucrase isomaltase |
| Slc27a1/2 | Solute carrier family 27 (fatty acid transporter), member 1/2 |
| Snap25 | Synaptosome associated protein 25 |
| SNP | Single nucleotide polymorphism |
| SNS | Sympathetic nervous system |
| SOCS3 | Cytokine signalling 3 |
| SRC2 (NCOA2) | Nuclear receptor coactivator 2 |
| Srebp1 | Sterol regulatory element binding protein 1 |
| STAT | Signal transducer and activator of transcription |
| SVF | Stromal vascular fraction |
| SWI/SNF | Switch/Sucrose Non-Fermentable |
| Syt1/4/5 | Synaptotagmin 1/4/5 |
| TAG | Triacylglyceride |
| Tbp | TATA-box binding protein |
| TCA | Tricarboxyclic acid |
| TD-NMR | Time-domain nuclear magnetic resonance |
| TES | Transcriptional end site |
| TET1-3 | Ten eleven translocase 1-3 |
| Tfam | Transcription factor A, mitochondrial |
| TGFb1 | Transforming growth factor beta 1 |
| Tmem26 | Transmembrane protein 26 |
| TNFα | Tumour necrosis factor alpha |
| Top2a | DNA topoisomerase II alpha |
| TSS | Transcriptional start site |
| Tst | Thiosulfate sulfurtransferase |
| TWIST1 | Twist family bh transcription factor 1 |
| TZD | Thiazolinedione |
| Ucp1 | Uncoupling protein 1 |
| UPLC | Ultra performance-liquid chromatography |
| WAT | White adipose tissue |
| WGA | Whole genome amplification |
| WT | Wildtype |
| ZFP516 | Zinc finger protein 516 |
| ZIC1 | Zinc finger protein of the cerebellum 1 |

**Table of Contents**

**Table of Figures**

# 1. Introduction

## 1.1. Obesity

### 1.1.1. The obesity epidemic

The World Health Organisation defines obesity as "abnormal or excessive fat accumulation that presents a risk to health" [1]. In adults, being overweight is classified as having a body mass index of over 25kg/m$^2$, while obesity is classified as a body mass index of over 30kg/m$^2$. The global obesity epidemic is associated with 2.8 million deaths per year [2]. Additionally, obesity contributes to the prevalence of numerous cardiometabolic disease risk factors, including non-alcoholic fatty liver disease (NAFLD), hypertension, type 2 diabetes, hyperlipidaemia and stroke, as well as being associated with an increased risk of certain cancers (including mammary, renal, oesophageal, gastrointestinal and reproductive cancers), sleep apnoea, osteoarthritis, and gynaecological problems [3]. To put just two of these comorbidities in context, 44% of type 2 diabetes and 23% of ischaemic heart disease is attributable to obesity [4]. The direct cost of obesity to the NHS in 2007, excluding the cost of associated diseases, was £2.3 billion, and the direct cost of being overweight was £1.9 billion [5]. The impact of obesity now poses a global health challenge.

In 2016, 39% of adults were overweight, and 13% were obese – figures that have nearly tripled since 1975 [4]. This dramatic rise in the number of cases of obesity in the last 40 years has been attributed to multiple underlying causes; the most widely accepted of which are increased access to energy-dense, high-sugar, high-fat foods, and decreased activity levels due to sedentary lifestyles [6, 7]. However, as a complex disease, obesity is a result of a combination of both environmental and genetic factors. Studying all causal factors will add to our understanding of the disease and improve our ability to treat it.

### 1.1.2. The thrifty genotype hypothesis

The 'thrifty genotype hypothesis', put forward in 1962 by J.V. Neel, proposes that there has been evolutionary selection for genes that contribute to increased fat deposition, for use as an energy storage in times of food shortage [8]. Today, the prevalence of these genes in combination with greater food availability causes increased susceptibility to disease rather than putting us at an evolutionary advantage over our leaner relatives. While there has been debate over the validity of the thrifty genotype hypothesis due to conflicting evidence [9, 10], recent studies have undisputedly found genetic factors that contribute to susceptibility to obesity. Identification of such 'thrifty' allele variants could provide new targets for therapeutic intervention of obesity and type 2 diabetes.

### 1.1.3. The genetic influence on obesity

The identification of the obese (*Ob*) gene in 1994 [11, 12], later named leptin, lead to the discovery of a population of severely obese individuals with mutations in the gene who, when treated with a recombinant form of the leptin protein, recovered remarkably, decreasing fat mass by 15.6kg in a year [13].

Monogenic mutations in the leptin signalling pathway are rare and account for only 1-5% of severe obesity [14]. However, the discovery of a direct genetic influence opened up the field of study to other candidate genes. It is now estimated that genetic differences account for between 40-70% of the variation in obesity susceptibility [15, 16]. Mutations in *MC4R*, *PCSK1*, and enzymes required for the processing of POMC have since been found to cause human obesity, as well as other components of the neural circuit that regulates food intake including *BDNF* and *SIM1* [17].

Genome wide association studies (GWAS) have provided several key candidate genes for common polygenic obesity and its metabolic complications [18-28], most notably *FTO* (fat mass and obesity associated) [29]. Single nucleotide polymorphisms (SNPs) in the *FTO* gene region on chromosome 16 were strongly associated with type 2 diabetes and obesity [29]. However, many other findings from GWAS have proved controversial, due to poor replicability of results [30, 31].

## 1.2. Adipose tissue biology

### 1.2.1. White adipose tissue

Adipose tissue, made up of adipocytes with unilocular lipid droplets, is present in discrete depots in both mice and humans. Classical adipose tissue is known as white adipose tissue (WAT), which is mainly responsible for storing excess energy for use in peripheral tissues. In mice and humans, the largest WAT depots are: subcutaneous/inguinal, retroperitoneal, mesenteric and gonadal/epididymal; with smaller depots including pericardial, intramuscular, omental and perirenal.

WAT is a dynamic energy store in a state of constant flux, storing energy in the form of triglycerides (through the process of esterification/lipogenesis) and mobilising energy from triglycerides in the form of fatty acids and glycerol ( through hydrolysis/lipolysis) [32]. During times of energy shortage, a greater net rate of lipolysis occurs. During lipolysis, triacylglyceride (TAG) is hydrolysed sequentially to form diacylglyceride (DAG) and then monoacylglyceride (MAG) with the release of a fatty acid at each step. MAG is then hydrolysed to release a final fatty acid and glycerol. Hormone sensitive lipase (HSL) is the enzyme that controls the initial rate-limiting step of lipolysis (hydrolysis of TAG) [33]. HSL activity is increased by catecholamines and adrenocorticotropic hormone (ACTH) and inhibited by insulin. Alterations in lipolysis are often associated with obesity. For example, a

decrease in basal rates of lipolysis was observed in obese subjects, with a concomitant decrease in HSL mRNA expression, protein expression and enzyme activity [34].

White adipose tissue is also a major endocrine organ, secreting hormones such as leptin and adiponectin – to name two of the most prominent – and the list of adipose-secreted proteins is still growing [35]. They include cytokines, proteins involved directly in lipid metabolism, those involved in the complement system and those involved in vascular haemostasis [36]. For many of these proteins, the functional significance of their secretion from adipose tissue is undetermined. However, this importance of the secretory functions of WAT is demonstrated in conditions such as cancer cachexia [37], malnutrition [38] and anorexia nervosa [39-42], during which there are markedly decreased levels of WAT, resulting in significant modulation in the production of most of the adipose-secreted proteins. For example, in anorexia nervosa patients and other states of energy deprivation, hypoleptinaemia is associated with amenorrhoea [39]. This is thought to be because in healthy patients, luteinising hormone (LH) and oestradiol levels are regulated by leptin, so hypoleptinaemia leads to loss of LH and oestradiol regulation [40]. Thus a critical leptin threshold value for amenorrhoea has been set at 2μg/L [41, 42]. This demonstrates the importance of the secretory functions of WAT.

### 1.2.2. Brown adipose tissue

Brown adipose tissue (BAT) is responsible for the production of extra heat in response to cold exposure. BAT was identified as a thermogenic organ in 1961 [43], and in 1978, Foster et al. demonstrated the thermogenic activation of BAT in rats acclimatised to the cold [44].

In infants, BAT is present in several depots, including interscapular, supraclavicular, suprarenal, pericardial, para-aortic and around the pancreas, kidney and trachea [45]. In adults, however, fluorodeoxyglucose positron emission tomography (FDG PET) studies have revealed that BAT is mainly limited to the supraclavicular and neck region, with some additional activity in the paravertebral, mediastinal, para-aortic, and suprarenal regions [46, 47]. In mice, BAT is highly active and the main BAT depot is located in the interscapular region [48].

Until recently, BAT was thought only to have a functional role in rodents and human newborns, but in 2009, a series of papers were published demonstrating its function and activity in adults [49, 50]. In 2011 it was shown that BAT consumes more glucose per gram of tissue than other tissues, and this was increased 12-fold in response to cold exposure, indicating that BAT is far from redundant in human adults [51].

***Non-shivering thermogenesis***

The mechanism of action for heat production in BAT is *via* non-shivering thermogenesis, a process mediated mainly by mitochondrial uncoupling protein 1 (UCP1), whose expression is mainly limited to BAT. There are five known homologues of the uncoupling proteins (UCP1-5), but UCP1 is the only form that has proven thermogenic capacity [52].

UCP1 is a transmembrane proton transporter that decreases the proton gradient across the inner mitochondrial membrane, which is generated in oxidative phosphorylation of the tricarboxylic acid (TCA) cycle. It does so by acting as a proton 'leak', allowing protons to be transported across the inner mitochondrial membrane, down the gradient, thus uncoupling proton transport from ATP synthesis (demonstrated in Figure 1.1). By decreasing the proton gradient, UCP1 decreases the rate of ATP production but increases the rate of substrate oxidation, generating heat as a by-product.

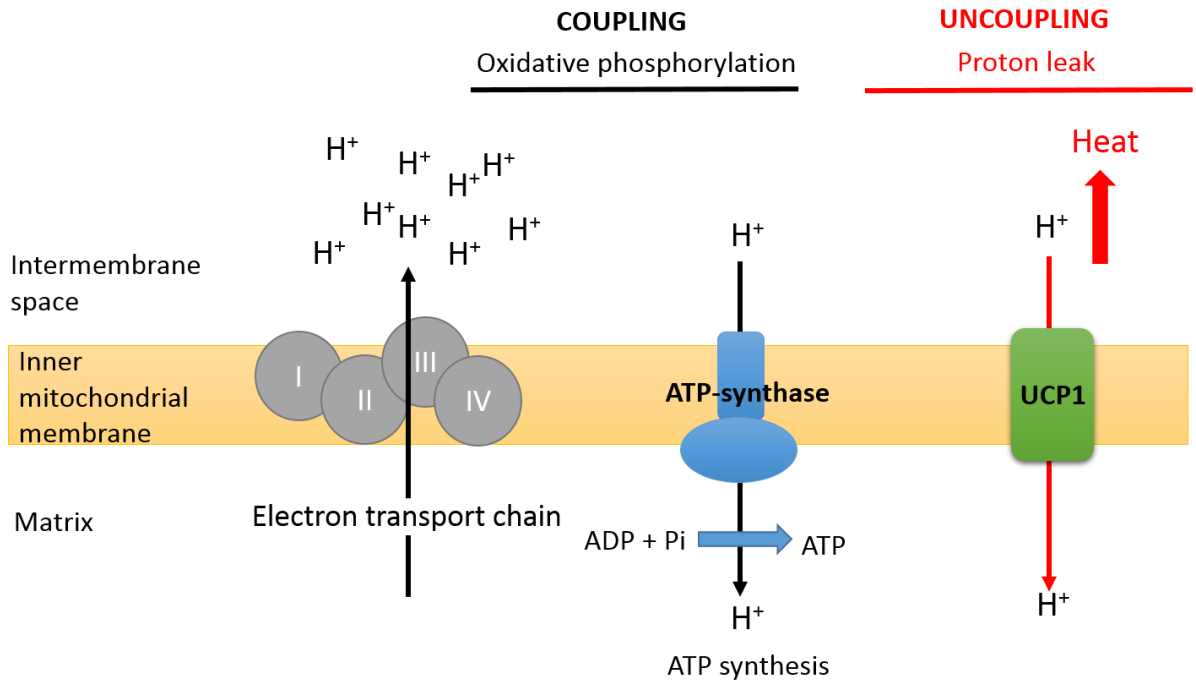


Figure 1.1. The mechanism of action of UCP1.

The electron transport chain pumps protons across the mitochondrial matrix into the intermembrane space, generating the proton gradient that is required for ATP-synthase. The production of ATP via ATP-synthase requires the transport of protons from the intermembrane space into the mitochondrial matrix. However, UCP1 in brown adipose tissue transports protons across the inner mitochondrial membrane without the production of ATP, acting as a proton 'leak'. This uncouples proton transport from ATP synthesis, decreasing the proton gradient generated by the electron transport chain. This increases the rate of substrate oxidation in the electron transport chain without increasing the production of ATP, generating heat as a by-product. Image adapted from Brondani et al. 2012 [53].

***BAT activation***

The level of activity of BAT varies between species [54] and individuals [55-57]. BAT mass and activity has been shown in several independent studies to be increased in females as compared to males [55, 56, 58] and also decreased with age [59]. BAT has also been shown to have seasonal variability [56], with around a three-fold increase in the number of individuals with measurable BAT activity in the winter months in the UK compared to summer months, and also a four-fold mean increase in the activity of BAT – as measured by PET/CT – in patients whose BAT activity was measured monthly.

As the thermogenic organ, exposure to cold temperatures is a potent stimulus of BAT activation [49-51]. This activation is dependent upon innervation of the tissue from the sympathetic nervous system (SNS). Cold exposure induces the release of norepinephrine in brown adipocytes, which binds to β3-adrenergic receptors in the mature brown adipocyte cell membranes. The β3-adrenergic receptors are coupled with guanine nucleotide-binding proteins (G-proteins), which activate adenylyl cyclase and its downstream signalling pathway (cAMP, protein kinase A, and p38MAPK).

This signalling pathway in turn activates lipolysis-stimulating enzymes, such as hormone-sensitive lipase, adipose triacylglycerol lipase and monoacylglycerol lipase, increasing the availability of free fatty acids (substrates for oxidation within the mitochondria) [60]. In addition, the transcription factor ATF2 (activating transcription factor 2) is activated, which directly triggers UCP1 transcription [61]. The process of browning is also dependent on β3-adrenergic receptors (further discussed in section 1.2.3) [62].

In addition to cold exposure, chronic treatment (three days or longer) with thiazolinediones (TZDs), a group of PPARγ agonists (such as rosiglitazone), induces browning of WAT [63-66]. The long-believed hypothesis for TZD-induced BAT activation was that it occurred simply as a result of increased binding of PPARγ agonists to PPAR response elements on beige-selective genes [67, 68]. However, it has since been suggested that TZDs increase the stability of PRDM16 (a key transcriptional co-regulator in BAT and beige activation) from 5.9 hours to 17.5 hours [69].

Furthermore, a group of novel activators of BAT have been identified that are associated with exercise and act independently of the SNS. These include cardiac natriuretic peptides [70], interleukin-6 (IL-6) [71], β-aminoisobutyric acid (BAIBA) [72], fibroblast growth factor 21 (FGF21) [73] and irisin [74-76]. Of these, the most extensively studied is irisin, a myokine released from muscles following exercise [75]. In 2012, Boström et al. showed that irisin binds to the surface of white adipocytes, inducing the expression of UCP-1, and inducing the browning of subcutaneous WAT in mice [75]. This was associated with weight loss, an increase in total body energy

expenditure, and improved glucose tolerance. Finally, BAT activity and abundance is known to decrease with age in both humans [50, 77] and mice [78].

***The tricarboxylic acid cycle***

The tricarboxylic acid (TCA) cycle takes place in the mitochondrial matrix and produces the substrates required for the electron transport chain (see Figure 1.2). As such, changes in the levels of TCA cycle metabolites can influence substrate availability, with subsequent effects on the rate of the electron transport chain, proton transport and ATP production.

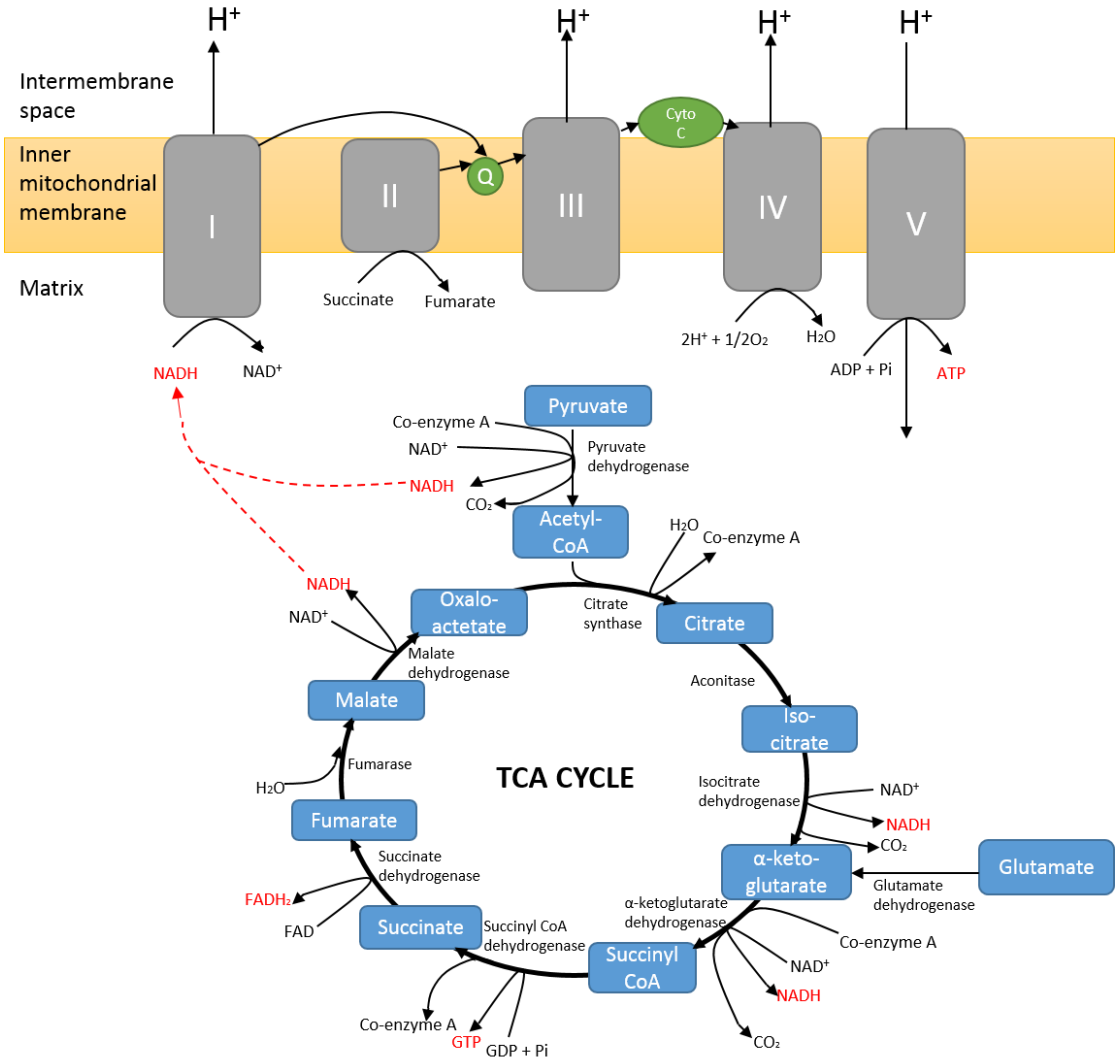


Figure 1.2. The tricarboxylic acid (TCA) cycle and electron transport chain.
Q = conenzyme Q; Cyto C = cytochrome C; NADH = nicotinamide adenine dinucleotide; ADP = adenosine diphosphate; ATP = adenosine triphosphate; FADH = flavin adenine dinucleotide; GTP = guanosine triphosphate. Adapted from Osellame et al. 2012 [79].

Upon BAT activation, there is an increase in rate of glucose uptake into BAT [80]. This was demonstrated by Ouellet et al. in 2012 [80] using PET-CT analysis of $^{18}$F-fluorodeoxyglucose ($^{18}$FDG), a radioactive glucose analogue. This was accompanied by an increased uptake of saturated fatty acid (measured using fatty acid tracer $^{18}$F-fluoro-thiaheptadecanoic or $^{18}$FTHA) and non-esterified fatty acids [80]. In addition, the rate of TCA cycle oxidation was measured using $^{11}$C-acetate, a tracer for acetate. Acetate is the main input molecule to the TCA cycle, in the form of acetyl-CoA. $^{11}$C-acetate levels were increased in BAT throughout cold exposure, indicating increased oxidative metabolism [80]. These findings were confirmed by Blondin et al. in 2014 [81]. Taken together, this indicates an increased rate of oxidation within the TCA cycle, and thus an increased rate of turnover of TCA cycle metabolites.

In addition, in human males, cold-induced increases in BAT activity are associated with increased BAT glutamate uptake [82]. Glutamate is a precursor to α-ketoglutarate, and converted to α-ketoglutarate in a reaction catalysed by the enzyme glutamate dehydrogenase.

***A therapeutic target***

Due to its potential to increase energy expenditure, increasing BAT activity is a therapeutic target for the treatment of obesity. Estimations suggest that 50g of active BAT in humans could equate to around a 5–20% increase in resting energy expenditure [49, 83], which could equate to a loss of 4–4.5kg of fat mass per year [84]. Indeed, increased BAT or beige activity in mouse models is associated with a leaner phenotype [75, 85-88], while mice lacking BAT or beige adipose tissue activity are susceptible to obesity [89, 90]. Furthermore, human BAT activity has an inverse correlation with body mass [91].

BAT activation may also have beneficial metabolic effects outside of its ability to increase energy expenditure. It has been suggested that BAT activation could delay the development of type 2 diabetes due to increased oxidation of excess glucose and lipids [92]. A recent study by Lee et al. [93] demonstrated that cold-induced BAT activation increased insulin sensitivity in humans, although further study is needed in this area.

Cold-induced BAT activation has also been shown to reduce plasma triacylglycerol levels in mice [94, 95]. Furthermore, SNS-induced BAT activation decreased plasma triacylglycerols in hyperlipidaemic mouse models through increased uptake of these specific lipids into BAT [96], which subsequently decreased the cholesterol levels and slowed down the rate of atherosclerosis development. This has been confirmed in a human study, in which 68 hypercholesterolaemic patients showed reduced levels of total serum cholesterol and serum LDL cholesterol following exposure of the whole body to cold water for 5–20 minutes per day for 90 days [97].

Therefore, the beneficial effects of therapeutic BAT activation may not be solely limited to the generation of a negative energy balance.

### 1.2.3. Beige adipose tissue

UCP1 expression is almost exclusively limited to brown adipose tissue as the main thermogenic organ [98]. However, it is now well established that in certain populations of white adipose tissue (WAT), UCP1 expression can be induced [63, 99], as well as the expression of a panel of genes associated with uncoupled proton transport and heat production [100]. These populations of WAT are known as 'beige' or 'brite' adipocytes, and can be activated, like BAT, by cold exposure or sympathetic innervation [101].

Beige adipocyte populations are present in subcutaneous white adipose tissue, while visceral white adipose tissue is typically non-browning [102]. However, beige adipocytes lack other intrinsic characteristics associated with brown adipocytes, such as the myf-5 cellular lineage and myocyte-associated genes [99] and the expression of transcription factors PRDM16, ZIC1, LHX8 and MEOX2 [63]. They also retain certain characteristics unique to WAT, such as HOXC9 expression [63]. The induction of browning in WAT has been the subject of extensive research in recent years due to its potential therapeutic application in the treatment of obesity.

### 1.2.4. Bone marrow adipose tissue

Marrow adipose tissue (MAT) is an anatomically and functionally distinct adipose depot located in the marrow cavity of bones. Bone marrow adipocytes occupy over 70% of the bone cavity volume [103]. While the presence of adipose tissue in bone marrow has been recognised for around 100 years [104-107], it was only with the discovery that adipose tissue is also an endocrine organ (rather than an inert energy storage organ) [108] that the possibility of MAT as an important factor in energy metabolism was considered.

***A distinct depot***

It has been proposed that MAT is similar to brown adipose tissue (BAT) [109], and that it has comparable functions in thermogenesis. MAT and BAT have overlapping gene expression profiles (including expressing *UCP1*, *PRDM16*, *DIO2*, and *PGC1a*) and show a comparable decrease in these genes during ageing and in diabetes [109]. However, MAT is unlike BAT both histologically and structurally.

Histologically, MAT looks identical to white adipose tissue (WAT) [110]. MAT and WAT also exhibit similar lipid contents, being made up mostly of triglycerides[111]. Furthermore, MAT, like WAT, can function as an adipokine-secreting endocrine organ (discussed further on page 11).

However, despite similar lipid content, the lipid saturation profiles of WAT and MAT differ [112], with a greater proportion of saturated fatty acids and a lower proportion of monounsaturated fatty acids in MAT compared to WAT. MAT also has a distinct gene expression profile in comparison to WAT [113], with higher expression of genes associated with early adipogenesis (e.g. *CEBPb*, *RGS2*) and a lower expression of mature adipocyte-specific genes (e.g. *PPARg*, *FABP4*, *PLIN1*, *CFD*). A group of genes that could be linked to MAT-bone signalling have also been identified, including *SFRP4*, *TNFa*, *TGFb1*, *GPR109A*, and *IL-6* [113].

MAT also responds differently to WAT in response to energy deficit: in rabbits fasted for 3 weeks, the ability of MAT to esterify fatty acid was not altered; whereas that of perinephric WAT was decreased by 60% [114]. Furthermore, in animal models of calorie restriction (CR) including in rabbit [115] and mouse [116], MAT has been shown to increase in volume in response to energy deficit, in contrast to the decreased WAT mass that is observed in response to energy deficit. This observation in MAT has been verified in several human studies investigating cohorts of patients with anorexia nervosa [117-119].

Thus, the characteristics of MAT are distinct from other previously well-characterised adipose tissue depots. This leaves the function of MAT a question largely unanswered.

***Mechanisms for MAT development and deposition***

MAT development differs from typical WAT development in several ways:

*MAT development*

Visceral WAT development and constitutive MAT development occur at similar stages of development (Table 1.1). However, in adulthood, WAT expansion depends primarily on hypertrophy (cell size increase), with a generally very tightly maintained adipocyte cell number in healthy adults. Hyperplasia (cell number increase) is therefore reserved as a secondary mechanism for lipid storage when capacity is exceeded [120, 121]. In contrast, expansion of MAT is dependent on both hypertrophy and hyperplasia: 66.2% of MAT expansion is dependent on adipocyte size alone; and 97.2% is dependent on the combination of *both* adipocyte size and number [122].

In addition, MAT behaves differently to WAT in response to certain dietary stimuli. As discussed on page 8, MAT is increased in CR and anorexia nervosa [116, 123, 124]. This apparently contradictory observation has led to the theory that MAT may act as a reserve energy storage for times of severe starvation that can be utilised to provide several extra days of life during the final stages of starvation [125]. This supports the idea that WAT and MAT may respond differently to nutritional status. Consistent with this, MAT does not generally correlate with commonly used clinical measures of adiposity, such as body mass index, waist-to-hip ratio and visceral to subcutaneous fat ratio [126-128].

| | **Subcutaneous WAT** | **Visceral WAT** | **Constitutive MAT** | **Regulated MAT** |
|---|---|---|---|---|
| Mice | Embryonic days 14-18 [129] | Several weeks after birth [129] | 1-4 weeks after birth [130] | Develops in response to various stimuli throughout life [130, 131] |
| Humans | Final third of gestation [132] | Final third of gestation [132] | At birth or slightly before birth (further expansion 4-8 weeks of age) [110, 133] | |

Table 1.1. The stages of development of adipose tissue.
The stages of development at which subcutaneous and visceral white adipose tissue (WAT), and constitutive and regulated marrow adipose tissue (MAT) are formed.

*The origin of MAT*

WAT is thought to be of mesodermal origin [134], with adipocytes derived from self-renewing mesenchymal stem cells. Adipocyte progenitor cells are characterised by the expression of PPARγ, marking commitment to the adipogenic lineage, yet they do not accumulate lipid [135]. A study by Rodeheffer et al. [136] identified a subset of adipocyte progenitor cells expressing CD29, CD34, Sca-1 and CD24 (negative markers for the haematopoietic lineage), which have the potential to regenerate an entire fat depot in lipodystrophic mice and stimulate *de novo* vascularisation. BAT, on the other hand, is thought to be of distinct origin from WAT. BAT is thought to share a common early developmental program with skeletal muscle, and the transcriptional signature of BAT differentiation may act to inhibit myogenesis [137]. Brown adipocytes, but not white or beige adipocytes, were shown to arise from myogenic marker *Myf*5-expressing precursors [138].

It is thought that MAT adipocytes, like WAT adipocytes, differentiate from mesenchymal stem cells and can further differentiate into white and beige adipocytes [139, 140]. Some recent studies have identified the leptin receptor (LepR) as a marker for adult bone marrow adipocyte progenitors [141], and showed that conditional knockout of LepR in Prx1-Cre positive cells (a mesenchymal stem cell marker) caused increased osteogenesis, decreased adipogenesis, and accelerated fracture healing [142], indicating that leptin/LepR signalling to bone marrow mesenchymal stem cell populations is required for bone marrow adipogenesis. Furthermore, a study by Ambrosi et al. [143] identified the properties of bone marrow adipocyte precursors using flow cytometry, isolating a population of $CD45^{-}CD31^{-}Sca1^{+}CD24^{+/-}$ adipocyte progenitor cells: the same markers used to identify white adipocyte progenitors. In addition, the bone marrow adipocyte progenitor cell population had a gene expression profile (including PPARγ and CEBPα) and *in vitro* adipogenic capacity that most closely resembles inguinal (subcutaneous) WAT.

***MAT contribution to local and systemic metabolism***

The triglycerides in MAT have been shown to affect regulation of the populations of osteoblasts, osteoclasts and blood cells [111, 144], contributing to the hypothesis that MAT may influence the local metabolism and growth of bones.

Comprising around 7% of the total fat mass in an average adult [128], MAT is also thought to make a significant contribution towards systemic metabolism, particularly in individuals with an exaggerated MAT:WAT ratio, such as those with anorexia nervosa or MAT-sparing lipodystrophy. In these individuals, it is estimated that MAT comprises around 30-40% of the total fat mass [110]. Cases of congenital lipodystrophy (CGL) have been pivotal in the study of the role of MAT in systemic metabolism, due to the fact that some CGL manifest as MAT-depleting (CGL1, CGL2) and some are MAT-sparing (CGL3, CGL4) [110]. The prevalence of hyperinsulinemia, high serum triglycerides, acanthosis nigricans (a sign of insulin resistance), and diabetes is higher in patients with CGL1 and CGL2 in comparison to patients with CGL3 or CGL4 [110], suggesting that the presence of MAT in CGL4 could contribute to the reduced severity of diabetes and insulin resistance.

The endocrine properties of MAT are also thought to contribute to systemic metabolism. In cultured explants of rabbit WAT and MAT, adiponectin was found to be expressed at higher levels in MAT than WAT [123]. This finding was also confirmed in humans, with MAT adipocyte cultures demonstrating a greater capacity for adiponectin secretion than WAT [123]. Adiponectin is a peptide hormone associated with improved glucose tolerance, insulin sensitivity, cell survival and vascular function [145]. Levels of circulating adiponectin are generally inversely correlated with WAT mass, so that obesity is generally associated with hypoadiponectiaemia [146], and low circulating

adiponectin is a proposed biomarker for risk of both cardiometabolic disease and cancer [147]. The role of specific MAT-derived adiponectin is a subject of ongoing research, although CR studies suggest that MAT-derived adiponectin is required for CR-derived adaptations in skeletal muscle, such as upregulation of transcripts involved in mitochondrial function (including *Ppargc1a*, *Tfam* and *Acadm*) [148]. The potential for MAT-derived adiponectin to impact on other systemic functions, such as glucose tolerance and hepatic gene transcription, is a subject of ongoing research (reviewed in [149]).

It is also thought that MAT has some capacity for leptin expression and secretion, first demonstrated in cultured adipocytes differentiated from bone marrow-derived mesenchymal stem cells *in vitro* [150-152]; a finding confirmed in primary bone marrow adipocytes *in vitro* [153, 154]. Leptin expression at the transcript level in isolated bone marrow adipocytes has also been shown *in vivo* in mice [113] and rabbits [124]. Leptin is a satiety hormone, and depletion of the leptin gene or the leptin receptor results in insatiable hunger and severe obesity [108, 155]. Leptin also has effects on energy balance, fertility and immune function [156], and as such MAT-derived leptin may have the potential to influence any of these systemic functions.

***Regulated and constitutive MAT***

MAT is present in the marrow of long bones in two distinct depots: regulated (rMAT) and constitutive (cMAT). The two depots differ in their histological profiles, their fatty acid content, and their stage of development [130]. cMAT develops 1-4 weeks after birth in mice (at the same time as WAT development); appears histologically as confluent, rounded adipocytes; and has a greater proportion of unsaturated fatty acids. rMAT develops later in life in response to certain metabolic or endocrine stimuli or disease states (see Table 1.2); histologically is present as smaller, more discrete adipocytes; and has a higher proportion of saturated fatty acids compared to cMAT [130].

| **Stimulus/disease state** | **Human MAT response** | **Rodent MAT response** | **Reference** |
|---|---|---|---|
| Calorie restriction/Anorexia nervosa | Increased | Increased | [123, 124, 157] |
| High fat diet/Obesity | Increased | Increased | [158-163] |
| Type I Diabetes | No change | Increased (tibia/fibula) or no change (vertebrae) | [164, 165] |
| Type II Diabetes | Increased or no change | Increased | [166-168] |
| Cold exposure | - | rMAT decreased, cMAT no change | [130] |
| Congenital lipodystrophy 1 | Absent | Not applicable | [110] |
| Congenital lipodystrophy 2 | Absent | Not applicable | [110] |
| Congenital lipodystrophy 3 | Retained | Retained | [110, 130] |
| Congenital lipodystrophy 4 | Retained | rMAT decreased, cMAT no change | [110, 130] |
| Ageing | Increased | Increased | [127, 130] |
| Glucocorticoid treatment | Increased | Increased | [169, 170] |
| Oestrogen deficiency | Increased | Increased | [171, 172] |

Table 1.2. Marrow adipose tissue response to various stimuli.
Adapted from Scheller et al. 2016 [173].

***MAT and obesity***

As shown in Table 1.2, MAT is increased in states of obesity. This increase is particularly associated with an increase in visceral fat: in a study on 47 pre-menopausal women of varying BMI, there was a positive correlation between the amount of visceral adipose tissue and amount of MAT [159], a finding confirmed in 35 healthy obese men [158]. In mice, both long-term (12 weeks) and short-term (2 and 3 weeks) high fat diet (HFD) was associated with increased MAT, with contradictory findings on the associated effect on bone mass [160, 162]. Additionally, both regular diet- and HFD-fed mice with access to an exercise wheel exhibited decreased MAT by more than half compared to those without access to an exercise wheel [163], demonstrating that MAT is highly responsive to exercise.

***The effect of MAT on bone structure and bone mineral density***

Increases in MAT are associated with decreased bone mineral density following the menopause [174] and in various human disease states, including ageing [127, 175] and anorexia nervosa [117]. The

inverse association between MAT content and bone mineral density has also been demonstrated in animal models of ageing [176], ovariectomy [177], calorie restriction [116] and glucocorticoid treatment [178]. There are two hypotheses to explain the contribution of MAT expansion to the process of bone demineralisation. Firstly, it has been suggested that adipogenesis and osteoblastogenesis are competitive processes, with increases in pro-osteogenic factors (growth hormone, Wnt proteins, insulin-like growth factor 1) associated with an increase in adipogenesis [179-181]. The alternative hypothesis is that certain paracrine factors secreted by MAT can inhibit osteoblastogenesis and favour adipogenesis, such as such as Wnt signaling inhibitors [182] and chemerin [183].

## 1.3. Physiological control of food intake

### 1.3.1. Leptin

Leptin is a 16kDa protein secreted from adipose tissue in response to eating. Frequently referred to as the satiety hormone, leptin is secreted into the blood, attaches to the leptin binding protein, and reaches the hypothalamus *via* the cerebrospinal fluid (CSF). In the brain, it acts by decreasing neuropeptide Y, which suppresses appetite [184]; and promoting α-MSH (α-melanocortin stimulating hormone) synthesis, which decreases hunger [185].

Recent evidence also demonstrates that leptin influences energy metabolism as well as energy intake. For example, in rodents, leptin treatment increases energy expenditure and decreases fat mass without affecting lean mass [186, 187]. In addition, in mice genetically lacking leptin (*Ob*/*Ob* mice), recombinant leptin treatment normalises serum glucose, insulin and lipid concentration [186]. Leptin is also involved in numerous other processes, including fertility [188-190], puberty [191], angiogenesis [192, 193] and bone metabolism [194].

### 1.3.2. Leptin receptors

Leptin acts by binding to its receptors (OB-R), of which there are 7 known isoforms (OB-R a-f), produced by alternative splicing [195]. Leptin receptors are single membrane-spanning receptors with homology to the cytokine receptor superfamily. OB-R a, b, c, d & f contain transmembrane domains and can be divided into two groups: those that have a short amino acid residue intracellular domain (short form: includes OB-Ra, OB-Rc, OB-Rd and OB-Rf) and those with a long amino acid residue intracellular domain (long form: OB-Rb only) [195]. OB-Rb is mainly expressed in the hypothalamus [196] and is responsible for the anorectic action of leptin. The long form has two Janus kinase (Jak) sites in the intracellular domain while the short form has only one. The long form activates the signal transducers and activators of the transcription family STAT [197]. Short leptin isoforms are able to

activate some signal transduction cascades, although the effect of short isoform activation differs from that of long isoform activation [198, 199].

The short forms are expressed in a variety of tissues with distinct tissue distributions [200]. It was initially suggested that the main function of the short form receptors is to internalise and degrade leptin [201]. However, the short form leptin receptors are now believed to be important for the peripheral metabolic effects of leptin [202]. Leptin has been suggested to have direct peripheral action *via* the short-form receptors in key metabolic organs including skeletal muscle, pancreas, liver, gastrointestinal tract and adipose tissue [202].

OB-Re is the soluble leptin receptor and has no transmembrane domain. This isoform is thought to be either a result of alternative transcript splicing or a consequence of transmembrane Ob-R receptor destruction [203]. Plasma Ob-Re can bind serum leptin and inhibit its signal transduction. It can also regulate serum leptin levels and act as a carrier protein, delivering the hormone to its membrane receptors to initiate cellular signal transduction [204].

### 1.3.3. Serum leptin fluctuations

Serum leptin levels increase in response to feeding, particularly in response to foods with a high glycemic index (GI) [205, 206]. Plasma leptin levels are positively correlated with BMI [207, 208], and leptin increases not linearly but exponentially with fat mass [209]. Conversely, starvation causes hypoleptinaemia, a change that takes place acutely, even prior to the depletion of adipose tissue [210]. Leptin levels increase diurnally between midnight and early morning, acting to suppress appetite during the night [211]. However, this diurnal variation in leptin levels can be modified by meal timing [212].

In a study of 1062 male office workers, leptin levels were found to be increased in those who rated themselves as more psychologically stressed [213]. In addition, physical exercise (12 weeks aerobic exercise training) causes a chronic reduction in plasma leptin in females but not males. These changes were seen in the absence of a reduction in body fat [214]. Glucocorticoids directly stimulate leptin synthesis in cultured adipocytes [215, 216], and chronic cortisol elevation in humans causes increased leptin expression [217]. For a full summary of conditions known to influence leptin levels, please see Table 1.3.

| Site of leptin secretion | Increase | Decrease |
|---|---|---|
| Adipose tissue | Feeding (especially high GI foods) | Fasting |
| | Overfeeding | Starvation |
| | Obesity | Testosterone |
| | Insulin | Beta-adrenergic agonists |
| | Glucocorticoids | Thiazolidinediones (in vitro) |
| | Acute infection | Thyroid hormone |
| | Cytokines (TNF-α, IL-1, LPS) | Cold exposure |
| Placenta | Insulin | Smoking |
| | Glucocorticoids | Low birth weight |
| | Hypoxia | - |
| Skeletal muscle (rat) | Glucosamine | - |
| | Glucose | - |
| | Lipids | - |
| Stomach fundus (rat) | - | Feeding |
| | | |

Table 1.3. Conditions that regulate plasma leptin levels.

Table adapted from Ahima et al. 2000 [218]

### 1.3.4. Regulation of leptin plasma levels

Leptin is regulated at multiple levels: expression, secretion and protein binding. It has been suggested that insulin can stimulate leptin expression and secretion in adipocytes *in vitro* [219, 220], although there is contradictory evidence for this [221, 222]. Similarly, *in vivo*, some groups have reported that insulin increases plasma leptin levels in rodents and humans [223, 224], while other groups have not observed any acute change in leptin expression or secretion in response to insulin [225, 226].

Another known regulator of leptin secretion is cold exposure [227], which acts by activating the sympathetic nervous system and β3-adrenergic receptors, increasing the circulating levels of norepinephrine, in turn decreasing plasma insulin and leptin levels [228-230] and leptin mRNA expression in adipose tissue [231]. Sympathetic innervation and β3-adrenergic receptor activation in adipose tissue has been shown to be the mechanism responsible for decreasing leptin gene expression

in response to leptin injections [232] and also for fasting-induced reduction in circulating leptin levels [233].

Another method of regulation of serum leptin levels is through sequestering of the protein in the serum by the soluble leptin receptor (OB-Re) [234]. The ratio of serum leptin to OB-Re provides the measure of free leptin index (FLI), which is proposed to be a more accurate determinant of leptin action than serum leptin levels alone [235]. An example in which OB-Re may be actively regulating free leptin levels is in anorexia nervosa. In this case, plasma leptin levels are decreased and OB-Re levels are increased, resulting in a decreased FLI [236]. This suggests that high OB-Re levels in anorexia nervosa may act to suppress leptin action during energy deficiency. Weight recovery in anorexic patients was associated with a decrease in plasma OB-Re and an increase in plasma leptin, with no change in FLI [236].

### 1.3.5. Leptin deficiency

In *ob*/*ob* mice, a mutation in the leptin gene coding sequence results in leptin deficiency and obesity. In *db*/*db* mice, mutations in leptin receptors are associated with an almost identical phenotype [197]. Treatment with recombinant leptin reduces fat mass in *ob*/*ob* mice but not *db*/*db* mice.

In humans, mutations in the *LEP* gene result in hyperphagia and severe obesity from childhood [155]. Following the first identification of a mutation in the human *LEP* gene in 1997 [155], a further seven distinct human mutations have been identified. While these mutations vary in structure, the result *in vivo* is the absence of plasma leptin. Treatment with a recombinant form of the protein, Metreleptin, in these patients lead to a "rapid change in eating behaviour, a reduction in daily energy intake, and substantial weight loss" [237].

In addition, polymorphisms in the leptin receptor gene *LEPR* have been associated with a similar clinical presentation including hyperphagia and obesity [238]. These polymorphisms were accompanied by high plasma leptin levels, indicating leptin resistance [238].

### 1.3.6. Leptin resistance

The discovery of leptin as a satiety hormone was met with much excitement regarding its potential application as a treatment for obesity. However, while recombinant leptin therapy is effective in treating monogenic forms of obesity that involve mutations in leptin and its signalling pathway [239] this possibility of its application in polygenic obesity was soon disregarded when it was found that leptin sensitivity, much like that of insulin in Type 2 diabetes, is plastic and overexposure to the hormone results in leptin resistance [240]. This is the case in obesity, in which high levels of leptin

are secreted due to increased adipose tissue, but the subject no longer receives the satiety signals. In this regard, plasma leptin levels can be used to predict the physiological potency of leptin, such that *ob/ob* mice show marked responses to injected leptin, while hyperleptinemia results in diminished leptin response [241].

There are a number of hypotheses for a molecular explanation for leptin resistance, including alterations in the transport of leptin across the blood brain barrier (BBB), alterations in cellular OB-Rb signalling and perturbations in developmental programming [242-244]. It is possible that all of these mechanisms may act together to give the combined effect of leptin resistance. Although there are no changes in the transcription or abundance of OB-Rb in the hypothalamus in most cases of leptin resistance [245, 246], the majority of studies in the field confirm that defects in OB-Rb signalling play a crucial role [242, 243, 247].

One hypothesis for leptin resistance is that leptin transport across the BBB is altered. In humans, it was found that the ratio of leptin in the CSF compared to the blood is lower in obese people compared to healthy weight controls [248]. It has been suggested that obesity causes high levels of triglyceride transport across the BBB, which can in turn affect the transport of leptin across the BBB. In support of this, a study using CSF from Lou/C rats, an inbred strain of Wistar origin that are resistant to age- and diet-related obesity, found decreased levels of triglycerides in the CSF of the Lou/C rats compared to age-matched Wistar controls, which could be consistent with increased leptin transport across the BBB [249]. Consistent with this, they found improved hypothalamic leptin signalling in Lou/C rats, indicated by increased pSTAT3/STAT3 (signal transducer and activator of transcription 3) ratio following acute peripheral leptin administration, as well as by decreased hypothalamic mRNA expression of the suppressor of SOCS3 (cytokine signalling 3), known to downregulate leptin signalling. All of these changes were found in the absence of changes in leptin transporter expression in the choroid plexus.

However, changes in the leptin receptor are not believed to be the main cause of leptin resistance. This is because, although there is a deficit in the transfer of leptin from the plasma to the CSF in obesity, obese subjects still have 30% more leptin in their CSF compared to lean subjects, which fails to prevent obesity [248]. Leptin mRNA levels indicate that the amount and quality of leptin receptors in the hypothalamus are normal in the majority of obese subjects [246]. Therefore, it is more likely that leptin resistance in obesity develops from a post-receptor deficit, similar to the mechanism seen in type 2 diabetes. For example, leptin resistance may be caused by defects in the JAK/STAT pathway downstream of leptin receptor activation. Phosphotyrosine phosphatase (PTP1B) recognises a specific consensus substrate motif found in JAK2. Over-expression of PTP1B resulted in hypophosphorylation of endogenous JAK2 and blocked the leptin-induced transcription of endogenous SOCS3 and c-fos in

a hypothalamic cell line [250]. PTP1B appears to be a negative mediator of both the JAK/STAT and MAPK pathways in leptin receptor signalling and therefore may be implicated in leptin resistance [250].

## 1.4. Epigenetics

The most widely accepted definition of epigenetics is the study of heritable phenotype changes that do not involve alterations in the DNA sequence [251-253]. Epigenetics is usually used to describe molecular mechanisms that affect transcription without change to the primary nucleotide sequence. Examples include histone modifications, DNA methylation, and can include non-coding RNAs with transcription-modulating properties, such as microRNAs.

Epigenetic modifications can persist through multiple cell divisions, throughout life and may be heritable throughout multiple generations [254]. They can also be responsible for tissue-specific gene expression and developmental changes in gene expression [255]. Furthermore, they are also dynamically influenced in various environmental exposures and disease states, most notably cancer (reviewed in [256] and [257]).

### 1.4.1. DNA packaging and chromatin accessibility

To enable several metres of eukaryotic DNA to fit within a cell nucleus of 2-10μm, DNA must be efficiently packaged, while still remaining accessible to the critical protein machinery that allow it to function [258]. The histone proteins are a solution to this problem, allowing around 147 base pairs of DNA to wrap around a histone octamer (2 copies each of H3, H4, H2A and H2B), forming a nucleosome complex which repeats throughout the DNA [259]. Chromatin occurs in distinct domains: regions that are compacted (heterochromatin) and regions that are relaxed (euchromatin). Euchromatin is typically transcriptionally permissive, while heterochromatin is typically transcriptionally repressive [260]. Chromatin state is influenced by several factors, such as histone chaperones that can facilitate deposition and eviction of histones [261, 262], histone variants in the nucleosome core particle [263], chromatin remodellers that use ATP to evict histones [264], and small chemical modifications to histones and DNA [265-268], which compose a large part of the mechanisms under the term “epigenetics”.

### 1.4.2. Histone post-translational modifications

A huge number of histone modifications, such as lysine acetylation, lysine and arginine methylation, lysine ubiquitination, arginine citrullination, lysine sumoylation, ADP-ribosylation, proline isomerization, and serine/threonine/tyrosine phosphorylation can occur on histones [265, 269], although only a few have known transcriptional regulatory function [270]. Histone 3 lysine 4

trimethylation (H3K4me3) [271-273] and histone 3 lysine 36 trimethylation (H3K36me3) [270] are associated with transcriptional activation. Histone 3 lysine 27 trimethylation (H3K27me3) [274], histone 3 lysine 9 di- and tri-methylation (H3K9me2/3) [269, 275] and histone 4 lysine 20 trimethylation (H4K20me3) [276, 277] are four marks that are associated with transcriptional repression. In addition, the "histone code" hypothesis suggests that in addition to the role of histone modifications mediating chromatin compaction or relaxation, they may be able to selectively recruit effector proteins that dock onto histone modifications and elicit a transcriptional response [270, 278] that may well be contradictory to the direct physical effect of the histone modification on chromatin structure [279].

### 1.4.3. DNA methylation

Methylation of the C5 position of the cytosine in a CpG dinucleotide, mediated by DNA methyltransferase enzymes 1-3 (DNMTs), generates 5-methylcytosine (5mC) [280]. 5mC is associated with long-term transcriptional repression, particularly when present in gene promoters. DNA methylation is essential for normal development and is associated with a number of key developmental processes including genomic imprinting, X-chromosome inactivation and repression of transposable elements. DNA methylation may influence gene transcription in two ways: either DNA methylation can physically prevent the binding of transcriptional proteins [281]; or methylated DNA may be bound by methyl-CpG-binding domain proteins (MBDs). MBD proteins are able to recruit further repressive proteins to the locus, such as histone deacetylases, thus generating compact heterochromatin [282].

### 1.4.4. CpG islands

Chemical instability of methylated CpG dinucleotides has resulted in an evolutionary global depletion of CpGs and a lower-than-expected incidence of CpG sites within the genome [283]. The exception to this is within CpG-rich regions known as CpG islands, which are constitutively unmethylated [284]. Around 50% of CpG islands are located in gene promoters, and another 25% are located in gene bodies, where they often serve as alternative promoters [284]. Likewise, around 60-70% of gene promoters in mice and humans contain CpG islands [285, 286].

### 1.4.5. Active and passive DNA demethylation

The methyl group of 5mC can be removed in a cell type-specific manner. This removal can be achieved passively through failure of DNMT1 during DNA replication [287], or actively through enzymatic DNA demethylation. During active DNA demethylation, 5mC is oxidized to sequentially produce 5-hydroxymethylcytosine (5hmC), 5-formylcytosine (5fC), and 5-carboxylcytosine (5caC) in a manner independent of DNA replication [288] by the action of the ten-eleven-translocation (TET)

enzymes [289]. Following oxidation, the DNA base-excision repair (BER) pathway can remove the methylated cytosine and replace it with an unmodified cytosine. Furthermore, it has been suggested that passive DNA demethylation is enhanced by active DNA demethylation, because DNMT1 activity can be reduced by 5hmC *in vitro* [288, 290].

### 1.4.6. DNA hydroxymethylation

As well as being an intermediate in active DNA demethylation, 5hmC is also a stable, functional and relatively abundant epigenetic mark involved in transcriptional regulation [291]. 5hmC is 10- to 100-fold more abundant than 5fC/5caC and it is relatively enriched in neurons, stem cells, and decreased in cancer cells [292-294]. An increasing number of studies demonstrate that 5hmC plays important roles during maintenance of pluripotency in embryonic stem cells (ESCs), central nervous system development and tumorigenesis [295].

5hmC was initially identified in 1952 in viral DNA [296, 297], not long after the discovery of 5mC; but it wasn't until 2009 that it gained attention following the discovery that it was abundant in Purkinje fibres and granule cells [298, 299]. Shortly after, it was discovered in all cell types in the mouse, with particularly high levels in the central nervous system [300].

Increased levels of 5hmC are present in the gene bodies of actively transcribed genes, and TET1 is often present at the transcriptional start site of genes with CpG promoters that are marked by the bivalent histone signature of H3K27me3 and H3K4me3 [301]. Because of this, it is assumed that 5hmC and TET proteins may initiate active gene expression by modulating chromatin accessibility of the transcriptional machinery, or by inhibiting repressor binding.

In support of this, 5hmC is enriched within gene bodies, promoters, and transcription factor-binding regions [302]. In addition, 5hmC accumulates in gene-rich regions marked by H3K4me2/3, as demonstrated by immunostaining [301, 303]. The relationship between 5hmC peaks and gene expression level is complicated. For example, actively transcribed genes have depleted 5hmC in their transcriptional start site regions, while genes of low expression show 5hmC peaks at promoters in both embryonic stem cells and neural progenitor cells [304]. To complicate it further, 5hmC peaks in gene bodies are positively correlated with gene expression levels in embryonic stem cells, but with lower expression levels in neural progenitor cells [304]. In this regard, patterns of 5hmC peaks seem to be a cell type-dependent regulatory network rather than simple activation or repression of gene activity.

Furthermore, during cell differentiation, patterns of 5hmC peaks and troughs are affected by the presence of histone modifications, epigenetic marker binding proteins, and chromatin configuration.

5hmC is present at high levels at the transcriptional start sites of genes whose promoters have dual histone marks (H3K27me3 for transcriptional repression and H3K4me3 for transcriptional activation) [305]. 5hmC levels are also high at "poised" and active enhancers labelled with H3K4me1, H3K18ac, and H3K27ac [303].

5hmC is also highly enriched at polycomb target gene promoters where it is associated with the generation of the repressive histone mark H3K27me3 and transcriptional repression [306, 307]. TET1 is necessary for chromatin binding of the Polycomb Repression Complex 2 (PRC2), which is required for initial targeting of genomic regions to be silenced. Therefore, 5hmC has both activating and repressive influences on transcription [307].

5hmC levels are highly dynamic, and can be altered in states of disease [308] or drug treatment [309, 310]. For example, in mice treated with phenobarbital (a rodent hepatocarcinogen) for 4 weeks, 5hmC at specific loci in liver DNA were dramatically changed [309, 310]. In the promoters of genes displaying highly upregulated expression, increased levels of 5hmC and decreased levels of 5mC were observed in addition to increased levels of the activating histone mark H3K4me2.

### 1.4.7. The Ten Eleven Translocase enzymes

The Ten Eleven Translocase (TET) enzymes, which include TET1, TET2 and TET3, were identified in 2009 as homologues of J-binding protein 1 & 2 (JBP1 & 2) and members of the 2-oxoglutarate (2OG)- and Fe(II)-dependent oxygenase superfamily [299, 311, 312]. TET1 was first identified as a fusion partner of the *MLL* gene in acute myeloid leukaemia [313]. All three TET isoforms have been shown to oxidize 5mC into 5caC efficiently *in vitro* and *in vivo* [314], although TET depletion studies suggest that TET1 is responsible primarily for activity in the gene promoters, while TET2 is more active at CpGs in gene bodies [315].

The three TET isoforms show temporal and tissue-specific patterns of expression [316-318]. TET1 is highly expressed in embryonic stem cells [299] and primordial germ cells [319], suggesting an association with the pluripotent state. TET2 is most widely expressed in somatic tissues, especially haematopoietic cells [320], and has overlapping roles with TET1 in regulating haematopoietic stem cell (HSC) maintenance, hematopoietic homeostasis, and leukemogenesis [321]. TET3 is most highly expressed at the oocyte to zygote stage of development, and contributes to paternal global DNA demethylation [322].

Because the TET1 and TET2 isoforms in humans show higher activity for 5mC than for 5hmC/5fC, it is not easy to oxidize it to 5fC and 5caC once 5hmC is established in genomic DNA [323]. However,

TET3 acts as 5caC reader during 5caC excision in BER, since its CXXC domain shows high affinity for 5caC [324].

Finally, although the enzymatic activity of the TET proteins has been shown to be highly important for their function, one study suggested that TET proteins might also exert functions independently of their catalytic activity [325]. In this study, it was reported that TET1 associates with the Sin3a co-repressor complex in 293T and mouse embryonic stem cells (mESCs). Importantly, they found that the upregulation of TET1 target genes upon *Tet1* knockdown can also be observed in DNMT triple knockout ES cells in which both 5mC and 5hmC modifications are absent. These results suggest that TET1 might repress gene transcription in a manner independent of their catalytic activity.

### 1.4.8. The *Tet1* knockout mouse model

A study published in 2011 was the first to investigate the effects of *Tet1* deletion [326]. Initial studies on *Tet1* KO in ESCs found that levels of global 5hmC was reduced by around 35%, and subtle differences occurred in global gene expression (221 genes were significantly dysregulated > 2-fold; mostly genes involved with development). However, *Tet1* KO ESCs were still pluripotent. In addition, a tetraploid complementation assay was carried out. This is a test for assessing pluripotency as the cells of the recipient tetraploid (4n) blastocyst can only contribute to the trophectoderm but not the epiblast, thus generating embryos that are generated exclusively from the injected diploid mESCs [327]. The tetraploid complementation assay revealed that *Tet1* KO ESCs still supported development of live-born mice, although differentiation *in vitro* was skewed towards mesoderm and endoderm developemnt.

The same study generated the first *Tet1* KO mouse [328], which has a global knockout (KO) of the *Tet1* gene. *Tet1* KO mice are viable, fertile and grossly normal, although 75% of KOs were slightly smaller at birth. In this study, *Tet1* KO mice were reported to be born at expected Mendelian ratios [328], although subsequent studies have contradicted this [329-331]. Yamaguchi et al. reported that progenies resulting from mating between *Tet1* KO males and wildtype females display several variable phenotypes including placental, fetal and postnatal growth defects, and some early embryonic lethality [331].

A number of studies have used the *Tet1* global KO mouse model to investigate the function of TET1 in various tissues. For example, the *Tet1* KO mouse was found to display aberrant hypermethylation in the paternal allele of differential methylated regions of imprinted genes in sperm, which can be traced back to primordial germ cells, indicating that TET1 acts to wipe out remaining methylation, including imprinted genes, at the late reprogramming stage [331]. In addition, *Tet1* KO oocytes were reported to display univalent chromosomes, DNA double-strand breaks, and defective DNA

demethylation and decreased expression of a subset of meiotic genes [330], indicating that TET1 is important for meiosis. A further study using a *Tet1* KO mouse model found that *Tet1* KO causes altered expression of neuronal activity-regulated genes and compensatory upregulation of active demethylation pathway genes [332]. In addition, *Tet1* KO mice displayed an enhanced fear conditioning response and object location memories, suggesting that TET1 plays an important role in maintaining the epigenetic state of the brain associated with memory consolidation and storage [332]. A further study found that *Tet1* KO caused an increase in $H_2O_2$-induced apoptosis and an increase in sensitivity to oxidative stress of cerebellar granule cells, suggesting a role for TET1 in neuronal protection against oxidative stress [333]. Thomson et al. also characterised the liver epigenome of the *Tet1* KO mouse [308] and found a dramatic reduction in 5hmC over a large number of gene promoters, suggesting that TET1 is important for liver function.

Further studies have generated and characterised the phenotypes of other *Tet* isoform knockouts, including double and triple knockouts (summarised in Table 1.4).

| Genotype | Preimplantation development | Postimplantation development | Postnatal development | References |
|---|---|---|---|---|
| *Tet1*$^{-/-}$ | Normal | Small body size | Small body size | [326] |
| *Tet2*$^{-/-}$ | Normal | Normal | Spontaneous myeloid leukemia | [334-337] |
| *Tet1*$^{-/-}$ *Tet2*$^{-/-}$ | Normal | Normal, some defects in chimeric embryos | Some perinatal lethality. Viable and normal mice were also obtained | [338] |
| *Tet3*$^{-/-}$ | Normal | Normal | Neonatal lethality | [339] |
| *Tet3*$^{mat-/pat+}$ | Normal, but blockage in paternal genome reprogramming | A high frequency of degeneration and variable multi-organ abnormalities | Neonatal lethality and small body size | [339] |
| *Tet1*$^{-/-}$*Tet3*$^{-/-}$ | Severe loss of Nanog expression or aberrant coexpression of Nanog and Cdx2 | Global loss of 5hmC and gain of 5mC, dysregulation of lineage markers, poor ectoderm and endoderm development | Perinatal lethality | [329] |
| *Tet1*$^{-/-}$ *Tet2*$^{-/-}$ *Tet3*$^{-/-}$ | Impaired differentiation | Growth retardation or morphological defects. | Perinatal lethality | [340] |

Table 1.4. Phenotypes of *Tet* knockout mice.

Table adapted and expanded upon from Tan et al, 2012 [341].

## 1.5. Epigenetics and metabolism

### 1.5.1. The ‘thrifty phenotype’ and ‘thrifty epigenotype’ hypotheses

In addition to the ‘thrifty genotype hypothesis’ discussed previously in section 1.1.2, the ‘thrifty phenotype hypothesis’ [342] and the ‘thrifty epigenotype hypothesis’ [343] propose the importance of environmental influence (e.g. food shortage or availability) on the epigenome, gene expression and consequently phenotype.

The most well-known example of the thrifty phenotype/epigenotype is the 'Dutch Hunger Winter' study, in which a cohort of 300,000 men exposed during the first half of gestation to the Dutch famine in 1944-45 had significantly increased obesity rates at the age of 19 [344]. On the other hand, those exposed to famine during the last trimester or the first few months of life had significantly decreased rates of obesity. A later study identified increased DNA methylation levels in whole blood samples of those exposed to famine in early gestation, but not mid or late gestation [345], indicating that the inclination towards the 'thrifty' or obese phenotype is associated with changes in the epigenome. This has justified further investigation into the influence of the epigenome in adipose tissue and the development of obesity.

### 1.5.2. The role of TCA cycle metabolites in control of epigenetic factors

The TET enzymes are part of a group of α-ketoglutarate dependent dioxygenases [289]. It has also been shown that succinate and fumarate can inhibit the activity of enzymes in this group, including the TETs [346]. This provides a mechanism by which the rate of metabolite oxidation in the TCA cycle of adipose tissue can affect TET activity. This may subsequently influence levels of 5mC and 5hmC in DNA in the tissues of interest. Other members of the α-ketoglutarate dependent dioxygenases include the Jumonji C (JmjC)-domain-containing demethylases (JMJD), a group of histone demethylases [289]. Therefore, there is reason to believe that changes in metabolite concentrations could also influence histone modifications.

In support of this hypothesis, intracellular α-KG has been shown to maintain embryonic stem cell pluripotency by controlling H3K27me3 and DNA methylation [347]. Isocitrate dehydrogenases 1 and 2 (IDH1 and IDH2), the enzymes that catalyse the formation of α-KG from isocitrate within the TCA cycle, are frequently mutated in several types of cancer [348-350]. The mutant IDH enzyme produces 2-hydroxyglutarate from α-KG, which acts as an inhibitor of α-KG-dependent enzymes including the TETs and JMJDs. In addition, mutations in IDH2 have been shown to increase levels of H3K9me3 and H3K27me3 in the 3T3-L1 adipocyte cell line, specifically in the promoter regions of *Pparg* and *Cebpa* [351] (see Figure 1.3). This was associated with a decrease in capacity for *in vitro* adipogenesis.

Other TCA cycle metabolites that can influence epigenetic enzyme activity include NAD+, which is required for the activity of the NAD+-dependent histone deacetylases (sirtuins). Moreover, acetyl-CoA, a key metabolite in the TCA cycle, can serve as a donor for histone acetylation. It has been shown that changes in acetyl-CoA availability can control histone acetylase activity, with resulting modulation of differentiation of 3T3-L1 pre-adipocytes and embryonic stem cells [352, 353]. The interaction between TCA cycle metabolites and epigenetic factors are summarised in Figure 1.3.

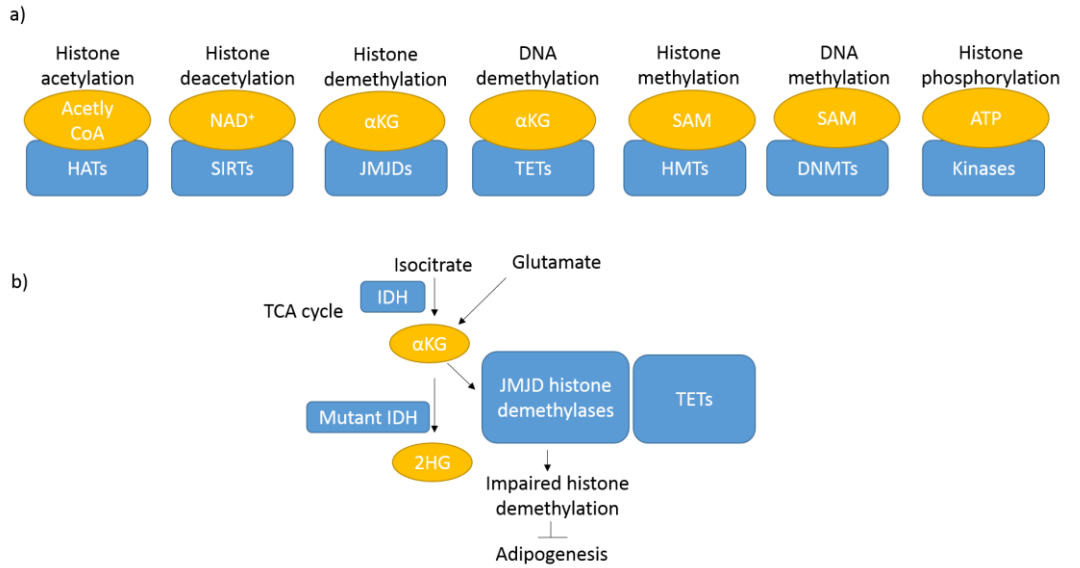


Figure 1.3. The role of metabolites in regulating epigenetic factors.

a) Metabolites of the tricarboxylic acid cycle can modulate a variety of epigenetic factors. Acetyl-CoA and S-adenosyl methionine (SAM) are donors for histone acetyltransferases (HATs) and histone and DNA methyltransferases (HMTs and DNMTs), respectively. NAD+ and ATP regulate sirtuin demethylases (SIRTs) and kinases, respectively. α-ketoglutarate (α-KG) is a cofactor of JMJD histone demethylases (JMJDs) and ten eleven translocase methylcytosine dioxygenases (TETs). b) The effects of altered metabolite availability on adipogenesis. Isocitrate dehydrogenase (IDH) catalyses isocitrate to produce α-KG in the tricarboxylic acid (TCA) cycle. However, mutations in the IDH gene lead to the production of 2-hydroxyglutarate (2HG) from α-KG, which in turn inhibits enzymatic activities of the α-KG-dependent histone and DNA demethylases, such as JMJD and TETs, thus inhibiting adipogenesis. Figure adapted from Inagaki et al. 2016 [354].

### 1.5.3. Metabolic changes in obese adipose tissue

A number of key metabolic changes are characteristic of adipose tissue in obesity. Hypertrophied adipocytes in obese adipose tissue display hyperlipolytic activity, generating excess free fatty acids and glycerol [355, 356]. In addition, the production and secretion of uric acid from adipose tissue is increased in obesity [357]. Cummins et al found that adipose tissue levels of succinate and malate in high fat-fed mice were increased compared to control-fed animals, and that metabolites that can enter the Krebs cycle *via* anaplerosis (e.g. glutamine) were mostly decreased in high-fat-fed mice, suggesting altered mitochondrial metabolism [358]. Another study using a genetically obese mouse model (*Ob/Ob*) [359] found that static levels of glutamate and many constitutive metabolites of the TCA cycle (such as α-ketoglutarate, succinate, fumarate, and malate) were all increased in WAT, but not in liver or skeletal muscle. Using *in vivo* metabolic turnover analyses, the same study suggested that these increases in glutamate and TCA cycle metabolites were due to the cataplerotic TCA cycle flux in obese adipose tissue.

### 1.5.4. Epigenetic changes in obesity

Metabolite modulation in obese adipose tissue, as described above, could therefore influence epigenetic modifiers (summarised in Figure 1.3). Indeed, it has been suggested that epigenetic changes could account for a portion of the heritable component of obesity [15].

For example, a study examining global histone methylation in obesity [360] demonstrated a 40% decrease in levels of histone H3K4me2 (H3 lysine 4 dimethylation) in adipocytes of overweight compared with lean individuals, and increased levels lysine 4 trimethylation was shown in adipocytes of obese and diabetic individuals.

A 2015 meta-analysis on studies published between 2008-2013 [361] found that of the 46 studies included, 15 studies investigated global DNA methylation in obesity, 13 investigated DNA methylation in specific candidate genes in obesity, 5 used genome-wide approaches, 8 investigated DNA methylation profiles in relation to weight loss interventions and 9 investigated relationships of DNA methylation at early life with either parental health measures or later life health outcomes. The majority of studies investigating global DNA methylation found no association between obesity measures and global DNA methylation [362-366], with a few exceptions: two studies on women found a negative correlation between global methylation and BMI [367, 368]. On the other hand, a further two studies including both male and female subjects reported a positive correlation between global methylation in peripheral blood leukocytes and BMI [369, 370]; and another study reported an increase in global DNA methylation in obese women compared to lean women [371]. This demonstrates the contradictory nature of the findings of the field: while some studies have discovered a correlation between global methylation and obesity, most found no correlation. In addition, both global CpG hypomethylation and global CpG hypermethylation have been associated.

Several studies have employed a candidate gene approach focusing on a range of genes involved in obesity, appetite regulation, metabolism, insulin signalling, immunity, circadian clock regulation, growth and imprinted genes. Decreased methylation has been reported in tumour necrosis factor alpha (*TNFα*) in peripheral blood leukocytes [372] pyruvate dehydrogenase kinase 4 (*PDK4*) in muscle [373] and leptin (*LEP*) in whole blood [374]. Increased methylation has been observed in proopiomelanocortin (*POMC*) in whole blood [375], PPARγ coactivator 1 alpha (*PGC1α*) in muscle [373], and *CLOCK* and aryl hydrocarbon receptor nuclear translocator-like (*BMAL1*) genes in peripheral blood leukocytes in obese compared to lean subjects [376]. In addition, methylation at the IGF2/H19 imprinting region in blood cells has been consistently associated with measures of adiposity [377, 378].

Genome-wide approaches have revealed small but abundant alterations in methylation at specific sites. Obesity-associated differentially methylated regions have been found in the genome in both obesity candidate genes [379] and in genes with a wide range of other functions, including immune response [380], cell differentiation [379] and transcriptional regulation [381].

## 1.6. Epigenetics and adipose tissue biology

### 1.6.1. TET1 in adipose tissue development

DNA methylation can affect the binding of many DNA-binding proteins to their target sequences [282]. Therefore, it is possible that 5hmC may also be involved in regulating protein-DNA interactions. A number of studies suggest that the TET enzymes play a crucial role in the development or function of adipose tissue, through interaction with the transcription factor peroxisome proliferator-activated receptor gamma (PPARγ). PPARγ is a nuclear receptor involved in adipocyte differentiation and activation of adipocyte-specific gene expression (such as *ADIPOQ*, *FABP4*, *ADSF* and *GLUT4*). PPARγ recruits TET enzymes in a process facilitated by the CCCTC-binding factor (CTCF) [382] and directs local demethylation around PPREs resulting in the transcription of adipocyte-specific genes [383]. Enrichment of 5hmC has been identified at over 20% of PPARγ binding sites, suggesting this modification is functionally important in gene regulation at these sites [384]. Moreover, double knockout (DKO) of *Tet1* and *Tet2* inhibited the adipogenic differentiation of mouse embryonic fibroblasts (MEFs) *in vitro*, with a marked reduction in the number of lipid droplets and reduced mRNA expression of the adipogenic marker genes *Pparγ*, *C/ebpα*, and *Igf1* [385]. The reduced adipogenesis in DKO MEFs was associated with pronounced hypermethylation of promoter regions of genes involved in adipogenesis (*Igf1* and *Pparg*) and adipocyte function (*Foxc1* and *Foxc2*) [385].

A recent study [386] found that 5hmC enrichment inhibits the binding of C/EBPβ (CCAAT/enhancer-binding protein beta) – a transcription factor expressed by committed pre-adipocytes – to target DNA sequences. C/EBPβ expression, together with C/EBPδ expression, initiates expression of C/EBPα and PPARγ, which in turn promote differentiation by activating adipose-specific gene expression [387]. PPARγ binds with C/EBP*α* to the promoter/enhancer of the gene encoding the adipocyte fatty acid binding protein aP2 (FABP4) [388, 389]. While 5hmC enrichment was found to inhibit C/EBPβ binding to DNA target sites, binding was increased by 5mC, 5fC and 5caC [386].

These data suggest that activation of adipogenic-specific genes requires TET-mediated maintenance of low methylation levels in the corresponding promoters.

### 1.6.2. Epigenetics in thermogenic activation of brown and beige adipose tissue

***Transcriptional control of BAT activation***

Thermogenic activation of BAT and beige adipose tissue at the molecular level relies heavily upon transcriptional regulation of the BAT and beige gene programmes, a set of key genes involved in crucial aspects of BAT function; including glucose and fatty acid uptake, UCP1 gene expression and uncoupled cellular respiration. Examples of these key genes include *UCP1*, *β3-AR*, *CPT1b*, *GLUT-1*, *GLUT-4*, and *ZFP516*. Also frequently included in the BAT and beige thermogenic gene programmes are the transcription factors involved in regulation of the above genes, such as *PGC1α*, *C/EBPβ*, *PPARα*, *PRDM16* and *EBF2*. The functions and interactions of these transcription factors are summarised in Figure 1.4.

As previously mentioned, PR-domain containing protein-16 (PRDM16) is a well-established key transcription factor in BAT and beige adipocytes. Expression of PRDM16, together with its co-regulator EHMT1, and the transcription factor EBF2, distinguishes the brown and beige adipocytes from their mesenchymal precursors [138, 390, 391]. Ectopic expression of PRDM16, together with its binding partners CCAAT/enhancer-binding protein-β (C/EBPβ) and PPARγ, is sufficient to convert nonadipogenic cells – including skin fibroblasts and myoblasts in both human and mouse – into brown adipose lineage [138, 392, 393]. When activated, PRDM16 acts as a coregulator for transcription factors PPARγ, PPARα, c/EBPβ, and Pgc1α to induce transcription of brown fat-specific genes [138, 392-394]. EBF2 interacts with PPARγ to directly regulate PRDM16 expression [395]. Loss of Ebf2 in mouse brown preadipocytes reduced expression levels of genes associated with the BAT gene programme, while ectopic Ebf2 expression in myoblasts induced a brown-like gene expression profile [395].

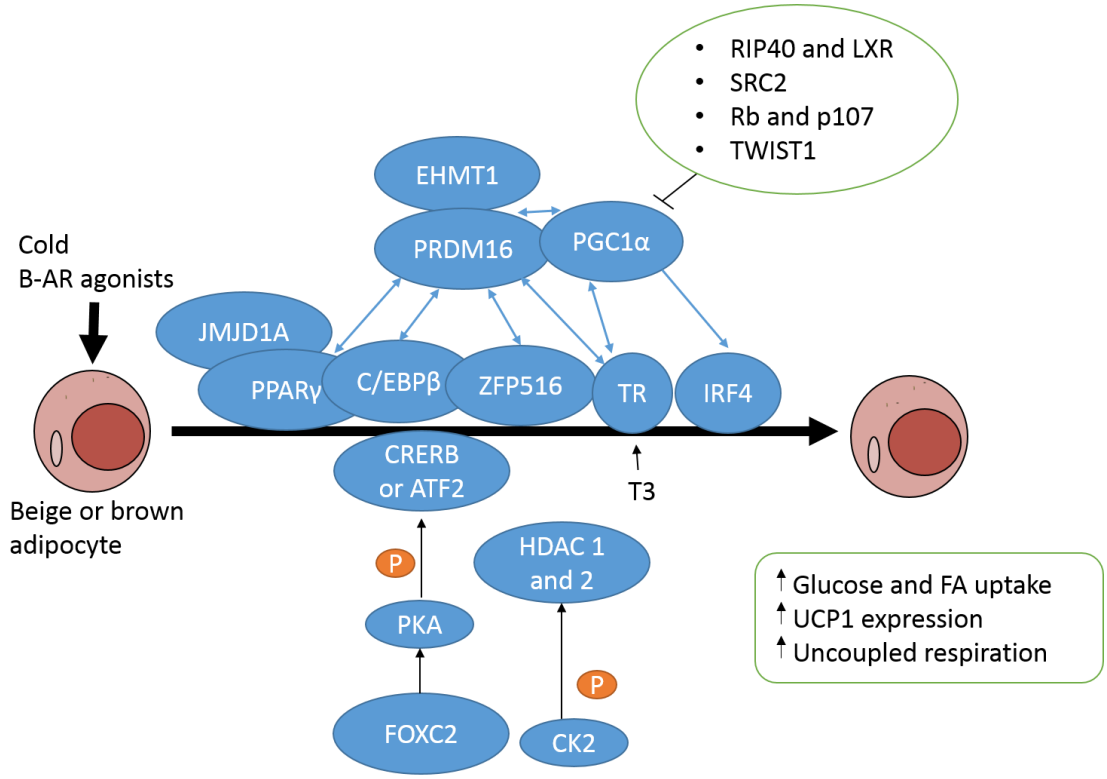


Figure 1.4. Transcription factors and coregulators responsible for the activation of brown and beige adipose tissue-specific gene programme.

Blue double-headed arrows indicate protein interaction and complex formation; black arrow-headed and bar-headed lines show stimulatory and inhibitory effects, respectively. Figure adapted from Inagaki et al. 2016 [354].

***Epigenetic control of BAT activation***

The dependence of BAT and beige adipose tissue on transcriptional activation of the thermogenic gene programme suggests that transcriptional regulation – including epigenetic control of transcription – is a major regulator of BAT and beige adipocyte function. Recent studies have revealed that a number of epigenetic modifications are required for the activation of BAT and beige thermogenic capacity.

*Histone modifications*

A 2014 paper demonstrated that PRDM16-dependent activation of the BAT gene program is dependent upon the binding of PRDM16 to MED1, a component of the mediator complex, which subsequently causes alterations in the chromatin architecture at key thermogenic genes. MED1 recruits PRDM16 to superenhancers of key BAT-selective genes [396]. Knockout of *Prdm16* in cultured brown adipocytes disrupted chromatin architecture at *Pgc1* and *Ppara*, and "superenhancer" activity of thermogenic genes [396] (superenhancers are large clusters of transcription factor binding sites that drive the expression of cell identity genes [397]). In particular, PRDM16-MED1-mediated

changes in the chromatin landscape of thermogenic genes changes the proximity of the enhancer region to the gene promoter [396, 398].

A 2017 study showed that histone deacetylase 3 (HDAC3) is required to activate brown adipose tissue [399]. BAT-specific *Hdac3* ablation in mice exposed to cold exposure were unable to regulate their body temperature and suffered severe hypothermia. *Ucp1* expression in these mice was nearly absent, and expression of mitochondrial oxidative phosphorylation genes was significantly decreased. The study gave a suggestion for the molecular basis for the dependence of BAT activation on HDAC3: although HDAC3 normally acts as a transcriptional corepressor, it is able to function as a coactivator of oestrogen-related receptor α (ERRα) in BAT. ERRα activation is required for the transcription of *Ucp1* and *Ppargc1a*, which is controlled by HDAC3-mediated deacetylation of the PGC-1α protein.

Just a month later, an independent group published that HDAC3 in WAT contributes to maintenance of WAT identity and acts as a "molecular brake" to prevent browning [400]. Adipose-specific knockout of *Hdac3* in mice induced *de novo* fatty acid synthesis and β-oxidation. This subsequently increased WAT oxidative capacity and browning. This was accompanied by increased histone acetylation – a mark of transcriptional activation – in the enhancer regions of *Pparg* and *Ucp1* and the putative regulatory regions of *Ppara*. In addition, HDAC1 was shown to inhibit thermogenesis through deacetylation of histone 3 lysine 27 (H3K27) on the regulatory regions of *Ucp1*. This was associated with a reduction in Atf2-mediated transcription of *Ucp1* [401].

In addition, an epigenome profiling study in 2016 tracking the differentiation of a mesenchymal stem cell line into brown adipocytes found that the presence of two histone markers were indicators for brown preadipocytes: H3K4me1 and H3K27me3 [402]. However, the removal of H3K27me3 was required for cells to progress through the late stage of brown adipogenesis. H3K4me1, on the other hand, was found to remain present in the late stage of brown adipogenesis, indicating its involvement in poising the thermogenic genes for transcriptional activation [402].

Further enzymes that have been shown to be involved in transcriptional activation of thermogenic genes include the Jumonji C (JmjC)-domain-containing demethylases (JMJD). In particular, JMJD1A has been implicated [403]. The phosphorylated form of the protein forms a complex with the SWItch/Sucrose Non-Fermentable (SWI/SNF) chromatin remodeller, which together is recruited to the PPAR response elements of key thermogenic genes, including *Ucp1* and *Adrb1* (β3-adrenoreceptor), where it demethylates H3K9me2. Histone demethylation at this site reduces the distance between transcription factor-bound enhancers and the thermogenic gene promoters [403]. The study found that these changes occurred within minutes, peaking just 60 minutes after the initial protein phosphorylation occurred [403]. The stability of histone markers provides a mechanism by

which such epigenetic changes may provide a form of "epigenetic memory", which can activate thermogenic gene expression faster in response to future exposure to the cold [403].

Furthermore, Lysine-specific histone methylase 1 (LSD1) is required for transcriptional activation of the thermogenic gene programme [404]. Mice with a BAT-specific inactive *Lsd1* mutation – but not a knockout of *Lsd1* – had BAT that was histologically more similar to WAT (with an increase in adipocyte size and number of unilocular lipid droplets), an increase in expression of WAT-selective genes (such as *Bmp4*, *Egfr*, *Pdk3* and *Apoe*) and a decrease in expression of BAT-selective genes (such as *Ucp1*, *Slc27a2*, *Cox8b* and *Prdm16*). The fact that the enzymatic capacity of the protein was inactivated demonstrates that the specific histone demethylase activity of LSD1 is required for BAT gene expression.

Recently, Shapira et al. [405] demonstrated that the EBF2-mediated transcriptional activation in BAT is in part controlled by the histone reader Double PHD Fingers 3 (DPF3). EBF2 was shown to physically interact with the chromatin remodeller BRG1 and the BAF chromatin remodelling complex in brown adipocytes to regulate BAT identity and function [405]. A key regulatory component of the BAF complex is DPF3, a histone reader protein capable of binding methylated and acetylated lysine residues on histones 3 and 4. *In vitro* knockdown of *Dpf3* by 80% revealed that *Dpf3* expression was specifically required for both basal brown fat gene expression and function, and for β-adrenergic-stimulated upregulation of the thermogenic gene programme [405]. This suggested that the histone-modifying properties of Dpf3 are involved in transcriptional activation of the thermogenic gene programme.

*DNA methylation and hydroxymethylation*

Despite the known importance of transcriptional regulation in BAT activation, as of yet there is no published data on the methylation states of CpGs in key BAT genes and their influence on gene expression. The dependence of the TET enzymes on the availability of key TCA cycle metabolites [346] provides further justification for investigating the role of DNA methylation states in BAT and beige activation.

***Metabolite changes in BAT activation***

As discussed previously, the activity of many epigenetic modulators is dependent upon the presence of various metabolites. Given the known role of JMJD activity in BAT thermogenic gene expression [403], it is plausible that α-KG availability is central to modulating the activity of these enzymes in activation of BAT gene expression. It is therefore not too large a leap to hypothesise that the TET enzymes may be similarly modulated in response to α-KG changes in BAT activation.

Data from our collaborators demonstrate that in humans exposed to mild cold exposure (18°C), there is a decrease in glutamate concentrations in the interstitial fluid within the supraclavicular brown adipose tissue [82]. This indicates an increased uptake of glutamate into the BAT, suggesting an increased rate of glutamate oxidation and uptake into the TCA cycle.

Glutamate is a precursor to α-KG, and is converted to α-KG by the enzyme glutamate dehydrogenase (GDH). Therefore, increased utilisation of glutamate in activated BAT may modulate α-KG levels, and could subsequently influence the activity of the α-ketoglutarate dependent dioxygenases. This is further evidence that BAT activation could influence TET activity and consequently alter CpG methylation states, which may be a key factor in the transcriptional activation of the thermogenic gene programme.

## 1.7. Preliminary studies

Recent studies in our lab, using a colony of *Tet1* KO mice [328], show that male *Tet1* KO mice have an obesity-resistant phenotype when maintained on a high fat diet (HFD), with reduced weight gain and the maintenance of insulin sensitivity (Lyall et al, unpublished). These studies were aimed at establishing genome-wide differences in hepatic gene expression and 5hmC profiles in *Tet1* KO compared to littermate wildtype (WT) animals. However, the metabolic phenotype of the *Tet1* KO mouse has not been further characterised, and the mechanisms accounting for the differences in weight gain are still unclear. My project aims to use the *Tet1* KO mouse as a model in which to understand the effects of epigenetic dysregulation on obesity and metabolism, and investigate the mechanisms behind the differences in weight gain, focusing specifically on the adipose tissue phenotype.

## 1.8. Hypotheses & aims

### 1.8.1. Hypotheses:

1. *Tet1* KO causes alterations in the adipose tissue hydroxymethylome and transcriptome, which lead to decreased adiposity.
    - Global deletion of *Tet1* results in decreased 5hmC in adipose tissue DNA and subsequent transcriptional effects.
    - Global deletion of *Tet1* results in reduced capacity for adipogenesis due to transcriptional effects mediated by the PPAR family of transcription factors.
2. Reduced food intake in the *Tet1* KO mouse is sufficient to account for the reduced weight gain.

- *Tet1* KO mice have reduced transcription of *Lep* mRNA across all adipose tissue depots, and a corresponding reduction in plasma leptin.
- KO mice have significantly reduced food intake over the 11-week HFD.
- Decreased *Lep* transcription and serum leptin protein levels in KO mice allow KOs to retain leptin sensitivity, while WT mice become leptin resistant on HFD.
- Decreased *Lep* transcription is the result of *Tet*1-mediated changes in 5mC and/or 5hmC levels.

**3.** The reduced adiposity of *Tet1* KO mice on HFD also manifests in reduced MAT.

- The amount of MAT in the bone marrow cavity of *Tet1* KO mice is reduced when compared to their wildtype littermates.
- The change in MAT is associated with changes in bone mineral density and bone structure.

**4.** Cold exposure induces changes in hydroxymethylation levels as a result of altered levels of metabolites.

- Increased glutamate uptake into the brown adipose tissue, as previously observed in humans [82], also occurs in mouse brown and beige adipose tissue when animals are exposed to a temperature of 4°C, but not in white (non-browning) adipose tissue.
- This causes an increase in the levels of α-ketoglutarate in mouse brown and beige adipose tissue, but not in white (non-browning) adipose tissue.
- Changes observed in glutamate and α-ketoglutarate levels in mouse brown and beige adipose tissue modulate TET activity.
- Changes in TET activity as a result of cold-induced brown and beige adipose tissue activation cause global changes in CpG hydroxymethylation, particularly in genes key to thermogenic activation.
- Changes in the hydroxymethylome are associated with modulation of gene expression in brown and beige adipose tissue.

### 1.8.2. Aims:

**1.** To further characterise the metabolic phenotype of *Tet1* KO mice *in vivo*.

- Investigate the energy expenditure, respiratory exchange ratio and activity levels of the *Tet1* KO mouse.
- Characterise the adipose tissue hydroxymethylome and transcriptome of *Tet1* KO mice.
- Characterise the effect of *Tet1* depletion on adipocyte differentiation and function *in vitro.*

**2.** To investigate physiological control of food intake in the *Tet1* KO mouse

- Investigate *Lep* mRNA levels across a range of WT and KO mouse adipose tissue depots.
- Investigate serum leptin protein levels in the WT and KO mice.
- Investigate the food intake phenotype of the *Tet1* KO and WT mice through weekly food intake tracking.
- If a difference in food intake is observed over the 11-week HFD, carry out paired feeding studies to determine whether the difference in food intake is accountable for the difference in weight gain.
- Investigate the leptin sensitivity of the WT and KO mice.
- Investigate the role of CpG methylation and hydroxymethylation in *Lep* transcription by interrogating existing hMeDIP-seq data from WT and KO mouse mesenteric adipose tissue, and through bisulfite conversion pyrosequencing to obtain methylation data at a higher resolution (base-pair resolution).
- Investigate whether knocking down *Tet1 in vitro* drives the same changes observed in the *Tet1* KO *in vivo.*

**3.** To investigate any changes in the levels of MAT in high fat-fed *Tet1* KO mice.

- Quantify the volume of bone marrow cavity occupied by MAT in high fat-fed *Tet1* KO mice.
- Investigate the bone structure and bone mineral density phenotype of *Tet1* KO mice challenged with a HFD.

**4.** To interrogate the role of *Tet1* in the activation of cold-induced thermogenesis in brown, white and beige adipose tissue

- Confirm, using indirect calorimetry, that cold-induced BAT and beige upregulation occurs in the animals exposed to a temperature of 4°C.
- Investigate changes in glutamate levels, α-ketoglutarate levels and TET activity in the brown, beige and white adipose tissue of mice exposed to cold (4°C), room temperature (21°C) and thermoneutrality (30°C) for 48 hours.
- Investigate changes in DNA hydroxymethylation and associated alterations in gene expression in the brown, beige and white adipose tissue of mice exposed to cold (4°C), room temperature (21°C) and thermoneutrality (30°C) for 48 hours.

# 2. Methods

## 2.1. Buffers and solutions

**Alkaline Lysis Reagent**: 25mM NaOH, 0.2mM disodium EDTA, pH 12.0 was prepared by dissolving the salts in water prior to adjusting the pH.

**Tris-HCl 40mM pH8.0**: Prepared by dissolving Tris-HCl in water, prior to adjusting the pH to 8.0.

**TBE buffer (10X)**: 1M Tris base, 1M boric acid and 0.02M EDTA was prepared in distilled water. 100mL was diluted in 1L distilled water to make 1X solution.

**Krebs phosphate buffer**: 118mM NaCl, 5mM KCl, and 1.2mM $MgSO_4$ was prepared in 800mL distilled water. 120mls of 100mM $Na_2HPO_4$ was added, and pH 7.4 was achieved by dropwise addition of 100mM $NaH_2PO_4$. Volume was adjusted to 1L with distilled water.

**Full Krebs buffer**: Full Krebs buffer was prepared on the day of use by adding the following to Krebs phosphate buffer: $CaCl_2$ to a final concentration of 1.265mM, glucose to a final concentration 1mg/ml, and bovine serum albumin to a final concentration of 1%.

**Sorenson's buffer**: 0.133M $Na_2HPO_4$ and 0.133M $KH_2PO_4$ was prepared in 1L distilled water.

**TE (Tris-EDTA) buffer**: 10mM Tris-Cl and 1mM EDTA was prepared in 1L distilled water, with a pH of 7.4.

**DNA immunoprecipitation buffer**: 100mM Na-Phosphate pH 7.0 (mono and dibasic), 1.4 M NaCl, and 0.5 % Triton X-100 were prepared in 10mL in distilled water and 0.22µm sterile filtered.

**Proteinase K digestion buffer**: 50mM Tris-HCl pH 8.0, 10mM EDTA, 0.5% SDS were prepared in 10mL prior to each procedure in distilled $H_20$ and 0.22µm sterile filtered.

## 2.2. Animal maintenance and *in vivo* experiments

### 2.2.1. *Tet1* global knock out mouse breeding

B6;129S4-*Tet1*tm1.1Jae/J heterozygote mice (4 pairs) were purchased from Jackson Laboratories, Maine, US. Heterozygote mice were interbred to generate homozygous knockout and wildtype progeny. The breeding population was maintained as heterozygous *Tet1*$^{+/-}$.

### 2.2.2. Genotyping of *Tet1* knockout offspring

Mouse genotype was determined by PCR for exon 4, the absent region in the knockout allele. Mouse DNA was prepared using a "HotSHOT" genomic DNA preparation method (first published by Truett et al. [406]). Ear clip biopsies were heated to 95ºC in 75µL Alkaline Lysis Reagent for 30 minutes. When cooled to 4°C, 75µL Tris-HCl 40mM pH 8.0 was added.

2µL of this prepared DNA was added to 6µL Maxima Hot Start Green PCR Master Mix (Thermo Fisher Scientific, London UK); 0.06µL wildtype forward primer (100µM); 0.06µL mutant forward primer (100µM); 0.06µL common reverse primer (100µM); 3.82µL nuclease-free $H_2O$. Primer sequences are shown in Table 2.1. Primer sequences for *Tet1* genotyping PCR Thermal cycler steps are shown in Table 2.2. Products were run on a 3% agarose gel at 70V for 1.5 hours in TBE buffer. Mutant bands were determined to be 681bp and wildtype bands 300bp.

| **Primer name** | **Primer sequence (5'→3')** |
|---|---|
| Wildtype forward | TCA GGG AGC TCA TGG AGA CTA |
| Mutant forward | AAC TGA TTC CCT TCG TGC AG |
| Common reverse | TTA AAG CAT GGG TGG GAG TC |

Table 2.1. Primer sequences for *Tet1* genotyping PCR.

| **Step no.** | **Duration of cycle (hh:mm:ss)** | **Temperature ($^0$C)** | |
|---|---|---|---|
| 1 | 00:02:00 | 94 | |
| 2 | 00:00:20 | 94 | |
| 3 | 00:00:15 | 65 | |
| 4 | 00:00:10 | 68 | |
| 5 | - | - | Repeat steps 2-4 for 10 cycles |
| 6 | 00:00:15 | 94 | |
| 7 | 00:00:15 | 60 | |
| 8 | 00:00:10 | 72 | |
| 9 | - | - | Repeat steps 6-8 for 28 cycles |
| 10 | 00:02:00 | 72 | |
| 11 | ∞ | 10 | |

Table 2.2. Thermal cycler conditions for *Tet1* genotyping PCR protocol.

### 2.2.3. Animal husbandry and diets

All experiments were carried out under UK home office licence. All animal experiments were reviewed by the University of Edinburgh Animal Welfare and Ethics Review Board prior to their initiation. C57BL/6J mice (Charles River, Tranent, UK) or B6;129S4-*Tet1*tm1.1Jae/J mice (Jackson Laboratories, Maine, USA) were maintained under conditions of controlled lighting (lights on 7:00 am to 7:00 pm) and temperature (22°C ± 2ºC). Between 12-23 weeks of age, male *Tet1*$^{-/-}$ (KO) mice and littermate *Tet1*$^{+/+}$ (WT) controls were given free access to high fat diet (HFD) chow (58% fat by

caloric basis) (formula D12331; Research Diets Inc., USA) for 11 weeks to induce obesity, or control diet (formula D12328; Research Diets Inc., USA). Diet was obtained from Research Diets, New Brunswick, NJ, USA. Composition of the diet is shown in Table 2.3. Mouse body weight and food intake was measured weekly.

| | **High fat diet D12331** | **Control diet D12328** |
|---|---|---|
| Kcal/gram | 5.56 | 4.07 |
| Kcal%<br>Protein<br>Carbohydrate<br>Fat | <br>16.4<br>25.5<br>58.0 | <br>16.4<br>73.1<br>4.8 |
| Sucrose (g/kg) | 175 | 0 |
| Maltodextrin 10 (g/kg) | 170 | 170 |
| Coconut oil, Hydrogenated (g/kg) | 333.5 | 40 |
| Soyabean oil (g/kg) | 25 | 25 |

Table 2.3. Composition of rodent diets.

### 2.2.4. Paired feeding protocol

The paired feeding study was carried out for 11 weeks to assess the impact of food intake on weight gain in WT and *Tet1* KO mice. KO mice were given *ad lib* access to HFD and food intake was measured daily (weighed to the nearest 10mg). Cages were also checked daily to ensure there was no shredded diet on the floor of the cage or under bedding. Littermate WT food allowance was then paired to the mean KO food intake for the previous day. Body weights of WT and KO mice were measured weekly.

At the start of the study, food intake was not normalised to body weight: WT mice were given exactly the same amount of food as KO. However, by week 3 of the paired feeding study it became apparent that the WT mice were not gaining weight, and were in fact losing weight. After a re-analysis of starting body weight it became apparent that, in this particular cohort of WT and KO mice, the KO mice had a significantly lower starting body weight than the KO mice, and pairing WT food intake exactly to KO food intake resulted in weight loss. Therefore, from week 3 onwards, I began normalising food intake to total body weight for each individual animal.

### 2.2.5. Indirect calorimetry

Indirect calorimetry was carried out to analyse the source of respiration substrate. This can be determined using oxygen input and carbon dioxide output of the animals. Animals were kept in Metabolic PhenoCages under the TSE PhenoMaster system (TSE Systems, Germany). In the PhenoCages, animals were given bedding, access to food and water hoppers that were attached to weight sensors, and a dark tube also attached to weight sensors allowing intermittent measurement of body weight. The cages are also equipped with the ActiMot2 system (TSE systems), allowing measurement of locomotor activity using infrared light beams. The cages are fully sealed, allowing quantification of oxygen and carbon dioxide flow. Measurements for all parameters were taken at 15-minute intervals throughout the experiment.

Before entering the Metabolic PhenoCages, animals were trained on the TSE drinking water bottles for 7 days to adjust to the different nozzle. Also before the 24-hour measurement period, a 48-hour acclimatisation period was allowed so that animals were adjusted to the new environment.

Respiratory exchange ratio (RER) was calculated within the TSE PhenoMaster software. RER can be used as a measure of respiratory substrate. E.g. an RER of 0.7 indicates a greater proportion of fatty acid oxidation, while an RER of closer to 1.0 indicates mostly carbohydrate metabolism. For a more detailed explanation, see the calculation below:

**Oxidation of one carbohydrate molecule:**

$6\ O_2 + C_6H_{12}O_6 \Rightarrow 6\ CO_2 + 6\ H_2O + 38\ ATP$

Therefore: $RER = VCO_2/VO_2 = 6\ CO_2/6\ O_2 = 1.0$

**Oxidation of one fatty acid molecule:**

$23\ O_2 + C_{16}H_{32}O_2 \Rightarrow 16\ CO_2 + 16\ H_2O + 129\ ATP$

Therefore: $RER = VCO_2/VO_2 = 16\ CO_2/23\ O_2 = 0.7$

Energy expenditure (EE) is also be calculated within the TSE PhenoMaster software, using $VCO_2$ and $VO_2$, using an adapted Weir formula [407]. This value is then normalized to lean mass.

$EE = [3.941*(VO_2) + 1.1068\ (VCO_2)] *1.44$

***High fat diet indirect calorimetry***

All parameters were measured for two 24-hour periods at room temperature: once before starting the high fat diet, and once after 7 weeks of high fat diet.

***Cold exposure indirect calorimetry***

Light was set to 80% between the hours of 7am and 7pm; humidity was set to a constant of 40%; and temperature was also set to a constant (either 4°C, 21°C or 30°C). Measurements were taken for a single 24-hour period during which time the desired temperature was stable.

### 2.2.6. Venesection

1mm of tail was snipped off at the distal end with fine scissors. Animals were allowed to move freely on the top of the cage and blood encouraged from the wound. Blood was either collected into an EDTA tube (Microvette® CB 300 K2E; Sarstedt, Numbrecht, Germany) by capillary action, or applied directly to glucometer strip (Accu-check, Roche, Burgess Hill UK). Tubes were spun at 10,062 x *g* for 10 minutes at 4ºC. The supernatant was removed and stored at -80°.

### 2.2.7. Glucose tolerance testing

After 10 weeks maintained on high fat diet, glucose tolerance tests were performed on mice. Mice were fasted for 6 hours prior to insulin tolerance test. Mice were given an intraperitoneal injection of D-(+)-Glucose (Sigma-Aldrich G8270, Dorset, UK) at a concentration of 2g/kg body weight, diluted in 0.9% saline solution. Blood glucose measurements were made at baseline, 15, 30, 60 and 90 minute time points.

### 2.2.8. Leptin treatment

Leptin treatment was carried out before and after 6 week *ad lib* HFD. Before *ad lib* HFD, WT and KO animals were treated intravenously (tail vein) with 0.9% physiological saline (Thermo Fisher, Hampshire, UK) or 3mg/kg leptin (Sigma-Aldrich, Dorset, UK). Animals were held in mouse restrainers during treatment to ensure safe delivery of the injection. Both treatments were given to each animal, i.e. each animal served as its own saline control in order to provide paired analysis, with 4 days recovery between treatments (with saline treatment being carried out prior to leptin treatment). Injections were carried out at 9am and food intake was then measured every hour for 12 hours following treatment (9am to 9pm). This process was repeated after animals were given *ad lib* access to HFD for 6 weeks.

### 2.2.9. Carbon dioxide asphyxiation

Mice were killed to obtain tissue by exposure to carbon dioxide gas in a rising concentration in a sealed box, followed by confirmation by cervical dislocation.

### 2.2.10. Tissue harvesting

All mice were fasted overnight prior to culling and culled between 0800 and 1030 hours, to achieve consistency. Tissue was dissected immediately after culling, in order to preserve RNA integrity. Blood was collected by cardiac puncture. Liver, adipose depots (mesenteric, retroperitoneal, subcutaneous, epididymal and brown adipose) and bones (lumbar vertebrae, caudal vertebrae, femur and tibia) were dissected. All tissue was weighed, snap frozen on dry ice and stored at -80°C. Sections of epididymal adipose tissue and brown adipose tissue were fixed in 10% neutral-buffered formalin solution for 48 hours, and bones were also fixed in 10% neutral-buffered formalin solution for 24 hours. In the case of adipose tissue being taken for tissue culture, adipose depots were dissected and placed immediately into full Krebs phosphate buffer at 37ºC.

## 2.3. Bone phenotyping and bone marrow adipose tissue quantification

### 2.3.1. X-ray

After bones were fixed in 10% neutral-buffered formalin solution for 24 hours, they were X-rayed using a Faxitron (Biooptics, Arizona, USA). The exposure was set to 15 seconds at 22kV. X-ray images were analysed using ImageJ (NIH, USA), employing the measurement tool and the threshold tool.

### 2.3.2. Decalcification

Bones were washed 3 times for 10 minutes in distilled water on a shaker at room temperature, to remove traces of formalin. They then underwent decalcification in 14% EDTA solution on a shaker at 4ºC for 2 weeks. The EDTA solution was replaced every 3-4 days. After 2 weeks of decalcification, the EDTA solution was aspirated and replaced with PBS (Gibco, UK). At this stage, vertebrae were embedded in paraffin for histology, while the tibiae were stained using osmium tetroxide (Agar Scientific, UK).

### 2.3.3. Osmium tetroxide staining of bone marrow adipose tissue

Femurs and tibiae were immersed in a 1% osmium tetroxide (Agar Scientific, UK) solution for 24 hours. Osmium tetroxide reacts with alkene bonds within unsaturated fatty acids, resulting in covalent incorporation of the osmium atom and allowing visualisation of adipose tissue within the bone marrow. After 24 hours staining, bones were washed three times in Sorenson's buffer (two hours per wash).

### 2.3.4. X-ray microtomography

Osmium-stained tibiae were embedded in 1% agarose in 7mL Bijou tubes of 22.5mm diameter. The Bijou tubes were placed in the SkyScanner 1172 µCT system (Bruker, MA, USA) and scanned using the following settings: source voltage 54kV, source current 185µA, exposure time 885ms.

### 2.3.5. X-ray microtomography analysis

Trabecular and cortical bone volume, bone surface area, and bone surface to volume ratio were quantified using CTan analysis software, ver. 1.13 (Bruker, MA, USA). Cortical bone was analysed in 650 x 100µm sections, starting from the growth plate down. Trabecular bone was analysed in 225 x 100µm sections, starting from the growth plate down. Marrow adipose tissue volume (post decalcification and osmium staining) was quantified using the same software. MAT quantification was divided into three regions of the marrow cavity: 100 x 100µm sections from the growth plate (proximal); from there to the tibia-fibula junction (medial); and from the tibia-fibula junction to the end of the marrow cavity (distal).

## 2.4. Adipose tissue fractionation and culture

### 2.4.1. Plastic Culture Materials

The stromal vascular fraction (SVF) of adipose tissue was cultured and differentiated on collagen-coated plates (Corning, Chester, UK) in a 12-well format.

### 2.4.2. SVF culture media

All chemicals were purchased from Sigma-Aldrich, Dorset, UK, unless otherwise stated.
Initial SVF isolation was carried out in Full Krebs solution, consisting of 118mM NaCl; 5mM KCl; 1.2mM $MgSO_4$; adjusted to pH 7.4 with phosphate buffers using anhydrous solids $Na_2HPO_4$ and $NaH_2PO_4$; and made up to Full Krebs Buffer on the day of use with 1.265mM $CaCl_2$; 1mg/mL Glucose; and 1% w/v Bovine Serum Albumin.

Once isolated, the SVF was cultured in SVF Maintenance Media, consisting of DMEM/F-12 Hams (4.5g/L Glucose) (Thermo Fisher Scientific, Paisley, UK); 10% newborn calf serum (Thermo Fisher Scientific, Paisley, UK); 2mM Glutamine (Thermo Fisher Scientific, Paisley, UK); 100 units/mL Penicillin (Thermo Fisher Scientific, Paisley, UK); 100µg/mL Streptomycin (Thermo Fisher Scientific, Paisley, UK).

On initiation of adipocyte differentiation, culture media was changed to Differentiation Media, consisting of normal SVF Maintenance Media with 1nM triiodothyronine (VWR International Ltd, Birmingham, UK).

In all procedures, all media and solutions used in cell culture were pre-incubated at 37ºC.

### 2.4.3. Adipose tissue fractionation

Epididymal adipose tissue and brown adipose tissue was dissected and immediately collected in 8mL Full Krebs Buffer. The collected adipose tissue was washed twice in Dulbecco's Phosphate Buffered Saline (Thermo Fisher Scientific, Paisley, UK), then transferred to Full Kreb's Buffer with 2mg/mL collagenase (Worthington Biochemical Coorporation, New Jersey, USA). The tissue was finely cut into small pieces 1-3mm diameter, and incubated in a shaking water bath for 15 minutes at 37ºC. The digest was stopped by removing it from the incubator to room temperature and adding 10mL Full Krebs Buffer.

The digest was centrifuged at 1,500 x *g* for 15 minutes at room temperature and the pellet was resuspended in 5mL Krebs Buffer, before being strained through a plastic mesh (100µm aperture) to remove remaining adipocytes or undigested tissue. Cells were centrifuged again at 1,200 x *g* for 5 minutes at room temperature. The supernatant was removed and the pellet resuspended in 3mL Maintenance Media. The cells were counted using a haemocytometer, before being plated into a 6-well plate at a density of ~500+ cells/$mm^2$.

### 2.4.4. SVF culture

The SVF isolate was maintained in an incubator at 37°C / 5% $CO_2$ / 95% relative humidity until they reached 100% confluence. Maintenance Media was replaced every 2-3 days.

### 2.4.5. Adipocyte differentiation

Two days after 100% confluence was reached, the Maintenance Media was substituted for Differentiation Media, and the following factors were supplemented to the media to induce adipocyte differentiation: 1µM Rosiglitazone (Tocris Bioscience, Bristol, UK); 250µM IBMX (Cambridge Bioscience, Cambridge, UK); 33µM Biotin (Sigma-Aldrich, UK); 17µM Pantothenic acid (Sigma-Aldrich, Dorset, UK); 200pM T3; 10µg/ml Apo-Transferrin (Sigma-Aldrich, Dorset, UK); 5µg/ml Insulin (Novo Nordisk, West Sussex, UK); 100nM Dexamethasone (Sigma-Aldrich, Dorset, UK). After 2 days, Rosiglitazone and IBMX supplementation was ceased. Two weeks were allowed for cells to develop into mature adipocytes.

### 2.4.6. Oil Red O stain

After two weeks of culture in Differentiation Media, the media was removed from one well per animal, and replaced with 2mL 10% formalin. Cells were incubated in formalin at room temperature

for 5 minutes. Formalin was gently removed using a P1000 pipette, and replaced with another 2mL 10% formalin. Cells were incubated in formalin at room temperature for another 1 hour. After 1 hour, formalin was removed and washed out with isopropanol. The isopropanol was removed and cells were allowed to air-dry. Cells were then incubated with 1mL 3.5% Oil Red O solution (Sigma-Aldrich, Dorset, UK) for 10 minutes, before the solution was aspirated. Oil Red O binds to lipids within the adipocytes, allowing visualisation and quantification of lipid. A blank well was also stained for a background reading. Wells were then washed three times with $dH_2O$, and imaged using the Axiovert 200 (Zeiss, Birmingham, UK). 1mL isopropanol was then added to each well to elute the Oil Red O. 200µL of the eluted Oil Red O stain was plated into one well of a microplate, and light emission was read at 500nm using a spectrophotometric OptiMax Tunable Microplate Reader (Molecular Devices, CA, USA).

In parallel to Oil Red O staining, RNA was extracted from cells. Cells were washed and agitated in 1mL of Qiazol (Qiagen, Manchester, UK), and RNA was subsequently extracted according to the protocol of RNeasy mini lipid kit (Qiagen, Manchester, UK), followed by reverse transcription-PCR (see below for further details). The resulting cDNA was used in qPCR for positive and negative markers of adipocyte differentiation and candidate genes of interest.

### 2.4.7. siRNA transfection

In vitro *Tet1* knockdown was carried out in primary preadipocytes isolated from inguinal adipose tissue of wildtype C57BL/6J mice, cultured on collagen I-coated plates (Corning, Deeside, UK) for up to 3 passages, following a previously published protocol [408]. In the evening before the transfection, confluent preadipocytes in 12-well collagen I-coated plates were trypsinzed and seeded 1:1. The following afternoon (allowing enough time for the preadipocytes to adhere to the bottom of the well), cells were transfected with siRNA using HiPerFect reagent (Qiagen, Manchester, UK). For one well of a 12-well plate, 40nM siRNA was mixed with 6 µl HiPerFect reagent in a total of 200µl serum free α-MEM (without antibiotics) and incubated for 15 min at room temperature. During the incubation, 200µl growth media (α-MEM with 10% FBS without antibiotics) was added to each well. The plate was swirled intermittently during the incubation to prevent cells from drying out. The pre-incubated siRNA-HiPerFect mix was added dropwise to the wells, resulting in total 400µl of α-MEM with 5% FBS. After gently rocking the plate, it was transferred to cell culture incubator. After overnight transfection, cells were re-fed with regular growth media and differentiation was initiated. Cells were differentiated using the protocol above (section 2.4.5) for 5 days, after which RNA was extracted.

## 2.5. Molecular biology

### 2.5.1. RNA extraction

Adipose RNA was extracted from tissue and purified using the RNeasy Lipid Tissue Mini Kit (Qiagen, Manchester, UK) with Qiazol (Qiagen, Manchester, UK), according to the manufacturer's instructions in the 'RNeasy Lipid Tissue Handbook'. Tissue was cut into small pieces 17-25mg and placed in a 2mL microcentrifuge. Tubes were placed at room temperature, and 1mL QIAzol Lysis Reagent was added. Tissue was homogenised using the TissueRuptor (Qiagen, Manchester, UK). Samples were then incubated at room temperature for 5 minutes, before 200µL chloroform (Sigma Aldrich, Dorset, UK) was added to each sample, and samples were incubated for 2-3 minutes at room temperature. Samples were then centrifuged at 10,000 x *g* for 15 minutes at 4ºC. The upper, aqueous phase was transferred to a new tube, and an equal volume of 70% ethanol (Fisher Scientific, Loughborough, UK) added. Samples were vortexed and transferred to an RNeasy Mini spin column, which was then centrifuged at 7000 x *g* for 15 seconds. 700µL Buffer RW1 was added, and then tubes were centrifuged at 7000 x *g* for 15 seconds. Samples were washed twice with Buffer RPE, before RNA was eluted in 40µL RNase-free water. Once extracted, RNA was handled on ice and stored at -80ºC.

### 2.5.2. RNA quantification and integrity

RNA was quantified with the Qubit 2.0 Fluorometer (Invitrogen, Paisley, UK) using DNA "broad range" standards as per manufacturer's instructions for DNA samples. DNA integrity was determined by resolving extraction products on a 1.5% agarose gel and staining with gel red (Cambridge Bioscience, Cambridge, UK) 0.005% final concentration.

### 2.5.3. Reverse transcription (RT)

RT was carried out using the High-Capacity cDNA Reverse Transcription Kit (Thermo Fisher, UK) according to kit protocol. 800ng RNA was used per reaction. Reaction components are shown in Table 2.4. Tubes were sealed and briefly centrifuged, and then placed in the thermal cycler under the conditions shown in Table 2.5.

| **Component** | **Volume (µL)** |
|---|---|
| 10× RT Buffer | 2.0 |
| 25× dNTP Mix (100 mM) | 0.8 |
| 10× RT Random Primers | 2.0 |
| MultiScribe™ Reverse Transcriptase | 1.0 |
| Nuclease-free $H_20$ | 4.2 |

Table 2.4. RT-PCR reaction components.

| **Temperature (°C)** | **Time (minutes)** |
|---|---|
| 25 | 10 |
| 37 | 120 |
| 85 | 5 |
| 4 | ∞ |

Table 2.5. Thermal cycler conditions for RT-PCR.

### 2.5.4. Reverse transcriction-quantitative polymerase chain reaction (RT-qPCR)

2µl of the reverse-transcribed cDNA was used in the reaction mixture shown in Table 2.6. A list of all primer sequences used for RT-qPCR analysis of gene expression is shown in Table 2.7. A water and non-reverse transcriptase control were used routinely. All assays were carried out in triplicate. Once the mixture had been pipetted into a 384-well PCR plate (Thermo Fisher, West Sussex, UK), the plate was centrifuged for 2 minutes at 563 x *g* to ensure all liquid was mixed at the bottom of the well. The plate was inserted into the LightCycler® 480 Instrument (Roche, West Sussex, UK), and run on the program shown in Table 2.8.

The LC480 Software (Roche, West Sussex, UK) measured fluorescence throughout the experiment and plotted fluorescence against PCR cycle number. The crossing point (Cp) was calculated as the maximum point of the second derivative of the amplification curve. Triplicates were considered acceptable if the standard deviation of the Cp was less than 0.3 cycles. Negative controls were considered acceptable if the Cp of any signal was greater than 10 cycles higher than that of the lowest standard. Each assay was considered acceptable if the reaction efficiency was between 1.8 and 2.1. Relative levels of mRNA of unknown samples were interpolated from the standard curve and expressed relative to the abundance of a reference gene. Student's t-tests were carried out to ensure transcript quantities of reference genes were not significantly different between groups.

| **Reagent** | **Volume (µl)** |
|---|---|
| PerfeCTa® FastMix® II (Quanta Biosciences, Inc., USA) | 6.00 |
| Forward Primer (100µM) | 0.02 |
| Reverse Primer (100µM) | 0.02 |
| Water | 3.96 |

Table 2.6. qPCR reaction components per well.

| **Gene name** | **Forward primer sequence (5'→3')** | **Reverse primer sequence (5'→3')** | **UPL probe number** |
|---|---|---|---|
| *Tbp* | GGGAGAATCATGGACCAGAA | GATGGGAATTCCAGGAGTCA | 97 |
| *Actb* | CTAAGGCCAACCGTGAAAAG | ACCAGAGGCATACAGGGACA | 64 |
| *Tet1* | GGCTCCAGTTGCTTATCAAAA | CCCTCTTCATTTCCAAGTCG | 67 |
| *Tet2* | GGATGAGTTTGGGAGTACGG | TGACTGCAGAACCTCAATGG | 2 |
| *Tet3* | AGATGTGGCCTCAATGATGA | CATATTTGCAGCCGTTGAAG | 1 |
| *Lep* | CAGGATCAATGACATTTCACACA | GCTGGTGAGGACCTGTTGAT | 93 |
| *Pref1* | CGGGAAATTCTGCGAAATAG | TGTGCAGGAGCATTCGTACT | 80 |
| *Cd24* | CTGGGGTTGCTGCTTCTG | AACAGATGTTTGGTTGCAGTAAAT | 68 |
| *Cd34* | GCACCACTGGTTATTTCCTGA | TTTTCTTCCCAACAGCCATC | 19 |
| *Pdgfra* | GCGAGTTTAATGTTTATGCCTTG | GGCACAGGTCACCACGAT | 2 |
| *Hsd-1* | CGTTCCCAGAGCTTCAAAGT | AGGAGGGCATCCTTGAGTC | 98 |
| *Tst* | CCAGCTGGTGGACTCTCG | GTGGCCCGAGTCTAGTCCT | 104 |
| *Ucp1* | TCAGGATTGGCCTCTACGAC | TTAAGCCGGCTGAGATCTTG | 34 |
| *Tmem26* | TGGGGAATATCCTTGAGCTG | TCTAGTGATGGTGCCTCCAA | 7 |
| *Pgc1a* | CAGTCGCAACATGCTCAAG | GGGTCATTTGGTGACTCTGG | 6 |
| *Cebpa* | CCGACCTCTTCCAGCACA | GCTGTTCTTGTCCACCGACT | 2 |
| *Gata4* | GGAAGACACCCCAATCTCG | CATGGCCCCACAATTGAC | 13 |
| *Gata6* | GGTCTCTACAGCAAGATGAATGG | TGGCACAGGACAGTCCAAG | 40 |
| *Klf5* | CCGGAGACGATCTGAAACAC | CAGATACTTCTCCATTTCACATCTTG | 17 |
| *Srebp1* | CGTGGCAGCAGGACTGATA | AGGCCTCTGGGTCATCTACA | 68 |
| *Hsl* | CCTACGGGAAGGACAGGAC | CCTCCGTGGATGTGAACAA | 1 |
| *Atgl* | TGACCATCTGCCTTCCAGA | TGTAGGTGGCGCAAGACA | 104 |
| *Lpl* | GAAGTCTGACCAATAAGAAGGTCAA | TGTGTGTAAGACATCTACAAAATCAGC | 2 |
| *Slc27a1* | GACAAGCTGGATCAGGCAAG | GAGGCCACAGAGGCTGTTC | 70 |
| *Olr1* | CCCTTATTGTACAGTGGACACAAT | GATTCCTGTGAAGTGTTTTCTGC | 3 |
| *Fasn* | TCCACCAAATCCAACATGG | GTTGTGGAAGTGCAGGTTAGG | 1 |
| *Fabp4* | GGATGGAAAGTCGACCACAA | TGGAAGTCACGCCTTTCATA | 31 |
| *Gk* | ATGGTCTCCATCCCACTGTC | TCTTCTCATCCACTGATCCAAA | 16 |
| *Aqp7* | GGCTCCAGCCAGAAGTCA | GGGCCATTGTGGAGTTGT | 84 |
| *Pparg* | AAGACAACGGACAAATCACCA | GGGGGTGATATGTTTGAACTTG | 7 |
| *Adipoq* | GGAGAGAAAGGAGATGCAGGT | CTTTCCTGCCAGGGGTTC | 17 |
| *Igf1* | AGCAGCCTTCCAACTCAATTAT | GAAGACGACATGATGTGTATCTTTATC | 34 |

| | | | |
|---|---|---|---|
| *Ng2* | CTTGGCCTTGTTGGTCAGAT | CACCTCCAGGTGGTTCTCC | 16 |
| *Angptl4* | GGGACCTTAACTGTGCCAAG | GAATGGCTACAGGTACCAAACC | 83 |
| *Bcap31* | TATTGCTGGCTTTTCCTTGC | GCTGGGAGATGAGAGTCACC | 4 |
| *Top2a* | TGTATTAGAGTCACAATTGATCCAGA | CTGGAGGTCAGGAGTTGTCC | 33 |

Table 2.7. A list of all primer sequences and accompanying Roche Univeral Probe Library (UPL) probe number used for RT-qPCR analysis of gene expression.

| Stage | Temp (°C) | Acquisition mode | Hold (hh:mm:ss) | Ramp rate(°C/s) | Number of cycles |
|---|---|---|---|---|---|
| Preincubate | 95 | None | 00:05:00 | 4.8 | 1 |
| Program | 95 | None | 00:00:10 | 4.8 | 50 |
| | 60 | Single | 00:00:30 | 2.5 | |
| Cool | 40 | None | 00:00:30 | 2 | 1 |

Table 2.8. LightCycler® 480 Instrument thermal cycling program used with Roche Universal Probe Library assays for RT-qPCR candidate gene expression analysis.

### 2.5.5. RNA sequencing

RNA was deemed to be of suitable quality and integrity for sequencing with a RNA Integrity Number (RIN) of >8.0, determined using the 2100 Bioanalyzer using the RNA 6000 Nano Kit (Agilent Technologies, UK).

All library preparation, library quality control and sequencing was carried out by staff at the Wellcome Trust Clinical Research Facility, Edinburgh, UK. All products and kits were sourced from Illumina, Cambridge, UK, unless otherwise stated.

***Library Preparation***

Libraries were prepared from each total-RNA sample using the TruSeq Stranded Total RNA with Ribo-Zero kit according to the provided protocol. 500ng of total-RNA was processed to deplete rRNA before being purified, fragmented and primed with random hexamers. Primed RNA fragments were reverse transcribed into first strand cDNA using reverse transcriptase and random primers. RNA templates were removed and a replacement strand synthesised incorporating dUTP in place of dTTP to generate double stranded (ds) cDNA. AMPure XP beads (Beckman Coulter, High Wycombe, UK)

were then used to separate the ds cDNA from the second strand reaction mix, providing blunt-ended cDNA. A single 'A' nucleotide was added to the 3' ends of the blunt fragments to prevent them from ligating to another during the subsequent adapter ligation reaction, and a corresponding single 'T' nucleotide on the 3' end of the adapter provided a complementary overhang for ligating the adapter to the fragment. Multiple indexing adapters were then ligated to the ends of the ds cDNA to prepare them for hybridisation onto a flow cell, before 12 cycles of PCR were used to selectively enrich those DNA fragments that had adapter molecules on both ends and amplify the amount of DNA in the library suitable for sequencing.

***Library quality control***

Libraries were quantified by PCR using the Kapa Universal Illumina Library Quantification kit complete kit and assessed for quality using the Agilent Bioanalyser with the DNA HS Kit.

***Sequencing***

Sequencing was performed using the NextSeq 500/550 High-Output v2 (150 cycle) Kit on the NextSeq 550 platform. Libraries were combined in equimolar pools and run across 1 High-Output Flow Cell. All samples were sequenced to a depth of 33-63 million reads and percentage alignment was >94% for all samples.

### 2.5.6. Enzyme-linked immunosorbent assays (ELISA)

Both TET activity and plasma leptin levels were measured using ELISA-based assays according to kit instructions.

The TET activity assay was carried out using the Epigenase 5mC-Hydroxylase TET Activity/Inhibition Assay Kit (Colorimetric) (Epigentek, NY, USA). Prior to use in the assay, nuclear protein extraction was required. This was carried out using the NE-PER™ Nuclear and Cytoplasmic Extraction Reagents (Thermo Fisher Scientific, Perth, UK). 20mg tissue was homogenised using a Dounce homogeniser, and nuclear proteins were extracted according to kit instructions. 10µg of the resulting nuclear extracts per sample were used in the assay. The assay was then carried out according to kit instructions, and light emission was read at 450nm using a spectrophotometric OptiMax Tunable Microplate Reader (Molecular Devices, CA, USA). Assays were carried out in duplicate. Sample data was interpolated from the standard curve as recommended by the kit manufacturer.

The plasma leptin assay was carried out using the Mouse Leptin ELISA Kit (FineTest, China). 50µL fasted plasma sample was diluted 1:2 with Standard dilution buffer. The assay was then carried out according to kit instructions, and light emission was read at 450nm using the spectrophotometric

OptiMax Tunable Microplate Reader (Molecular Devices, CA, USA). Sample data was interpolated from the standard curve as recommended by the kit manufacturer.

### 2.5.7. Gas chromatography-mass spectrometry (GC-MS)

***Sample preparation***

The starting material (whole adipose tissue) was weighed out on a petri dish on dry ice. 30-50mg of starting material was used for brown adipose tissue and 70-100mg for white adipose tissue. Tissue was minced and homogenised using a pestle & mortar pre-cooled on dry ice. 1mL of 1:1 methanol (Fisher Scientific, Loughborough, UK): water mixture was added (previously prepared and cooled by storing at -20°C) containing 0.5µg of the internal standard d6-glutaric acid (Qmx Laboratories, Essex, UK). The mixture was sonicated for 75-90 minutes using the Bioruptor® (Diagenode, Seraing, Belgium) in an ice bath to maintain a cold temperature, refilling the ice every 10 minutes. An equal volume of ice cold HPLC grade chloroform (Fisher Scientific, Loughboroguh, UK) was added and tubes were vortexed vigorously for 1 minute. The mixture was placed on a shaker at 4°C for 5 minutes. Tubes were then centrifuged at 17,005 x *g* for 10 minutes at 4°C. The upper layer from the biphasic mixture was collected in a pre-cooled tube. Next, another cleaning step was carried out by repeating the addition of chloroform and continuing the protocol as above. Samples were dried completely using a Thermo Savant DNA 110 SpeedVac (Thermo Fisher, West Sussex, UK), then snap frozen and stored at -80°C until analysis.

***Derivatization***

All derivatization steps were carried out in a fume hood. The dried extract was incubated at 95°C in open tubes to remove any residual moisture in the samples. The dried extract was solubilised in 40µl of 2% methoxyamine HCl in pyridine (Sigma-Aldrich, Dorset, UK) followed by 60 minutes incubation at 60°C. Then 60µl N-tertbutyldimethylsilyl-N-methyltrifluoroacetamide (MTBSTFA) with 1% (w/v) tertbutyldimethyl-chlorosilane (TBDMSCI) (Sigma-Aldrich, Dorset, UK) derivatization reagent was added. The suspension was incubated for an hour at 60°C in a well-sealed tube to prevent evaporation. Finally the samples were centrifuged at 17,005 x *g* for 5 minutes and the clear supernatant was transferred to a chromatography vial with a glass insert (Thermo Fisher Scientific, Hertfordshire, UK) and proceeded immediately to GC-MS analysis.

***Gas chromatography-mass spectrometry***

Gas chromatography-mass spectrometry analysis was carried out by Dr Alpesh Thakker, University of Birmingham. For analysis of the derivatized samples, an Agilent 7890B Series GC/MSD gas chromatograph with a polydimethylsiloxane GC column coupled with a mass spectrometer (GC-MS) (Agilent Technologies UK Limited, Stockport, UK) was used.

Prior to sample analysis the GC-MS was tuned to a full width at half maximum (FWHM) peak width of 0.60 a.m.u. in the mass range of 50 to 650 mass to charge ratio (m/z) using PFTBA tuning solution. 1µl of sample was injected into the GC-MS in split mode 1:10 with helium carrier gas at a rate of 1.0mL $min^{-1}$. The inlet liner containing glass wool was set to a temperature of 270°C. Oven temperature was set to 100°C for 1 minute before ramping to 280°C at a rate of 5°C $min^{-1}$. Temperature was further ramped to 320°C at a rate of 10°C $min^{-1}$ held at 320°C for 5 minutes. Compound detection was carried out in full scan mode in the mass range 50 to 650 m/z, with 2-4 scans $sec^{-1}$, a source temperature of 250°C, a transfer line temperature of 280°C and a solvent delay time of 6.5 minutes. The injector needle was cleaned with acetonitrile three times before measurement commencement and three times following every measurement thereafter.

***Gas chromatography-mass spectrometry analysis***

The raw GC-MS data was converted to common data format (CDF) using the acquisition software and further processing of the isotope data including isotope correction and mass isotopomer analysis was performed on MetaboliteDetector software [409]. CDF files were calibrated to the retention index using MetaboliteDetector software with a confidence limit of >70% and change in retention index tolerance (ΔRI) of <5 units. Values for relative metabolite levels were normalised to the internal standard (d6-glutaric acid) and then normalised to starting weight of tissue. Missing values (e.g. caused by peak interference) were substituted for using the mean imputation method.

## 2.6. Epigenome profiling

### 2.6.1. DNA extraction

Adipose DNA extraction was carried out using DNeasy® Blood and Tissue kit (Qiagen, Manchester, UK), according to kit protocol for use on animal tissues, using a spin-column technique. Tissue was cut into small pieces (100mg), and 360µL Buffer ATL was added to each tissue sample in a microcentrifuge tube, followed by 40µL PureLink proteinase K (Qiagen, Manchester, UK). Tubes were vortexed and incubated at 56°C in a thermomixer overnight. Following incubation, tubes were vortexed thoroughly for 15 seconds, and 20µL RNase was added. The tubes were incubated at room temperature for 2 minutes, before 200µL Buffer AL was added, and vortexed again. 200µL 100% ethanol (Fisher Scientific, Loughborough, UK) was added, before mixing thoroughly again by vortexing. This mixture was transferred to a DNeasy mini spin column placed in a 2mL collection tube. Samples were centrifuged at 6000 x *g* for 1 minute. Flow-through was discarded. 500µL Buffer AW1 was added, samples were centrifuged again, and flow-through discarded again. This process was repeated using Buffer AW2. Samples were then eluted in 100µL Buffer AE. Once extracted, DNA was handled on ice and stored at -4ºC.

### 2.6.2. DNA Quantification and Integrity

DNA was quantified with the Qubit 2.0 Fluorometer (Invitrogen, Paisley UK) using DNA "broad range" standards as per manufacturer's instructions for DNA samples. DNA integrity was determined by resolving extraction products on a 1.5% agarose gel and staining with gel red (Cambridge Bioscience, Cambridge UK) to a final concentration of 0.005%.

### 2.6.3. Ultra performance-liquid chromatography

***Sample preparation***

2.5µg DNA in 43µL water, per sample, was incubated at 95°C for 10 minutes. 5µL of 10x T7 DNA polymerase reaction buffer and 10 U T7 DNA polymerase (Thermo Scientific, Renfrew, UK) was then added. The reaction was incubated overnight at 37°C, followed by inactivation by incubation at 75°C for 10 minutes. The samples were then centrifuged for 45 minutes at > 12,000 x *g*, the supernatant was aspirated and dried down using the speed vac, and stored at -80°C until time of analysis.

***Ultra performance-liquid chromatography***

UPLC was carried out by Dr Jimi Wills and Dr Andrew Finch of the mass spectrometry facility, Institute for Genetic and Molecular Medicine, University of Edinburgh. After reconstitution, 10µL polymerase-treated sample was loaded onto a HyperCarb column (Thermo Fisher Scientific, West Sussex, UK) and eluted using an Ultimate 3000 BioRS (Thermo Fisher Scientific, West Sussex, UK) system over a 5 minute gradient from 0 to 100% B, where A was 20mM ammonium carbonate and B was acetonitrile. Data were collected using a Q Exactive (Thermo Fisher Scientific, West Sussex, UK) scanning in negative mode at 70k resolution and a scan range of 300-350 m/z.

### 2.6.4. Bisulfite conversion pyrosequencing

All kits and hardware for this procedure were obtained from QIAGEN (Manchester, UK) unless otherwise specified. 500ng genomic DNA was used in the bisulfite conversion using the EZ DNA Methylation Kit (Zymo, CA, USA) according to kit instructions. Pyrosequencing assays were designed using the PyroMark Q24 Software v2.0.8. Biotinylated primers were HPLC-purified. 5µL AmpliTaq Gold® 360 Master Mix (Thermo Fisher Scientific, UK) was used for polymerase chain reaction amplification, with 1.5µL bisulfite-converted DNA and 5µM primer mix in a total reaction mixture of 10µL (made up with nuclease-free $H_2O$. The PCR mix was placed in a thermocycler which was operated according to the program shown in Table 2.9. Primer sequences are shown in Table 2.10. To confirm a single, correct product has been amplified, PCR products were run on 1.5% agarose gel for 25 minutes at 120V. Three water controls were routinely run and sequenced in parallel to all samples to ensure no contamination of reagents.

The PyroMark file for use on the PyroMark Q24 sequencing system was prepared with information regarding the well layout and amplicon sequence, in order to prepare the correct nucleotide dispensation order. Bisulfite conversion controls were added to the dispensation sequence before each potentially unconverted cytosine.

All buffers (1X Wash Buffer, Annealing Buffer, Denaturation Buffer and Binding Buffer) were purchased as part of the Pyrosequencing kit from QIAGEN, UK. All buffers were acclimatised to room temperature before starting the sequencing, and 50mL of each was placed in the relevant wells at the PyroMark Q24 Workstation, as well as 70% ethanol (Fisher Scientific, Loughborough, UK) and MilliQ distilled water. The enzyme and substrate (PyroMark Gold 24 Reagents, QIAGEN, UK) were reconstituted in $dH_2O$ and kept in aliquots at -20ºC until use. The annealing mix was prepared (0.3µM dilution of sequencing primer in Annealing Buffer) and the binding mix was prepared (40µL Binding Buffer, 18µL $dH_2O$, 2µL streptavidin sepharose beads per well). 60µL binding mix and 20µL PCR product per sample was mixed in a single well of a PCR plate (Thermo Fisher Scientific, West Sussex, UK). Next, the plate was sealed and vortexed for 7 minutes at 1400rpm. Meanwhile, the capture probes were washed in ethanol, followed by $dH_2O$, and the PyroMark plate was loaded with 25µL annealing mix. Once the vortex had finished, the contents of the binding mix plate was immediately aspirated with the capture probes with the vacuum pump turned on, so that the beads did not have a chance to settle. They were then washed in 70% ethanol, Denaturation Buffer and Wash Buffer in that order, followed by a 15-second drying period with the vacuum pump turned on. The vacuum pump was then turned off and the capture probes were inserted into the PyroMark plate containing the annealing mix, and shaken gently until the beads were dislodged from the probes. The vacuum pump was turned back on and the capture probes were washed twice in $dH_2O$, then air-dried for 30 seconds. The PyroMark plate containing the streptavidin-captured DNA and primer mix was incubated for 2 minutes at 80°C and then 5 minutes at room temperature. Meanwhile, the PyroMark cartridge was loaded with the appropriate amount of enzyme, substrate and nucleotides as dictated by the software. The cartridge was then inserted into the sequencer, and the cooled PyroMark plate was inserted after. The previously designed assay program was initiated. Analysis of the sequencing results was carried out on PyroMark Q24 Software v2.0.8, and was subject to the software's in-built quality control measures (e.g. sufficient amplitude of peaks, no drift from baseline, no uncertainty of reading).

| **Temperature ($^0$C)** | **Time (hh:mm:ss)** | **Number of cycles** |
|---|---|---|
| 95 | 00:10:00 | - |
| 95 | 00:00:20 | 45 |
| 55 (annealing temp) | 00:00:20 | |
| 72 | 00:00:20 | |
| 72 | 00:07:00 | - |
| 4 | ∞ | - |

Table 2.9. Thermal cycler program for polymerase chain reaction amplification of bisulfite-converted DNA for use in bisulfite pyrosequencing.

| **Primer name** | **Sequence (5'→3')** |
|---|---|
| Forward | TTTGTTTTTTGAGGTGTTGGAAGTATTAT |
| Reverse (biotinylated) | CATACCTACCTACCCCTCTTA |
| Sequencing | ATGGAGTATTAGGTTGT |
| | |
| **Sequence to analyse (5'→3')** | TGTTGTTATT GTTGTTGGTT YGTTGGGTGG GGYGGGAGTT GGYGTTYGTA GGGATTGGGG TTGGT |

Table 2.10. Leptin promoter bisulfite pyrosequencing assay details. Forward, reverse and sequencing primer sequences, and sequence to analyse.

### 2.6.5. Hydroxymethylcystosine DNA immunoprecipitation (hMeDIP-seq)

***DNA shearing***

DNA was fragmented using the Covaris® E220 Focused-ultrasonicator (Covaris, Brighton, UK). 5µg DNA diluted in 130µL TE buffer was placed into a crimp cap microTUBE (Covaris, Brighton, UK). DNA was then sonicated in the conditions shown in Table 2.11. Quality of shearing was assessed by running in a 1.5% agarose gel in 0.5x TBE buffer for 90 minutes at 70 volts. Acceptable shearing was deemed as fragments between 100 and 600 base pair length with a mean of 200 to 300 base pairs and a uniform appearance between sheared samples.

| | |
|---|---|
| Peak Incident Power (W) | 175 |
| Duty Factor | 10% |
| Cycles per Burst | 200 |
| Treatment time (s) | 305 |
| Temperature ($^0$C) | 7 |

Table 2.11. Covaris conditions for DNA shearing.

***Hydroxymethylcystosine DNA immunoprecipitation (hMeDIP)***

2.5µg of sheared DNA was diluted up to 450ul in TE buffer in a 1.5ml Eppendorf® LoBind microcentrifuge tubes (Eppendorf, UK) and then denatured by placing in boiling water within a heat block for 10 minutes. Samples were immediately cooled on ice for 5 minutes. 50µl of 10X IP buffer was then added and vortexed briefly. 50µl 'input' was then removed and placed at 4$^0$C until the DNA clean up step below. 1µl of 5-Hydroxymethylcytosine (5-hmC) antibody (pAb) (Cat. No 39769; Active Motif, CA, USA) was then added to the remaining sample and incubated for 2 hours at 4$^0$C.

40µl of Dynabeads® Protein G for Immunoprecipitation (Invitrogen, Paisley, UK) were prewashed with 0.1% BSA in PBS for 5 minutes on rotating wheel at room temperature. The beads were collected on a magnetic rack and the supernatant was removed. To ensure all supernatant was removed, the beads were briefly centrifuged at 402 x *g* for 5 seconds, bound to the rack and the supernatant removed again. This washing step was repeated twice. The beads were then resuspended in 40µl of 1X IP buffer and added to the DNA/antibody mixture. This was then incubated for 1 hour at 4°C on a rotating wheel. The beads were then collected again on the magnetic rack. The supernatant was discarded, and the tube was centrifuged again at 402 x *g* for 5 seconds, beads bound to the magnetic rack and residual supernatant removed. The beads were then washed three times with 1mL of cold 1X IP buffer in the same manner as described above with BSA-PBS. The beads were then resuspended in 250µl of digestion buffer and 20ul of proteinase K 20mg/ml (Roche, UK) was added. The samples were then incubated in a thermoshaker overnight at 1000rpm and 55°C. Following this, the tubes were spun at 402 x *g* for 5 seconds, the beads were collected on a magnetic rack and the supernatant collected, containing DNA fragments enriched with 5hmC. Both the enriched fraction and input samples were then purified using the QIAquick PCR Purification Kit (Qiagen, UK) according to manufacturer's protocol, with elution into 22µl of water.

***qPCR of immunoprecipitated products***

The immunoprecipitated product was analysed by qPCR to determine the efficiency of the immunoprecipitation. Regions from the adipose tissue genome with known high or low 5hmC levels

were selected as positive and negative control regions. 10µl of the eluted DNA from purification was diluted 1:5 in water, and was used in the reaction mixture shown in Table 2.12, with primer sequences for control regions shown in Table 2.13.

A water control was used routinely. Standard curves were created using serial 1:2 dilutions of sonicated DNA. qPCR plates were centrifuged at 563 x *g* for 2 minutes prior to thermal cycling, to ensure all samples and mastermix were at the bottom of the well. The LightCycler® 480 Instrument (Roche, Sussex, UK) was used for temperature cycling (using the program shown in Table 2.14) and fluorescence quantifications.

The LC480 Software (Roche) measured fluorescence throughout the experiment and data was analysed as previously described in section 2.5.4.

| **Reagent** | **Volume (µl)** |
|---|---|
| SYBR green Master Mix (Roche, Burgess Hill, UK) | 5 |
| Forward Primer (100µM) | 0.02 |
| Reverse Primer (100µM) | 0.02 |
| Water | 1.96 |

Table 2.12. qPCR reaction components per well.

| **Gene & region** | **Control for 5hmC** | **Forward (5'→3')** | **Reverse (5'→3')** |
|---|---|---|---|
| H19 intragenic | Positive | GCCAAGAGAGAAGAAGGAGA | GAATGTTGAAGGACTGAGGG |
| Tex19.2 intragenic | Positive | GGGAGATATGTAAATGAGCTGG | CATCCTTACCTCCCTGACTGAG |
| Gapdh promoter | Negative | CCACTCCCCTTCCCAGTTTC | CCTATAAATACGGACTGCAGC |
| Zc3h3 promoter | Negative | ACAGAAAGGGTCGTTTGCAG | AGATGTTCCCTCTCCCCAAT |

Table 2.13. Primer sequences used in qPCR of hmC-dIP.

| Stage | Temp (°C) | Acquisition mode | Hold (hh:mm:ss) | Ramp rate (°C/s) | Number of cycles |
|---|---|---|---|---|---|
| Activation | 95 | None | 00:10:00 | 4.8 | 1 |
| Denaturation | 95 | None | 00:00:15 | 4.8 | 70 |
| | 60 | Single | 00:01:00 | 2.5 | |
| Melting curve | 95 | None | 00:00:05 | 4.8 | 1 |
| | 65 | None | 00:01:00 | 2.5 | |
| | 75 | Continuous (5 acquisitions per °C) | - | 0.11 | |
| Cool | 40 | None | 00:00:10 | 2.5 | 1 |

Table 2.14. LightCycler® 480 Instrument thermal cycling program used with SYBR Green assays for qPCR analysis of immunoprecipitated products.

***Whole genome amplification (WGA)***

WGA was performed using the SeqPlex Enhanced DNA Amplification Kit (SEQXE) (Sigma, UK), according to the manufacturer's instructions. 10µl of immunoprecipitation product and input sample were used. 15 cycles of DNA amplification was performed in a standard PCR machine (Techne Prime, Bibby Scientific, Birmingham, UK). For adaptor removal, all samples were quantified by nanodrop, the lowest DNA concentration was taken and volume required for 2.1µg calculated. This volume was then used for all samples in the adaptor removal step. Final elution was in 30ul of water.

***Ion Torrent Proton sequencing***

Proton sequencing was outsourced to the Wellcome Trust Clinical Research Facility at the Western General Hospital, Edinburgh, UK. All kits and hardware for this procedure were from Life Technologies (Paisley, UK) unless specified. Briefly, samples were quantified using the Qubit dsDNA HS kit and approximately 100ng of DNA was used to generate A DNA library from each sample using the Ion Xpress Plus Fragment Library Kit. During this process, DNA fragments are end repaired and then ligated to Ion specific barcode adaptors before being amplified (8 cycles) and twice purified using the Agencourt AMPure XP PCR clean up kit (Beckman Coulter, High Wycombe, UK) which size selects fragments approximately 100–250bp in length. Libraries were then quality controlled using the Agilent Bioanalyser DNA HS kit (Agilent, Santa Clara, US) and pooled in equimolar pairs prior to template preparation using the Ion PI™ Hi-Q™ OT2 200 Kit and sequencing

on the Ion Torrent semiconductor sequencer using the Ion PI™ Hi-Q™ Sequencing kit and an Ion PI™ Chip Kit v3. For consistency, each sample was sequenced on a PI chip with its own input.

## 2.7. Bioinformatic and statistical analysis

### 2.7.1. Statistical testing of null hypotheses

Statistical analysis was performed using GraphPad Prism 5 software. Comparisons between two groups were made using unpaired student's t-tests. Comparisons between two groups with repeated measures (e.g. weight gain measurements at multiple time points) were made using a two-way repeated measures ANOVA. Bonferonni post-hoc tests were also carried out to account for false discovery rate. The statistical analysis performed is listed in the legend of each figure. Data sets were routinely tested for normal distribution using the Shapiro-Wilks test. Non-parametric tests were used for data with non-parametric distribution. All values are represented as mean ± SEM with $p < 0.05$ deemed significant.

### 2.7.2. RNA-seq analysis

Raw data produced by the NextSeq 550 was uploaded to BaseSpace, a cloud-based data management and analysis service provided by Illumina. Here it was converted into FASTQ files in order to allow analysis using a number of apps accessible directly through BaseSpace. First, FASTQ files were aligned to RefSeq genome mm10 (Dec. 2011 GRCm38/mm10) using the RNA-seq Alignment workflow (v1.0), which, in addition to reference genome read alignment using STAR Aligner, also carried out the following functions:

- Fragments Per Kilobase of transcript per Million mapped reads (FPKM) estimation of reference genes and transcripts using Cufflinks 2.
- Assembly of novel transcripts with Cufflinks 2.
- Variant calling (single nucleotide variants and small indels) with the Isaac Variant caller.

Differential expression analysis was then carried out between test groups using the TopHat Alignment & Cufflinks Assembly and Differential Expression (v1.0) application, which then allowed download of tables with mean expression values for all annotated genes. Subsequent analysis was carried out in Excel.

Differential expression was deemed significant using a q value (p value adjusted for False Discovery Rate) of > 0.05 and a $\log_2$ fold change > 1.2. Pathway analysis was carried out on the Panther Classification System, using the statistical overrepresentation function, using input lists of significantly up- and down-regulated genes.

### 2.7.3. hMeDIP-seq analysis

Raw sequence data analysis from the semiconductor sequencer was processed using Ion Torrent Suite software version 4.0.2 (Life Technologies, Paisley, UK). This carries out quality control of the reads and generates binary alignment map (BAM) files suitable for export.

hMeDIP-seq analysis was carried out using the local university Galaxy Server (The Galaxy Project). The exported BAM files were uploaded to the server *via* a file transfer protocol client. BAM files were analysed using the "bamCompare" tool. This allowed binning of data into bins of 150 bases and subsequent subtraction of the input sequence values from the immunoprecipitated sequence values, allowing determination of 5hmC levels only in the immunoprecipitated sample and comparison between datasets. This step also allowed normalisation of read coverage to 1X to account for variations in the sequencing reactions. The output BIGWIG files were visualised in Integrated Genome Viewer (IGV, Broad Institute) and converted to WIG files using the "bigwigtowig" tool. WIG files were then converted to the mm9 build of the mouse genome Mouse July 2007 (NCBI37/mm9) to allow mapping to mm9 reference gene coordinates (using the tool "convert genome coordinates"). The mapped output files were then sorted by genome locus ("filter and sort") and sliding windows analysis was carried out to determine mean 5hmC levels at 5% intervals across every annotated gene (with all gene lengths normalised to 100%). This was carried out using the Galaxy tool named "Sliding window over length normalised regions of interest". The resulting tables were downloaded and analysis was completed in Excel to visualise and compare mean 5hmC levels across all genes and various subsets of genes.

# 3. Global *Tet1* knockout and the development of obesity

## 3.1. Introduction

Cytosine methylation (5mC) is associated predominantly with gene silencing [280], while cytosine 5-hydroxymethylation (5hmC) is associated with active gene transcription [291]. 5hmC also plays a key role in the process of DNA demethylation, catalysed by the α-ketoglutarate dependent Ten-Eleven-Translocation enzymes (TET1-3) [289]. The TET enzymes have been shown to play an important role in adipocyte differentiation and function [383, 410]. Peroxisome proliferator-activated receptor-γ (PPARγ), a master nuclear receptor critically involved in adipocyte differentiation and activation of adipocyte-specific gene expression, recruits TET1 to promote local demethylation around PPAR response elements (PPREs), thereby activating transcription of adipocyte-specific genes [383].

Previous studies in our lab, aimed at establishing genome-wide differences in hepatic gene expression and 5hmC profiles in *Tet1* KO mice compared to littermate wildtype (WT) animals, have found that *Tet1* KO mice are protected against diet-induced obesity (DIO), with maintenance of insulin sensitivity. However, the metabolic phenotype of the TET1 KO mouse has not been further characterised, and the mechanisms accounting for the differences in weight gain are still unclear. This project aimed to use the *Tet1* KO mouse as a model in which to understand the effects of epigenetic dysregulation on obesity and metabolism, and investigate the mechanisms behind the differences in weight gain, focusing specifically on adipose tissue phenotype.

## 3.2. Hypothesis & aims

**Hypothesis:**

*Tet1* KO causes alterations in the adipose tissue hydroxymethylome and transcriptome, which lead to decreased adiposity.

- Global deletion of *Tet1* results in decreased 5hmC in adipose tissue DNA and subsequent transcriptional effects.
- Global deletion of *Tet1* results in reduced capacity for adipogenesis due to transcriptional effects mediated by the PPAR family of transcription factors.

**Aims:**

- To further characterise the metabolic phenotype of *Tet1* KO mice *in vivo*.
- To characterise the adipose tissue hydroxymethylome and transcriptome of *Tet1* KO mice.
- To characterise the effect of *Tet1* depletion on adipocyte differentiation and function *in vitro.*

## 3.3. Methods

Male WT and *Tet1* KO mice (age range 12–23 weeks at the start of the diet intervention) were maintained on either control diet or HFD for 11 weeks. Body weight and food intake were tracked weekly, and Time-Domain Nuclear Magnetic Resonance (TD-NMR) was carried out to detect body composition. Indirect calorimetry ($VO_2$, $VCO_2$, respiratory exchange ratio, food & water intake, activity levels) was analysed immediately before the start of the diet intervention, and at 7 weeks HFD. Glucose tolerance tests were carried out at the end of the diet intervention.

After 11 weeks, mice were fasted for 16 hours, killed and adipose tissue and plasma were collected. The stromal vascular fraction, containing preadipocytes, was isolated from epididymal adipose tissue using the collagenase digestion method, cultured and differentiated *in vitro* on collagen-coated 6-well plates for 14 days using an adipogenic differentiation cocktail (1µM Rosiglitazone; 250uM IBMX; 200pM T3; 10µg/ml Apo-Transferrin; 5µg/ml Insulin; 100nM Dexamethasone) to observe intrinsic capacity for adipogenesis and gene expression. Fixed cells were stained with Oil Red O to observe lipid accumulation, and RNA was extracted for gene expression analysis by RT-qPCR.

RNA and DNA were extracted from mesenteric adipose tissue for RNA-sequencing (RNA-seq) and 5hmC-DNA-immunoprecipitation sequencing (hMeDIP-seq) studies, respectively. RNA-seq was carried out on the NextSeq 550 platform (Illumina) to a depth of ~60 million reads per sample. Analysis of RNA-seq data was carried out using Illumina's online platform, BaseSpace, using the differential expression application, Cufflinks. Genes were determined to be differentially expressed with a $\log_2$ fold change of > 1.2 and a q value < 0.05. hMeDIP-seq was carried out on the Ion Torrent platform. Analysis of hMeDIP-seq data was carried out using Galaxy to determine mean 5hmC levels per gene or sliding window analysis across 150bp regions across the gene.

## 3.4. Results

### 3.4.1. Weight gain, body composition and glucose and insulin tolerance of the *Tet1* KO mouse

*Tet1* KO mouse resistance to DIO was confirmed in three independent cohorts (Figure 3.1a). A significant difference in weight gain was also observed between WT and KO mice on control diet (CD, Figure 3.1a). Time Domain Nuclear Magnetic Resonance (TD-NMR) quantification of body composition revealed that the difference in weight on HFD appears to be almost entirely due to a difference in fat mass (Figure 3.1b). On HFD, both WT and KO mice have significantly decreased glucose tolerance, with an inability to return glucose levels to baseline within 90 minutes (Figure 3.1c) and no differences between genotypes were observed in glucose tolerance on glucose tolerance testing on control or HFD. However, insulin tolerance testing revealed that *Tet1* KO mice retain insulin sensitivity on HFD as compared to WT littermates (Figure 3.1d).

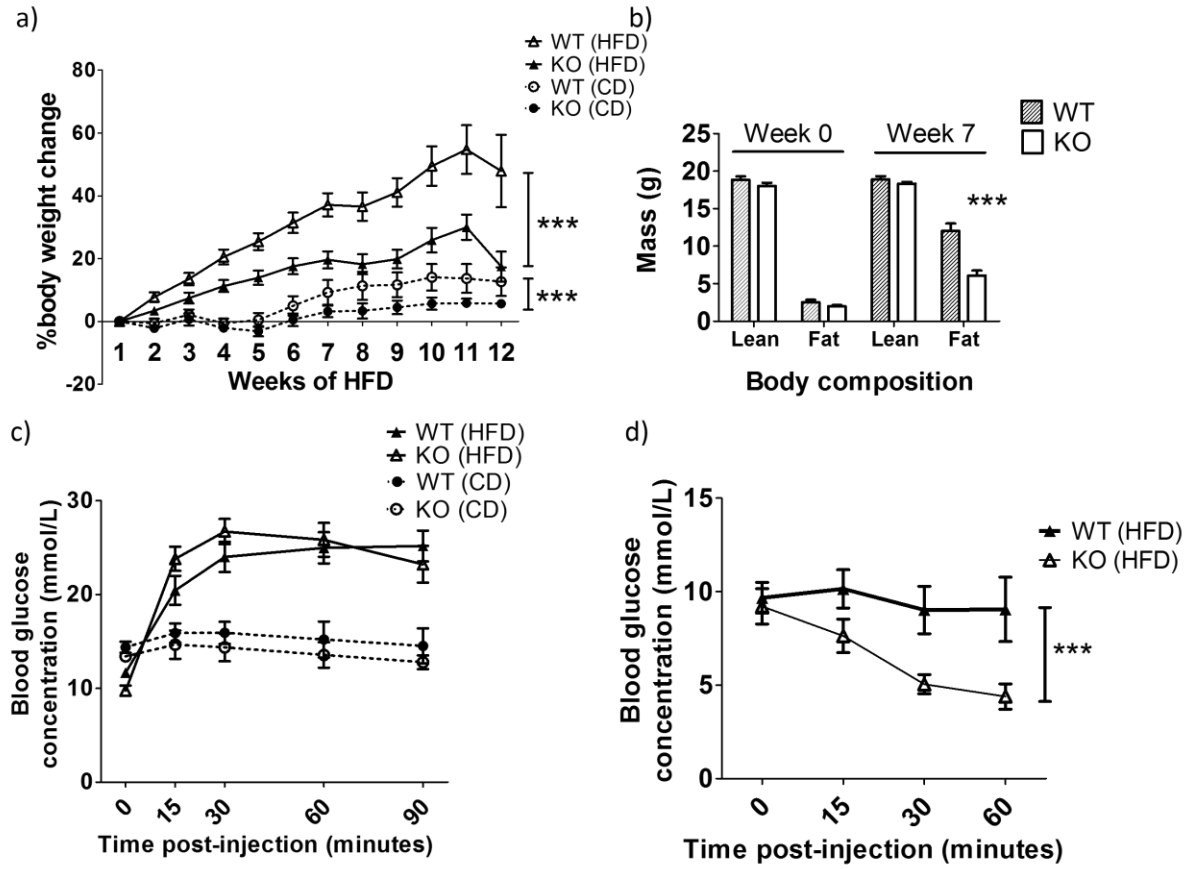


Figure 3.1. Metabolic phenotyping of the *Tet1* knockout mouse.

a) Percentage body change in weight of male wildtype (WT, n = 15) and *Tet1* knockout (KO, n = 14) mice on control diet (CD) (n = 6/group) and high fat diet over 11 weeks. ***p<0.001 by two-way repeated measures ANOVA. b) Body composition before and after high fat diet. ***p<0.001 by student's t test. c) Glucose tolerance tests of WT and KO mice on CD (n=6/group) and HFD (n = 10/group). d) Insulin tolerance tests of WT and KO mice, n = 10/group. ***p<0.001 by one-way repeated measures ANOVA. Insulin tolerance tests performed by Marcus Lyall. All data displayed as mean ± SEM.

### 3.4.2. Indirect calorimetry and activity levels

On HFD, *Tet1* KO mice expended fewer calories in total compared to WT littermates (Figure 3.2a). When analysed separately for light and dark phases, it is clear that the difference in energy expenditure occurs during the light phase – i.e. KO mice expended less energy than WT during the light or typically 'inactive' phase of the day (Figure 3.2b). This decrease in energy expenditure was not correlated with lean mass (Figure 3.2c).

Respiratory exchange ratio (RER) – i.e. ratio of oxygen inspired to carbon dioxide expired – is an indicator of fuel metabolism. During carbohydrate metabolism, there is an equal amount of $CO_2$ produced for $O_2$ consumed (RER = 1.0). During fat metabolism, there is less $CO_2$ produced

compared to $O_2$ consumed. Therefore, an RER of 0.7 indicates mostly lipid metabolism, while an RER of close to 1.0 indicates predominantly carbohydrate metabolism. Analysis of RER over time revealed a marked and consistent increased RER in KO as compared to WT, indicating preservation of a greater proportion of carbohydrate metabolism in the KO animals (Figure 3.3). Analysis by two-way ANOVA indicated that this change was statistically significant. Analysis of RER over time also showed that WT and KO mice had increased RER on chow as compared to HFD, and that on chow diet both WT and KO animals displayed normal diurnal variation in RER (increased RER during the dark phase, indicating increased carbohydrate metabolism during the 'active' phase). This diurnal variation was lost in both genotypes on HFD.

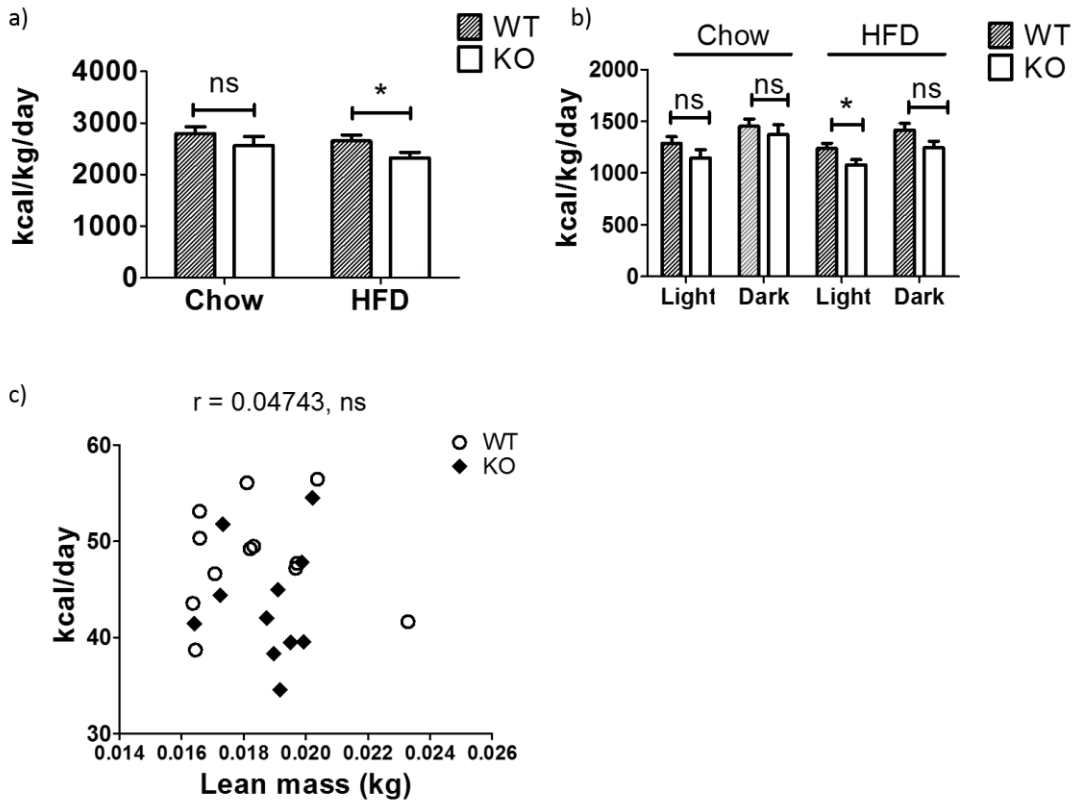


Figure 3.2. Kcalorie expenditure estimated from indirect calorimetry studies, using measurements of $VO_2$ and $VCO_2$.

a) Total kcal expenditure per kg lean mass per day of wildtype (WT) and knockout (KO) animals. *p<0.05 by student's t test. b) Total kcal expenditure per kg lean mass during the light phase (7am-7pm) and the dark phase (7pm-7am). *p<0.05 by student's t test. c) Kcal expenditure against lean mass values per animal. r = Spearman's correlation coefficient. All data is expressed as mean ± SEM. n = 12 and 11/group.

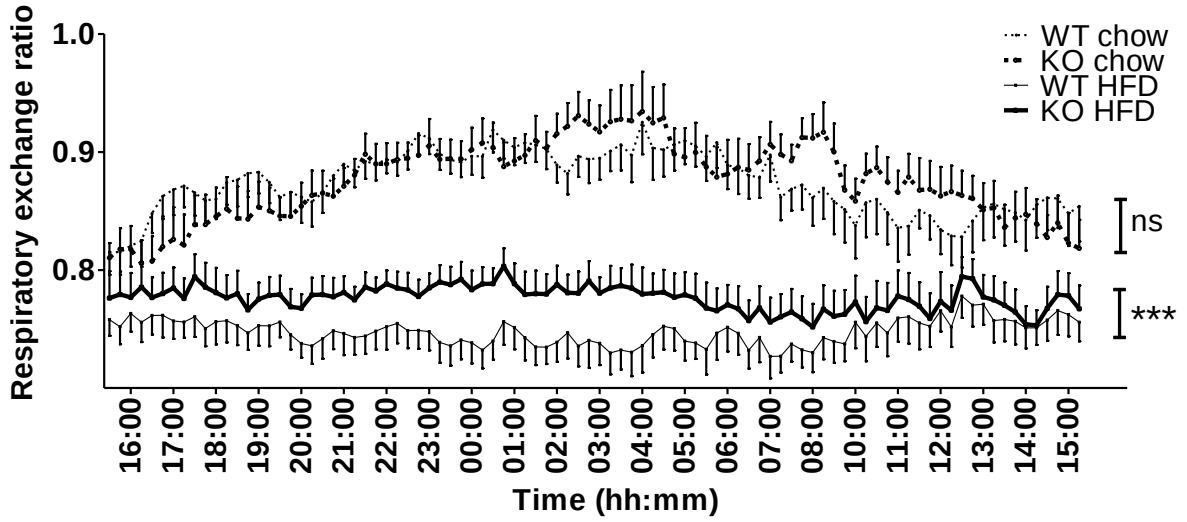


Figure 3.3. Respiratory exchange ratio of wildtype (WT) vs knockout (KO) mice on chow diet and high fat diet (HFD). n = 12 and 11/group. All data expressed as mean ± SEM. ns, not significant; ***p > 0.001 as determined by 2-way ANOVA.

The TSE PhenoMaster cages allowed measurement of movement by infrared light beams. While movement was markedly decreased in both genotypes on HFD compared to chow, no overall differences were seen between genotype on either diet (Figure 3.4a). However, analysis of the light and dark phases separately indicated that KO mice moved significantly more in the light phase compared to their WT littermates (Figure 3.4b). No differences were seen between genotypes in total distance travelled overall (Figure 3.4c) or when the light and dark phases were analysed separately (Figure 3.4d).

No differences were found in total food intake, either on chow or HFD (Figure 3.5a), and no differences were found in the light or dark phases when analysed separately (Figure 3.5b). When plotted against time, no differences were observed in cumulative food intake over 24 hours (Figure 3.5c).

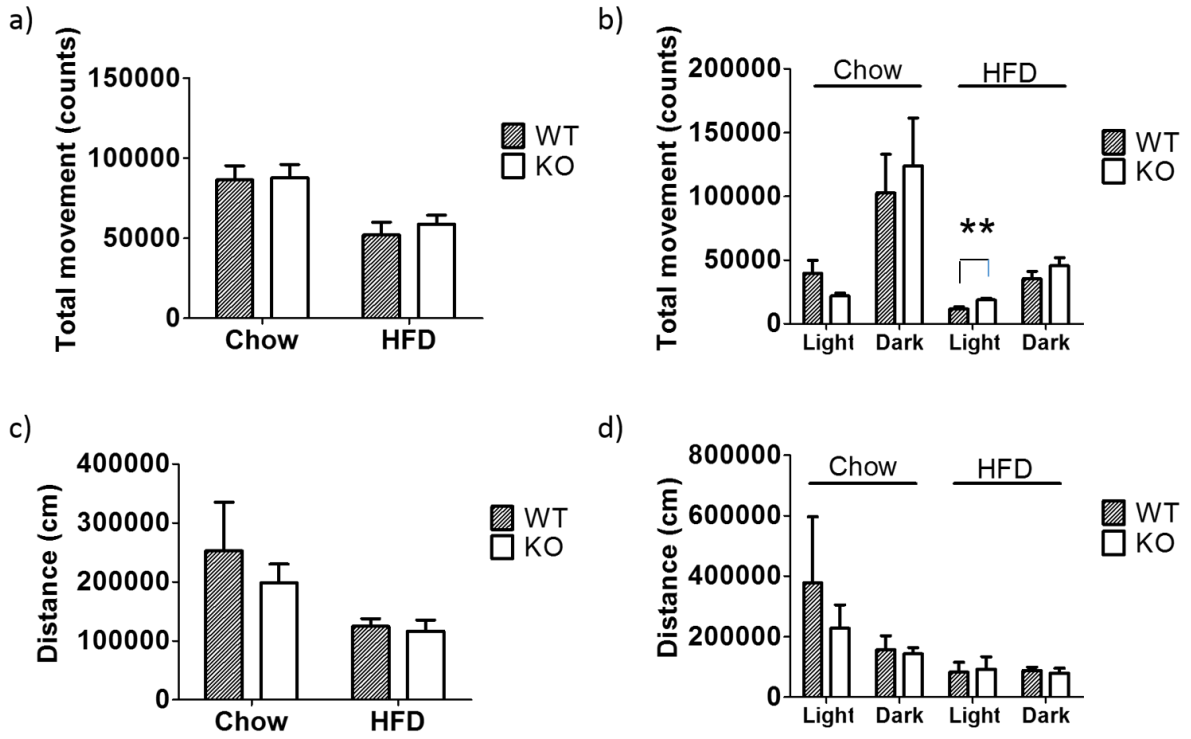


Figure 3.4. Movement and activity of wildtype (WT) and knockout (KO) mice.

a) Total movement of wildtype (WT) and knockout (KO) mice on both chow and high fat diet (HFD). b) Total movement of WT and KO mice on both chow and HFD in light and dark phases. **p<0.01 by student's t test. c) Total distance travelled by WT and KO mice on both chow and HFD in 24 hours. b) Total distance travelled in 24 hours by WT and KO mice on both chow and HFD in light and dark phases. n = 12/group. All data expressed as mean ± SEM.

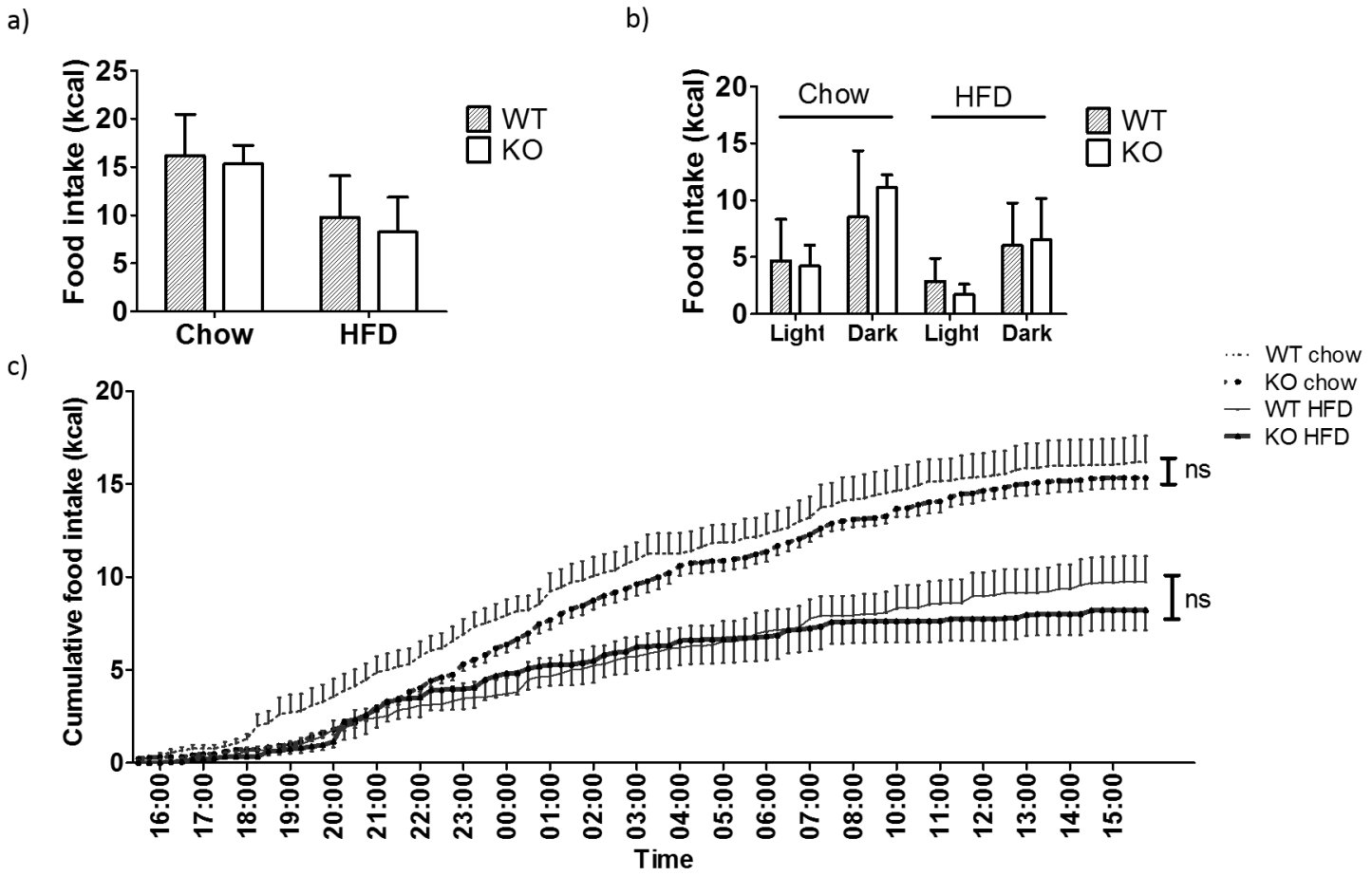


Figure 3.5. Food intake in wildtype (WT) and *Tet1* knockout (KO) mice.

a) Total 24-hour food intake in wildtype (WT) and *Tet1* knockout (KO) mice on chow and high fat diet (HFD). b) Food intake in light and dark phase on chow and HFD. c) Cumulative food intake in WT and KO mice over 24 hours on chow and HFD. n = 12/group. All data expressed as mean ± SEM. ns = not significant by two-way repeated measures ANOVA.

### 3.4.3. *In vitro* adipogenesis

Isolation and culture of preadipocytes from the stromal vascular fraction followed by *in vitro* differentiation revealed no differences in adipogenic capacity judging by the gross morphology of differentiated cells (Figure 3.6). This was the same for cells taken from WT and KO animals on a control diet (CD) or HFD. In addition, elution of the Oil Red O stain – which binds lipids within the cells – and quantification by photospectrometry revealed no difference in amount of lipid in the differentiated cells, on either CD (Figure 3.7a) or HFD (Figure 3.7b).

Candidate gene expression analysis was carried out by RT-qPCR for key genes involved in adipogenesis, and further genes of interest (Figure 3.7c). No difference was observed in the mRNA levels of any candidate genes except for a dramatic and significant decrease in leptin mRNA ($p < 0.01$).

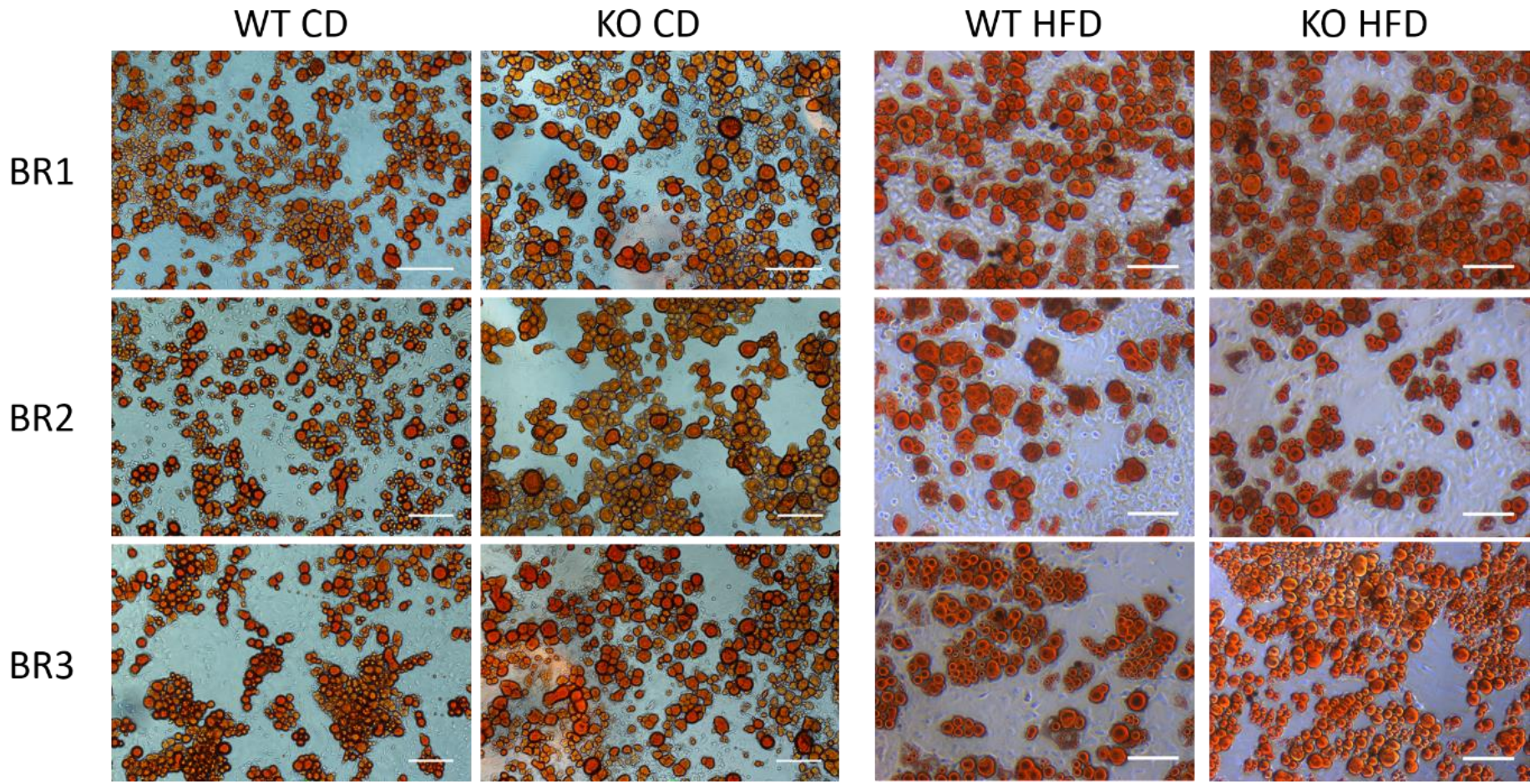


Figure 3.6. Mature adipocytes differentiated in vitro from primary isolated stromal vascular fraction preadipocytes, and stained with Oil Red O.
Cells taken from wildtype (WT) and knockout (KO) mice on both control diet (CD) and high fat diet (HFD). Images shown from biological replicates (BR) 1-3. Scale bar = 100µm.

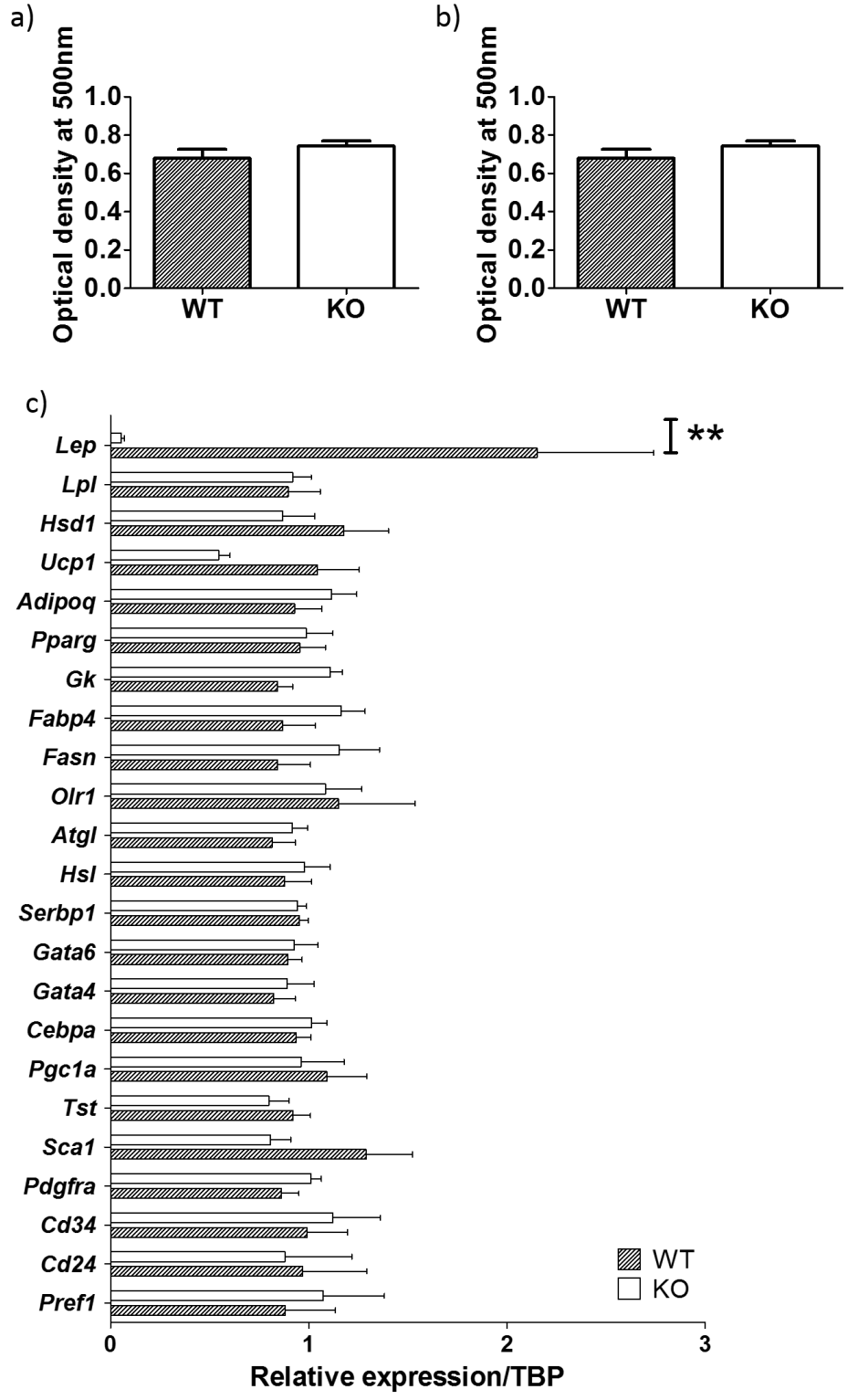


Figure 3.7. Lipid accumulation and gene expression of differentiated primary adipocytes from wildtype (WT) and knockout (KO) mice.

Quantification of Oil Red O staining from differentiated primary adipocytes from wildtype (WT) and knockout (KO) mice on both a) control diet (CD); and b) high fat diet (HFD) n = 5/group. c) Gene expression of candidate genes in differentiated primary adipocytes from WT and KO mice. n = 12/group. All data expressed as mean ± SEM. **p<0.01 by student's t test.

### 3.4.4. HFD mesenteric adipose tissue: RNA-sequencing analysis

RNA-seq analysis of mesenteric adipose tissue from WT and KO mice allowed hierarchical clustering of genes by Euclidean distance into two distinct groups, WT and KO (Figure 3.8a). In addition, gene expression was plotted as a scatterplot to visualise significantly upregulated and downregulated genes with a $\log_2$ fold change > 1.2 (Figure 3.8b). Also identified were a group of genes involved in metabolism with significantly decreased gene expression (Figure 3.8b). Statistical overrepresentation pathway analysis *via* PANTHER revealed several pathways that had increased representation in the list of significantly up- and downregulated genes. Of the list of upregulated genes, muscle organ development pathway genes were the most highly overrepresented, followed closely by synaptic vesicle exocytosis and acyl-coA metabolic processes (Figure 3.8c). Of the list of downregulated genes, almost all overrepresented pathways were involved in metabolic processes (Figure 3.8d), the top hit being gluconeogenesis, followed by cellular glucose homeostasis and monosaccharide metabolic processes. Other pathways overrepresented in the list of downregulated genes include lipid, fatty acid and cholesterol metabolic processes, carbohydrate metabolic processes, and lipid transport.

Of note, *Tet1* expression was *not* found to be downregulated in the *Tet1* knockout mouse mesenteric adipose tissue RNA-seq data (see Figure 3.9a). However, the absence of *Tet1* mRNA and protein was confirmed in epididymal adipose tissue (see Figure 3.9b & c). Therefore, it is likely that lack of differential *Tet1* expression in the mesenteric adipose tissue is due to the generally low expression of *Tet1* in normal, WT mesenteric adipose tissue at this developmental stage, making the lack of *Tet1* expression in the *Tet1* KO mouse mesenteric adipose tissue undetectable. However, lack of *Tet1* could have had an impact in mesenteric adipose tissue at earlier developmental stages.

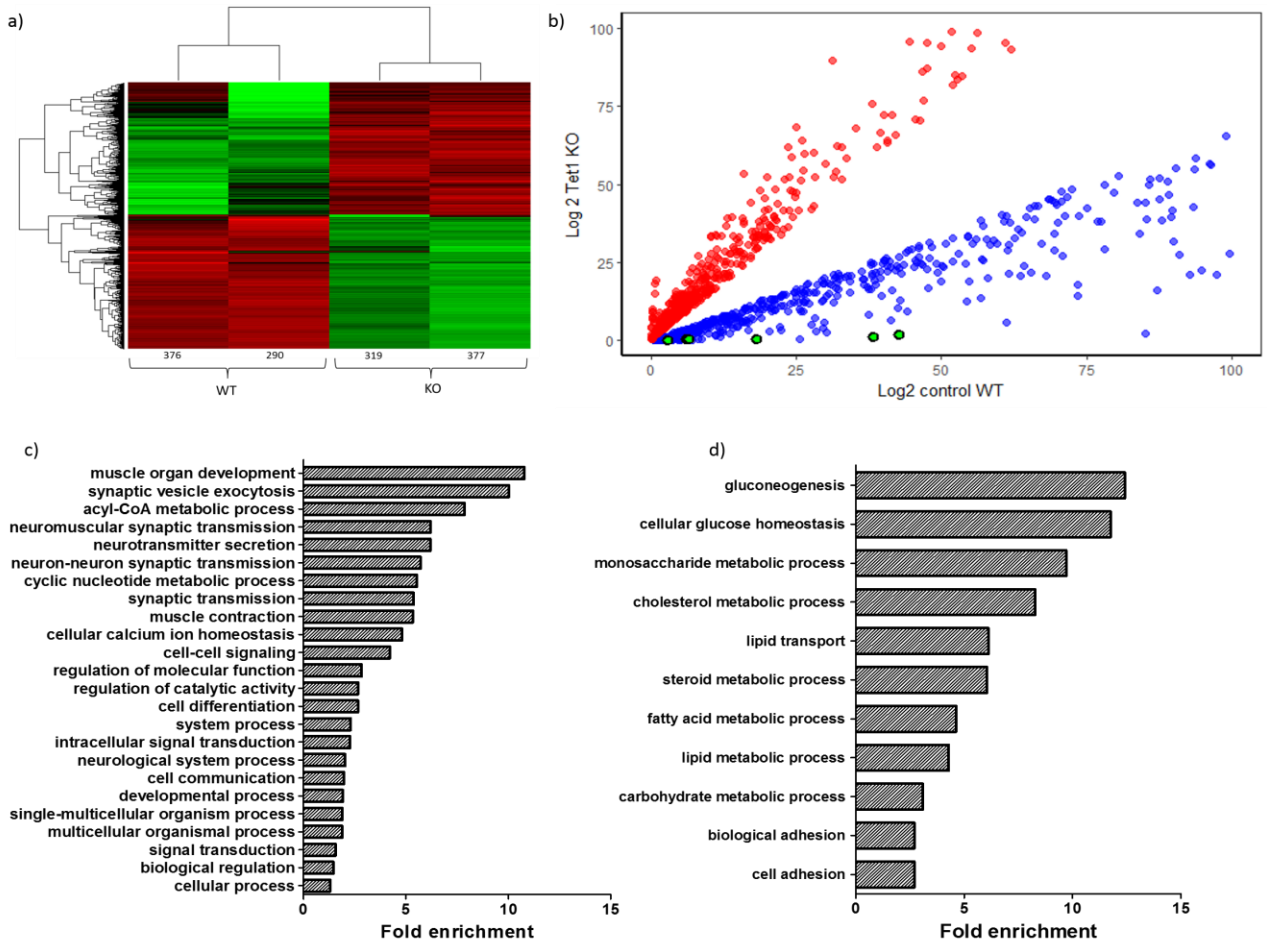


Figure 3.8. RNA-seq analysis.

a) Heatmap showing all 1353 significantly ($log_2$ fold change > 1.2; q < 0.05) differentially expressed genes clustered by Euclidean distance. b) Scatterplot showing significantly upregulated (red) and downregulated (blue) genes in knockout (KO) vs wildtype (WT) animals. In green are a subset of downregulated genes involved in metabolism. c) Statistical overrepresentation pathway analysis of significantly upregulated genes ($log_2$ fold change > 1.2; q < 0.05); and d) significantly downregulated genes. False Discovery Rate > 0.05. n =3/group.

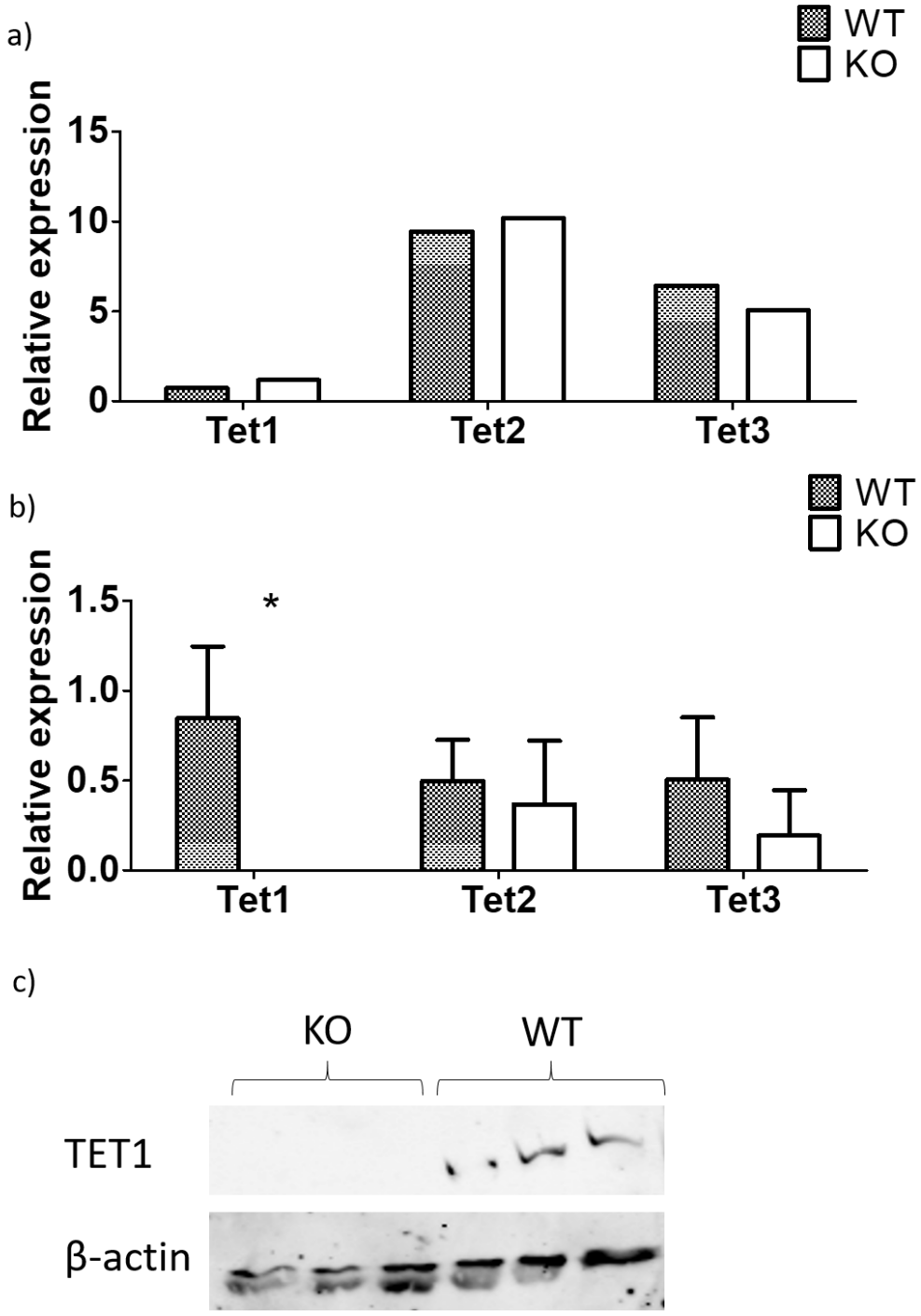


Figure 3.9. *Tet* mRNA and protein levels in mesenteric and epididymal adipose tissue from wildtype (WT) and *Tet1* knockout (KO) mice.

a) *Tet* mRNA levels in mesenteric adipose tissue ($n$ = 3/group), determined by RNA-seq. b) *Tet* mRNA levels relative to TBP in epididymal adipose tissue, determined by qPCR ($n$ = 4 and 3/group). Data expressed as mean ± SD. *$p<0.05$ by student's t test. c) Western blot for TET1 protein levels in epididymal adipose tissue from WT and KO mice.

### 3.4.5. HFD mesenteric adipose tissue: DNA immunoprecipitation-sequencing

Genome-wide 5hmC levels, when compared across every annotated gene in the mouse genome, were not different in high fat-fed KO *vs* WT mouse mesenteric adipose tissue (Figure 3.10). In fact, a notably high correlation was observed between WT and KO average gene 5hmC levels, with a Spearman's correlation coefficient value (r) of 0.9843 (Figure 3.11a). However, a subset of genes with significantly reduced 5hmC levels were identified (Figure 3.11a & Figure 3.11b). When analysed against the corresponding RNA-seq data, decreased average 5hmC levels correlated with decreased gene expression of only 3 genes (*Angptl4*, *Bcap31* and *Top2a*) (Figure 3.11b). Statistical overrepresentation pathway analysis *via* PANTHER using lists of genes with significantly increased or decreased mean 5hmC generated no significant results.

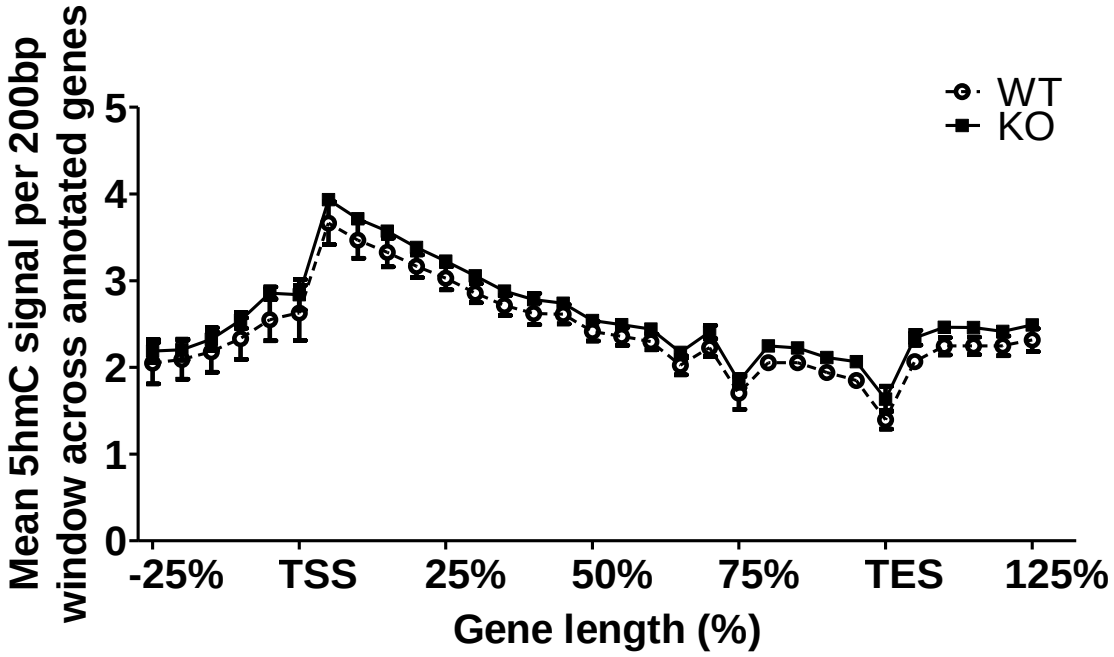


Figure 3.10. Sliding window analysis of 5-hydroxymethylcytosine DNA immunoprecipitation sequencing data. Gene length represents every annotated gene in the mouse genome normalised to 100%. n = 3/group. Data expressed as mean ± SEM.

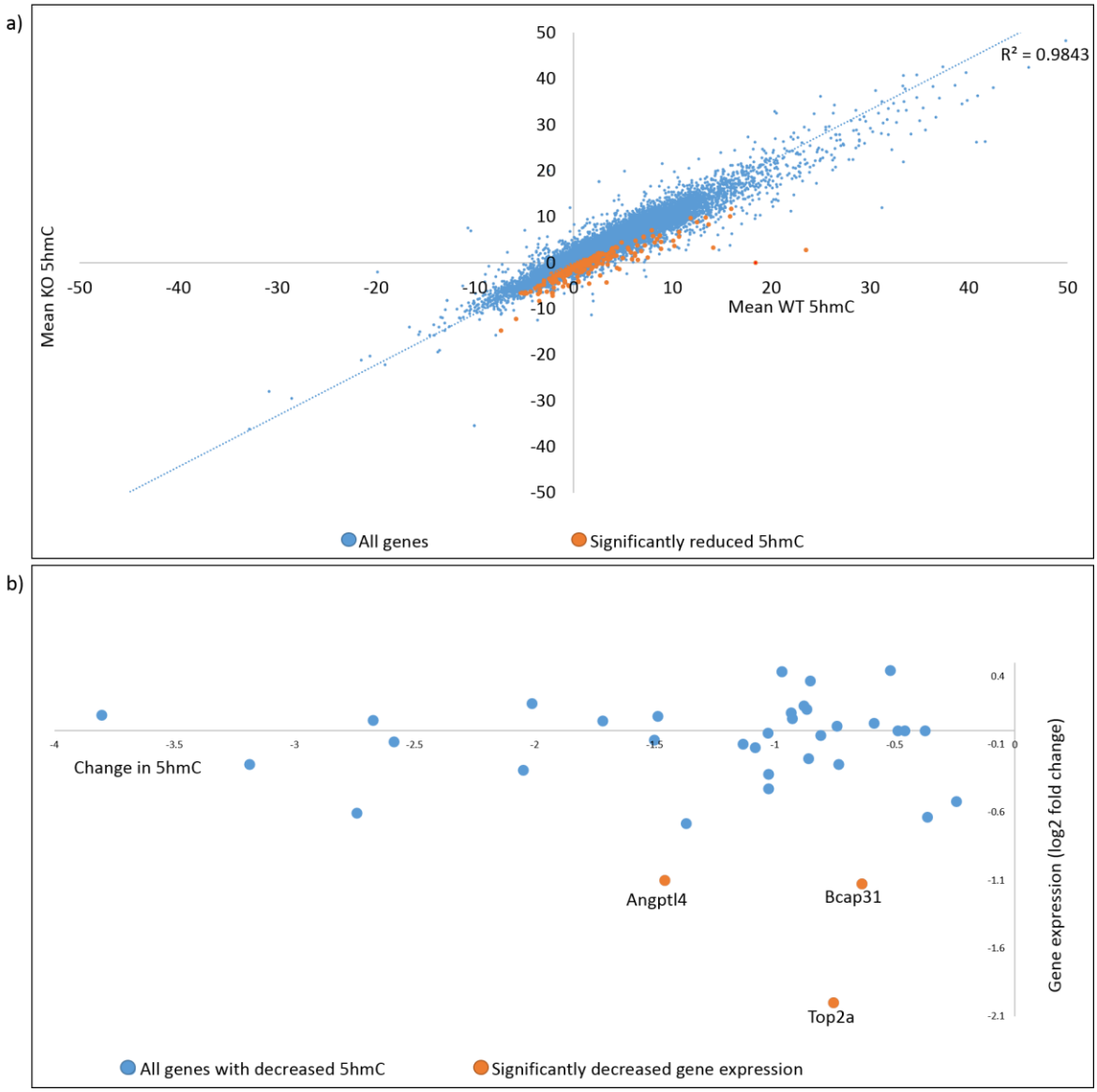


Figure 3.11. The relationship between mean 5hmC and gene expression.

a) Correlation between mean 5hmC levels across genes of adipose tissue from wildtype (WT) and knockout (KO) mice. Spearman's correlation coefficient ($R^2$) is displayed above the trendline. Orange points represent mean 5hmC levels that are significantly decreased in KO adipose tissue genes as compared to WT. b) Scatter plot showing all genes with significantly decreased 5hmC, and their correlating gene expression taken from transcriptomics data. Orange data points represent genes that have both significantly decreased 5hmC and significantly decreased gene expression. Gene names for these points are annotated. n = 3/group.

## 3.5. Discussion

In summary, I have confirmed that *Tet1* KO mice are protected against DIO in a further three independent cohorts, and identified the difference in weight gain as a difference in fat mass deposition. Indirect calorimetry studies suggest that KO mice are paradoxically expending fewer calories, a measurement that is unrelated to lean mass. Calorimetry studies also suggest that the KO mice are metabolising a greater ratio of carbohydrate to fat compared to their WT littermates. In addition, there is a suggestion of increased movement during the light phase in KO compared to WT, which also contradicts the observation of decreased calorie expenditure. Meanwhile, no change was observed in the 24-hour food intake.

*In vitro* studies using preadipocytes isolated from the stromal vascular fraction of WT and KO animals revealed no intrinsic differences in capacity for adipogenesis, except for a change in leptin expression. RNA-sequencing revealed a multitude of differentially regulated pathways, the top hits being muscle organ development (upregulated) and gluconeogenesis (downregulated). hMeDIP-seq data indicated a striking similarity in 5hmC levels between WT and KO animals with no difference in global 5hmC levels across the length of a gene. Of the genes that did have significantly decreased 5hmC levels, only three had a corresponding decrease in gene expression.

Based on these studies, the decrease in adipose tissue accumulation in KO mice does not appear to be the result of a primary adipose tissue phenotype.

### 3.5.1. Calorie expenditure and activity levels

Indirect calorimetry studies suggested that, on HFD, *Tet1* KO mice expend fewer calories than WT mice. This is paradoxical in several ways: firstly, a lean phenotype would normally be associated with *increased* calorie expenditure; and secondly, analysis of movement and activity levels would suggest that the KO mice had increased activity levels, which again is normally associated with increased calorie expenditure.

I considered that the decreased calorie expenditure could be accounted for simply by normalising to lean mass. However, this was not the case. When calorie expenditure is presented in association with lean mass, no correlation is observed ($r = 0.04743$, ns), suggesting that the decreased calorie expenditure is not simply a result of decreased lean body mass.

It is possible that the KO animals are burning fewer calories as a result of having decreased fat stores. Despite having a lower metabolic rate compared to lean mass, adipose tissue still has a metabolic energy requirement. When calorie expenditure is presented in association with total body weight,

which accounts for the metabolic effects of both fat mass and lean mass, there is an increased correlation, although it is still not significant (r = 0.2595, p = 0.23) (see Figure 3.12). This suggests that the decreased calorie expenditure in *Tet1* KO mice on HFD (and not on chow diet) could be simply the result of decreased total body weight.

Furthermore, calorie expenditure was only significantly reduced in the light phase (i.e. when animals are moving less), suggesting that during the active (dark) phase, calorie expenditure is normal. *Tet1* KO mice did show significantly increased movement on HFD (measured by number of counts using infrared sensors) during the light phase only. However, this was not shown in the dark phase (typically the more active phase) and was not accompanied by an increase in distance travelled.

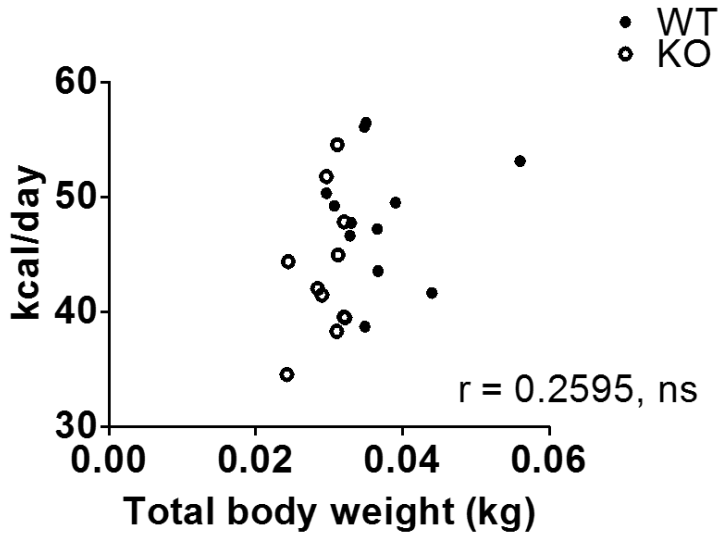


Figure 3.12. The association between calorie expenditure and body weight.

### 3.5.2. Food intake

Food intake was measured over the 24-hour calorimetry measurement period. Although no significant changes were observed in food intake over 24 hours, this may not be a long enough time period to be able to accurately judge changes in food intake. Because the time period is short, small changes in food intake in individual animals (e.g. caused by being in a new environment: new cages, new food hoppers, new water hoppers) could skew the data. Ideally, food intake analysis should be carried out over the total 11-week diet period and this is explored further in Chapter 4.

### 3.5.3. In vitro differentiation

When primary preadipocytes from *Tet1* KO and WT mice were cultured and differentiated *ex vivo*, no differences were observed in gross adipocyte morphology, lipid quantity (as measured by Oil Red O staining and spectroscopy) or gene expression of candidate genes. The only change observed was a significant and drastic reduction in leptin mRNA levels. Given that leptin is an adipokine secreted in

response to food intake, it was unexpected to see differential regulation of the gene *ex vivo*, when removed from food intake stimuli – and particularly such a marked reduction. In addition, reduced leptin mRNA was also identified in the RNA-seq data from mesenteric adipose tissue. This gives me further justification to investigate the food intake/leptin phenotype of the *Tet1* KO mice (see Chapter 5).

### 3.5.4. RNA-seq analysis

A large amount of differential gene expression was observed in mesenteric adipose tissue analysed by RNA-seq, and clustering analysis revealed two distinct groups of gene expression: WT and KO.

In the list of significantly upregulated genes, the pathway "muscle organ development" was the most overrepresented, with 4 genes (*Cacnb2*, *Unc13a*, *Unc13b* and *Myom1*) being present against an expected occurrence of 0.37. The *Unc13* gene products, which are homologous to human *UNC13* products [411], are members of the protein kinase C superfamily that lack a kinase domain, and mutations in this gene result in severely uncoordinated movement and increased accumulation of the neurotransmitter acetylcholine [412]. Of relevance, *Unc13b* expression is known to be both upregulated and activated in the kidney in hyperglycaemia, where it is thought to mediate apoptosis in glomerular cells [411, 413]. As hyperglycaemia is associated with apoptosis in multiple tissues [411], it could be plausible that *Unc13b* plays a role in hyperglycaemia-mediated apoptosis in adipose tissue. The caveat to this is that glucose tolerance tests of the *Tet1* KO mouse indicated that both fasted plasma glucose levels and plasma glucose clearance following glucose injection were no different to those of WT mice, so there is no hyperglycaemia in KOs compared to WTs. Meanwhile, *Myom1* encodes the protein myomesin 1, which is a structural stabilising protein of the muscle filaments, and *Cacnb2* encodes a calcium voltage-gated channel involved in muscle contraction. Upregulation of *Myom1* and other genes in the "muscle organ development" pathway in *Tet1* KO mice could be related to the increased percentage lean mass of the KO mice as compared to WTs.

Of the list of downregulated genes, many pathways involving metabolic processes were overrepresented, including gluconeogenesis, cellular glucose homeostasis and monosaccharide metabolic processes. Other pathways overrepresented in the list of downregulated genes include lipid, fatty acid and cholesterol metabolic processes, carbohydrate metabolic processes, and lipid transport. The downregulation of genes in the gluconeogenesis pathway (*Rbp2, Ranbp3l, Fbp2*) ties in with the increased obesity of the WT mice, given that obesity is associated with an increased contribution of gluconeogenesis to glucose production [414]. In addition, 26 genes in the list of downregulated genes come under the pathway "lipid metabolic processes", against an expected occurrence of 6.06. These are: *Ptchd4, Fasn, Acss2, Hnf4a, Rdh7, Anxa2, Mttp, Cyp4f14, Pnpla3, Apoa4, Apoa1, Mup3, Mup20, Insig1, Prkag3, Acaa1b, Hacd2, Cyp3a13, Nsdhl, Cyb5b, Hnf4g, Cyp4a10, Me1, Dbi, Slc27a2,* and

*Cyp4a14*. Decreased expression of lipid metabolic genes in the *Tet1* KO mouse is probably secondary to its lean phenotype, given that the contribution of lipids to energy expenditure is higher in obese as compared to control subjects [415], a finding also supported by my indirect calorimetry respiratory exchange ratio data in WT and KO mice, which indicated that WT mice were burning a greater proportion of lipids to carbohydrates than KO mice.

Conversely, a further 13 genes in the list of downregulated genes come under the pathway "carbohydrate metabolic processes", against an expected occurrence of 4.19: *G6pdx, Fbp2, Rbp2, B3gnt3, Mgam, Pgd, Ranbp3l, Rgn, Gpt, Gys2, Nsdhl, Ntsr2* and *Sis*. These genes are involved in a range of processes including enzymes involved in the pentose-phosphate pathway (*G6pdx*, *Pgd*), generation of TCA cycle intermediates (*Gpt*), gluconeogenesis (*Fbp2*), polysaccharide digestion (*Mgam*) and glycogen synthesis (*Gys2*). The downregulation of carbohydrate metabolic processes in the *Tet1* KO mouse could be secondary to its increased food intake and therefore decreased requirement for carbohydrate metabolism in adipose tissue.

The same could be said for all of the metabolic processes downregulated in the KO mice. Indeed, previous RNA-seq studies using C57 mice on control or high fat diet have found genes involved with amino acid metabolism are enriched in the list of differentially expressed genes [416], suggesting some overlap in the differential expression of metabolism pathway genes between this study and my study. However, the pathway analysis used in this study was done using a list of all differentially regulated genes, and was not separated into up- and down-regulated genes. Also, it is important to bear in mind possible species differences in gene expression between humans and mice. An RNA-seq study of abdominal fat in genetically fat and lean chickens also found upregulation of genes involved in adipogenesis and lipogenesis [417], again providing an overlap in pathways with my own data (e.g. lipid transport is a key process required for local adipose lipogenesis). Moreover, a study using microarray data from subcutaneous WAT from 209 female and 95 male subjects of varying overweight and obese states reported downregulation of genes encoding TCA cycle enzymes, including mitochondrial pyruvate carrier 1 (*MPC1*), pyruvate carboxylase (*PC*), pyruvate dehydrogenase (*PDHA1*), and citrate synthase (*CS*), amongst others, in lean subjects [418]. Although these genes specifically are not altered in expression in the *Tet1* KO mouse, this reinforces the idea that the changes observed in metabolic pathways are secondary to the lean phenotype of the *Tet1* KO mouse.

Furthermore, as none of these genes flagged in the pathway analysis overlap with the list of genes with significantly altered 5hmC, it is unlikely that these changes in expression are caused by the absence of *Tet1*, at least not the enzymatic effects of TET1. It is possible that TET1 is exerting effects on gene expression non-enzymatically, given that one 2011 study suggested that TET proteins might

also exert functions independently of their catalytic activity [325]. In this study, it was reported that the upregulation of TET1 target genes upon *Tet1* knockdown can also be observed in DNMT triple knockout ES cells in which both 5mC and 5hmC modifications are absent, suggesting that TET1 might repress gene transcription in a manner independent of their catalytic activity. However, it is also possible that TET1-mediated 5hmC is not in fact involved in the transcriptional regulation of these genes, but rather other epigenetic factors (e.g. histone modifications, non-coding RNAs) or transcription factors are responsible.

Importantly, the RNA-seq data suggested that *Tet1* expression was *not* downregulated in the *Tet1* KO mouse mesenteric adipose tissue, a finding confirmed by qPCR. However, the downregulation of *Tet1* mRNA and protein in the *Tet1* KO mouse was confirmed in epididymal adipose tissue (see Figure 3.9). Therefore, it is likely that lack of differential *Tet1* expression in the mesenteric adipose tissue is due to the generally low expression of *Tet1* in normal, WT mesenteric adipose tissue at this developmental stage, making the lack of *Tet1* expression in the *Tet1* KO mouse mesenteric adipose tissue undetectable. However, lack of *Tet1* could still have had an impact in mesenteric adipose tissue at earlier developmental stages.

### 3.5.5. The *Tet1* KO hydroxymethylome

The highly significant correlation between WT and KO average 5hmC levels was one of the most surprising findings of this study. Previous studies have reported a drastically decreased global hydroxymethylome in the *Tet1* KO liver tissue [308], although recent studies from our lab in older mice have found contradictory evidence for this (Lyall et al. unpublished). Regardless of the liver phenotype, the lack of changes in the adipose tissue hydroxymethylome may be due to a compensatory action of the other TET isoforms, although mRNA levels of *Tet2* and *Tet3* were unchanged (data previously displayed in Figure 3.9). However, mRNA levels of the *Tet2* and *Tet3* do not necessarily reflect protein levels or enzyme activity. Unfortunately there is currently no method for measuring enzyme activity of the individual TET isoforms.

Statistical overrepresentation pathway analysis *via* PANTHER using lists of genes with significantly increased, decreased or all change (both up- and down-regulated) mean 5hmC generated no significant results, showing that no particular genes pathways were significantly altered in 5hmC levels and suggesting that TET1 is not involved in the regulation of specific pathways within obese mesenteric adipose tissue.

Only 3 genes were reduced in both expression and mean 5hmC levels in KO mice. These were: *Angptl4*, *Bcap31* and *Top2a*. These associations could be functionally relevant. For example, *Angptl4*, also known as *Fiaf* (fasting-induced adipose factor), encodes a novel adipokine that directly regulates

lipid metabolism, whose expression is under control of the PPAR family [419]. Given the previously discussed role of *Tet1* in transcriptional activation of PPARγ target genes [420], it is plausible that *Tet1* KO inhibits PPAR activation of *Angptl4*. On the other hand, it is well-established that *Angptl4* expression is decreased in states of hypoxia [421]. Given that hypoxia is increased in obese adipose tissue, it might be expected that *Angptl4* expression would be increased in the KO mouse, which exhibits decreased fat mass (therefore probably has less adipose tissue hypoxia). In this regard, decreased *Angptl4* expression in the *Tet1* KO mouse does not necessarily fit with its lean phenotype.

*Top2a* encodes DNA topoisomerase II, an enzyme that controls and alters the topologic states of DNA during transcription. *Top2a* has also been implicated in regulation of PPARγ activation of downstream genes [422, 423]. In 2015, Lehmann et al reported that topoisomerase II activity induces the recruitment of ADP-ribosyl transferase to the PPAR binding site upstream of PPAR target genes, which is necessary to communicate the signal of endogenous PPAR ligand binding [422]. Since TET1 is also involved with PPAR activation of target genes [420], *Top2a* could be synergistically downregulated. However, *Top2b*, a paralogue of *Top2a*, has decreased mean 5hmC but its mRNA expression is unchanged, suggesting that perhaps 5hmC is unrelated to gene expression in this case.

In fact, these three associations could be simply be associations without any functional relevance. To test this, I could carry out *in vitro* TET inhibition studies to determine if it is the enzymatic function of TET that causes decreased expression of these three genes (although this would not allow me to look at the activity of the different TET isoforms).

To determine whether these three genes had altered expression as a primary result of *Tet1* KO or as a secondary result of a lean phenotype, I carried out qPCR analysis of these genes in mesenteric adipose tissue from control-fed WT and KO mice. Although I was unable to design a working assay for *Angptl4*, the expression levels of *Bcap31* and *Top2a* are displayed in Figure 3.13. As shown in Figure 3.13, both *Bcap31* and *Top2a* expression is unchanged in a range of adipose tissue depots taken from mice fed a control diet for 11 weeks. This suggests that the changes in the expression of these genes are a result secondary to the reduced adiposity of the KO mice rather than a primary result of the *Tet1* gene deletion.

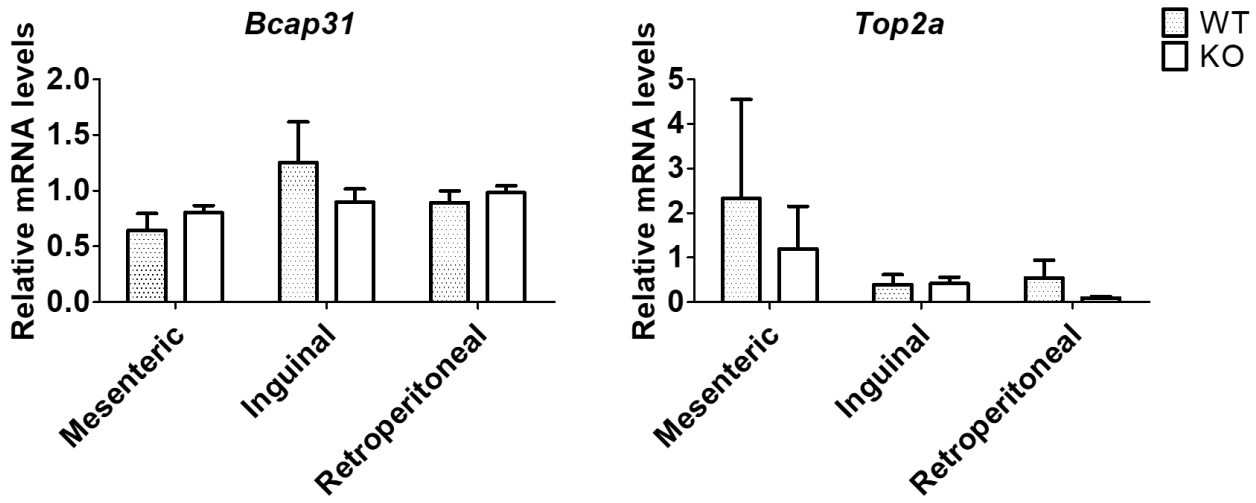


Figure 3.13. Relative mRNA expression of *Bcap31* and *Top2a* in mesenteric, inguinal and retroperitoneal adipose tissue depots from wildtype (WT) and *Tet1* knockout (KO) mice fed a control diet for 11 weeks.

### 3.5.6. A limitation of the high fat diet sequencing study

The above findings highlight a limitation of the RNA-seq and hMeDIP-seq studies: control samples were not sequenced from animals on control diet. Therefore, it is impossible to tell from the sequencing analysis alone whether changes in gene expression are primary, due to the *Tet1* KO, or secondary, due to the decreased fat of the KO mice. However, RNA from control diet-fed animals was used for validation of key genes of interest, such as the changes in *Bcap31* and *Top2a* (shown in Figure 3.13) and the change in leptin mRNA (data shown in Chapter 4).

In addition, findings from the indirect calorimetry may also be secondary to the obese/lean phenotype. For example, the observed decrease in respiratory exchange ratio (RER) in KO mice, indicating increased metabolism of carbohydrate, could simply be the result of decreased fat stores; therefore animals are obtaining a greater proportion of their energy from carbohydrate (i.e. directly from food) rather than lipid (i.e. from their own adipose stores). The fact that no difference was observed in RER between WT and KO on chow diet supports this hypothesis.

Furthermore, it has been shown that changes in diet can strongly influence the serum metabolite profile of mice, especially those involved with energy metabolism and glucose utilisation, even when plasma is collected from animals in a fasted state [424]. The modified nutrient composition and lower protein availability of the high fat diet can instantly modulate serum metabolite levels even before the occurrence of obesity, because many metabolites derive from *de novo* synthesis from dietary components [425]. Indeed, it could be that in my study the expression of the enzymes involved in metabolic pathways may also be altered in response to altered dietary nutrient intake, rather than in response to obesity, or indeed the KO of *Tet1*.

In summary, I have shown in a further three independent cohorts that *Tet1* KO mice are partially resistant to diet-induced obesity. This does not seem to be the result of an altered capacity for adipogenesis, or the result of 5hmC-mediated transcriptional changes. The mechanism behind the reduced weight gain of the *Tet1* KO mouse will be explored further in Chapter 4.

# 4. Physiological control of food intake in the *Tet1* knockout mouse

## 4.1. Introduction

The findings from Chapter 3 indicated that that the obesity-resistant phenotype of the *Tet1* KO mouse was not a primary adipose tissue phenotype, but may be a phenotype secondary to *Tet1* deletion in other tissues. However, the observation that *Lep* mRNA levels (coding for the protein leptin) were significantly and markedly decreased in the mesenteric adipose tissue of *Tet1* KO mice when compared to wildtype called for further examination of the leptin phenotype, and by extension, the food intake phenotype.

While no significant differences were observed in the 24-hour food intake of the KO and WT mice, KO food intake was consistently lower than that of WT, indicating that analysis of food intake over a longer period of time, i.e. 11 weeks of high fat-feeding, may provide greater power to reveal any genotype differences.

Leptin is the satiety hormone secreted from adipose tissue in response to eating. In particular, leptin is secreted at higher levels following feeding with foods with a high glycemic index [205]. Mutations in the *LEP* gene result in an insatiable appetite and severe obesity from childhood [155], and plasma leptin levels are negatively correlated with BMI [207]. The discovery of leptin as a satiety hormone was met with much excitement regarding its potential application as a treatment for obesity. However, while recombinant leptin therapy is effective in treating monogenic forms of obesity that involve mutations in the leptin gene and its signalling pathway [239], the possibility of its application in more complex, polygenic obesity was soon disregarded when it was found that leptin sensitivity, much like that of insulin, is plastic and overexposure to the hormone results in leptin resistance [240]. This is the case in obesity, in which high levels of leptin are secreted due to increased food intake and increased adipose tissue, but the subject no longer receives the satiety signals [241].

In this chapter I further investigated the food intake phenotype of the *Tet1* knockout mouse, examined the *Lep* mRNA and leptin protein levels and its leptin sensitivity, and further probed the role of TET1 in regulating *Lep* transcription.

## 4.2. Hypotheses & aims

**Hypotheses:**

- *Tet1* KO mice have reduced transcription of *Lep* mRNA across all adipose tissue depots, and a corresponding reduction in plasma leptin.
- KO mice have significantly reduced food intake over the 11-week HFD.
- Decreased *Lep* transcription and serum leptin protein levels in KO mice allow KOs to retain leptin sensitivity, while WT mice become leptin resistant on HFD.
- Decreased *Lep* transcription is the result of TET1-mediated changes in 5mC and/or 5hmC levels.

**Aims:**

- Investigate *Lep* mRNA levels across a range of WT and KO mouse adipose tissue depots.
- Investigate serum leptin protein levels in the WT and KO mice.
- Investigate the food intake phenotype of the *Tet1* KO and WT mice through weekly food intake tracking.
- If a difference in food intake is observed over the 11-week HFD, carry out paired feeding studies to determine whether the difference in food intake is accountable for the difference in weight gain.
- Investigate the leptin sensitivity of the WT and KO mice.
- Investigate the role of CpG methylation and hydroxymethylation in *Lep* transcription by interrogating existing hMeDIP-seq data from WT and KO mouse mesenteric adipose tissue, and through bisulfite conversion pyrosequencing to obtain methylation data at a higher resolution (base-pair resolution).
- Investigate whether knocking down *Tet1 in vitro* drives the same changes observed in the *Tet1* KO *in vivo.*

## 4.3. Methods

To investigate food intake, male WT and *Tet1* KO mice (age 12-23 weeks at the start of the study) were maintained on CD or HFD for 11 weeks, and food intake and body weight was tracked weekly. In the case of the paired feeding study, KO food intake on HFD was measured daily and daily WT food allowance was matched to KO *ad lib* food intake for the previous day. See section 2.2.4 for further details on the paired feeding protocol.

The leptin treatment study was carried out before and after 6-week *ad lib* HFD (section 2.2.8). Animals were treated with saline or leptin (3mg/kg) at 9am and food intake was measured hourly for

12 hours following treatment (9am–9pm). In all animal studies, after 11 weeks (or 6 weeks for the leptin treatment study), mice were killed, and adipose tissue and fasted plasma were collected.

In vitro *Tet1* knockdown was carried out in primary preadipocytes isolated from inguinal adipose tissue of wildtype C57BL/6J mice, cultured on collagen I-coated plates (Corning, Deeside, UK) for up to 3 passages, following a previously published protocol [408]. In the evening before the transfection, confluent preadipocytes in 12-well collagen I-coated plates were trypsinzed and seeded 1:1. The following afternoon (allowing enough time for the preadipocytes to adhere to the bottom of the well), cells were transfected with siRNA using HiPerFect reagent (Qiagen, Manchester, UK). For one well of a 12-well plate, 40nM siRNA was mixed with 6 µl HiPerFect reagent in a total of 200µl serum free α-MEM (without antibiotics) and incubated for 15 min at room temperature. During the incubation, 200µl growth media (α-MEM with 10% FBS without antibiotics) was added to each well. The plate was swirled intermittently during the incubation to prevent cells from drying out. The pre-incubated siRNA-HiPerFect mix was added dropwise to the wells, resulting in total 400µl of α-MEM with 5% FBS. After gently rocking the plate, it was transferred to cell culture incubator. After overnight transfection, cells were re-fed with regular growth media and differentiation was initiated. Cells were differentiated using the adipocyte differentiation protocol (section 2.4.5) for 5 days, after which RNA was extracted.

## 4.4. Results

### 4.4.1. Further analysis of food intake

Food intake was examined throughout the whole 11-week high fat diet (HFD) and control diet (CD) rather than just during the 24-hour period in metabolic cages. Figure 4.1 shows that genotype had a significant overall effect on food intake over time on both CD (Figure 4.1a) and HFD (Figure 4.1b), with KO animals eating significantly fewer weekly calories over the 11 week diet intervention, as analysed by two-way ANOVA. However, t-tests analysing the total 11-week calorie intake indicated a significant decrease only on HFD (Figure 4.1d), not CD (Figure 4.1c). This suggested that decreased food intake in KO mice on CD was an emerging property of genotype that was dependent on the variable of time. These data support the hypothesis that the decreased adiposity of the *Tet1* KO mouse is a result of decreased food intake.

This decreased food intake observed has an effect on body weight on both diet interventions (Figure 4.2). As discussed in Chapter 3, *Tet1* KO mice gained significantly less weight on HFD (Figure 4.2). In the CD study, two-way ANOVA indicated that genotype had an overall significant effect on weight gain over 11 weeks on CD (Figure 4.2).

In addition, feed efficiency (ratio of calorie input to weight gain) was analysed to indicate the efficiency with which WT and KO animals convert calories to kg body mass (Figure 4.3a). No significant difference was observed in feed efficiency, suggesting that there is no difference in the nutrient absorption or energy production of WT and KO animals, but rather that any differences observed are more likely to be a result of neuroendocrine control of food intake. Furthermore, analysis of covariance (ANCOVA) revealed that there was a correlation between food intake and weight gain (Figure 4.3b). Pearson's correlation coefficient for these data is 0.5853 ($p = 0.0009$), indicating a highly significant positive correlation.

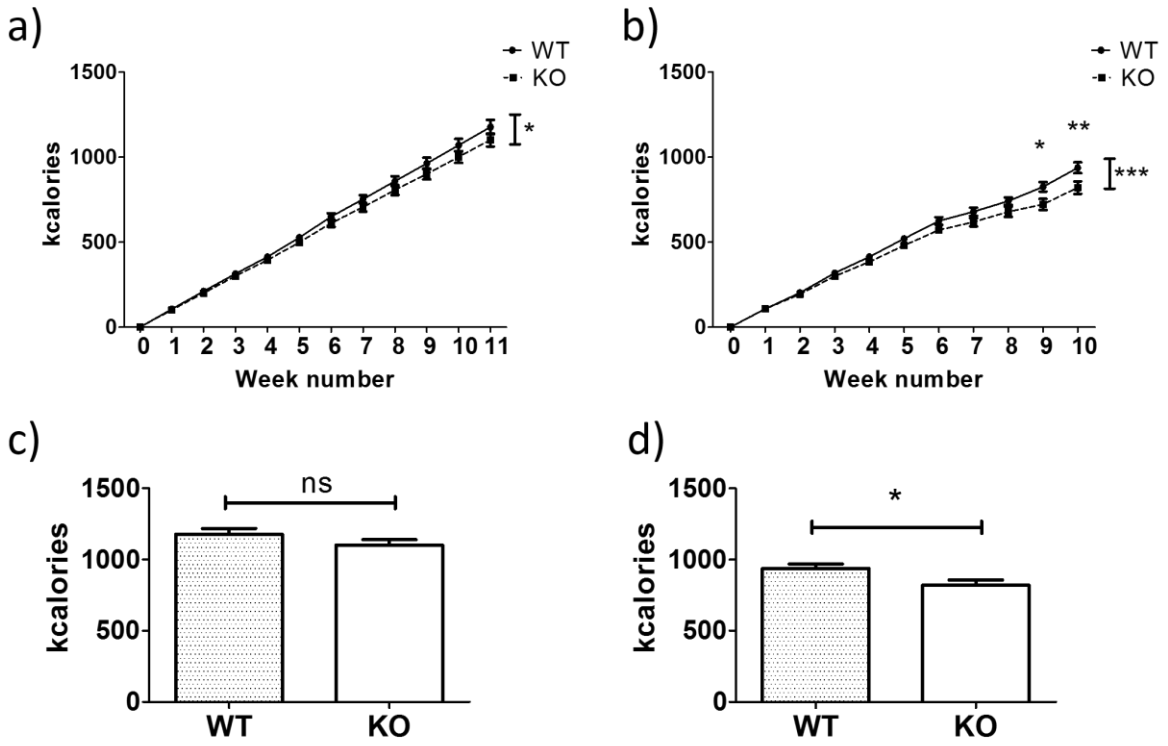


Figure 4.1. Food intake of *Tet1* knockout (KO) and wildtype (WT) mice.

Food intake of *Tet1* knockout (KO) and wildtype (WT) mice maintained on a) control diet (n = 5/group) and b) high fat diet (n = 15/group) for 11 weeks. Mean ± SEM. *p<0.05; **p<0.01; ***p<0.001. Analysed using a repeated measures ANOVA with Bonferroni post-hoc tests. c) Total food intake over 11 weeks on control diet (n = 5/group) and d) high fat diet (n = 8/group). Analysed using student's t-test. Mean ± SEM.

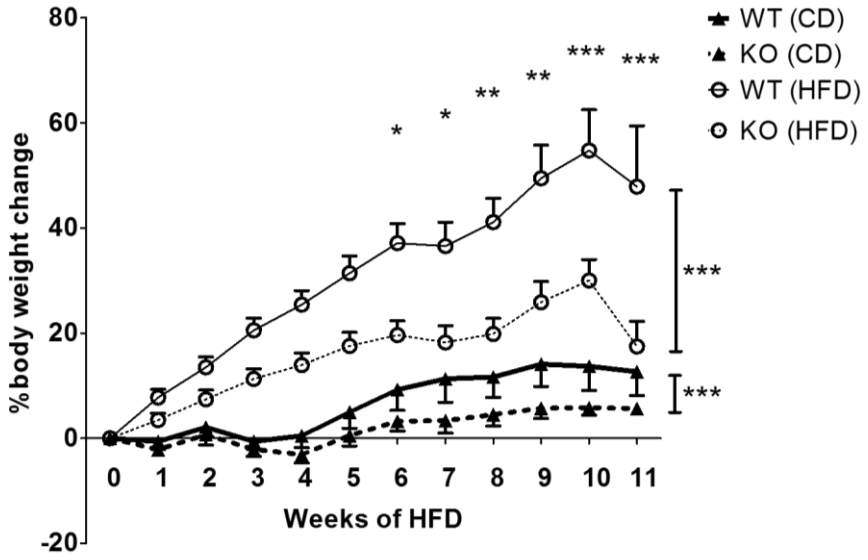


Figure 4.2. Weight gain over time on control diet (CD) and high fat diet (HFD).

*p<0.05; **p<0.01; ***p<0.001. Analysed using two-way repeated measures ANOVA with Bonferroni post-hoc tests.

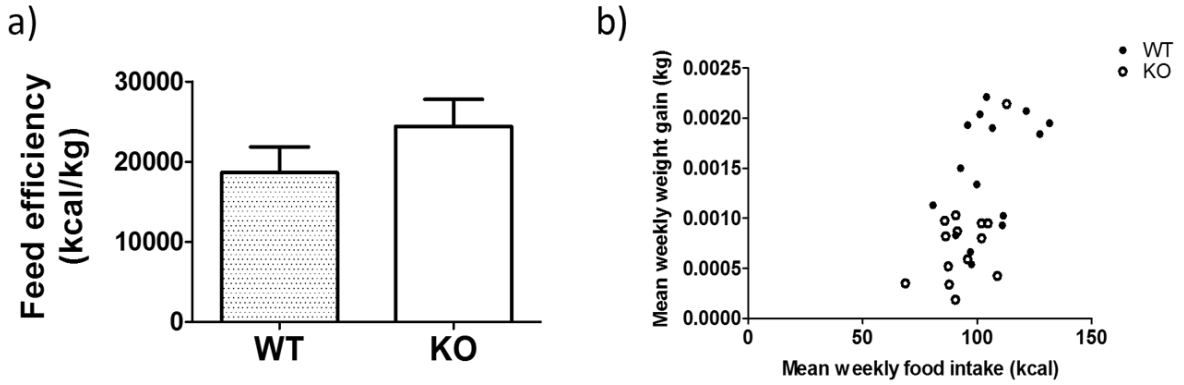


Figure 4.3. The relationship between food intake and weight gain.

a) Feed efficiency in wildtype (WT) and *Tet1* knockout (KO) mice on high fat diet. Mean ± SEM, n = 9/group.

b) Analysis of co-variance in food intake and weight gain on high fat diet. Pearson's correlation coefficient = 0.5853 (p = 0.0009)

### 4.4.2. Paired feeding

To confirm that the difference in weight gain the *Tet1* KO mouse was due to a decreased food intake, a paired feeding study was carried out (Figure 4.4) in which KO mice were given *ad lib* access to HFD, their food intake was measured daily and WT mice were fed exactly the same amount of HFD. Figure 4.4 showed that when WT mouse food intake was paired to KO, the weight gain of the two groups was comparable, indicating that the KO adipose phenotype is indeed due to decreased food intake.

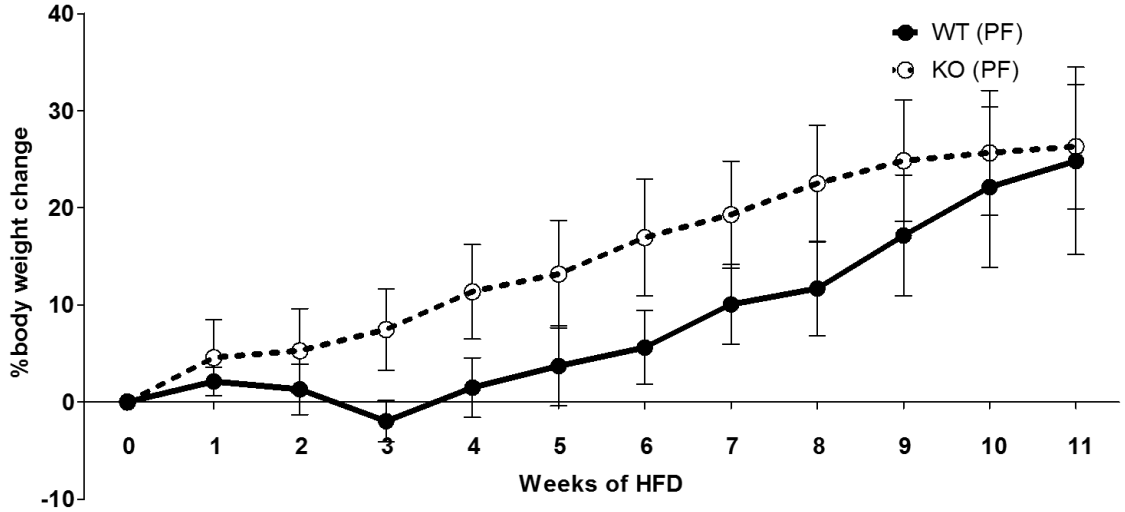


Figure 4.4. Weight gain in wildtype (WT) and *Tet1* KO mice under paired feeding (PF) protocol on high fat diet. Mean ± SEM; n = 5/group.

### 4.4.3. Leptin expression

Results from the RNA sequencing study in section 3.4.4 showed that leptin expression was significantly reduced in the mesenteric adipose tissue of *Tet1* KO mice. To further investigate this phenotype, *Lep* mRNA levels were measured in various adipose tissue depots and also in RNA from primary adipocytes differentiated for two weeks *in vitro* (Figure 4.5a). In all adipose tissue depots, and even when adipocytes had been cultured *in vitro* for 2 weeks, leptin mRNA levels were significantly decreased. Consistent with the reduction in mRNA, leptin protein in fasted plasma samples was also significantly decreased (Figure 4.5b). The reduction in *Lep* mRNA is also observed in animals fed control diet for 11 weeks, but only in the inguinal adipose depot and in adipocytes differentiated *in vitro* (Figure 4.5c). This suggests that the reduction in leptin expression in *Tet1* KO mice may be intrinsic, rather than an effect of reduced weight gain on HFD. Although, as the reduction in *Lep* expression is only present on CD in the inguinal adipose depot and *in vitro*, it could be that HFD can exaggerate the differences in *Lep* expression.

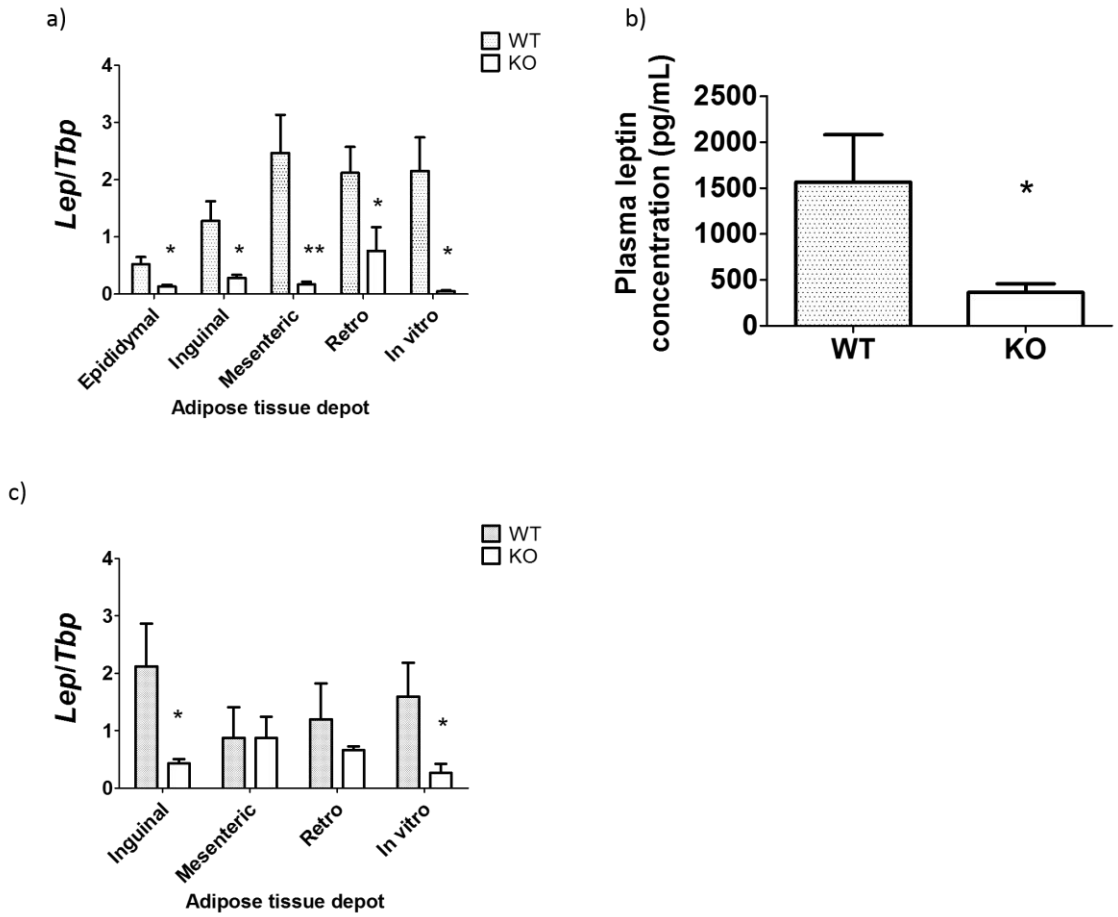


Figure 4.5. Leptin levels in wildtype and *Tet1* knockout mice.

a) Leptin mRNA levels in inguinal, mesenteric and retroperitoneal (retro) adipose tissue depots and *in vitro* taken from wildtype (WT) and *Tet1* knockout (KO) mice on 11-week high fat diet. Mean ± SEM, n = 6/group. Analysed by student's t test. b) Leptin protein levels in fasted plasma samples of WT and *Tet1* KO mice after 11-week high fat diet. Mean ± SEM, n = 6/group. Analysed by student's t test. c) Leptin mRNA levels in inguinal, mesenteric and retroperitoneal (retro) adipose tissue depots and *in vitro* taken from WT and *Tet1* KO mice on 11-week control diet. Mean ± SEM, n = 5/group. Analysed by student's t test. *p<0.5; **p<0.01.

### 4.4.4. Leptin sensitivity

Reduced leptin transcription and circulating leptin levels were consistent with lower fat mass. However, reduced food intake implies that the KO mice are more sensitive to the reduced levels of the appetite-suppressing hormone. To test this, leptin sensitivity was tested by injecting leptin intraveneously (corrected for total body weight) at 9am and measuring the effect on food intake over the following 12 hours (9am to 9pm). WT and KO animals were treated with 3mg/kg recombinant leptin and food intake was tracked for the following 12 hours. This study was carried out immediately before (Figure 4.6a) and immediately after (Figure 4.6b) animals were given *ad lib* access to HFD for 6 weeks. Food intake is decreased in KO animals after leptin treatment, as compared to vehicle

treatment, but WT food intake is unchanged. This occurs even before the 6-week HFD, indicating that the KO mice are intrinsically more leptin sensitive.

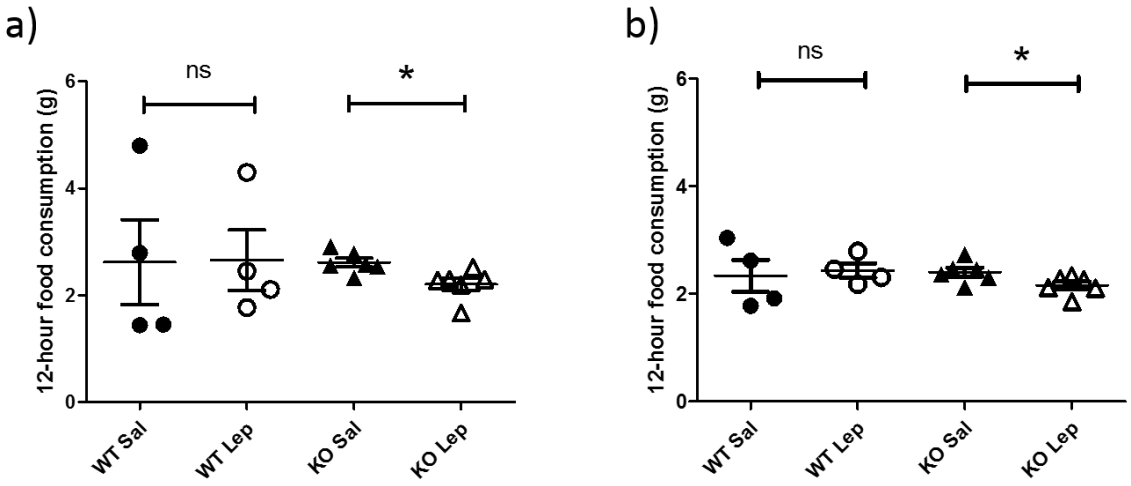


Figure 4.6. 12-hour food intake of wildtype (WT) and *Tet1* knockout (KO) mice treated with leptin.
12-hour food intake of wildtype (WT) and *Tet1* knockout (KO) mice treated with saline (Sal) or leptin (Lep) a) before 6-week *ad libitum* high fat diet; and b) immediately after 6 week *ad libitum* high fat diet. Statistical significance calculated using a student's t-test. Mean ± SEM; n = 4 and 6/group, respectively. *$p<0.05$.

### 4.4.5. Leptin promoter methylation status

To investigate the upstream mechanisms of regulation of leptin transcription, the DNA immunoprecipitation sequencing (hMedIP-seq) data were mined to reveal 5hmC levels across sliding 200bp windows of the *Lep* gene (Figure 4.7a) and the *Lep* promoter (Figure 4.7b) in mesenteric adipose tissue taken from WT and KO mice fed an 11-week HFD. No differences were observed in 5hmC levels across sliding windows. In addition, mean 5hmC levels across the leptin gene (Figure 4.7c) were unchanged. Bisulfite conversion pyrosequencing was carried out in DNA from inguinal adipose tissue of control diet-fed WT and KO mice (in which differences in *Lep* expression was observed – see Figure 4.5c), to determine 5mC levels at specific CpGs in a region of the leptin promoter proximal to the transcriptional start site (Figure 4.7d). Again, no significant differences were found in methylation levels in the leptin promoter. Based on these analyses, it appears that leptin promoter methylation/hydroxymethylation is not the main mechanism of transcriptional control under these circumstances.

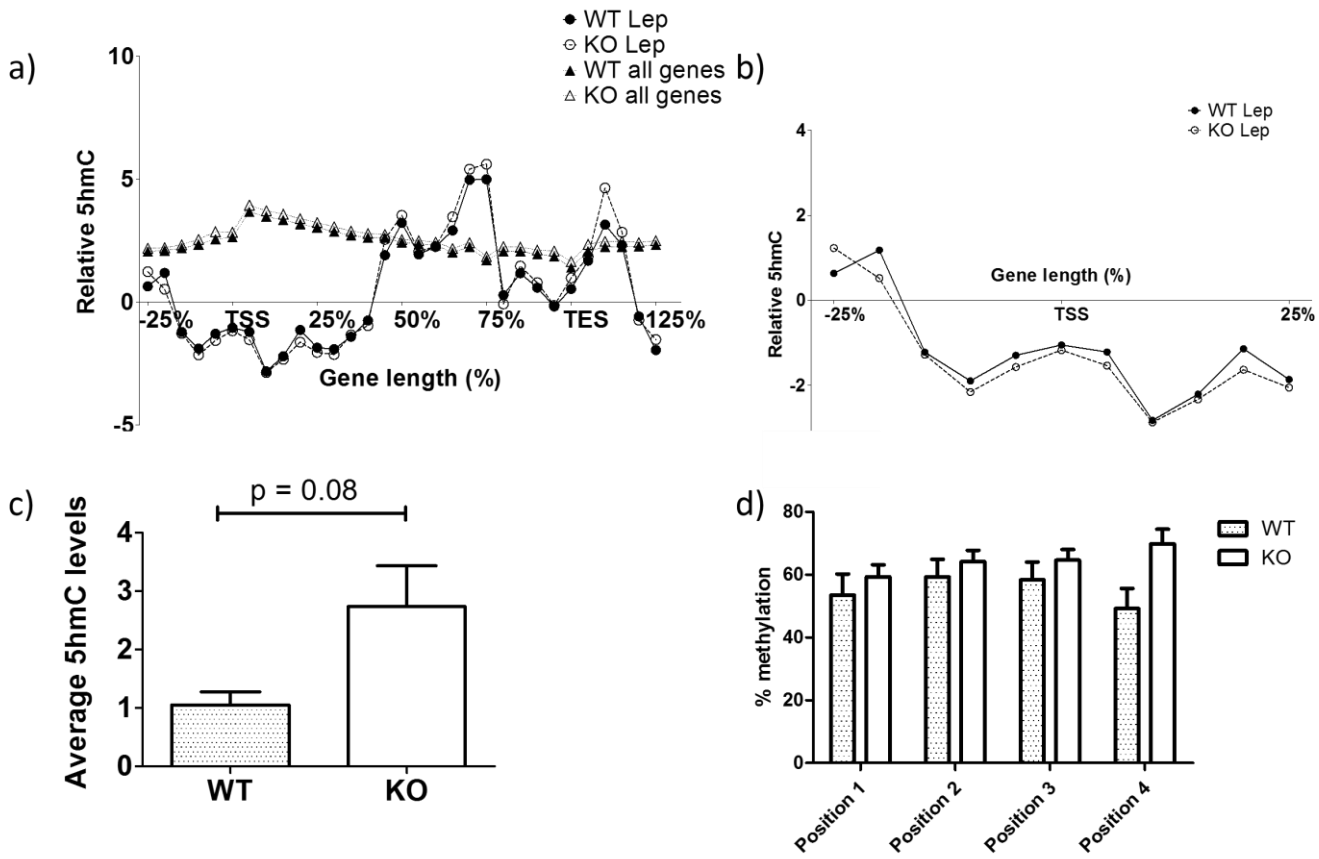


Figure 4.7. Cytosine hydroxymethylation and methylation levels of the leptin gene in wildtype and *Tet1* knockout mice.

a) Gene hydroxymethylation (5hmC) levels across sliding 200bp windows in the *Lep* gene in wildtype (WT) and *Tet1* knockout (KO) mice, as determined by DNA immunoprecipitation sequencing. Plotted against mean sliding window analysis for all genes for comparison. TSS = transcriptional start site; TES = transcriptional end site. Mean ± SEM, n = 3/group. b) An enlarged view of 5hmC levels across the leptin promoter (TSS ± 25%). c) Mean total gene hydroxymethylation levels in the *Lep* gene in WT and *Tet1* KO mice, as determined by DNA immunoprecipitation sequencing. Mean ± SEM, n = 3/group. d) Leptin promoter percentage methylation levels in inguinal adipose tissue from control diet-fed wildtype (WT) and *Tet1* knockout (KO) mice in the promoter region proximal to the transcriptional start site, as determined by bisulfite conversion pyrosequencing. Mean ± SEM, n = 6/group.

### 4.4.6. In vitro *Tet1* knockdown

Finally, a protocol for *Tet1* knockdown by siRNA was optimised in primary preadipocytes, intended for use as an *in vitro* model to further investigate the mechanisms behind TET1-mediated downregulation of *Lep* transcription. *Tet1* was successfully knocked down in primary preadipocytes (Figure 4.8a). However, *Tet2* and *Tet3* transcription appear to respond in a compensatory fashion with upregulation of transcription of these two isoforms.

Furthermore, following 5 days of differentiation in order to produce cells that are mature adipocyte-like, *Tet1* expression decreased in the negative control, such that the knockdown no longer produced a significant effect on *Tet1* transcription. To further confirm this, a timeline study was carried out in which *Tet* expression was measured daily over a period of 5 days of differentiation (Figure 4.8b). While this study was carried out only with $n = 1$ due to limitations of tissue availability, it appears that *Tet1* expression does indeed decrease over 5 days of differentiation, while *Tet2* may increase slightly, and *Tet3* expression does not seem to change.

No change was observed in leptin expression following *Tet1* knockdown (Figure 4.8c). This model therefore requires further development if it is to be used to investigate the role of TET1 in regulating *Lep* transcription.

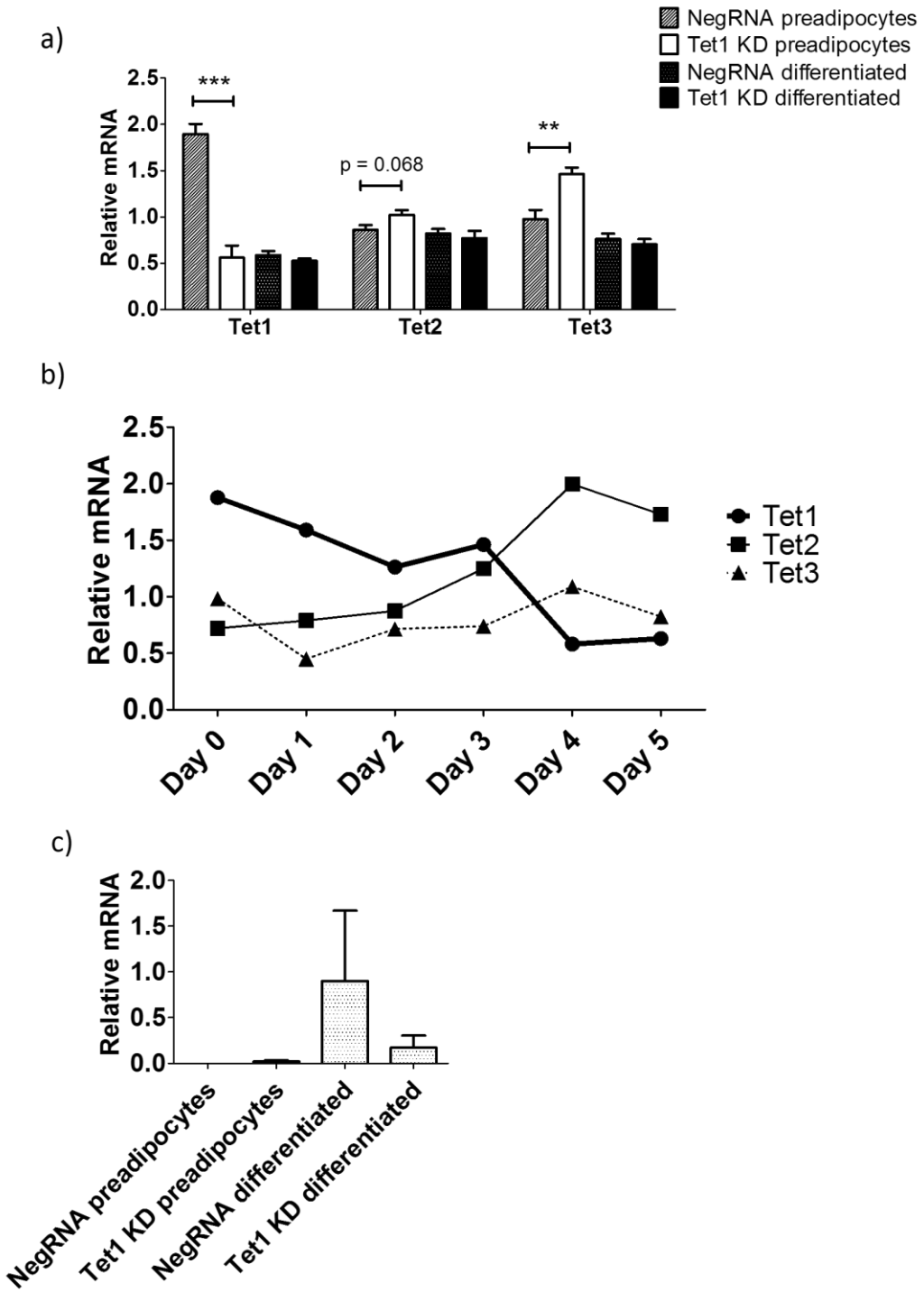


Figure 4.8. *Tet1* knockdown in primary preadipocytes followed by 5 days of adipocyte differentiation. a) *Tet1, Tet2 and Tet3* mRNA levels in preadipocytes and differentiated adipocytes treated with negative control RNA (NegRNA) or *Tet1*-targeted siRNA (*Tet1* KD). Mean ± SEM, n = 4/group. Statistical significance determined using student's t-test. *p<0.01; **p<0.001. b) *Tet1, Tet2 and Tet3* mRNA levels measured daily in primary preadipocytes (Day 0) followed by 5 days of exposure to an adipocyte differentiation cocktail. n = 1/group. c) Leptin mRNA levels in preadipocytes and differentiated cells treated with negative control RNA (NegRNA) or *Tet1*-targeted siRNA (*Tet1* KD). Mean ± SEM, n = 4/group. Statistical significance determined using students t-test.

## 4.5. Discussion

### 4.5.1. *Tet1* knockout mice have decreased food intake

In this chapter, I determined that *Tet1* KO mice had significantly decreased food intake on an 11-week HFD and an 11-week CD. This reduction in food intake results in a significant reduction in weight gain on both diet interventions. Analysis of food intake by food conversion ratio suggests that the ratio of calorie input to weight gain is no different between WT and KO animals, indicating that the food intake is sufficient to account for differences in weight gain. To further support this, a highly significant ($p = 0.0009$) positive correlation was observed by analysis of covariance (ANCOVA) of food intake versus weight gain. ANCOVA analysis was chosen in these circumstances based on the recommendations of the Speakman guide to analysis of mouse metabolism [426]. In addition, a paired feeding HFD study revealed that reducing WT food intake to that of the KO food intake was sufficient to normalise any differences in weight gain on HFD, suggesting that the food intake phenotype of the KO mice is the predominant mechanism behind the KO lean phenotype.

### 4.5.2. Leptin transcription is decreased in the *Tet1* knockout mouse

Further mRNA studies in this chapter found that leptin was significantly reduced in KO animals in a range of adipose tissue depots taken from WT and KO animals after 11-week HFD, a finding confirmed in the plasma protein levels of leptin. Furthermore, this reduction in leptin mRNA is also observed in certain adipose depots from animals fed for 11 weeks on CD, further reinforcing the idea that the reduction in leptin transcription in the *Tet1* KO mouse is unrelated to decreased fat mass, opening up the possibility that leptin transcription is decreased due to a primary effect of *Tet1* KO.

### 4.5.3. Leptin sensitivity is increased in the *Tet1* knockout mouse

Leptin treatment studies revealed that KO mice have increased leptin sensitivity compared to WT mice, even before *ad lib* HFD. Since leptin sensitivity is decreased in obesity [241], we may expect KO mice to have increased sensitivity due to their decreased adiposity, but the fact that leptin sensitivity was increased even before *ad lib* HFD in the KO mice suggests that the increased leptin sensitivity in the KO mice is intrinsic rather than a result of decreased levels of obesity in the KO mice. My working hypothesis is that decreased *Lep* transcription occurs as a direct result of *Tet1* KO. This results in decreased plasma leptin, allowing the KO mice to retain leptin sensitivity and moderate their food intake appropriately. Meanwhile, the WT mice have leptin levels that reflect their greater fat mass and the expected development of leptin resistance in obesity, so that they can't moderate their food intake.

### 4.5.4. Leptin and epigenetics

Melzer et al. demonstrated that methylation of the *LEP* promoter can modulate or silence *LEP* transcription when driving the expression of a luciferase reporter gene in a human adipose cell line [427], suggesting that leptin promoter methylation can modulate gene expression. The leptin promoter is methylated in both human and mouse somatic tissues and displays epigenetic variation which is highly associated with transcription [428, 429]. A mosaic pool of unmethylated and densely methylated *Lep* epialleles exists in mouse adipose tissue, compared to DNA from brain, liver and spleen in which *Lep* epialleles are mostly hypermethylated [429]. Analysis of dIP-seq data did not suggest that there was any overall difference in 5hmC levels in the *Lep* gene of *Tet1* KO mice (neither across sliding 200bp windows nor across the total gene), and bisulfite conversion pyrosequencing did not reveal any difference in 5mC at specific CpGs upstream of the leptin promoter – a region in which methylation levels are thought to be important for transcriptional regulation [429]. Although bisulfite pyrosequencing does not distinguish between 5hmC and 5mC, based on the lack of changes observed in 5hmC in the dIP-seq data, it can be inferred that the levels of 5mC are unchanged too. My results do not fit with the suggestion that leptin expression is modulated by promoter DNA methylation: in inguinal adipose tissue taken from mice on an 11-week CD, although leptin expression is significantly reduced ($p = 0.0358$) in KO mice, leptin promoter methylation is unchanged. According to these previous studies, a significant reduction in leptin expression would be associated with an increase in leptin promoter methylation. One explanation could be that I only examined 4 CpGs within the leptin promoter due to the logistics of designing an effective assay for the promoter region. The sites of these CpGs within the leptin promoter are displayed in Figure 4.9. Perhaps examination of further CpGs in the proximal *Lep* promoter may reveal further differences. On the other hand, the 4 CpGs within my assay include a CpG that has been described as "key" for leptin modulation: the CpG within the C-EBPα binding motif (labelled position 4 in Figure 4.7b; or position 11 in Figure 4.9), which has been suggested to prevent C-EBPα binding when methylated, thus downregulating transcription [427]. Another CpG considered to be key in human leptin transcriptional regulation is the CpG in the TATA-box just upstream of the transcriptional start site, which is not present in the mouse promoter (see Figure 4.9), so I am unable to draw comparisons with this site.

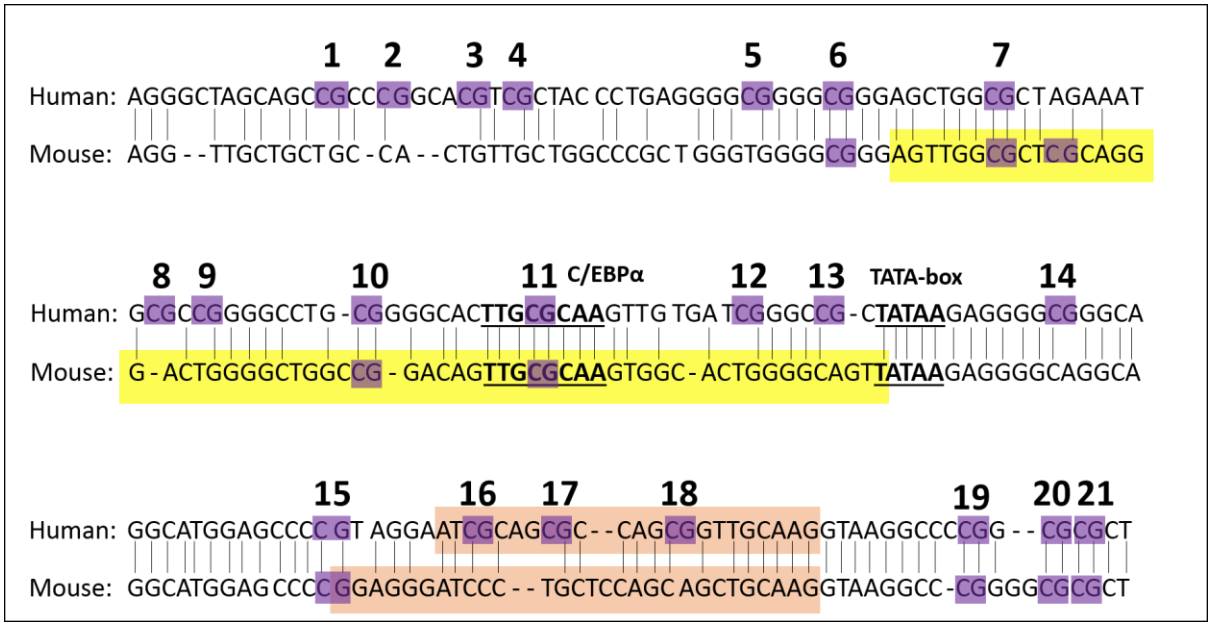


Figure 4.9. The leptin promoter in human and mouse.
CpG sites are highlighted in purple and numbered 1-21. The region covered by my bisulfite pyrosequencing assay is highlighted in yellow. Exon 1 is highlighted in red. The C/EBPα binding site and the TATA-box are underlined in bold and labelled. Base pairs homologous between human and mouse are indicated by a black line between lines. Figure adapted from Stöger et al. 2006 [429].

In 2008, Stöger speculated that the leptin gene may be responsive to environmental cues and can therefore acquire a "thrifty epigenotype", i.e. an epigenome that confers greater energy efficiency in an individual or predisposes one to obesity [343]. For example, in Pima Indians, plasma leptin concentrations are lower in individuals with a tendency to gain weight, but no allelic *LEP* variants have been identified in this population [430, 431], suggesting that epiallele variants may be responsible for variation in plasma leptin.

Indeed, it has been found that the methylation status of the proximal leptin promoter was highly correlated to transcriptional activation or silencing, and that *in vitro* demethylation (by decitabine) was sufficient to increase leptin transcription in primary fibroblasts, and even induce *de novo* leptin expression in HeLa cells [432]. Furthermore, *in vitro* differentiation of preadipocytes to adipocytes correlates with reduction of methylation at the promoter and induction of *LEP* expression [427, 433], while whole adipose tissue contains *LEP* epialleles with lower methylation levels compared to that of peripheral blood leukocytes [429], suggesting the importance of DNA demethylation in mature adipocyte expression of *LEP*.

Regarding the role of *LEP* promoter methylation in obesity, much of the data is contradictory. As *LEP* expression is increased in obesity [434], and *LEP* promoter demethylation correlates with induction of *LEP* expression in adipocyte differentiation [427, 433], it could be hypothesised that the obesity-

associated increase in *LEP* expression correlates with decreased methylation. Indeed, methylation of the *LEP* promoter in humans is negatively correlated with BMI [435]. In addition, in the adipose tissue of diet-induced obese (DIO) mice, leptin promoter methylation was decreased by HFD feeding during the first 8 weeks [436]. Contradictory to this, the same study reported that promoter methylation decreased after 12 weeks of HFD feeding compared to control diet fed mice, although *Lep* expression was still increased in DIO mice [436]. The authors suggested that the decrease in *Lep* promoter methylation in obesity was due to a transcriptional negative feedback mechanism, which was still insufficient to return *Lep* expression back to normal levels. Further studies support these observations. For example, in high fat-fed Wistar rats, the *Lep* promoter had increased methylation compared to control-fed rats [437]. Moreover, obese subjects who underwent weight loss of 5% body mass or higher had decreased leptin methylation compared to subjects who lost less than 5% body mass [438].

Finally, to further contradict the evidence, Fan et al. reported no difference in *Lep* promoter methylation in high fat-fed mice as compared to control-fed mice [439], and Okada et al. also reported that high fat-fed C57BL/6J mice displayed no differences in *Lep* promoter methylation as compared to control-fed animals [440], despite the observation of obesity-associated increase in *Lep* expression in both studies.

Given that *Lep* promoter methylation was decreased by HFD during the first 8 weeks but then subsequently decreased after 12 weeks compared to control-fed mice [436], it could be possible that the contradictory findings in this field are dependent on the duration of study or the severity of obesity observed. If this is the case, this could explain the lack of changes observed in the methylation levels of the *Lep* promoter in the *Tet1* KO mice, as my HFD intervention was 11 weeks, slightly shorter than the duration of study in the Shen study at which *Lep* promoter methylation was found to be increased [436]. At present, there are no reports of time course studies investigating the *Lep* methylation levels throughout the duration of HFD, but based on the current literature, I believe these studies would be insightful.

It could also be possible that DNA methylation of the *Lep* promoter is a contributor to transcriptional regulation, rather than the sole or primary driver. Indeed, Shen et al. observed a whole host of epigenetic changes in the *Lep* promoter in concomitance with the changes in DNA methylation [436]: these included increased MBD2 binding; decreased H3 and H4 acetylation and H3K4 methylation; decreased binding of RNA polymerase II at the leptin promoter; increased HDAC1, 2 and 6 binding. These changes were associated with nucleosome compacting resulting in transcriptional repression. It was suggested that these epigenetic modifications were also part of the feedback regulation mechanism that occurs as a result of increased *Lep* gene expression [436].

It could be that, in the particular case of the *Tet1* KO mice, some of these other epigenetic mechanisms described above may be primarily responsible for transcriptional repression of *Lep*, which is why I have observed no differences in the methylation of the *Lep* promoter. On the other hand, DNA methylation of the *Lep* promoter may not play a role at all in the regulation of *Lep* transcription, but could instead be a by-product of chromatin state. In any case, based on my data, TET1 is not required for methylation or hydroxymethylation of the *Lep* promoter.

While methylation has been shown to be an important regulator in tissue-specific and obesity-specific regulation of leptin transcription, hydroxymethylation of the *Lep* promoter remains unexplored. While the data from my hMeDIP-seq study can provide suggestions into this, unfortunately the resolution of such studies is insufficient, given that we can only examine the data across 200bp windows. To examine the 5hmC levels at base pair resolution in the *Lep* promoter, oxidative bisulfite sequencing would need to be carried out.

### 4.5.5. Central control of obesity

It is perhaps unsurprising that the mechanism behind the "lean" phenotype of the *Tet1* KO mouse is involved in central pathways rather than peripheral adipose tissue pathways, given that the majority of approved pharmaceutical interventions for the treatment of obesity target pathways within the central nervous system. For example, Lorcaserin, approved for the treatment of obesity in 2012, selectively activates serotonin 2C receptors on anorexigenic neurons in the hypothalamus. It acts to inhibit appetite stimulation and promote satiety, although its exact mechanism remains unclear [441].

Another effective pharmaceutical strategy for obesity treatment is combination treatment with Bupropion (a dopamine and norepinephrine reuptake inhibitor) and Naltrexone (an opioid receptor antagonist) [442-444]. Again, although the precise mechanism of action is not entirely understood, activity has been observed in both the hypothalamic melanocortin system and the mesolimbic reward system, both of which are important for control of food intake and body weight [444]. Bupropion has been shown to stimulate POMC neurones in the arcuate nucleus of the hypothalamus, while the addition of naltrexone prevents the autoinhibition from β-endorphins, thus facilitating continued weight loss [444].

Phentermine and topiramate combination therapy is also used to treat obesity. Weight loss by phentermine, a sympathomimetic amine anorectic, is thought to be mediated by release of catecholamines in the hypothalamus, which mediates appetite suppression and decreased food consumption [441] The mechanism of action of topiramate, an antiepileptic drug and neurostabilizer, is unclear but it has been suggested to be related to appetite suppression and increased satiety by

increasing γ-aminobutyrate, modulating voltage-gated ion channels, inhibiting carbonic anhydrase, and inhibiting AMPA/kainite excitatory glutamate receptors [445, 446]. Topiramate is a histone deacetylase, which can be recruited by methyl-CpG binding proteins such as DNMTs, MBDs and MECP2 [445, 447]. Therefore, it is tempting to speculate that TET1 may also interact with this mechanism through its action on 5mC conversion and/or demethylation.

These few examples demonstrate how central control of food intake and appetite are more desirable and effective pharmaceutical targets than targeting peripheral metabolism, digestion or nutrient absorption. This helps explain why we see such a prominent effect of *Tet1* KO on weight gain, given that knockout of the gene seems to have an effect on the central leptin signalling pathway resulting in decreased food intake.

### 4.5.6. An *in vitro* model for investigating the role of TET1 in leptin regulation

The attempt to develop an *in vitro* model of *Tet1* knockdown in adipocytes for further investigating the role of TET1 in leptin transcription was complicated by the compensatory upregulation of *Tet2* and *Tet3* isoforms, as well as the observation that *Tet1* transcription appeared to decrease throughout differentiation, thus rendering the knockdown insignificant after 5 days. In addition, while 5 days of exposure to the adipocyte differentiation cocktail was selected in an attempt to compromise between optimal differentiation time and siRNA knockdown duration, it seems that 5 days of differentiation is not long enough, given that *Lep* transcription is not significantly upregulated in this time, and its expression is also highly variable between replicates, indicating that the cells within each well have differentiated to varying degrees. Thus while this is not a suitable model to investigate the role of TET1 on leptin transcription, it has revealed interesting compensatory behaviour in the other TET isoforms.

This is consistent with findings in studies in haematopoietic cells by the Rao group, which showed that TET2 and TET3 have overlapping and compensatory functions in haematopoietic cells [334, 448]. In addition, other groups have demonstrated that TET1 and TET2 have overlapping and compensatory roles [326, 449], as knockdown or knockout of TET1 or TET2 result in only a partial decrease in 5hmC. Furthermore, Fujiki et al. also generated data to support this compensatory relationship in adipocytes, such that TET1 and TET2 appear to have complementary roles during the demethylation that occurs at key CpGs throughout adipogenesis [420]. Therefore, my finding of upregulation of *Tet2* and *Tet3* following knockdown of *Tet1* is in agreement with the literature on this topic.

My observation that *Tet1* expression decreases throughout the first 5 days of adipogenesis may or may not be in agreement with the literature. In NIH/3T3 and 3T3-L1 cells, Western blotting of the three

TET proteins revealed that the amounts of TET1 and TET2 proteins were expressed constantly in both cell lines throughout adipogenic differentiation [420]. However, the Western blots in this study were interpreted in a binary manner (present or not present) and were not quantified. To look at the images of the Western blots in the supplementary figures of the study, TET1 bands appear to decrease by 5 days of differentiation in the 3T3-L1 cells, and TET2 appears to increase, which is consistent with my findings. In the same study, the TET3 protein was present at lower levels [420], which is indeed in agreement with my results. Obviously any interpretation of the results from my *Tet* expression timeline should acknowledge the lack of an adequate number of replicates (n = 1), and so any interpretation is little more than speculation. It is also important to remember that mRNA studies may not always be representative of the amount of protein present or the activity of the protein.

### 4.5.7. Therapeutic application of TET1-mediated effects on the leptin pathway

While *Tet1*-mediated maintenance of leptin sensitivity is effective in reducing food intake and adipose tissue expansion, there are several pitfalls to using this strategy as a potential treatment for obesity. Firstly, we have not examined the other unknown effects of *Tet1* KO. As *Tet1* is expressed across a wide variety of tissues [289], it is likely to have other unknown effects. On the other hand, as we have already established that the TET isoforms have overlapping and compensatory roles [334, 420, 448], therapeutically inhibiting TET1 may not have any effect at all. In addition, the role of TET1 in obesity and control of food intake may not be conserved between species. In this respect, it would be an insightful pilot study to investigate *Tet1* variants in human obese and non-obese populations.

However, the knowledge that epigenetic regulators such as the HDAC inhibitor topiramate [445, 447] are an effective and current treatment for obesity provides justification to explore other epigenetic modifiers. Deacetylation of histones by HDACs is associated with chromatin condensation and of transcriptional repression. Consequently, HDACs inhibitors induce histone hyperacetylation and directly to alter transcription of a subset of genes [445, 450, 451].

Regardless of the direct clinical application of these findings, it is useful to understand the role of *Tet1* in the development of obesity, as it helps us to understand the mechanisms behind the development of obesity. A greater understanding of disease pathogenesis will bring us closer to developing new and more effective strategies to combat the epidemic. While there is still much to be discovered surrounding the role of TET1 in the development of obesity, I have determined that it exerts its effects centrally via the leptin signalling pathway, rather than peripherally in adipose tissue or other metabolic organs. Thus while this PhD began as an investigation into the adipose tissue phenotype of the *Tet1* KO mouse, it has resulted in an investigation into the behaviour (food intake) and central signalling pathways (leptin). Further studies may investigate the effects of *Tet1* on the downstream leptin signalling pathway in the brain: for example, is leptin transport altered in the *Tet1* KO mouse?

Are the downstream pathways, such as Jak/STAT activation, altered? In addition, it would be useful to generate an adipose-specific *Tet1* KO, in order to confirm that deletion of *Tet1* in the adipose tissue is entirely responsible for the reduction of leptin transcription.

# 5. TET1 in marrow adipose tissue

## 5.1. Introduction

Marrow adipose tissue (MAT) is the adipose that is present in the bone marrow cavity. It has been recognised as an adipose tissue for around 100 years [104-107] but its function remains largely unknown. MAT has been compared to brown adipose tissue (BAT) due to its overlapping gene expression profile [109], but its histology [110] and its lipid profile [111] more closely resembles that of white adipose tissue (WAT).

As discussed in Chapter 1, it has been shown that TET1 interacts directly with the transcription factor PPARγ, mediating CpG hydroxymethylation upstream of adipocyte-specific genes [420], thus providing a molecular mechanism by which TET1 expression or activity can influence adipose development. Furthermore, previous studies in our lab have found that, when fed a HFD, *Tet1* KO mice display an obesity-resistant phenotype. Based on this evidence, I sought to characterise the effects of *Tet1* KO on MAT development. Furthermore, an increase in MAT is often associated with a decrease in bone mineral density following the menopause [174] and in various human disease states, including ageing [127, 175] and anorexia nervosa [117]. Based on this evidence, my study also aimed to investigate the effect of global *Tet1* KO on bone mineral density and bone structure, and its association with changes in MAT.

## 5.2. Hypothesis & aims

**Hypotheses:**

- The reduced adiposity of *Tet1* KO mice on HFD will also manifest in reduced MAT. The amount of MAT in the bone marrow cavity of *Tet1* KO mice will be reduced when compared to their wildtype littermates.
- The change in MAT will be associated with changes in bone mineral density and bone structure.

**Aims**:

- Investigate the bone structure and bone mineral density phenotype of *Tet1* KO mice challenged with a HFD.
- Quantify the volume of bone marrow cavity occupied by MAT in high fat-fed *Tet1* KO mice.

## 5.3. Methods

Male WT and *Tet1* KO mice (age 12–23 weeks at the start of the study) were maintained on HFD for 11 weeks. After 11 weeks, mice were killed and lumbar vertebrae, tail vertebrae, femurs and tibiae were collected. Bones were fixed in 10% neutral-buffered formalin solution for 24 hours, and then X-rayed using a Faxitron (Biooptics, Arizona, USA). The exposure was set to 15 seconds at 22kV. X-ray images were analysed using ImageJ (NIH, USA), employing the measurement tool and the threshold tool.

Bones were washed 3 times for 10 minutes in distilled water on a shaker at room temperature, to remove traces of formalin. They then underwent decalcification in 14% EDTA solution on a shaker at 4ºC for 2 weeks. Then the tibiae were immersed in a 1% osmium tetroxide (Agar Scientific, UK) solution for 24 hours. Osmium tetroxide reacts with alkene bonds within unsaturated fatty acids, resulting in covalent incorporation of the osmium atom and allowing visualisation of adipose tissue within the bone marrow. After 24 hours staining, bones were washed three times in Sorenson's buffer (two hours per wash).

Osmium-stained tibiae were embedded in 1% agarose in 7mL Bijou tubes. The Bijou tubes were placed in the SkyScanner 1172 µCT system (Bruker, MA, USA) and scanned using the following settings: source voltage 54kV, source current 185µA, exposure time 885ms.

Trabecular and cortical bone volume, bone surface area, and bone surface to volume ratio were quantified using CTan analysis software, ver. 1.13 (Bruker, MA, USA). Cortical bone was analysed in 650 x 100µm sections, starting from the growth plate down. Trabecular bone was analysed in 225 x 100µm sections, starting from the growth plate down. Marrow adipose tissue volume (post decalcification and osmium staining) was quantified using the same software. MAT quantification was divided into three regions of the marrow cavity: 100 x 100µm sections from the growth plate (proximal); from there to the tibia-fibula junction (medial); and from the tibia-fibula junction to the end of the marrow cavity (distal).

## 5.4. Results

### 5.4.1. *Tet1* KO does not affect bone size, bone mineral density or bone structure.

Bone structure and bone mineral density were assessed to investigate whether global *Tet1* KO has any impact on these parameters. X-ray analysis of bones from *Tet1* KO mice revealed no differences in bone mineral density of tibiae or femurs (see Figure 5.1 and Figure 5.2). Likewise, no differences were determined in bone length of tibiae or femurs (Figure 5.2). µCT analysis of tibiae before demineralisation confirmed that there was no difference in the amount of trabecular bone, the structure of trabecular or cortical bone (based on surface to volume ratio) or the cortical thickness (Figure 5.3).

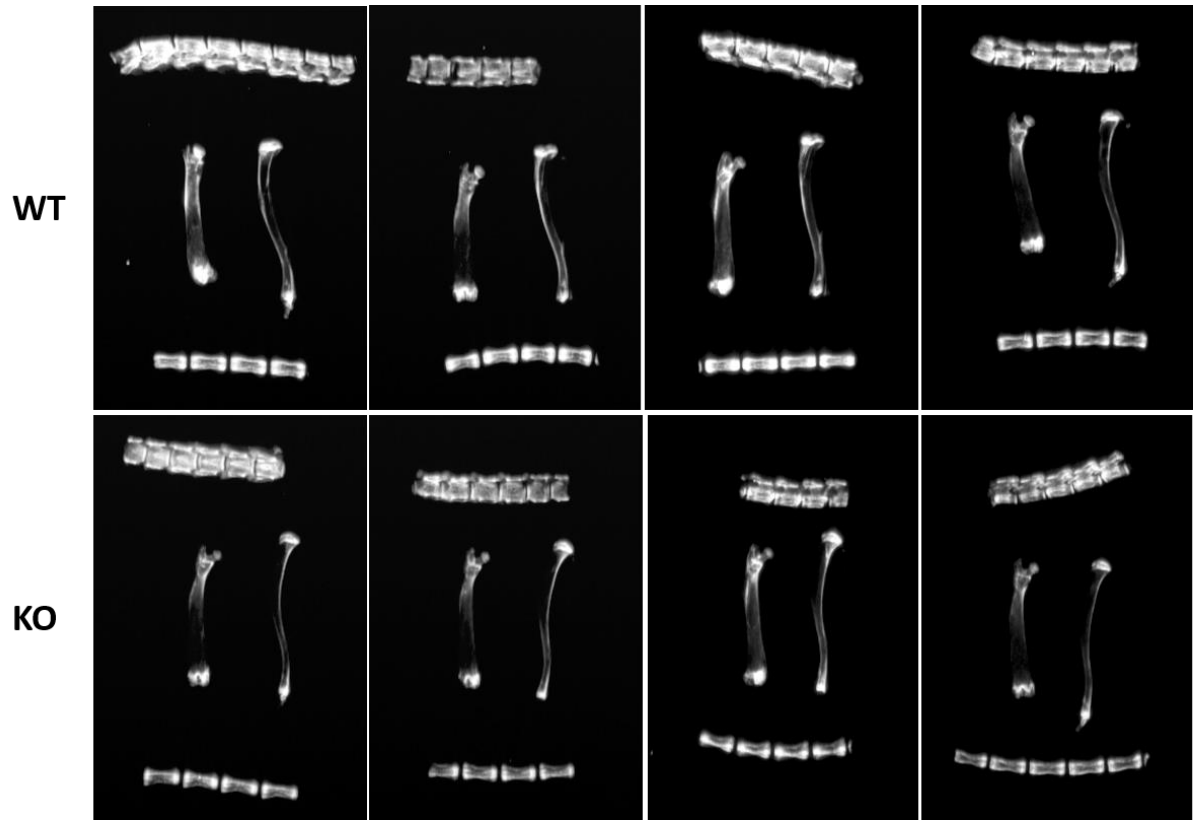


Figure 5.1. X-ray image of mouse wildtype (WT) and *Tet1* knockout (KO) bones.
Horizontally arranged: Lumbar (top) and caudal (bottom) vertebrae. Vertically arranged: Femur (left) and tibia (right).

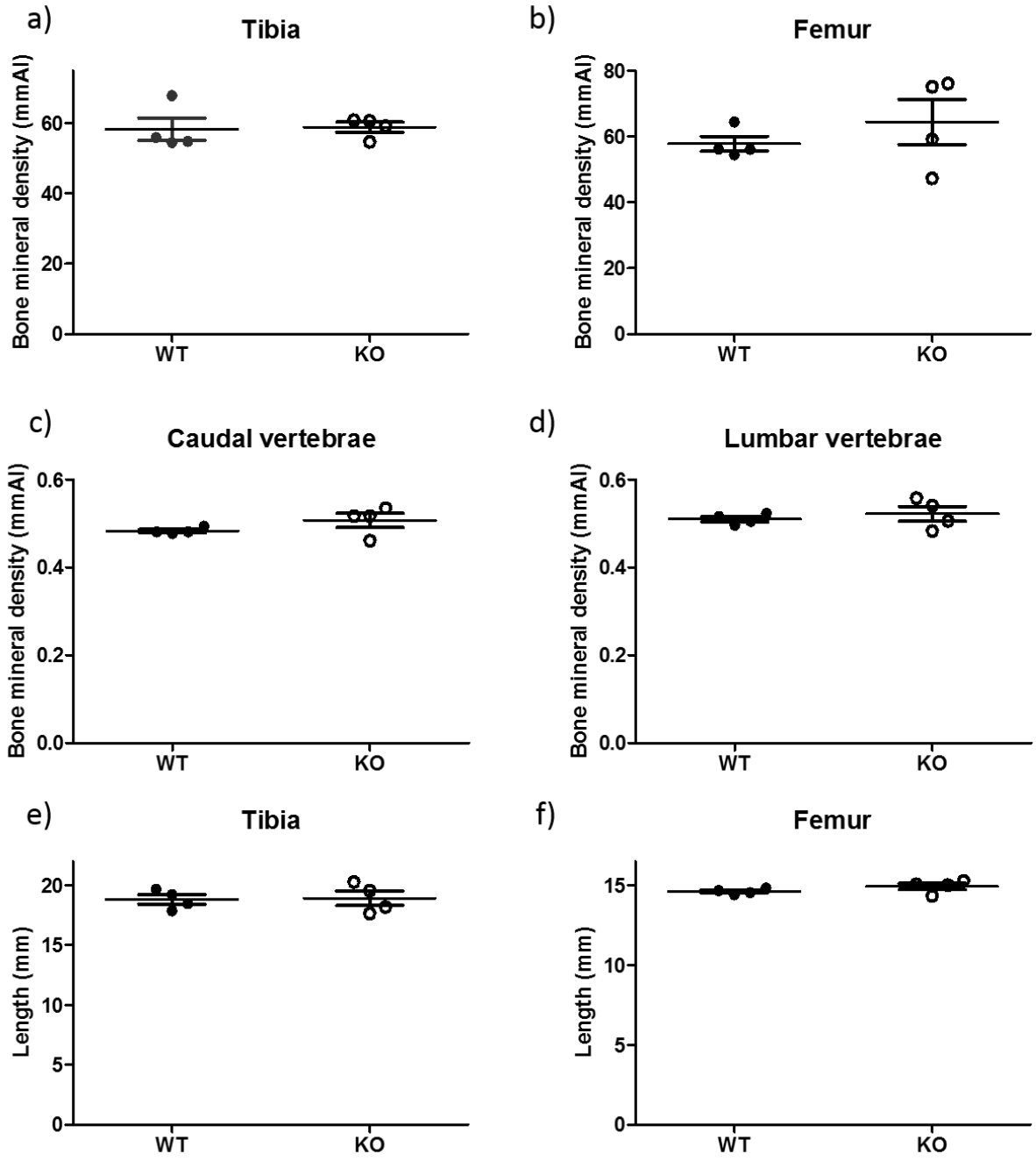


Figure 5.2. Bone mineral density of wildtype (WT) and *Tet1* knockout (KO) mice.

Bone mineral density of (a) Tibiae; (b) Femurs; (c) Caudal vertebrae; and (d) Lumbar vertebrae. Bone length of (e) Tibiae; and (f) Femurs. Mean ± SEM. *n* = 4/group.

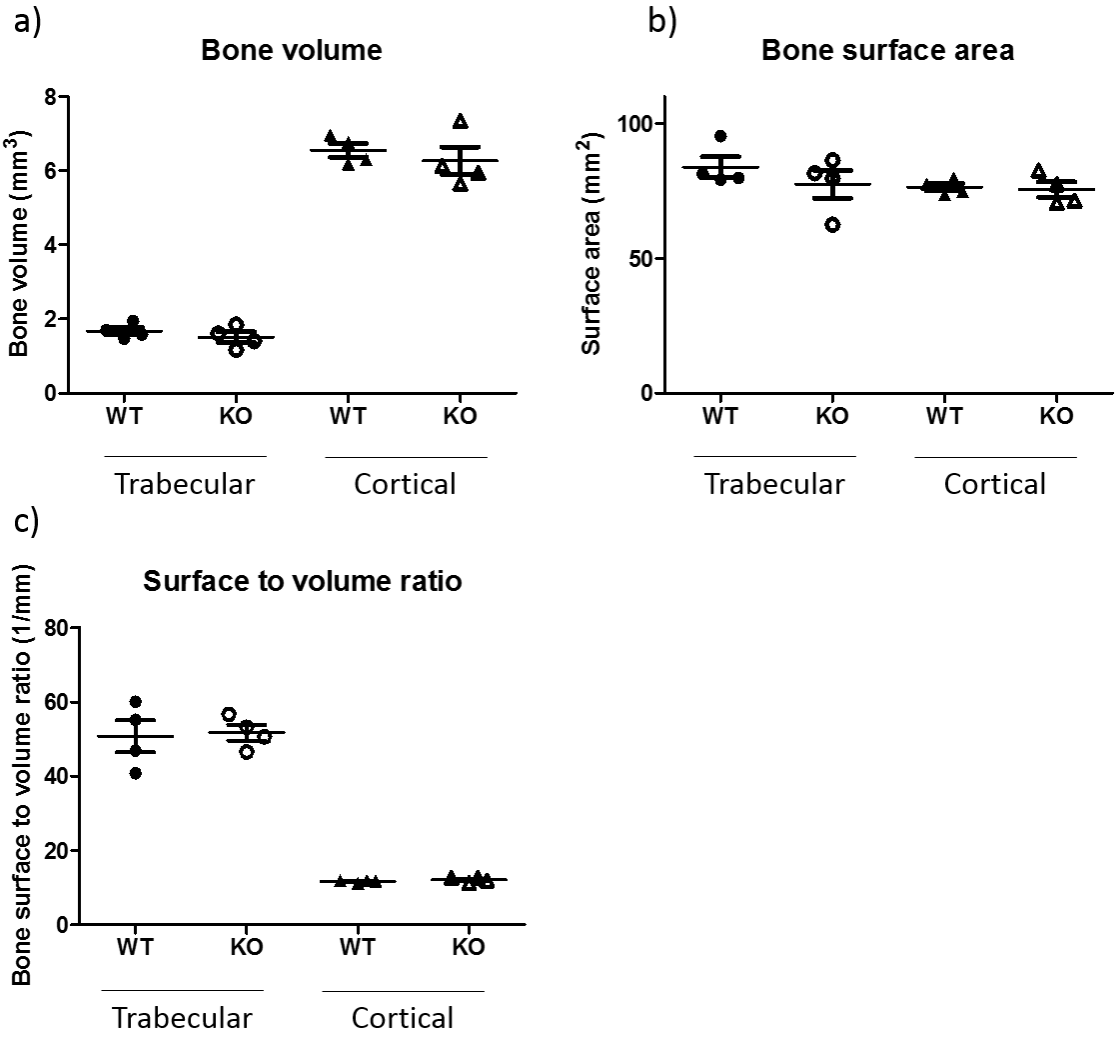


Figure 5.3. Bone structure in wildtype (WT) and *Tet1* knockout (KO) mice.
µCT analysis of a) Bone volume; b) Bone surface area; and c) Bone surface to volume ratio of trabecular and cortical bone of tibiae. Mean ± SEM. *n* = 4/group.

### 5.4.2. *Tet1* KO does not alter bone marrow adiposity

µCT analysis of tibiae after demineralisation and osmium tetroxide staining allowed visualisation and quantification of adipose tissue. Three-dimensional renders were constructed to allow visualisation of adipose tissue within the bone marrow cavity (Figure 5.4). Quantification revealed no differences between WT and KO in the volume of adipose tissue as a percentage of bone marrow cavity volume. Regional analysis of MAT (Figure 5.5) revealed that most adipose tissue was present in the distal tibia (constitutive MAT). WT and KO MAT volume percentage did not differ at the regional level.


Figure 5.4. Three-dimensional renders of mouse wildtype (WT) and *Tet1* knockout (KO) tibia and fibula. Bone is shown in grey and marrow adipose tissue shown in red.

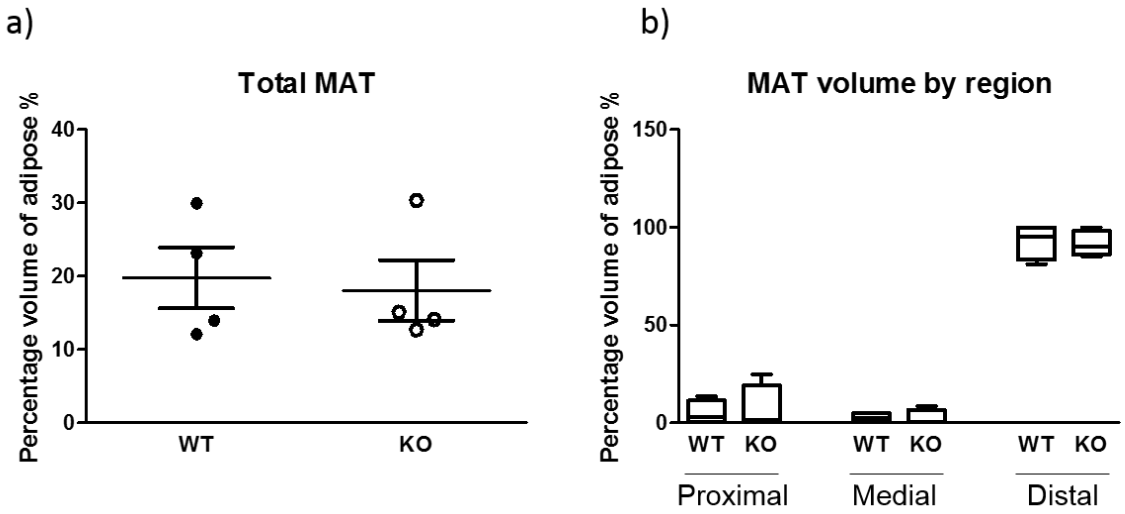


Figure 5.5. Percentage volume of tibia marrow cavity occupied by marrow adipose tissue (MAT). a) Total marrow adipose tissue volume. b) Marrow adipose tissue volume according to bone cavity region. Mean ± SEM. *n* = 4/group.

## 5.5. Discussion

In this diet-induced obesity mouse model, global knockout of *Tet1* had no effects on bone marrow adiposity. Bone structure and bone mineral density were also analysed and no changes were found. This is in contrast to the effects of *Tet1* deficiency in the visceral and subcutaneous white adipose tissue depot, which are markedly reduced in comparison to WT littermates following challenge with a HFD. This suggests that MAT development and deposition is controlled by an alternative mechanism to typical WAT.

### 5.5.1. *Tet1* KO response to HFD

It is possible that differences in MAT accumulation between KO and WT were present in mice on HFD but were too small to detect in this study, although initial power calculations indicated that $n = 5$ would be sufficient to determine a difference if there was one. The lack of an obvious difference in MAT accumulation between KO and WT is in contrast to the changes in non-MAT depots, in which the *Tet1* KO mouse does exhibit reduced adipose tissue deposition on a HFD. Nevertheless, *Tet1* KO mice do show an increase in non-MAT fat mass from baseline, albeit not to the same extent as WT littermates (see Chapter 3). In other words, both groups of animals have increased WAT that could be classed as 'overweight' or 'obese'. Whether there are differences in MAT between lean *Tet1* KO and WT mice (maintained on standard chow) is unknown, so that it is not possible to say whether any obesity-associated increase in MAT occurs in both groups of animals to the same extent. To further investigate this, analysis of WT and KO MAT at baseline (i.e. before starting the HFD) would need to be carried out.

### 5.5.2. Adipose tissue deposition: MAT *vs* WAT

Another potential explanation for the differential deposition of MAT and WAT in *Tet1* KO mice is that MAT development and deposition is controlled by fundamentally different mechanisms to WAT; and that these mechanisms may not be affected by *Tet1* depletion in the same way. However, evidence for the developmental origin of MAT, as discussed in section 1.2.4 (page 9), would suggest that MAT adipocytes differentiate from the same $CD45^{-}CD31^{-}Sca1^{+}CD24^{+/-}$ adipocyte precursor population as WAT adipocytes [143]. This does not support the idea that alternative MAT accumulation explains the differential adipose tissue accumulation in WAT and MAT depots of the *Tet1* KO HFD model.

On the other hand, the dependence of adult MAT expansion on both hyperplasia and hypertrophy [122] in contrast to adult WAT expansion, which depends primarily on hypertrophy [120, 121], could provide an explanation for the differential accumulation of MAT and WAT in *Tet1* KO mice on a HFD. The expansion of adipose tissue by either hyperplasia or hypertrophy is recognised to have both

environmental and genetic determinants. In a high fat diet study using obesity-prone C57BL/6 mice and obesity-resistant FVB/N mice, C57BL/6 mice relied on adipocyte hyperplasia to a greater extent than the leaner FVB/N mice [452], indicating that genetic differences in adipocytes may play a fundamental role in determining inter-individual differences in adipose tissue expansion.

Ehrlund et al. [453] described a specific transcriptional profile associated with adipocyte hypertrophy, showing that a number of genes that are normally expressed either transiently or specifically during late adipogenesis are also expressed in obese hypertrophic WAT. Furthermore, the expression of genes *CCL2* [454], *EBF1* [454], *DUSP1* [454] and *PLXND1* [455] have all been implicated in adipocyte hypertrophy. Thus, any effects of *Tet1* deletion which predominantly affect the transcription of genes involved in hypertrophy may have more effects on WAT expansion – which depends primarily on hypertrophy – than on MAT expansion - which depends on both hypertrophy and hyperplasia. In this scenario, hyperplasia may provide a compensatory mechanism to allow adipose tissue expansion in the bone marrow when hypertrophy is inhibited. To assess this hypothesis further, it would be useful to compare MAT histology between WT and KO mice and analyse cell size and number.

The implication that TET1 is involved in the transcriptional activation of genes downstream of the transcription factor PPARγ [420] (further discussed in section 1.6.1) may be important. In the mouse, adipose PPARγ activation in transgenic mice expressing a VP16-PPARγ fusion protein (that activates PPARγ independent of ligand availability) has been shown to reduce hypertrophy [456]. Given the finding that TET1 is required for PPARγ activation [420], it is plausible that knockout of *Tet1* could influence adipocyte hypertrophy *via* the reduced activation of PPARγ. This again provides a mechanism by which WAT expansion (hypertrophy) could be reduced, while MAT expansion (hypertrophy and hyperplasia) may still be able to function due to the compensatory action of hyperplasia.

To further assess the impact of HFD on MAT in *Tet1* KO mice, future studies should analyse MAT adipocyte size and number to investigate the extent of hyperplasia and hypertrophy in WT and KO high fat-fed mice. It might also be insightful to analyse MAT volume in WT and KO mice on a standard chow diet to observe if differences are present at baseline. In addition, longitudinal studies could be carried out using high-resolution MRI to observe the changes in MAT content in WT and KO mice over time. In addition, it would be interesting to observe the effect of *Tet1* KO in CR-associated MAT expansion, as this may interrogate the role of *Tet1* in different pathways involved in MAT expansion.

# 6. Metabolite availability and TET activity in cold-induced thermogenesis

## 6.1. Introduction

The increase of research investigating brown adipose tissue (BAT) in the last 10 years reflects its potential for use in the treatment of obesity. In both humans and rodents, activation of BAT has been shown to significantly increase energy expenditure [49, 83], increase glucose and lipid oxidation [92], delay the development of Type 2 diabetes [92, 93], reduce triacylglycerol levels [94, 95] and reduce cholesterol levels, slowing down the progression of atherosclerosis [96, 97]. In addition, certain depots of white adipose tissue (WAT), known as "beige" adipose tissue, are able to exhibit properties of BAT, including the expression of a thermogenic gene programme [63, 99, 100]. The browning of WAT has been shown to have similar beneficial effects on metabolic health [75, 457, 458].

At the molecular level, BAT activation is controlled by transcriptional activation of a specific gene programme required for thermogenesis. The most notable of these genes is *UCP1*, coding for uncoupling protein 1, which acts as a proton leak in the mitochondrial membrane, and as such uncoupling proton transport and substrate oxidation from respiration. The result of this is a large increase in ATP requirements. Other genes considered to be crucial members of the thermogenic gene programme include *β3-AR*, *CPT1b*, *GLUT-4*, and *ZFP516* [459]. Also frequently included are the transcription factors involved in regulation of the above genes, such as *PGC1α*, *C/EBPβ*, *PPARα*, *PRDM16* and *EBF2*.

Given the dependence of BAT activation upon transcriptional activation of the thermogenic gene programme, transcriptional regulation – including epigenetic control of transcriptional regulation – is obviously a key element of BAT activation. There is abundant evidence for the role of epigenetic modifications – in particular histone modifications – in BAT activation [396-399, 403]. Specifically, histone deacetylase 3 (HDAC3) has been implicated: BAT-specific *Hdac3* ablation in mice exposed to cold temperatures results in the inability to regulate body temperature and subsequent severe hypothermia [399]. Furthermore, *Hdac3* in mouse WAT was shown to contribute to maintenance of WAT identity and act as a "molecular brake" to prevent browning [400]. In addition, Jumonji C (JmjC)-domain-containing demethylase 1A (JMJD1A) was shown to demethylate H3K9me2 in the PPAR response elements of key genes such as Ucp1 and Adrb1 (β3-adrenoreceptor), permitting transcription of these genes and contributing to the transcriptional activation of the thermogenic gene programme [403].

The JMJD enzymes are part of a group of α-ketoglutarate (α-KG) -dependent dioxygenases, a group of enzymes whose activity is dependent upon the availability of tricarboxylic acid cycle metabolite, α-KG, as a co-factor [289]. Other members of this group include the ten eleven translocase methylcytosine dioxygenases (TETs) [289, 347]. The activity of these enzymes is also inhibited by other by-product metabolites of the TCA cycle (succinate and fumarate) [346]. The dependence of such epigenetic regulators on the availability of α-KG, and their susceptibility to inhibition by succinate and fumarate, provides a mechanism by which changes in the rate of TCA cycle metabolite oxidation (such as those that take place in BAT activation) may influence the activity of this group of enzymes. Indeed, it is plausible that such modulation in intracellular α-KG levels may be required for epigenetic activation of the thermogenic gene programme.

Finally, our collaborators have demonstrated that in humans in mild cold exposure (18°C), there is a decrease in glutamate concentrations in the interstitial fluid within the supraclavicular brown adipose tissue [82]. This indicates an increased uptake of glutamate into the BAT, suggesting an increased rate of glutamate oxidation and uptake into the TCA cycle. Increased uptake of glutamate, the precursor to α-KG, into the TCA cycle of activated BAT could alter α-KG levels, and influence the activity of the α-ketoglutarate dependent dioxygenases with downstream effects on CpG methylation states.

While the role of histone modifications in BAT and beige activation has been extensively studied, the role of changes in CpG methylation state (mediated by the TET enzymes) has not. I aim to investigate whether activation of the thermogenic gene programme is associated with changes in DNA methylation/hydroxymethylation.

## 6.2. Hypotheses & aims

**Hypotheses**:

- Increased glutamate uptake into the brown adipose tissue, as previously observed in humans [82] will also occur in mouse brown and beige adipose tissue when animals are exposed to a temperature of 4°C, but not in white (non-browning) adipose tissue.
- This will cause an increase in the levels of α-ketoglutarate in mouse brown and beige adipose tissue, but not in white (non-browning) adipose tissue.
- Changes observed in glutamate and α-ketoglutarate levels in mouse brown and beige adipose tissue will modulate TET activity.
- Changes in TET activity as a result of cold-induced brown and beige adipose tissue activation will result in global changes in CpG hydroxymethylation, particularly in genes key to thermogenic activation.

- Changes in the hydroxymethylome will be associated with modulation of gene expression in brown and beige adipose tissue.

**Aims**:

- To confirm using indirect calorimetry that cold-induced BAT and beige upregulation occurs in the animals exposed to a temperature of 4°C.
- To investigate changes in glutamate levels, α-ketoglutarate levels and TET activity in the brown, beige and white adipose tissue of mice exposed to cold (4°C), room temperature (21°C) and thermoneutrality (30°C) for 48 hours.
- To investigate changes in DNA hydroxymethylation and associated alterations in gene expression in the brown, beige and white adipose tissue of mice exposed to cold (4°C), room temperature (21°C) and thermoneutrality (30°C) for 48 hours.

## 6.3. Methods

Male C57BL/6J mice (aged 12 weeks at the start of the study) were maintained at 30°C, 21°C or 4°C for 48 hours. Indirect calorimetry was carried out during the temperature exposure to analyse the source of respiration substrate (determined by respiratory exchange ratio). This can be determined using oxygen input and carbon dioxide output of the animals. Food and water intake and activity levels were also measured during this time. After 48 hours exposure to temperature, animals were immediately killed and adipose tissue – epididymal (WAT), brown adipose (BAT) and inguinal adipose (beige) tissue – was dissected.

30-100mg of whole WAT and BAT was used for gas chromatography-mass spectrometry (GC-MS) analysis of tissue polar metabolite levels. 1mL of 1:1 methanol: water mixture was added containing 0.5µg of the internal standard d6-glutaric acid. The mixture was sonicated for 75-90 minutes. An equal volume of ice cold HPLC grade chloroform was added and tubes were vortexed vigorously for 1 minute. The mixture was placed on a shaker at 4°C for 5 minutes. Tubes were then centrifuged at 17,005 x g for 10 minutes at 4°C. The upper layer from the biphasic mixture was collected in a pre-cooled tube. Another cleaning step was carried out by repeating the addition of chloroform and continuing the protocol as above. Samples were dried completely using a Thermo Savant DNA 110 SpeedVac, then snap frozen and stored at -80°C until analysis.

The dried extract was solubilised in 40µl of 2% methoxyamine HCl in pyridine followed by 60 minutes incubation at 60°C. Then 60µl N-tertbutyldimethylsilyl-N-methyltrifluoroacetamide with 1% (w/v) tertbutyldimethyl-chlorosilane derivatization reagent was added, and the suspension was incubated for an hour at 60°C. Finally the samples were centrifuged at 17,005 x *g* for 5 minutes and

the clear supernatant was transferred to a chromatography vial with a glass insert and proceeded immediately to GC-MS analysis. For analysis of the derivatized samples, an Agilent 7890B Series GC/MSD gas chromatograph with a polydimethylsiloxane GC column coupled with a mass spectrometer (GC-MS) was used. GC-MS was carried out by our collaborators from the University of Birmingham (Dr Alpesh Thakker, Dr Christian Ludwig, Prof Gareth Lavery and Dr Daniel Tennant).

RNA and DNA were extracted from BAT, WAT and beige adipose for RNA-sequencing (RNA-seq) and 5hmC DNA-immunoprecipitation sequencing (hMeDIP-seq) respectively. RNA-seq was carried out on the NextSeq platform (Illumina) to a depth of ~33 million reads per sample. Analysis of RNA-seq data was carried out using Illumina's online platform, BaseSpace, using the differential expression application, Cufflinks. Genes were determined to be differentially expressed with a $\log_2$ fold change of > 1.2 and a q value < 0.05. hMeDIP-seq was carried out on the Ion Torrent platform. Analysis of hMeDIP-seq data was carried out using Galaxy to determine mean 5hmC levels per gene or sliding window analysis across 150bp regions across the gene. In addition to hMeDIP-seq, global 5mC and 5hmC levels were analysed by Ultra Performance Liquid Chromatography (UPLC).

The TET activity assay was carried out using the Epigenase 5mC-Hydroxylase TET Activity/Inhibition Assay Kit (Epigentek, NY, USA). Prior to use in the assay, nuclear protein extraction was carried out. 10µg of the resulting nuclear extracts per sample were used in the assay, which was carried out according to kit instructions.

## 6.4. Results

### 6.4.1. Indirect calorimetry

Animals were kept in PhenoCages in the TSE PhenoMaster system, a closed system that allows measurement of oxygen and carbon dioxide flow and animal locomotor activity. System temperature was maintained at either 30°C (thermoneutrality), 21°C (room temperature) or 4°C (cold exposure) for 48 hours. Figure 6.1 displays indirect calorimetry data obtained from this study. Due to technical issues associated with the gas calibration process, unfortunately no useable indirect calorimetry data was obtained from the experiment at 30°C. Therefore 21°C is used as the control temperature for all indirect calorimetry/TSE data.

Calorie expenditure was significantly increased in mice exposed to 4°C when compared to room temperature controls (36.4 ± 2.6 *vs* 24.6 ± 0.3 kcal/hour/kg; $p = 0.0005$; $n = 8$/group) (Figure 6.1a), and food intake was increased accordingly (51.3 ± 2.5 *vs* 23.5 ± 3.1 kcal/hour/kg; $p = 0.000008$; $n = 8$/group) (Figure 6.1b). $VO_2$ and $VCO_2$ were significantly increased (Figure 6.1c and Figure 6.1d), indicating a greater metabolic rate, while respiratory exchange ratio (RER) was significantly decreased (Figure 6.1e), indicating a biological preference for fatty acid metabolism over carbohydrate metabolism under cold exposure. Movement and activity data shows that animals are inclined to reduce locomotor activity under cold exposure, presumably in an attempt to further conserve energy for heat. Daily distance travelled was significantly decreased (Figure 6.1f), as was daily counts of movement (Figure 6.1g). When movement was analysed separately as ambulatory (movement around the cage) and fine (small movements such as twitching of the ears and tail), both forms of movement were significantly decreased at 4°C compared to room temperature (Figure 6.1h).

Figure 6.2 shows the indirect calorimetric response during the first 12 hours of cold exposure, including the transient decrease in temperature to 4°C from ambient. The mean cage temperature appears to stabilise at around 5-6°C, which is slightly higher than the target system temperature of 4°C, most likely due to the body heat produced by the animals slightly raising temperature measurements within the cages. By observing the initial 12 hours including the transient decrease in temperature, we can observe the acute reaction to cold exposure.

Figure 6.2a shows the initial 12 hour response of RER with change in temperature. During the initial decrease in temperature from ambient to 4°C (the first 4 hours), RER decreases rapidly from 0.86 to 0.76. After 4 hours, RER increases again almost to starting level. This transient decrease in RER could be explained by a delay in the increase of food intake (Figure 6.2b). Rate of food intake appears to remain constant until around 16:00 hours, at which point the gradient of the slope increases. This delay in food intake increase may mean that the animals are forced to use adipose stores in order to

account for the increased energy expenditure (decreasing RER). When food intake is increased accordingly (after 16:00 hours) animals appear to metabolise more carbohydrate for respiration (increasing RER). Figure 6.2c displays the acute response of energy expenditure to cold exposure.

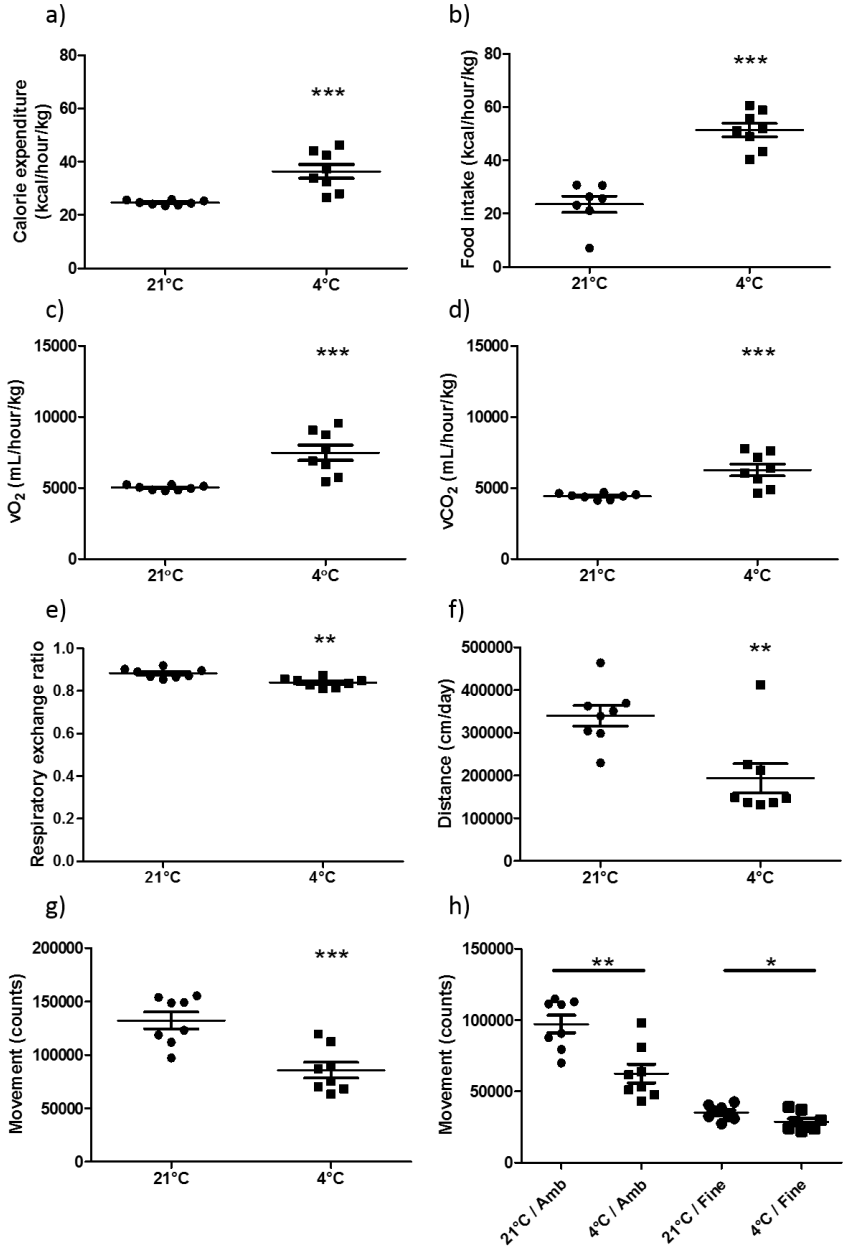


Figure 6.1. Indirect calorimetry data from mice maintained at 21°C (room temperature) and 4°C (cold exposure).

All calculations performed on data over 24 hours. All data presented as mean ± SEM or sum ± SEM (where appropriate, e.g. distance per day, movement per day). *n* = 8/group. a) 24-hour mean kcalorie expenditure. b) 24-hour mean food intake. c) $VO_2$ (volume of oxygen input). d) $VCO_2$ (volume of carbon dioxide output). e) Respiratory exchange ratio (RER): the ratio of $VO_2$ to $VCO_2$. f) Distance travelled over 24 hours. g) Total movement over 24 hours, measured by number of breaks of the detection lasers. h) Movement over 24 hours, represented as ambulatory movement (Amb) and fine movement. *p<0.05; **p<0.01; ***p<0.001; analysed by student's t test.

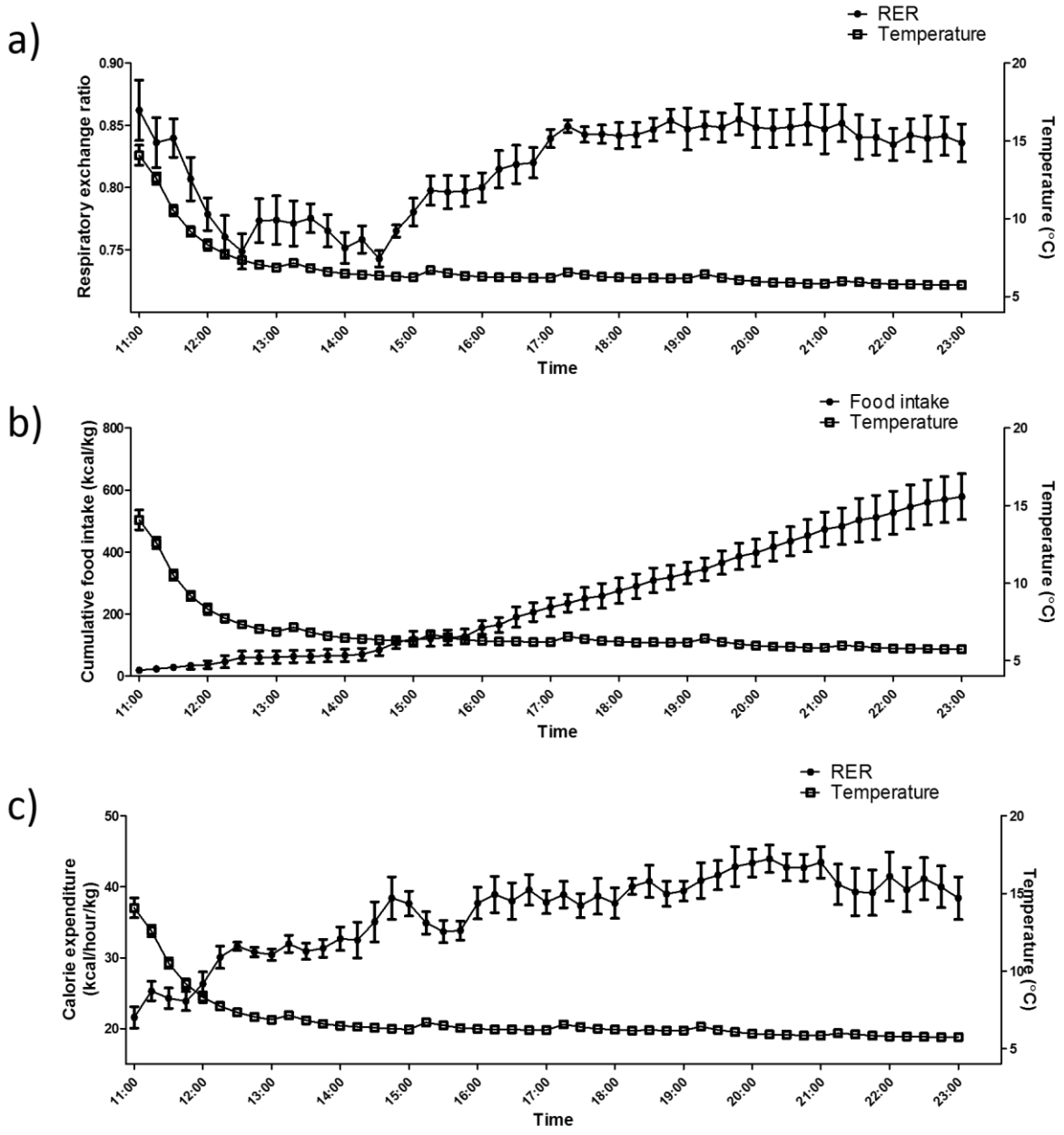


Figure 6.2. The indirect calorimetric response during the first 12 hours of cold exposure, including the transient decrease in RER following the initial reduction in temperature from room temperature.

Mean ± SEM. $n$ = 8. a) Respiratory exchange ratio. b) Cumulative food intake. c) Energy expenditure.

### 6.4.2. Metabolite levels

Steady state levels of polar metabolites in whole brown and white adipose tissue were measured using gas chromatography-mass spectrometry. TCA cycle metabolite levels are shown in Figure 6.3. Every detectable TCA cycle intermediate follows the same pattern: TCA cycle intermediate levels are increased in adipose tissue from animals exposed to 4°C when compared to 30°C. In addition, glutamate, a precursor for α-ketoglutarate, also follows the same pattern. This increase is observed in

both brown and white adipose tissue, although metabolite levels are consistently higher in BAT compared to WAT per mg tissue. All increases in metabolites are statistically significant ($p < 0.05$) except for those in α-ketoglutarate and succinate in BAT, which still follow the same pattern but the changes are not significant. It is possible that an increased number of biological replicates would yield significant changes in these metabolites.

The increase of TCA cycle metabolites in BAT from animals under cold exposure could represent increased rate of cycling in an effort to produce a greater amount of substrates to feed into the respiratory chain. However, we would not expect to observe the same phenomenon in white adipose tissue, which plays no role in thermogenesis.

Meanwhile, Figure 6.4 shows the levels of amino acids (and pyruvate) that feed into the TCA cycle. The levels of these precursor metabolites are likely to directly influence the levels of TCA cycle metabolites. For example, the decrease in histidine levels in BAT at 4°C could suggest an increased utilisation of histidine for generation of increased levels of glutamate.

While the scope for interpretation of steady state metabolite levels can be limited due to lack of information about carbon cycling, the ratios of certain metabolites can suggest further information. Figure 6.5a shows the ratio of α-ketoglutarate:(succinate + fumarate). As previously discussed, α-ketoglutarate is required as a substrate for the action of the TET enzymes, while succinate and fumarate can competitively inhibit the TET enzymes. Therefore changes in the ratio of TET-activating metabolites to TET-inhibitory metabolites could potentially influence TET activity. The ratio of α-ketoglutarate:(succinate + fumarate) is unchanged in BAT at 4°C, but it is trending towards an increase in WAT at 4°C.

Figure 6.5b (ratio of citrate:α-ketoglutarate), Figure 6.5c (ratio of malate:citrate) and Figure 6.5d (ratio of pyruvate:citrate) each represent NADH-forming steps in the TCA cycle. While there is no change in the pyruvate:citrate ratio, the citrate:α-ketoglutarate ratio is decreased in WAT at 4°C, and the malate:citrate ratio is increased in BAT at 4°C. A change in these ratios could indicate changes in the levels of NADH. In addition, Figure 6.5e shows the serine:glycine ratio, which is associated with 1C metabolism. The serine:glycine ratio is significantly increased in BAT at 4°C.

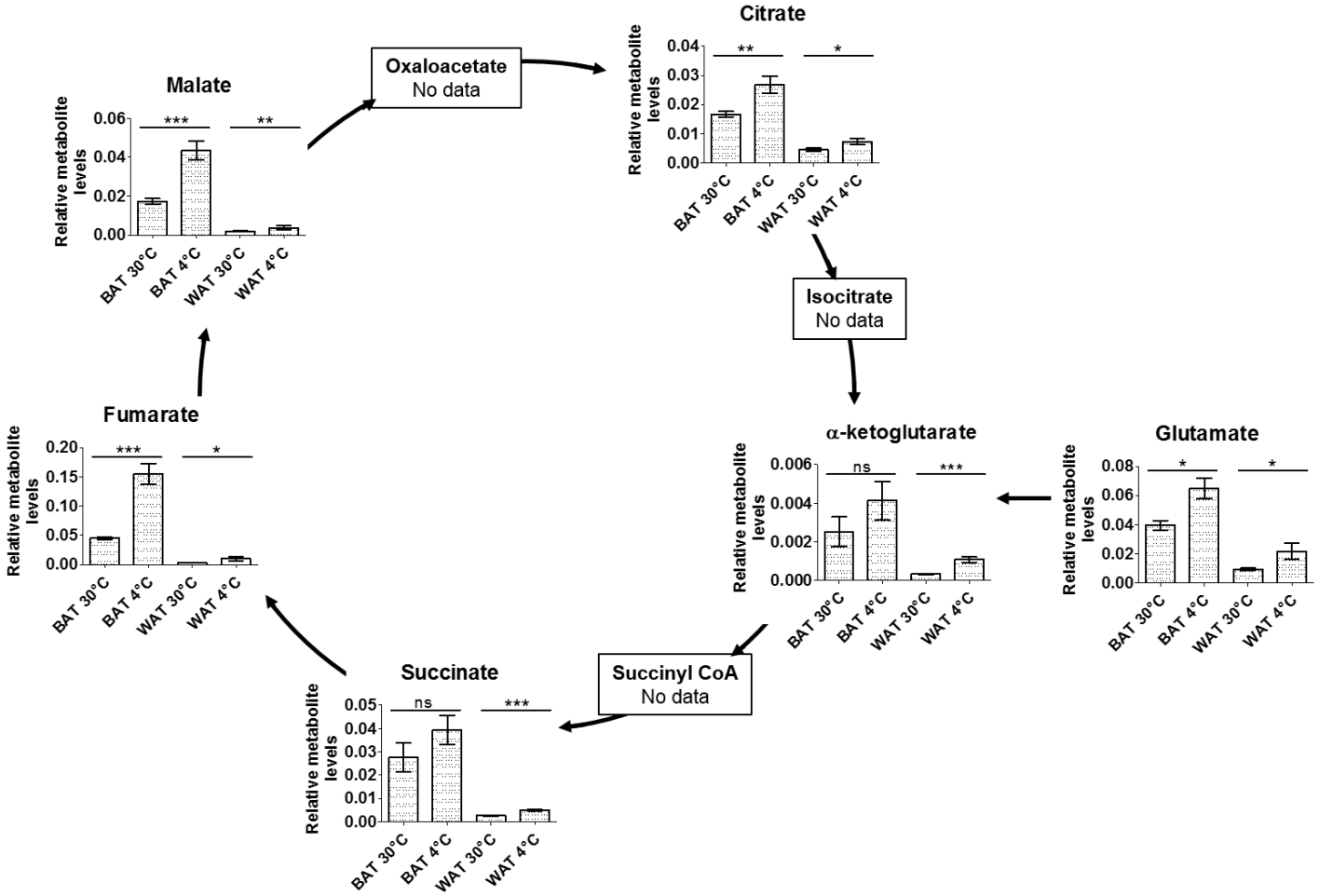


Figure 6.3. Levels of metabolites of the tricarboxylic acid cycle in whole brown adipose tissue (BAT) and white adipose tissue (WAT) from mice maintained at 30°C and 4°C for 48 hours.

As determined by gas chromatography-mass spectrometry (GC-MS). All data expressed as mean ± SEM, *n* = 5/group. Where "no data" is indicated, metabolites are unmeasurable using GC-MS due to chemical instability. *p<0.05; **p<0.01; ***p<0.001; ns = not significant; analysed by student's t test.

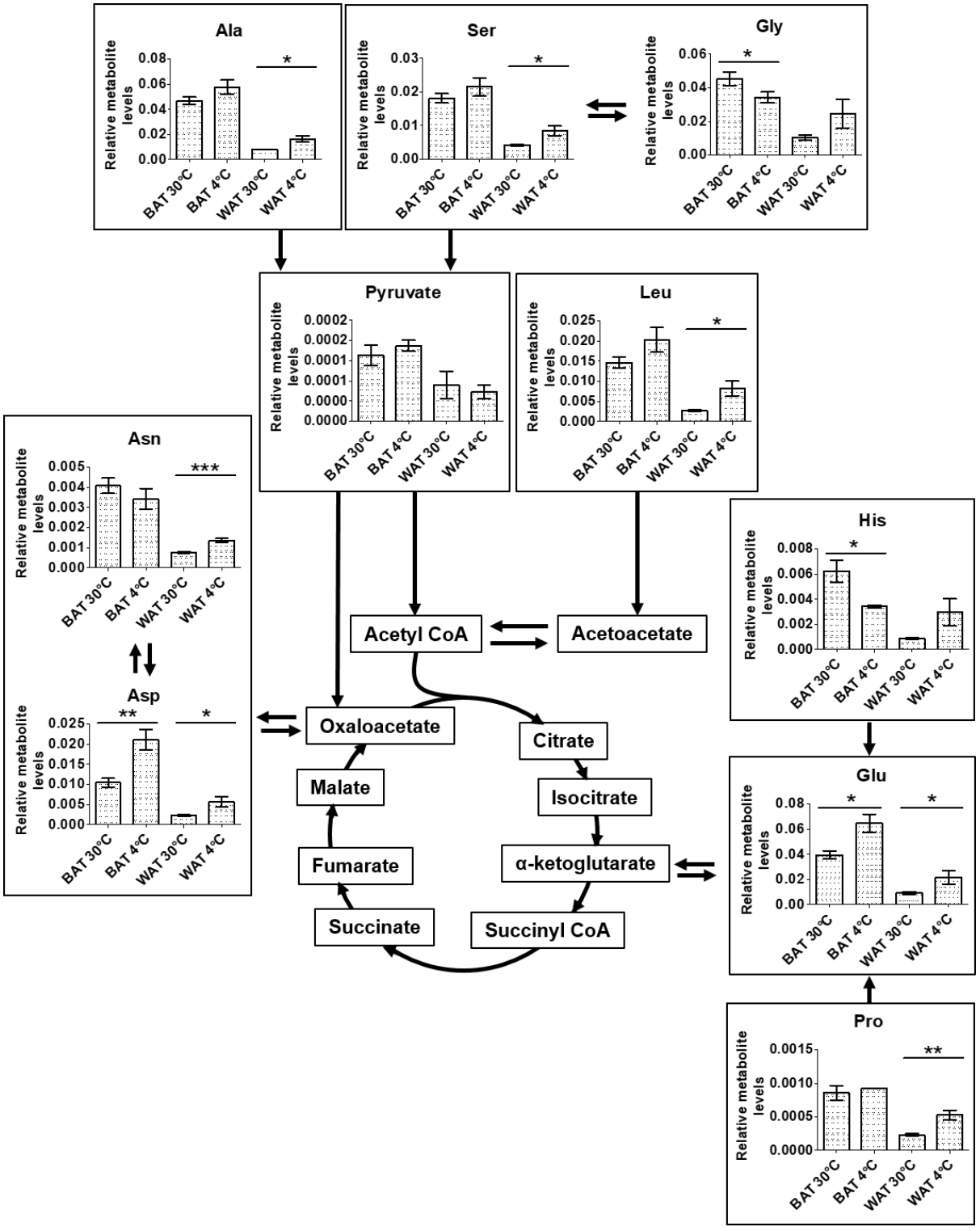


Figure 6.4. Levels of some of the amino acids that can feed into the tricarboxylic acid cycle in whole brown adipose tissue (BAT) and white adipose tissue (WAT) from mice maintained at 30°C and 4°C for 48 hours. As determined by gas chromatography-mass spectrometry. All data expressed as mean ± SEM, *n* = 5/group. *p<0.05; **p<0.01; ***p<0.001; ns = not significant; analysed by student's t test.

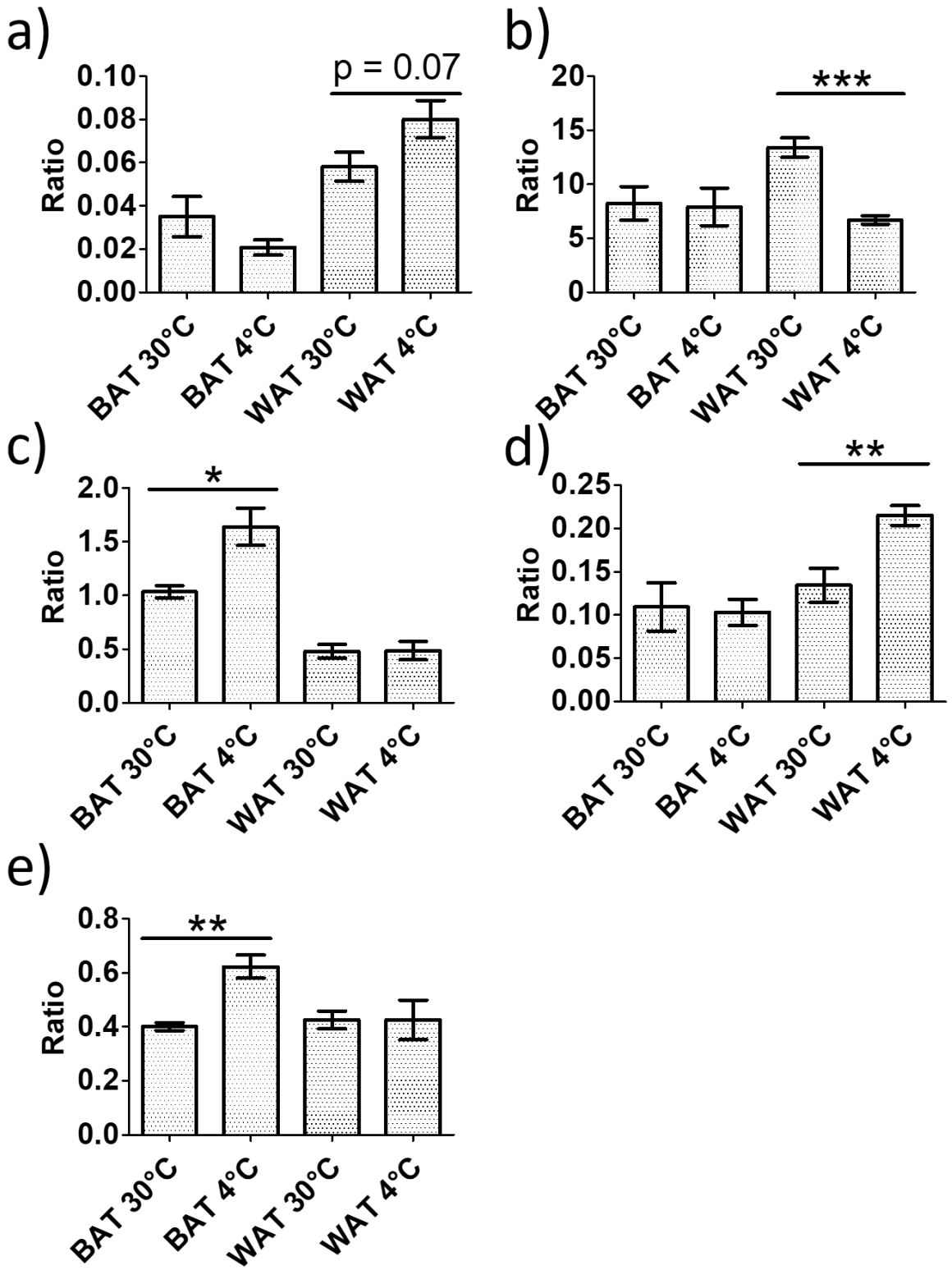


Figure 6.5. Metabolite ratios in whole brown adipose tissue (BAT) and white adipose tissue (WAT) from mice maintained at 30°C and 4°C for 48 hours.

Data presented as mean ± SEM, *n* = 5/group. a) Ratio of α-ketoglutarate:(succinate + fumarate). b) Ratio of citrate:α-ketoglutarate. c) Ratio of malate:citrate. d) Ratio of α-ketoglutarate:succinate. e) Ratio of serine:glycine. *p<0.05; **p<0.01; ***p<0.001; ns = not significant; analysed by student's t test.

### 6.4.3. RNA-sequencing

Initial analysis of RNA-sequencing data allowed hierarchal clustering of biological replicates by gene expression. Figure 6.6a, Figure 6.6c and Figure 6.6e show heatmaps illustrating significantly differentially expressed genes between groups, with a $\log_2$ fold change > 1.2, clustered by Euclidean distance, for BAT, beige and WAT, respectively. In BAT and WAT, gene expression profiles are replicable between samples and allow clustering into the two treatment groups (30°C and ●4°C). However, in beige adipose tissue, gene expression appears to be more variable between biological replicates, which prevents clustering into two distinct groups. Scatterplots in Figure 6.6b, Figure 6.6d and Figure 6.6f illustrate significantly up- and down-regulated genes with a $\log_2$ fold change > 1.2 in BAT, beige and WAT, respectively. In BAT, this comprises 2796 genes upregulated and 3087 downregulated; in beige: 582 upregulated and 80 downregulated; in WAT: 1890 upregulated and 1000 downregulated.

In BAT, activation of the thermogenic gene programme was observed (Figure 6.7a). In addition, *Ucp1* upregulation is observed at expected levels in BAT and beige (Figure 6.7b) (please note the break in scale of the y-axis). While *Ucp1* expression is technically upregulated in WAT, its expression is negligible compared to BAT and beige.

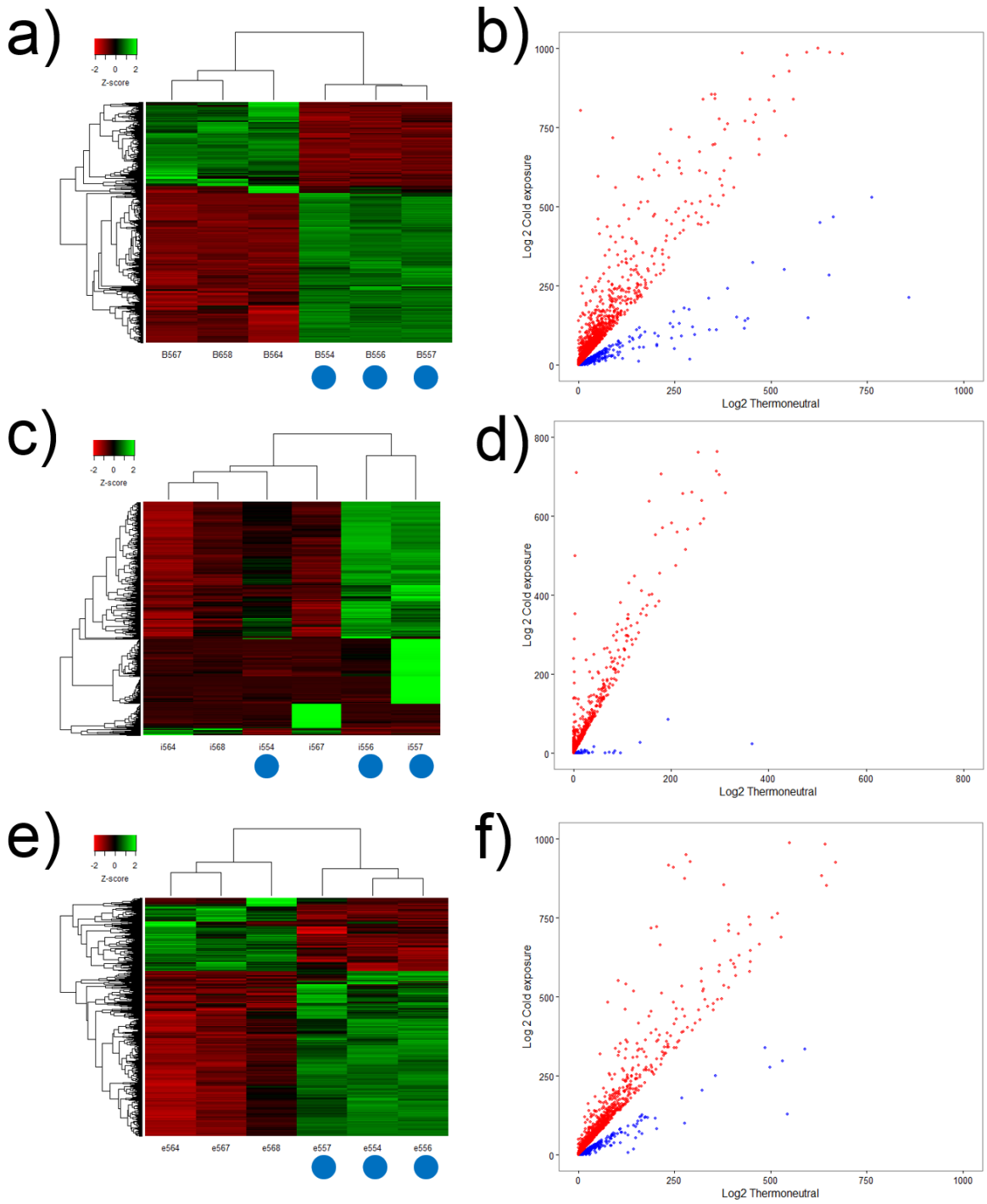


Figure 6.6. RNA-sequencing performed on whole brown adipose tissue (BAT), beige and white adipose tissue (WAT) from mice maintained at 30°C and 4°C for 48 hours.

Heatmaps illustrating significantly differentially expressed genes with a $\log_2$ fold change > 1.2, clustered by Euclidean distance, for BAT, beige and WAT are shown in **a**, **c** & **e** respectively. Blue circles (●) indicate samples from animals from the group exposed to 4°C. Scatter plots displaying genes that are significantly upregulated in the 4°C group (in red) and significantly downregulated (shown in blue) for BAT, beige and WAT are shown in **b**, **d** & **f** respectively.

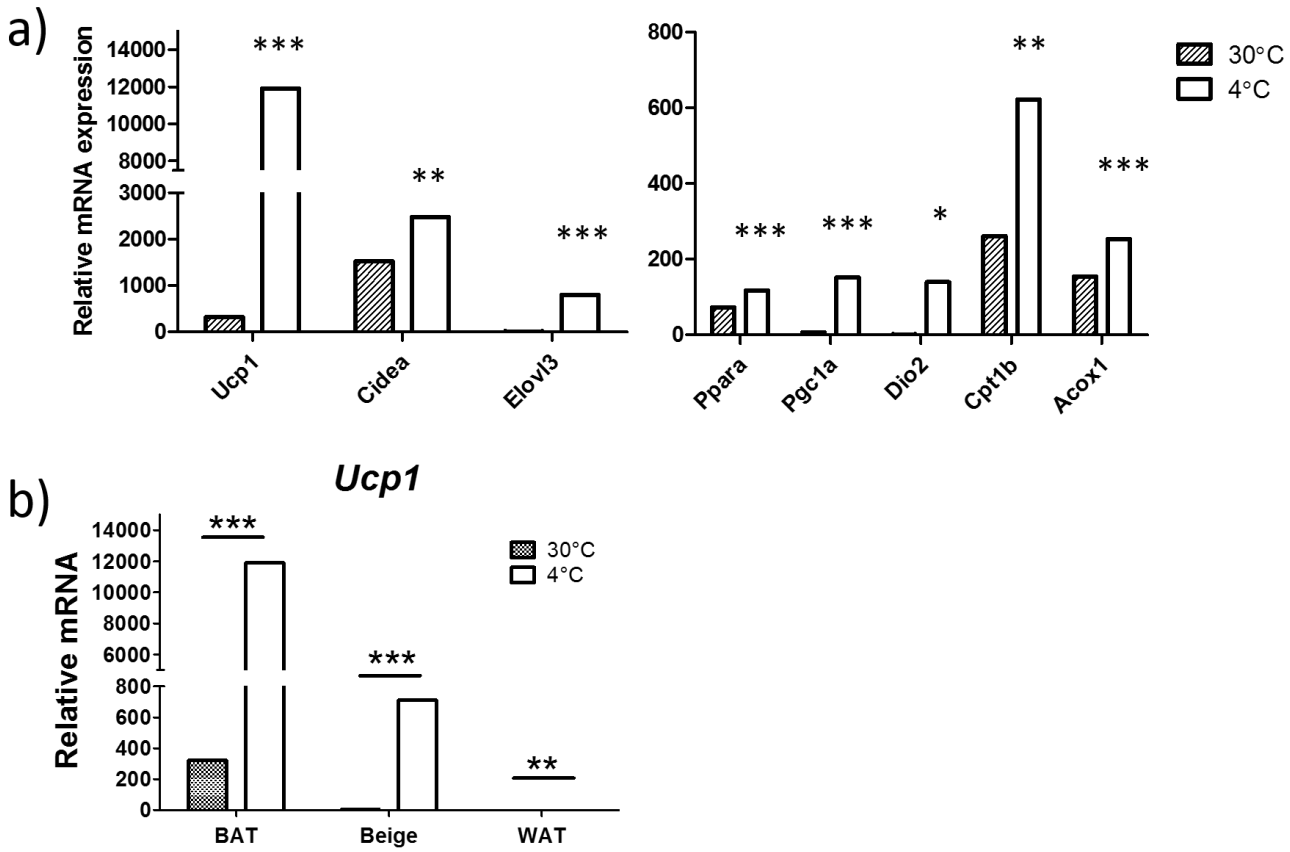


Figure 6.7. RNA-seq analysis of activation of the thermogenic gene programme.
a) Thermogenic gene programme activation in whole brown adipose tissue from mice exposed to 30°C or 4°C for 48 hours. b) *Ucp1* gene expression in whole brown adipose tissue (BAT), beige adipose tissue and white adipose tissue (WAT) from mice exposed to 30°C or 4°C for 48 hours. n = 3/group. *q<0.05; **q<0.01; ***q<0.001; significance determined by q-value estimation for false discovery rate control.

Pathway analysis revealed the most upregulated (Figure 6.8a, b & c) and downregulated (Figure 6.9a, b & c) pathways in BAT, beige and WAT, respectively. Many of the upregulated hits in BAT and beige support activation of the thermogenic gene programme, such as mitochondrial transport and organisation, TCA cycle, lipid & carbohydrate metabolic processes and generation of precursor metabolites. In WAT, the top upregulated hits suggest that WAT may be undergoing anabolic processes in order to store as much energy as possible. For example, the pentose-phosphate shunt (2nd upregulated hit) is a metabolic pathway parallel to glycolysis, whose primary function is to generate reducing equivalents, in the form of NADPH, used in reductive biosynthesis reactions within cells (e.g. fatty acid synthesis). It is considered an anabolic pathway, rather than catabolic.

Taking the RNA-seq data in combination with the GC-MS data, we can look at the changes in both genes and metabolites in the same pathway. Figure 6.10 shows changes in metabolites of the TCA cycle in a) BAT and b) WAT.

a)

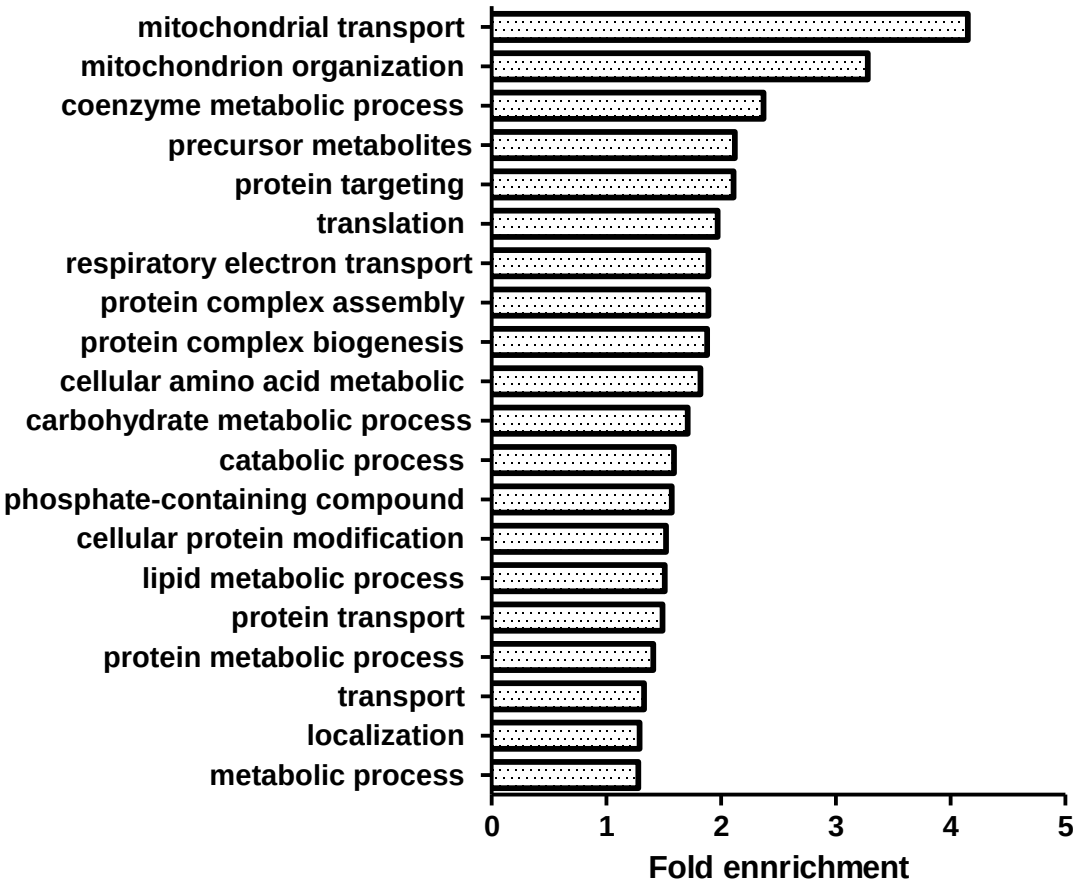
mitochondrial transport
mitochondrion organization
coenzyme metabolic process
precursor metabolites
protein targeting
translation
respiratory electron transport
protein complex assembly
protein complex biogenesis
cellular amino acid metabolic
carbohydrate metabolic process
catabolic process
phosphate-containing compound
cellular protein modification
lipid metabolic process
protein transport
protein metabolic process
transport
localization
metabolic process
0
1
2
3
4
5
Fold ennrichment

b)

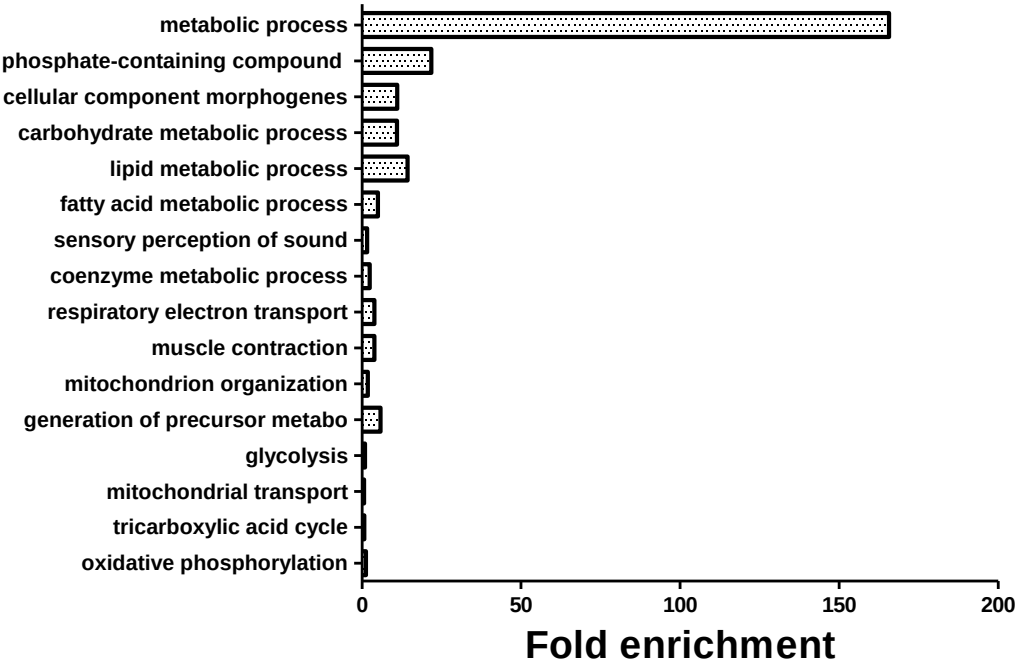
metabolic process
phosphate-containing compound
cellular component morphogenes
carbohydrate metabolic process
lipid metabolic process
fatty acid metabolic process
sensory perception of sound
coenzyme metabolic process
respiratory electron transport
muscle contraction
mitochondrion organization
generation of precursor metabo
glycolysis
mitochondrial transport
tricarboxylic acid cycle
oxidative phosphorylation
0
50
100
150
200
Fold enrichment

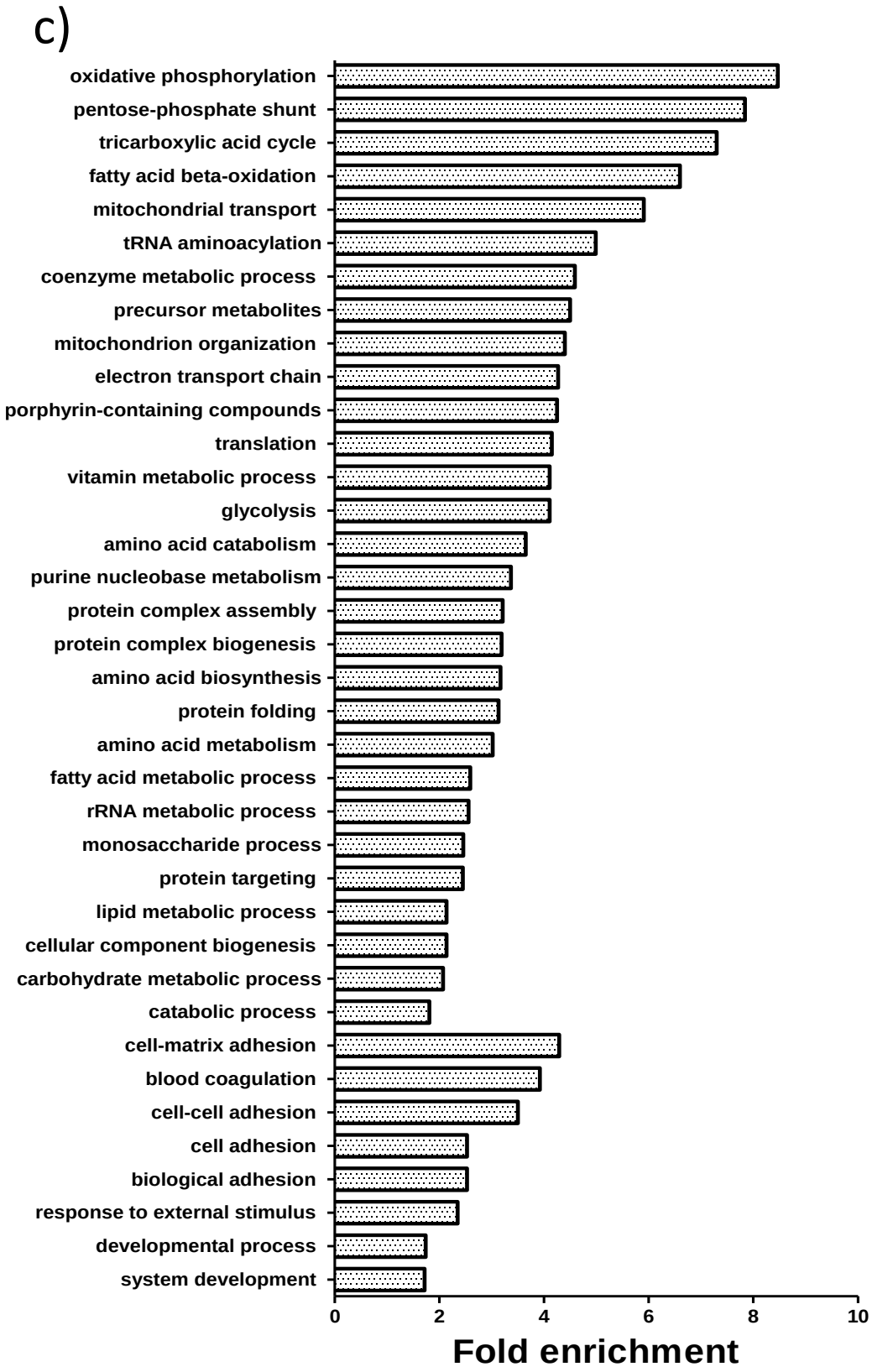


Figure 6.8. Pathway analysis of significantly upregulated genes in cold exposure

Pathway analysis of significantly upregulated genes in cold exposure in: a) brown adipose tissue; b) beige adipose tissue; and c) white adipose tissue.

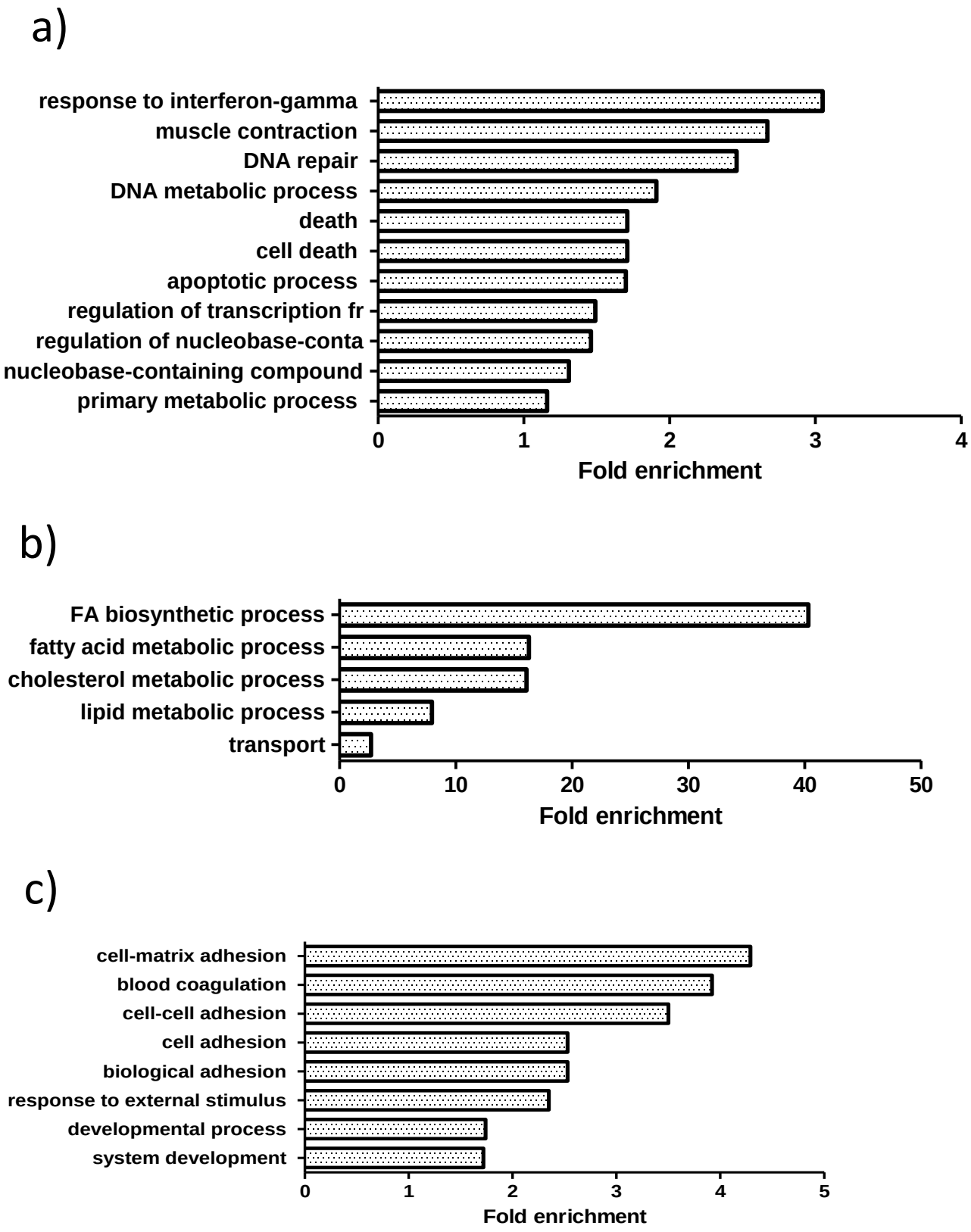


Figure 6.9. Pathway analysis of significantly downregulated genes in cold exposure.

Pathway analysis of significantly downregulated genes in cold exposure in: a) brown adipose tissue; b) beige adipose tissue; and c) white adipose tissue.

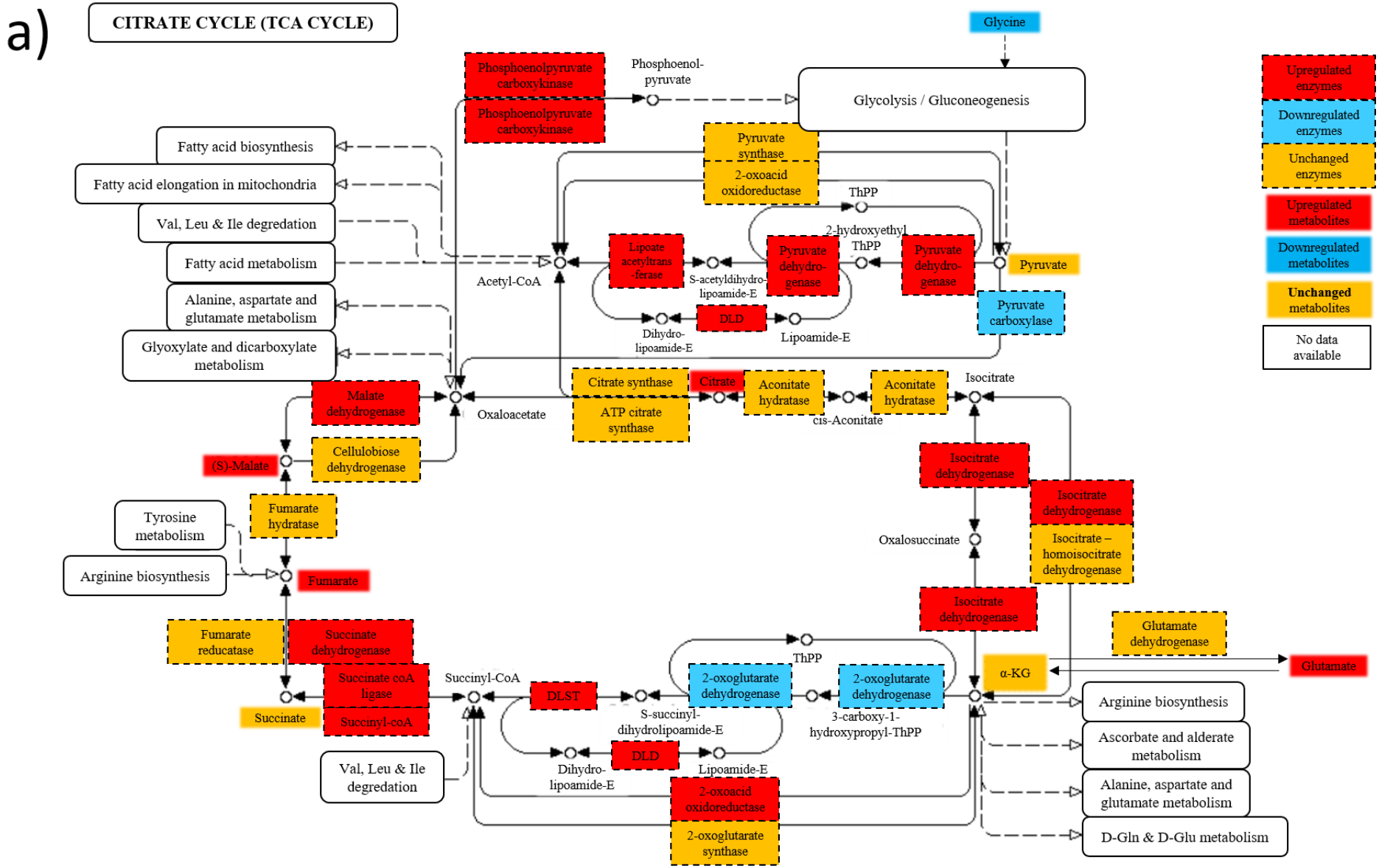
a)
CITRATE CYCLE (TCA CYCLE)
Glycine
Phosphoenolpyruvate carboxykinase
Phosphoenol-pyruvate
Glycolysis / Gluconeogenesis
Phosphoenolpyruvate carboxykinase
Fatty acid biosynthesis
Fatty acid elongation in mitochondria
Val, Leu & Ile degredation
Fatty acid metabolism
Alanine, aspartate and glutamate metabolism
Glyoxylate and dicarboxylate metabolism
Pyruvate synthase
2-oxoacid oxidoreductase
ThPP
2-hydroxyethyl ThPP
Lipoate acetyltrans-ferase
Pyruvate dehydro-genase
Pyruvate dehydro-genase
Pyruvate
Acetyl-CoA
S-acetyldihydro-lipoamide-E
DLD
Dihydro-lipoamide-E
Lipoamide-E
Pyruvate carboxylase
Malate dehydrogenase
Citrate synthase
Citrate
Aconitate hydratase
Aconitate hydratase
Isocitrate
Oxaloacetate
ATP citrate synthase
cis-Aconitate
(S)-Malate
Cellulobiose dehydrogenase
Isocitrate dehydrogenase
Tyrosine metabolism
Fumarate hydratase
Isocitrate dehydrogenase
Oxalosuccinate
Arginine biosynthesis
Fumarate
Isocitrate – homoisocitrate dehydrogenase
Isocitrate dehydrogenase
Glutamate dehydrogenase
Fumarate reducatase
Succinate dehydrogenase
ThPP
α-KG
Glutamate
Succinate coA ligase
Succinyl-CoA
DLST
2-oxoglutarate dehydrogenase
2-oxoglutarate dehydrogenase
Arginine biosynthesis
Succinate
Succinyl-coA
S-succinyl-dihydrolipoamide-E
3-carboxy-1-hydroxypropyl-ThPP
Ascorbate and alderate metabolism
Val, Leu & Ile degredation
DLD
Dihydro-lipoamide-E
Lipoamide-E
Alanine, aspartate and glutamate metabolism
2-oxoacid oxidoreductase
D-Gln & D-Glu metabolism
2-oxoglutarate synthase
Upregulated enzymes
Downregulated enzymes
Unchanged enzymes
Upregulated metabolites
Downregulated metabolites
Unchanged metabolites
No data available

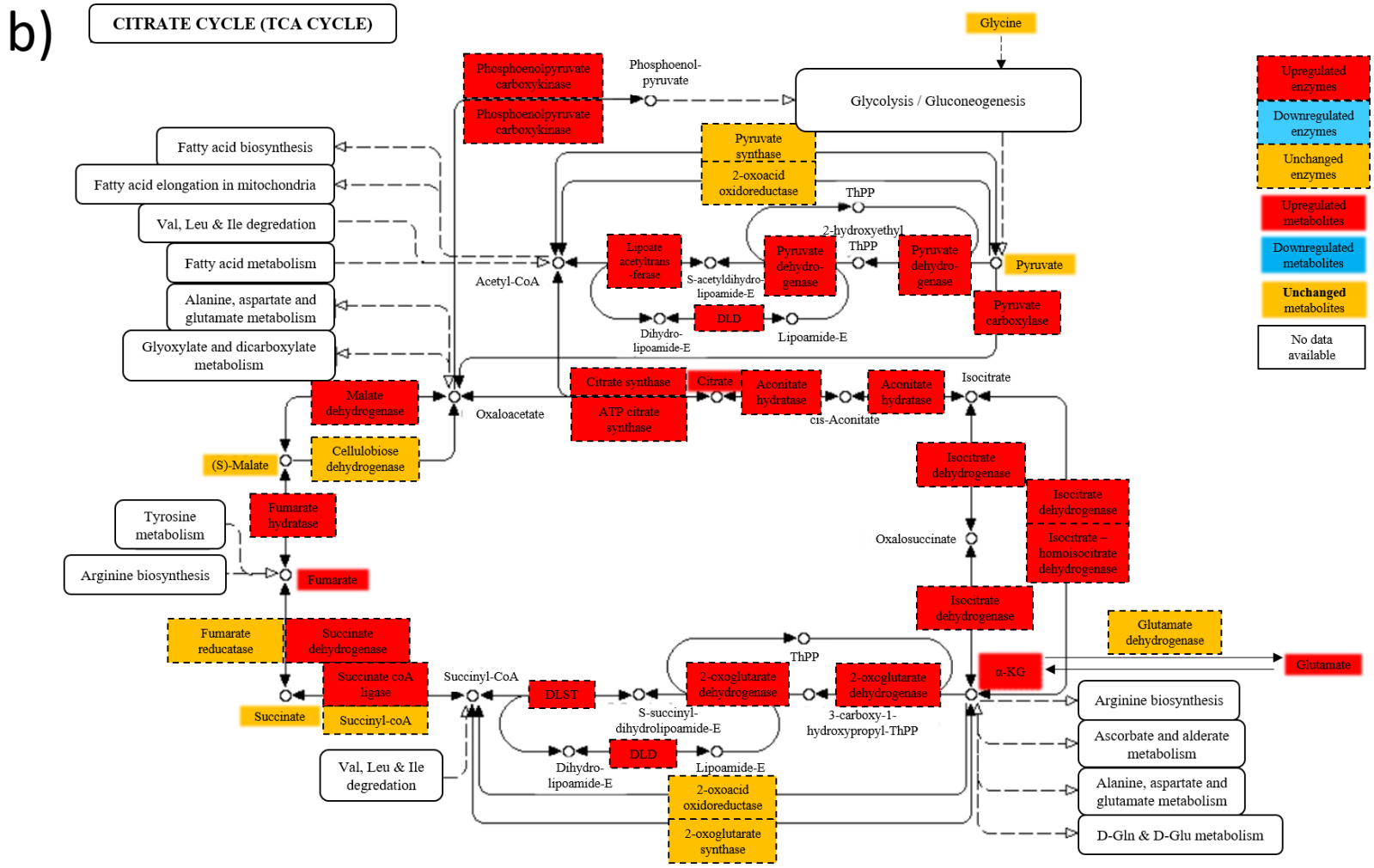


Figure 6.10. Up- and down-regulation of enzymes and metabolites of the tricarboxylic acid cycle.

Up- and down-regulation of enzymes and metabolites of the tricarboxylic acid cycle in a) whole brown adipose tissue; and b) whole white adipose tissue of mice exposed to 4°C for 48 hours.

### 6.4.4. TET expression and activity

Analysis of RNA-seq data showed that while *Tet1-3* mRNA levels appear to be reduced with cold exposure (Figure 6.11a-c), the only significant changes in mRNA levels are *Tet2* in BAT and *Tet1* in WAT. This correlates with a decrease in TET activity in WAT at 4°C (Figure 6.11d).

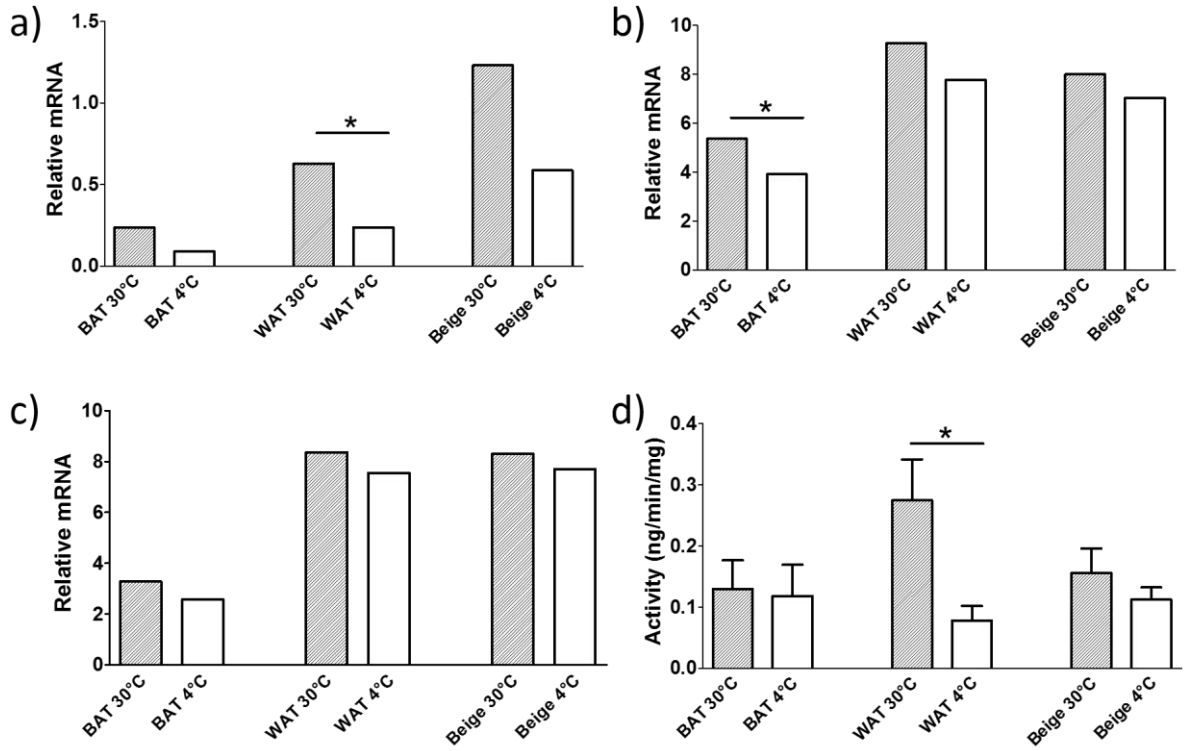


Figure 6.11. TET expression and activity in whole brown adipose tissue (BAT), white adipose tissue (WAT) and beige adipose tissue taken from mice maintained at 30°C or 4°C for 48 hours.

a) *Tet1* expression; b) *Tet2* expression; c) *Tet3* expression (mean, $n$ = 3/group; significance determined by q-value estimation for false discovery rate control); d) overall TET activity (mean ± SEM, $n$ = 5/group; significance determined using student's t test). *q<0.05; **q<0.01; q<0.001.

### 6.4.5. Global methyl- and hydroxymethylcytosine

No differences were observed in global 5-methylcytosine (5mC) or 5-hydroxymethylcytosine (5hmC), as detected using ultra performance-liquid chromatography (UPLC) (see Figure 6.12). No changes were observed in either BAT or WAT, although BAT has significantly lower 5mC levels compared to WAT.

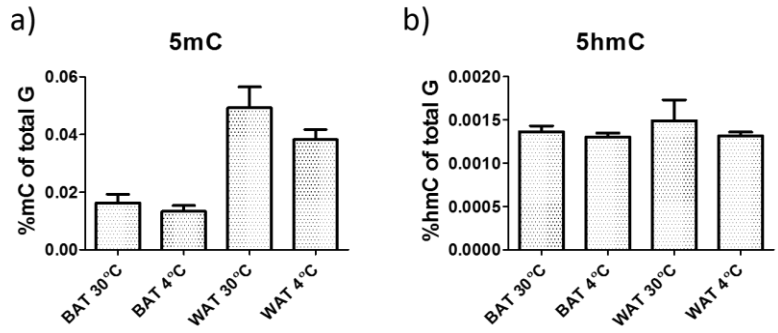


Figure 6.12. Global methyl- and hydroxymethyl-cytosine levels in brown and white adipose tissue at thermoneutrality or cold exposure.

a) 5-methlycytosine (5mC) and b) 5-hydroxymethylcytosine (5hmC) levels in whole brown adipose tissue (BAT) and white adipose tissue (WAT) from mice exposed to 30°C or 4°C for 48 hours, expressed as a percentage of total G. n = 5/group.

### 6.4.6. 5hmC DNA immunoprecipitation-sequencing (hMeDIP-seq)

Analysis of hMeDIP-seq data showing 5hmC levels across every gene, normalised to 100%, is shown in Figure 6.13a. Based on these data, 5hmC levels in BAT and WAT appear to decrease globally with 48 hours cold exposure, although with only one biological replicate, no solid conclusions can be drawn. In contrast to previous hMeDIP-seq data in WAT (see section 3.4.5) , a trough occurs in 5hmC levels specifically at the 10% position of the gene body in BAT at 30°C, BAT at 4°C, and WAT at 4°, but not in WAT at 30°C (Figure 6.13a). Previously, I have demonstrated a relative 5hmC peak at around 10% gene length in WAT, as shown in Figure 6.13b. Therefore, the epigenetic signature of BAT differs from WAT at this locus. In addition, cold exposure induces large changes in WAT 5hmC at this locus that closely resemble the 5hmC signature of BAT.

Further analysis identified a subset of genes with decreased 5hmC at 10% gene length in WAT at 4°C. I carried out statistical overrepresentation pathway analysis to investigate the genes that are decreased in 5hmC at 10% gene length in response to cold exposure (Figure 6.13c). The most highly enriched pathways are neuromuscular synaptic transmission, sensory perception of smell and perception of chemical stimuli. High correlations were observed between mean 5hmC levels at thermoneutral and cold exposure in both BAT (Figure 6.13d) and WAT (Figure 6.13e), with Spearman's correlation coefficient ($R^2$) > 0.95 in both cases, although statistical significance tests cannot be carried out due to the lack of biological replicates.

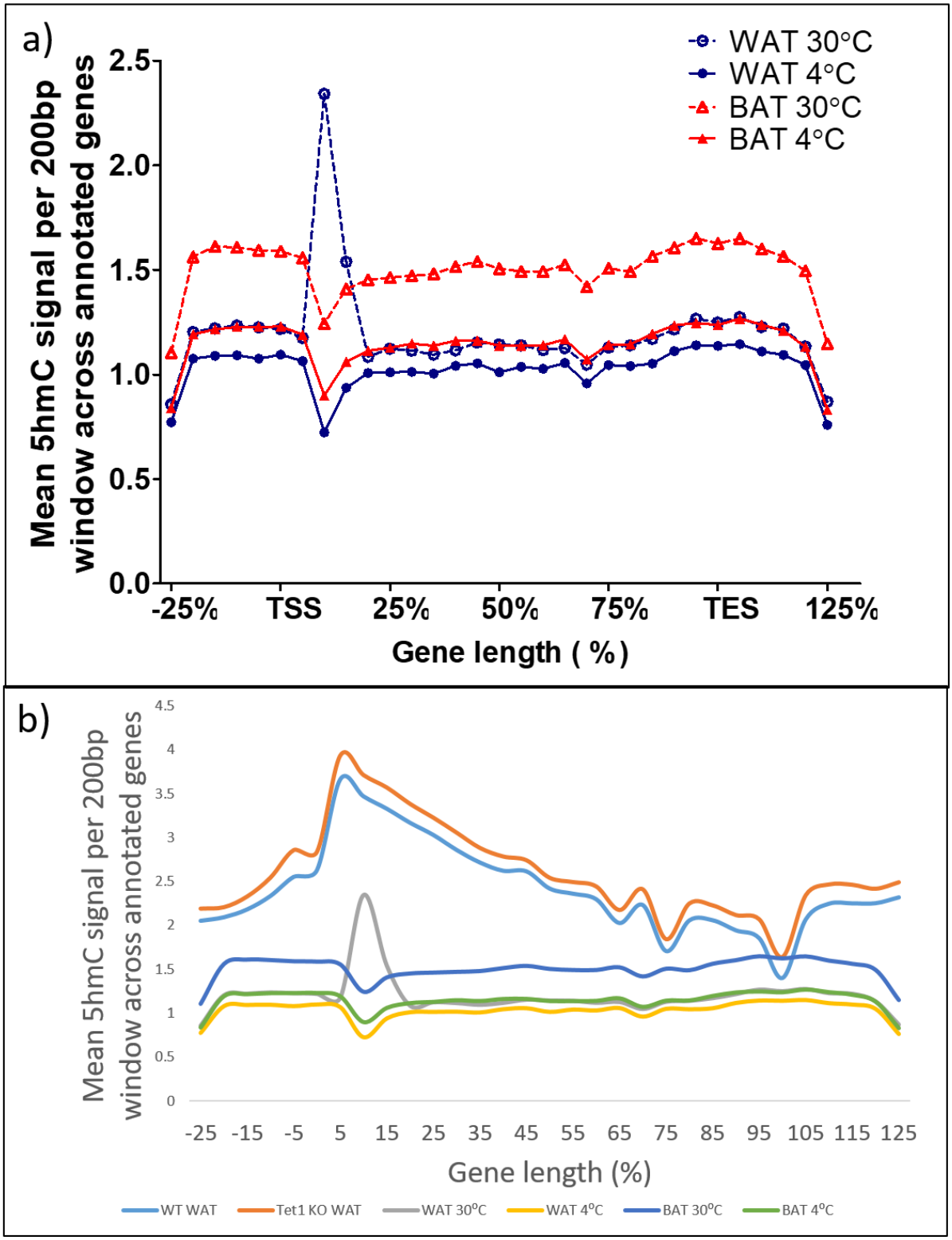
a)
Mean 5hmC signal per 200bp window across annotated genes
2.5
2.0
1.5
1.0
0.5
0.0
WAT 30°C
WAT 4°C
BAT 30°C
BAT 4°C
-25%
TSS
25%
50%
75%
TES
125%
Gene length ( %)
b)
Mean 5hmC signal per 200bp window across annotated genes
4.5
4
3.5
3
2.5
2
1.5
1
0.5
0
-25 -15 -5 5 15 25 35 45 55 65 75 85 95 105 115 125
Gene length (%)
WT WAT
Tet1 KO WAT
WAT 30°C
WAT 4°C
BAT 30°C
BAT 4°C

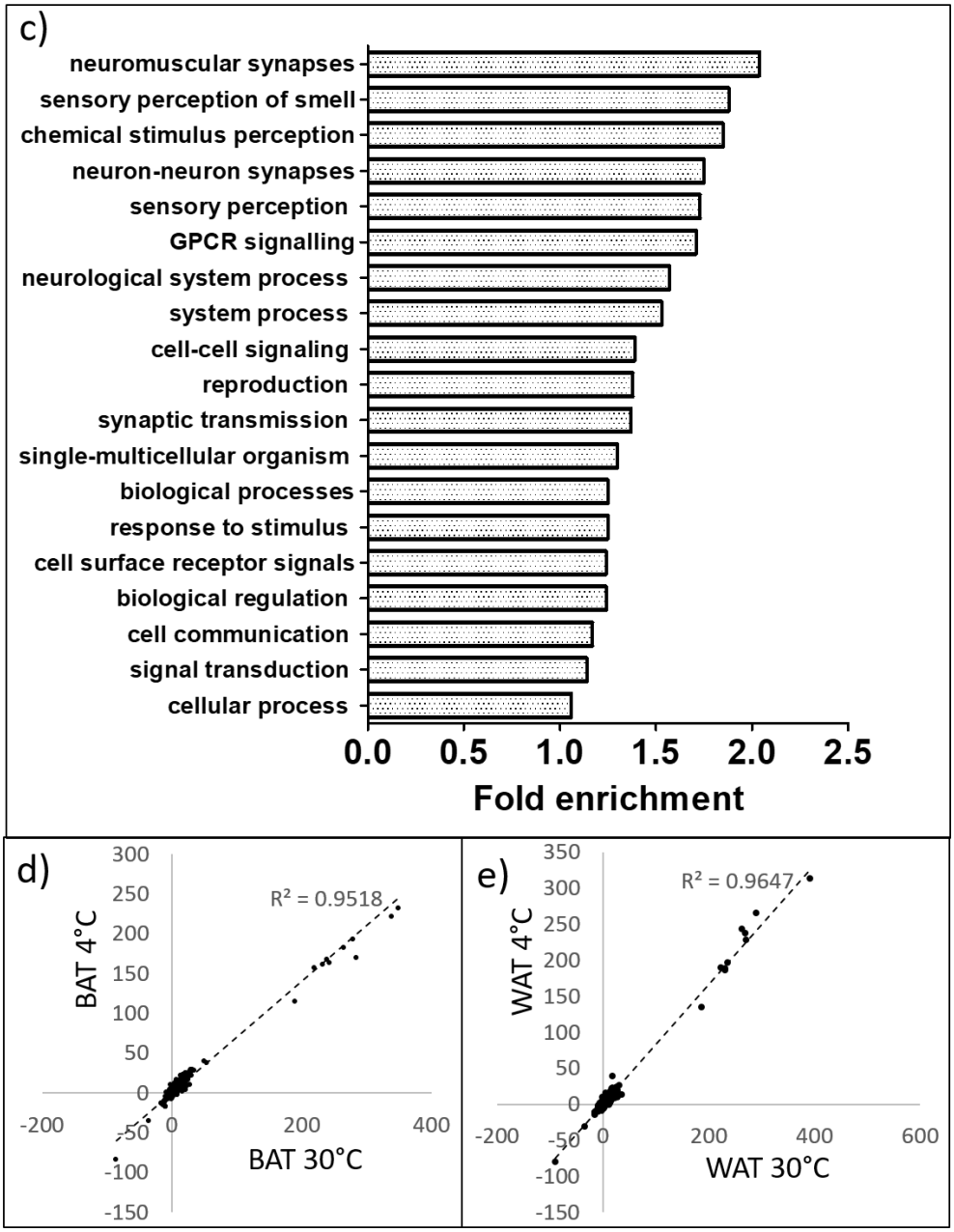


Figure 6.13. Analysis of 5-hydroxymethylcytosine DNA immunoprecipitation sequencing data for brown adipose tissue and white adipose tissue taken from animals exposed to 30°C or 4°C for 48 hours.
a) Sliding window analysis of 5-hydroxymethylcytosine DNA immunoprecipitation sequencing data for brown adipose tissue (BAT) and white adipose tissue (WAT) taken from animals exposed to 30°C or 4°C for 48 hours. Gene length represents every annotated gene in the mouse genome normalised to 100%. n = 1/group. b) Sliding window analysis of 5-hydroxymethylcytosine DNA immunoprecipitation sequencing data for WAT in wildtype (WT) and *Tet1* knockout (KO) mice (n = 3/group); compared to that of BAT and WAT taken from animals exposed to 30°C or 4°C for 48 hours (n = 1/group). c) Statistical enrichment pathway analysis for genes decreased in 5hmC (5hmC < 0) at 10% gene length in WAT. d) Mean gene 5hmC levels for thermoneutral (30°C) plotted against mean gene 5hmC levels in cold exposure (4°C) in BAT. e) Mean gene 5hmC levels for thermoneutral plotted against mean gene 5hmC levels in cold exposure in WAT. $R^2$ = Spearman's correlation coefficient.

## 6.5. Discussion

### 6.5.1. Validation of the cold exposure model

***Indirect calorimetry***

To summarise, my *in vivo* mouse model of cold exposure was validated by the observation of several of the effects of cold-induced thermogenesis. Firstly, indirect calorimetry showed a highly significant ($p = 0.00054$) increase in energy expenditure in animals maintained at 4°C for 48 hours with a concomitant increase in food intake. Respiratory exchange ratio was significantly decreased in cold exposure, indicating that animals are using a greater proportion of lipid for energy metabolism compared to carbohydrate, suggesting that they are using their adipose stores. Movement and activity levels were significantly decreased, suggesting that animals are preserving energy for heat generation. My findings agree with existing literature for the effects of cold exposure. It is well-established that fatty acids are a major energy source in activated BAT [460], thus RER would be expected to decrease. In male athletes, a seasonal reduction in the RER occurs during acute cold exposure (10°C) in winter [461] and a further study demonstrated that some individuals have increased $VO_2$ during a 24-h period of cold exposure (10°C) in winter [462]. Furthermore, in 17 male subjects, RER was significantly lower during both thermoneutral and cold exposures in winter than it was during the same periods in summer [463]. In addition, oxygen consumption increases between 2 to 4-fold in rodents after both acute and chronic cold exposure (4°C) [464, 465], a finding that supports the increased $VO_2$ and increased calorie expenditure observed by indirect calorimetry in my model.

In the first 5 hours of cold exposure, the decrease in RER is much greater. After 5 hours, RER returns to near-baseline levels. This indicates a difference in RER between acute and chronic cold exposure. Although there are no published data available on RER response in acute *vs* chronic cold exposure, there are known differences in other responses to acute *vs* chronic cold exposure. Most prominently, shivering is responsible for part of the acute response to cold exposure, but with cold adaptation, the shivering response goes away [464, 465] and the role of brown adipose tissue becomes more important. Therefore, the initial large decrease in RER observed in the first 5 hours of cold exposure could be a result of shivering thermogenesis. In addition, it could be the result of animals having to use their fat stores. Rodents often increase food intake in response to cold exposure [466, 467]. However, in my study, rate of food intake does not seem to increase until around 5 hours. Once food intake has increased to account for the extra energy expenditure, animals will be relying less heavily on their adipose stores for energy and therefore will use a greater proportion of carbohydrate, increasing RER.

***Transcriptomics***

In addition, RNA-seq data further validates my model of cold exposure. Upregulation of the thermogenic gene programme [468], including *Ucp1*, *Ppara*, *Cebpb*, *Dio*, *Elovl3* and *Pgc1a*, is observed. Furthermore, clustering of BAT & WAT RNA-seq samples by Euclidean distance allowed clustering into two distinct groups: cold exposure and thermoneutrality. On the other hand, beige adipose tissue RNA-seq data did not allow for clustering into their respective groups. This is probably due to large amount of transcriptional and metabolic heterogeneity within activated beige adipose tissue [469].

A large number of genes were up- and down-regulated in BAT (2974 up; 3087 down) and WAT (1890 up; 1000 down), and a distinctly lower amount of differential gene expression was observed in beige adipose tissue (582 up; 80 down). This could be again due to heterogeneity of the tissue and variability of gene expression from cell to cell compromising the analysis and the significance of RNA-seq results. The heterogeneity of beige adipose tissue is demonstrated in the seminal study by Wu et al., which showed that only ~40% of preadipocytes in subcutaneous adipose tissue can differentiate into UCP1-expressing beige adipocytes upon stimulation [99].

One surprising finding was the large number of changes in gene expression that occurred in WAT. Pathway analysis revealed that many of these transcriptional changes were related to fatty acid oxidation, lipid metabolic processes, catabolic processes and oxidative phosphorylation. It is already established that adrenergic stimulation increases catabolic metabolism in both BAT and WAT [470, 471] and upregulates *de novo* fatty acid synthesis, which allows cells to meet oxidative demand with enhanced synthesis [472-474]. This could account for many of the transcriptional changes observed in WAT, and indeed agrees with the results of the pathway analysis. Many of the changes in gene expression in WAT agree with previously published data of WAT in cold exposure: for example, decreased *Trib3* expression (a negative regulator of protein kinase B, which has been associated with improved adipose insulin sensitivity), increased *Hsd3b7* expression (hydroxy-delta-5-steroid dehydrogenase, a gene responsible for steroid biosynthesis) and increased *Dio2* (thyroid deiodinase I – a gene associated with increased thyroid action on cellular respiration) were all reported as "changes of note" in a 2013 study investigating gene expression in WAT in cold exposure [468], and these findings were all replicated in my sequencing data (see Figure 6.14).

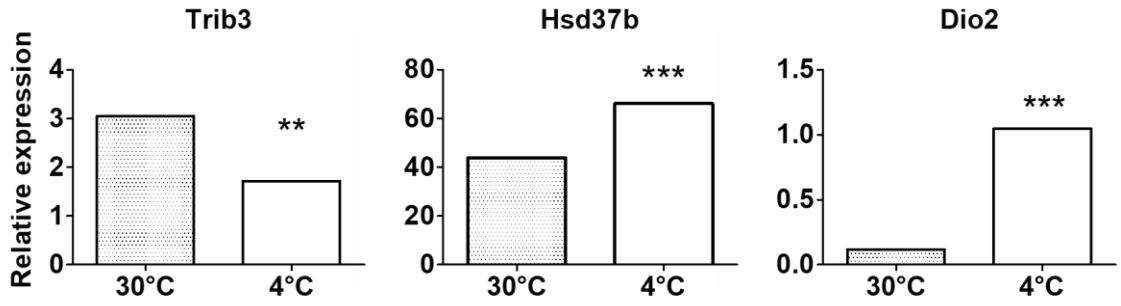


Figure 6.14. mRNA levels of *Trib3, Hsd3b7* and *Dio2.*

mRNA levels of *Trib3, Hsd3b7* and *Dio2* in WAT taken from mice maintained at thermoneutrality (30°C) or cold exposure (4°C) for 48 hours, determined by RNA-seq. n = 3/group. **q<0.01; ***q<0.001. Significance determined using q-value estimation for false discovery rate control.

### 6.5.2. Novel findings from the cold exposure model

***Analysis of whole tissue steady-state metabolite levels***

Although gene expression of activated BAT is well studied [475, 476], a surprisingly small amount of research has been published regarding metabolite levels in adipose tissue under cold exposure. Lu et al. examined the acute (up to 6 hours) metabolomic response in BAT and WAT [477] and found that lipid metabolism was activated within the first two hours of cold exposure, resulting in an increase in many lipid species including diglyceride, monoglyceride and fatty acids. They also reported significant changes in metabolites in the glycolysis and pentose-phosphate pathway after 4 hours of cold exposure. In particular, glutathione depletion in BAT was observed. With regards to the lipid species, I am unable to compare studies as I did not investigate the apolar fraction in my samples. However, my findings in the polar fraction reveal that all TCA cycle metabolites are increased in *both* BAT and WAT under cold exposure (with the exception of BAT levels of succinate and α-ketoglutarate), while Lu et al. did not observe any significant changes in polar metabolites in WAT, but nearly all polar metabolites were significantly altered in BAT with cold exposure. Similarly, this study reported that glutamate levels were increased in BAT but not WAT [477]. In my study, TCA cycle metabolite levels are higher in BAT than WAT, but fold-change increases with cold exposure are similar between tissues. This again highlights the difference between the acute response (as reported by Lu *et* al) and the chronic response to cold exposure (as investigated here).

A further study demonstrated that loss of the mechanistic target of the rapamycin complex 1 (mTORC1) affected glucose, lipid, and oxidative metabolism in the BAT of mice following chronic cold exposure (2 weeks) [478]. More recently, Hiroshima et al. [479] reported lower levels of glycolysis and gluconeogenesis intermediates in the BAT of rats exposed to 4°C for 48 hours compared to the group maintained at 22°C. In agreement with my data, they also reported higher levels of the TCA cycle metabolites. The decrease of glycolysis and gluconeogenesis intermediates

reported by Hiroshima et al. is contradictory to my study given that glycolysis-related genes were found to be overrepresented in the list of upregulated genes in WAT in cold exposure, but not BAT, and not enriched at all in the list of downregulated genes (in either tissue). Of the metabolites detected in my study, glycolysis and gluconeogenesis intermediates would include glycerol-3-phosphate (3-PG) and pyruvate. 3-PG is an intermediate in pyruvate generation. Hiroshima et al. reported a large decrease in 3-PG in BAT in cold exposure, but no change in pyruvate levels. On the other hand, I observed no changes in 3-PG or pyruvate in either BAT or WAT (see Figure 6.15). Therefore, despite the upregulation of glycolysis/gluconeogenesis intermediates reported in both studies, my data fail to support these findings. One difference between studies that could account for contradictory findings is that in my study thermoneutrality was used as a temperature control (30°C) whereas in the study mentioned above, room temperature (22°C) is used. However, these studies do support my findings of increased levels of TCA cycle metabolites in BAT.

Meanwhile, Nagao et al. [480] published a study investigating the metabolomic profile of obese adipose tissue and reported an increase in glutamate levels in obesity, accompanied by an decrease in transcription of the predominant glutamate transporter in adipose tissue, GLAST (Glutamate Aspartate Transporter) suggesting that downregulation of GLAST occurred in response to a negative feedback loop initiated by build-up of intracellular glutamate. By mining RNA-seq data from this study, I was able to show a similar decrease in GLAST expression in both BAT and WAT in cold exposure, as displayed in Figure 6.16. This suggests that GLAST could be responsible for the increase in intracellular glutamate levels in cold exposure, and that a similar negative feedback mechanism occurs in cold exposure as does in obesity.

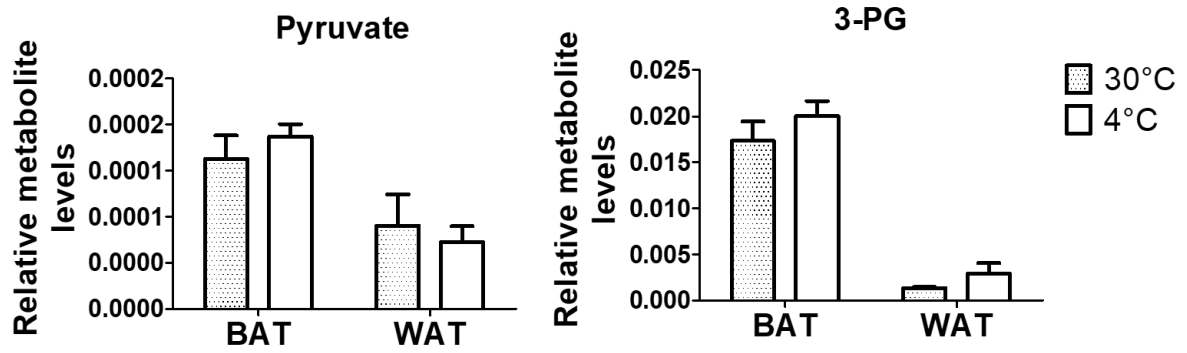


Figure 6.15. Relative levels of glycolysis/gluconeogenesis intermediates.
Relative levels of glycolysis/gluconeogenesis intermediates in brown adipose tissue (BAT) and white adipose tissue (WAT) from mice maintained at thermoneutrality (30°C) or cold exposure (4°C) for 48 hours. 3-PG = glycerol-3-phosphate. n = 5/group.

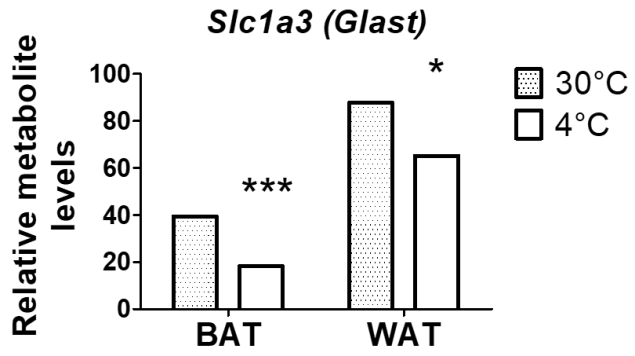


Figure 6.16. mRNA levels of the Glutamate-Aspartate Transporter, determined by RNA-seq.
mRNA levels of the Glutamate-Aspartate Transporter (GLAST), the predominantly expressed glutamate transporter in adipose tissue, under thermoneutrality (30°C) and cold exposure (4°C) in brown adipose tissue (BAT) and white adipose tissue (WAT). n = 3/group. **q<0.01; ***q<0.001. Significance determined using q-value estimation for false discovery rate control.

The increase in TCA cycle metabolites observed in my study could indicate increased flux rate of the TCA cycle. Alternatively, it could indicate decreased metabolite clearance. Unfortunately these data represent static mass spectrometry measurements and give little indication as to metabolite flux, so we can only speculate as to the cause of metabolite increase. A more informative method to use would be to use carbon-labelling methods, which would allow analysis of carbon cycling and from which we would be able to draw conclusions about metabolite flux. Furthermore, as whole tissue was used rather than isolated cells, there is no way of telling whether the increase in metabolites is intracellular or extracellular.

However, a potential approach to overcome this limitation is to estimate metabolic flux ratios (the relative contributions of each reaction feeding into a specific metabolite pool), as reviewed in [481]. Here I have analysed NADH-forming reactions (see Figure 6.5), given that these ratios can be used as substitutes for NAD+:NADH ratios, indicating the levels of oxidation or reduction. As the ratio of substrate:product is linked to the oxidation or reduction of NAD+/NADH, then a change in one suggests that there is a change in the other. For example, the conversion of α-ketoglutarate to succinate also reduces the reduction of NAD+ to NADH in a 1:1 ratio, i.e. for every mole of succinate produced, one mole of NADH is also formed.

However, in substrate:product ratios (e.g. α-KG:succinate), an increased ratio would suggest that the build-up of the substrate is not being matched by the degradation of the product, or that degradation of the product is more rapid that the production of the substrate. Given that the reaction also reduces NAD+ to NADH, an increase in the ratio could suggest that less NAD+ is being reduced – but could

also mean that the rate stays the same, and the product is being removed more rapidly. Changes in the NAD+:NADH ratio in the mitochondria could indicate an alteration in respiration.

Of the three reaction ratios representing NAD+:NADH, (citrate:α-KG; malate:citrate; α-KG:succinate), the results are contradictory. Two of the reaction ratios (malate:citrate in BAT; and α-KG:succinate in WAT) indicate an increased product:substrate ratio in cold exposure, suggesting a greater rate of product generation or decreased product clearance. This would also indicate greater levels of NAD+ reduction, suggesting that there is an increase in respiration. However, citrate:α-ketoglutarate is significantly decreased in WAT in cold exposure, suggesting lower levels of NAD+ reduction and decreased respiration rate. In addition, malate:citrate in WAT, α-KG:succinate in BAT, and citrate:α-KG in BAT all have unchanged ratios under cold exposure, indicating no change in NAD+ reduction and no change in rate of respiration. While these ratios can sometimes be helpful to analyse, in this case the amount of conflicting evidence makes it difficult to draw any conclusions.

I also analysed the ratio of (α-KG:succinate + fumarate) given that α-KG is a cofactor for TET enzymes and succinate and fumarate can inhibit TETs, so looking at this ratio can give an indication of TET inhibition or activation. There was no significant change in either BAT or WAT, although a p value of 0.07 in WAT suggests that the increase in (α-KG:succinate + fumarate) ratio may be trending towards significance and may just be underpowered. However, an increase in (α-KG:succinate + fumarate) ratio is inconsistent with the decrease in TET activity observed in WAT (discussed further in section 6.5.3).

Furthermore, analysing the serine:glycine ratio may be insightful, as this reaction produces one-carbon units for biosynthesis and methylation reactions [482, 483]. One-carbon metabolism integrates carbon units from amino acids (serine and glycine), and generates diverse outputs, such as the maintenance of redox status, the biosynthesis of lipids, nucleotides and proteins, and the substrates for methylation reactions, particularly those mediated by SAM (S-adenosyl methionine). The epigenetic reactions mediated by SAM involve the transfer of methyl groups onto the arginine and lysine residues of proteins, DNA histones, RNA and intermediary metabolites [484]. Therefore, one-carbon metabolism is thought to be tightly linked to histone methylation [485, 486]. The serine:glycine ratio is unchanged in WAT in cold exposure but increased in BAT. This suggests that BAT activation may increase the production of one-carbon units, which may have an impact on histone methylation. This provides justification to investigate the histone status of key genes in BAT in cold exposure.

Furthermore, analysis was carried out on mass spectrometry data of amino acid levels. Different amino acids can feed into the TCA cycle by acting as precursor molecules to TCA cycle metabolites. For example, aspartate, which feeds into oxaloacetate; and glutamate, which feeds into α-

ketoglutarate, follows similar patterns to the constitutive TCA cycle metabolites (increased at 4°C compared to 30°C; and increased in BAT compared to WAT). This suggests that these feeder amino acids are indeed involved with forming the relevant constitutive TCA cycle metabolites. On the other hand, asparagine, which also feeds into oxaloacetate, does not follow this same pattern, suggesting that aspartate is more closely involved with oxaloacetate formation compared to asparagine in this system.

Pathway analysis combining RNA-seq data of mRNA levels and mass spectrometry data of metabolite levels can provide a bigger overall picture as to what is changing in the TCA cycle. In BAT, there is upregulation of the expression of the majority of measured enzymes and metabolites, but a reduction is observed in the metabolite glycine and the enzyme pyruvate carboxylase, possibly suggesting lower rates of glycolysis in cold exposure in BAT, contrary to the published literature [477, 479]. On the other hand, pyruvate is unchanged. The combined pathway analysis also shows downregulation of the 2-oxoglutarate dehydrogenase (also known as α-ketoglutarate dehydrogenase), the enzyme that converts α-ketoglutarate to succinyl co-A. This could be an effect of the increased levels of α-ketoglutarate in cold exposure, such that 2-oxoglutarate dehydrogenase expression is decreased in order to limit the conversion of α-ketoglutarate to downstream succinate, thus acting to control the rate of reaction.

However, combined pathway analysis in WAT suggests that there is a greater upregulation of TCA cycle enzymes and metabolites in WAT compared to BAT, with a greater number of enzymes and metabolites upregulated. This TCA cycle upregulation could be occurring in WAT in order to fuel lipolysis. It is well-established that WAT contributes to BAT thermogenesis by mobilising energy stores in the form of lipolysis [460]. Indeed, this is the basis of many of the significantly upregulated gene pathways in WAT (e.g. β-oxidation, lipid metabolic processes – see Figure 6.8c). The reaction for one cycle of β-oxidation (fatty acid hydrolysis) is as follows:

$$C_n\text{-acyl CoA} + FAD + NAD^+ + H_2O + CoA \rightarrow C_{n-2}\text{-acyl CoA} + FADH_2 + NADH + H^+ + \text{acetyl CoA};$$

where $n$ = number of carbons in the acyl CoA chain. The substrates to this reaction are not generated from the TCA cycle, but rather the product (acetyl CoA) feeds into the TCA cycle. Therefore there is no obvious reason why upregulation of the TCA cycle enzymes and metabolites, or increased rate of TCA cycle flux, would be required from WAT under cold exposure. Indeed, increased levels of TCA cycle metabolites could be the result of either increased metabolite production or decreased metabolite clearance. In either case it is likely that these increases are the result of increased TCA cycle flux, although we cannot categorically conclude that using steady-state GCMS.

Glucose uptake studies have reported that 48 hours cold exposure increases glucose utilisation 4- to 20-fold in WAT, as well as 8-fold in the heart and 2- to 5-fold in skeletal muscle (compared to 110-fold in BAT) [487], suggesting increased rate of respiration in all these tissues. However, insulin responsiveness increased during cold acclimation in WAT, but decreased in BAT [487]. Another difference between BAT and WAT in cold exposure was that this increase in insulin responsiveness persisted in WAT after return to the warm for 18 hours, but in BAT, heart and skeletal muscle, glucose uptake returned to normal levels. This suggests that cold exposure produces more permanent alterations in glucose metabolism in WAT compared to the other tissues.

Clearly some of the functions of WAT in cold exposure are not fully understood, and further research is required in this area to determine the cause of/requirement for the increased glucose uptake, upregulation of TCA cycle enzymes and metabolites in WAT in cold exposure.

### 6.5.3. The effects of cold exposure on epigenetic factors

*Tet1* mRNA levels were reduced in WAT and *Tet2* mRNA levels were reduced in BAT. Furthermore, cold exposure significantly decreased overall TET activity in WAT but not BAT. This is perhaps unexpected given the near-significant finding of increased ratio of α-ketoglutarate:(succinate + fumarate) in cold exposure in WAT. This increase was not significant but a p value of 0.07 suggests that the experiment may simply have been underpowered. Indeed, power calculations suggest that a sample size of 10 per group would be required to give sufficient statistical power (0.8). An increased ratio of α-ketoglutarate:(succinate + fumarate) would indicate that there is a greater proportion of TET substrates as compared to TET inhibitory factors, which could theoretically be associated with an *increase* in TET activity, but this is not observed.

Decreased TET activity may be associated with an increase in 5mC and a decrease in 5hmC levels due to decreased demethylase activity upon 5hmC modifications. Indeed, *Tet1* KO embryonic stem cells (ESCs) have decreased global 5hmC by around 35% [326]. However, this is not reflected in 5mC or 5hmC levels as determined by ultra-performance liquid chromatography, as there is no change in the levels of either modification resulting from cold exposure.

hMeDIP-seq analysis provided interesting findings regarding the pattern of 5hmC in adipose tissue. In contrast to previously analysed hMeDIP-seq data from WAT (see Chapter 3), 5hmC in BAT across all genes (with normalised gene length) generally appears to trough at around 10% gene length, with another smaller trough at around 70% gene length. This was shown in BAT 30°C and 4°C and WAT at 4°C; but in WAT at 30°C, the 5hmC profile more closely resembles the 5hmC profile previously demonstrated in WAT (see section 3.4.5 and Figure 6.13b). Therefore, the epigenetic signature of BAT differs from WAT at this locus, suggesting that BAT has a unique 5hmC profile compared to

that of WAT. This alternative 5hmC profile may be involved in activation of the thermogenic gene programme, although further investigation is required into this hypothesis.

In addition, cold exposure induces large changes in WAT 5hmC at this locus that closely resemble the 5hmC signature of BAT. This finding suggests that changes in 5hmC at this locus occur in WAT as a result of cold exposure, and these changes may be involved with some of the transcriptional or even metabolomic changes that occur in WAT under cold exposure. However, this study only demonstrates an association between cold exposure and changes in 5hmC, and a tentative one at that given that the number of biological replicates is only one per group. Further study is required to determine whether these changes in 5hmC in WAT in cold exposure are causative of changes in gene expression.

The 5hmC profile in both BAT and WAT contrasts with the 5hmC profile published in other tissues including mouse liver [308, 488, 489], mouse brain [488], human chondrocytes [490], mouse embryonic fibroblasts [491], human embryonic stem cells [492], and human colon mucosa [493], which exhibit a large trough in 5hmC at the transcriptional start site (0% gene length) with fluctuating 5hmC levels intragenically; a pattern that is altered in various states including liver cancer [308] and states of active transcription [309]. Given that the pattern of 5hmC in WAT at room temperature and at thermoneutrality was the same in two separate experiments (the *Tet1* KO study and the cold exposure study, with a total n of 10), I propose that WAT and BAT have a distinct epigenetic signature with regards to 5hmC. The reason for this is unknown: perhaps it is the result of using whole tissue rather than a single isolated cell type. Whole adipose tissue is composed of many different cell types, including adipocytes, preadipocytes, stem cells, macrophages, neutrophils, lymphocytes, and endothelial cells [494]. With this mix of cells, many genes will be transcriptionally heterogeneous, and this could cause "noise" in the 5hmC signal at the transcriptional start site. The reason for the peak in 5hmC at 10% gene length in WAT (or trough in BAT) is unknown, and no published information is available on the typical hydroxymethyl state or its function this gene locus. Further work is required to determine the reasons for the unique 5hmC profile of adipose tissue.

The relevance of the subset of genes that have decreased levels of 5hmC specifically at 10% gene length is debatable. Statistical overrepresentation pathway analysis suggests that this subset of genes (5hmC > 0 at 10% gene length) are involved predominantly in synaptic transmission, sensory perception of smell and perception of chemical stimuli. However, many genes within the pathways "sensory perception of smell" and "perception of chemical stimuli" are notably small in gene length. For example the Olfactory Receptor (*Olfr*) genes, of which there are 800 in humans and 1400 in mice [495], make up a large part of these two gene pathways. *Olfr* genes are often only 2-5 Kb in length. This leaves them highly susceptible to analytical bias, given that a change in the 5hmC of these genes will weigh more heavily on the overall total gene (e.g. 200bp window of a 2 Kb gene = 10%; 200bp

window of a 15 Kb gene = 1.3%). Furthermore, the high number of these genes within the genome also predisposes the pathway "sensory perception of smell" to bias.

In addition, the relevance of the upregulated pathway "synaptic transmission" is also debatable. This pathway mainly includes synaptic neurotransmitter receptors such as gamma-aminobutyric acid receptor subunit gamma-2 (*Gabrg2*), acetylcholine receptor subunit beta (*Chrnb1*), neuronal acetylcholine receptor subunit beta-3 (*Chrnb3*), 5-hydroxytryptamine receptor 3B (*Htr3b*) and glycine receptor subunit alpha-4 (*Glra4*). It seems unlikely that the differential 5hmC profile of these genes in WAT would have any functional significance, given that these genes are largely expressed in neurones of the brain. Therefore, it is possible that the decrease in 5hmC at 10% gene length in WAT genes is not functionally relevant.

***Comparison of methods: UPLC vs hMeDIP-seq***

UPLC suggested that, while there was no difference in 5mC or 5hmC in WAT or BAT taken from mice at 30°C or 4°C, global 5mC levels – but not 5hmC levels – were significantly higher in BAT compared to WAT. While this cannot be compared with the hMeDIP-seq data as a 5mC assay was not carried out by this method, we can compare 5hmC data between methods. Indeed, DIP data supports the UPLC findings that there is little difference in 5hmC between tissues and between temperatures. DIP also provides further information as 5hmC levels can be compared at different regions within the gene, for example, allowing us to investigate 5hmC levels in promoter or intragenic regions.

### 6.5.4. Benefits and drawbacks of the mouse model of cold exposure

There is some debate surrounding the scope for the use of mice as a model for cold-induced thermogenesis. Although BAT has been identified to be functional in human adults [49, 50] with a high glucose demand that increases in response to cold exposure [51], species-specific differences have recently been identified in UCP-1 regulation [496]. Ramage et al. demonstrated that glucocorticoid treatment has opposing actions in BAT in humans and mice [496]: *in vitro* in human primary brown adipocytes, glucocorticoid treatment increased isoprenaline-stimulated respiration and UCP-1 expression. Similarly, *in vivo* in healthy male subjects exposed to the cold, glucocorticoid treatment increased BAT glucose uptake, increased supraclavicular skin temperature, and increased energy expenditure. However, in mouse primary brown adipocytes, glucocorticoid treatment displayed the opposite effect, decreasing isoprenaline-stimulated respiration and UCP-1 expression.

In addition to this, other differences exist between rodent and humans regarding BAT function. For example, cold exposure increases food intake in animal species including mice (as observed in this study), piglets [497], rats and birds [498], but not in humans [499]. Furthermore, it has been suggested

recently that human BAT may be more closely related to rodent beige adipose, rather than the classical rodent BAT [48, 500, 501]. This is important to bear in mind when considering the translatability of research in rodent models of cold-induced thermogenesis.

### 6.5.5. Conclusions

In summary, I have validated my mouse model of cold-induced thermogenesis with indirect calorimetry and transcriptomic data, although the differences between rodent and human BAT must be acknowledged. I have observed increases in all TCA cycle metabolites in cold exposure in both BAT and WAT (with the exception of succinate and α-ketoglutarate in BAT). The increase of these metabolites in BAT is supported by two independent studies, but these increases in WAT have not been previously reported and the reason behind the need for their upregulation requires further research. In the absence of any significant changes in the ratio of α-KG:succinate+fumarate, decreased TET activity was observed in WAT, but not BAT or beige adipose tissue. However, no changes were observed in the 5hmC levels globally (UPLC) or across genes (hMeDIP-seq). Interestingly, a large trough in 5hmC was observed at 10% gene length in BAT at 30°C and 4°C and WAT at 4°C, whereas in other WAT samples, a peak in 5hmC levels usually occurs at 10% gene length. The subset of genes with large decreases in 5hmC at this particular locus BAT at 30°C and 4°C and WAT at 4°C include genes involved with sensory perception of smell. The relevance of this in BAT and WAT is debatable. In conclusion, TET enzymes and 5hmC do not appear to be solely responsible for driving changes in gene expression on cold exposure, although they may act alongside other mechanisms to alter gene expression.

# 7. Discussion

## 7.1. Summary

In this thesis I have investigated the role of TET1 in adipose tissue in both diet-induced obesity and in cold exposure. The current extent of the obesity crisis highlights the need for a better understanding of adipose tissue biology and an option of pharmacological interventions. I have demonstrated that a lack of the *Tet1* gene causes decreased susceptibility to diet-induced obesity by reducing food intake, and that this may be linked to a reduction in *Lep* transcription. I have also demonstrated that TET activity is significantly decreased in white adipose tissue in cold exposure, but not in brown adipose tissue, although this is not associated with any significant changes in the ratio of TET "activating" to "inhibitory" metabolites, or with any global changes in 5hmC.

## 7.2. Novel findings of this thesis

### 7.2.1. The role of TET1 in obesity

A role for the TET enzymes in adipose tissue was first discussed in 2012 in a publication by Fujiki et al., which demonstrated that PPARγ recruits TET enzymes and directs local demethylation around PPREs resulting in the transcription of adipocyte-specific genes [383]. Further work demonstrates that this recruitment of the TET enzymes occurs in a process facilitated by the CCCTC-binding factor (CTCF) [382]. Enrichment of 5hmC has been identified at over 20% of PPARγ binding sites, suggesting this modification is functionally important in gene regulation at these sites [384]. Further, double knockout (DKO) of *Tet1* and *Tet2* inhibited the adipogenic differentiation of mouse embryonic fibroblasts (MEFs) *in vitro,* associated with pronounced hypermethylation of promoter regions of genes involved in adipogenesis and adipocyte function [385]. However, the work covered in this thesis explores for the first time the effects of *Tet1* deletion in adipose tissue *in vivo*. A schematic representing a summary of these findings is displayed in Figure 7.1.

| Body weight | Fat mass | Glucose tolerance | Insulin sensitivity | Movement | Respiratory exchange ratio | Energy expenditure | Food intake | Leptin sensitivity | Bone MAT |
|---|---|---|---|---|---|---|---|---|---|
| ↓ | ↓ | ↔ | ↑ | ↑ | ↑ (light phase only) | ↓ | ↓ | ↑ | ↔ |

Figure 7.1. A summary of the effects of *Tet1* knockout (KO) on the metabolic phenotype of mice exposed to high fat diet (HFD), as compared to wildtype (WT) littermates.

Firstly, these data support the hypothesis that *Tet1* deletion reduces fat accumulation in diet-induced obesity. However, after analysis of indirect calorimetry, *in vitro* adipocyte lipid accumulation and

transcriptomics, it can be concluded that this reduction in fat mass is not a primary result of *Tet1* deletion in adipose tissue. Analysis of food intake and paired feeding revealed that *Tet1* deletion is associated with decreased food intake. I proposed that decreased leptin transcription, decreased serum leptin and increased leptin sensitivity in the *Tet1* KO mouse is the mechanism or a contributing mechanism behind this decreased food intake. While leptin transcription and serum leptin were indeed decreased resulting in increased leptin sensitivity in the *Tet1* KO mouse, evidence from global hMeDIP-seq and bisulfite pyrosequencing of the leptin promoter suggested that the decrease in *Lep* transcription is not the result of TET1-mediated changes in 5hmC or 5mC in adipose tissue. This is in contrast to a number of studies demonstrating the close association between the methylation status of the *Lep* promoter and *Lep* transcriptional status [343, 427-433]. Thus, while this study adds novel findings to the field of obesity regarding TET1 in the central control of obesity, its contribution to the field of *Lep* epigenetics is inconsistent with much of the current literature.

While *Tet1* KO mice were found to have lower levels of most adipose tissue depots, the bone marrow adipose levels were unaltered in KO mice. This is unusual, given the fact that obesity is associated with increased MAT in both humans [158, 159] and rodents [160, 162], so even if TET1 does not directly affect MAT development or deposition, decreased levels of MAT would be expected in the *Tet1* KO mouse as a secondary result of decreased overall adiposity. A possible explanation for this lack of change is that, while KO mice were 'lean' relative to their WT littermates, they still gained some fat mass on HFD and therefore displayed increased adipose tissue levels compared to non-high fat-fed mice. Thus, it is possible that both WT and KO levels of MAT increased to similar extents. To confirm this hypothesis, a control diet study investigating MAT in WT and KO mice should be carried out.

### 7.2.2. The role of TET1 in cold exposure

While various histone modifiers have recently been reported to have influence over transcriptional activation of the thermogenic gene programme [399-405], this study is the first to my knowledge to investigate the role of CpG modifications in cold-induced thermogenesis. I found that, while global levels of 5hmC and 5mC are unchanged in whole brown and white adipose tissue in cold exposure, there is a key difference in BAT and WAT 5hmC profiles at 10% gene length (further discussed in Section 6.5.3). In addition, although a handful of publications have reported changes in metabolite levels in cold-exposed adipose tissue [477-479], this thesis demonstrates for the first time large changes in metabolite levels in whole WAT under cold exposure, contrary to the study by Lu et al. [477], which reported a lack of significant changes in the metabolite response to cold exposure in WAT. The increase in TCA cycle metabolites could indicate increased flux rate of the TCA cycle or decreased metabolite clearance. Further work is required to determine the cause of increased

metabolite levels in cold exposure. In summary, this thesis makes novel contributions to both fields of epigenetics in cold exposure, and metabolomics in cold exposure.

### 7.2.3. The role of TET1 in adipose tissue

***Tet1 expression in primary adipocytes***

For the first time to my knowledge, this thesis examines the expression of *Tet1* in preadipocytes throughout early differentiation, and finds that *Tet1* expression decreases throughout differentiation This is logical, given that TET1 has previously been reported to be associated with the pluripotent state [325, 326, 502]. Therefore, as preadipocytes differentiate away from the pluripotent state, *Tet1* expression decreases. Furthermore, *Tet2* and *Tet3* expression seem to increase with differentiation. This would perhaps be predicted for *Tet2*, which is more highly expressed in somatic cells [503], but not for *Tet3*, which is most highly expressed at the oocyte to zygote stage of development [504]. However, with n = 1, this study needs repeating if we are to draw any valid conclusions.

***Abnormal 5hmC patterns in adipose tissue***

This thesis has also revealed that 5hmC patterns in WAT and BAT differ from those published in mouse liver [308, 488, 489], mouse brain [488], human chondrocytes [490], mouse embryonic fibroblasts [491], human embryonic stem cells [492], and human colon mucosa [493], which exhibit a large trough in 5hmC at the transcriptional start site (TSS) with fluctuating 5hmC levels intragenically. Here, no trough was observed at the TSS in WAT, but a relative 5hmC peak was observed at ~10% gene length. While WAT displays a peak in 5hmC at 10% gene length, BAT displays a relative trough at this locus, suggesting that BAT has a unique 5hmC profile compared to that of WAT. This alternative 5hmC profile may be involved in activation of the thermogenic gene programme, although further investigation is required into this hypothesis. Furthermore, cold exposure induces large changes in WAT 5hmC at this locus that closely resemble the 5hmC signature of BAT, suggesting that changes in 5hmC occur at this locus in WAT as a result of cold exposure, and that these changes may be involved with some of the transcriptional changes that occur in WAT under cold exposure.

## 7.3. Limitations

### 7.3.1. Limitations of the *Tet1* knockout model

The *Tet1* KO mouse model used in this study is a global knockout. This has two main limitations: firstly, any effects observed in this model may be the result of *Tet1* deletion in other tissues. For example, the reduction in food intake observed in the *Tet1* KO mouse could be caused by 5hmC and associated gene expression changes in the brain. Secondly, the global *Tet1* KO mouse lacks *Tet1* throughout embryonic and postnatal development. Therefore, any changes observed in the KO mouse

may not be the direct result of *Tet1* deletion in adulthood, but rather secondary changes that occurred due to the lack of *Tet1* in development. This is particularly relevant given that *Tet1* is expressed more highly throughout development than in adulthood. To overcome these limitations, the development of an inducible Adipoq-Cre *Tet1* KO mouse would be beneficial. This would allow the deletion of *Tet1* specifically in WAT and BAT (adiponectin-expressing cells) at the desired stage of development.

A further limitation of this model is that the effects of *Tet1* deletion are difficult to discern from the effects of the altered HFD response of the KO mice. Although a control diet study was carried out to validate any findings of interest, the sequencing studies were not carried out control diet-fed animals due to constraints on number of animals and financial considerations. Therefore, the analysis of the sequencing studies is limited by this.

### 7.3.2. TET1 as a pharmacological target

In any study proposing to investigate the science of human disease, the clinical relevance should be assessed. TET1 may not be an appropriate pharmacological target in the treatment of obesity because of the ubiquitous nature of its expression and activity. Interfering with the expression or activity of TET1 *in vivo* is likely to have unknown off-target effects which could negatively impact on human health. Although there are a range of epigenetic therapies currently in clinical use and/or clinical trials, including DNA methylation inhibitors [505], bromodomain inhibitors [506], HAT inhibitors [507], histone methylation inhibitors [508], and HDAC inhibitors [509], these are generally approved for the use of cancers in which known epigenetic modulation occurs. Meanwhile, more work is required to investigate the epigenetic changes which underlie obesity. In addition, while rapid and often aggressive drug therapy is often required for the treatment of cancers, the off-target effects such as diarrhoea, fatigue, nausea, and anorexia [510] are tolerated. However, for obesity, in which treatment is less time-pressing, these side effects would be avoided.

Furthermore, the work in this thesis assumes that the role of TET1 in mouse adipose tissue is homologous to that of human adipose tissue. However, this may not be the case. As a pilot study in humans, it would be beneficial to examine the expression of *TET1* and the abundance of 5mC/5hmC in different adipose tissue depots and compare it to measures such as body mass index, hip-to-waist ratio and daily calorie intake. Furthermore, the role of adipose tissue may differ between mice and humans, particularly that of BAT. Although BAT has been identified to be functional in human adults [49, 50] with a high glucose demand that increases in response to cold exposure [51], species-specific differences have recently been identified in UCP-1 regulation [496]. Therefore, this work should be pursued in human cells or in human *in vivo* studies.

Finally, in this thesis, I demonstrate associations between 5hmC and gene expression but not causation. Epigenetics research often demonstrates associations between epigenetic changes and gene expression, or epigenetic changes and disease state, but determining functional changes is more challenging. However, while further work is required to assess the potential of TET1 as a pharmacological target, this thesis has begun to shed light on the role of TET1-mediated epigenetic changes in adipose tissue, a research field that was relatively unpursued.

## 7.4. Future directions

A number of future directions could be pursued following the findings of this thesis. Firstly, given the food intake and leptin expression phenotype of the *Tet1* KO mouse model, the role of TET1 in central control of food intake should be investigated further. I hypothesise that understanding the mechanism behind the reduced food intake of the KO mice could yield further avenues for therapeutic intervention, since the majority of approved pharmaceutical interventions for the treatment of obesity target pathways within the central nervous system, one of which is even an epigenetic modifier (topiramate). To investigate this, a neurone-specific *Tet1* knockout should be generated, for example using the mouse neurofilament-H (mNF-H)-cre transgenic mouse line, which specifically targets neurones in the cortex and hippocampus. This is particularly relevant given the importance of the hippocampus in control of food intake. Following the generation of neuronal *Tet1* KO mice, phenotypic screening should be carried out to determine food intake and indirect calorimetric response. In addition, gene expression and 5hmC/5mC profiling may reveal specific gene sets in which TET1 is likely to cause its effect.

The abnormal 5hmC profile of adipose tissue should be further investigated, with emphasis on determining any functional significance of the 10% gene length locus, despite the fact that pathway analysis of genes with altered 5hmC with cold exposure in WAT at this locus did not reveal highly enriched pathways of particular significance. I suggest that analysing the adipose tissue phenotype in Adipoq-Cre *Tet1* knockout mice would give insight into this. For example, it could be possible that TET1 does not play a large role in the regulation of adipose tissue gene expression, in which case, no changes would be observed in the Adipoq-Cre *Tet1* knockout.

An interesting avenue for further investigation would be to determine the cause of metabolite changes in cold exposure. For this, carbon labelling studies would be insightful, to determine the carbon flow within the TCA cycle and associated metabolites. This would demonstrate whether increased levels of TCA cycle metabolites in BAT and WAT in cold exposure are caused by increased metabolite production or decreased metabolite clearance. This knowledge would allow us to further understand metabolomic changes in cold exposure. Furthermore, novel findings could be generated from the

investigation of these changes in WAT, which have not been previously reported. Understanding the reason for increased TCA cycle metabolite levels in WAT would be very interesting and may reveal a novel role for WAT in cold exposure. To further investigate this, carbon labelling may again be insightful to observe the carbon flow within the TCA cycle. Following this, *in vitro* manipulation of the TCA cycle in adipocytes (e.g. by inhibiting various enzymes within the cycle) may reveal important roles for WAT in cold exposure.

I further propose that studies should be carried out in human adipose tissue to investigate expression levels of the TET enzymes in association with various metabolic parameters such as body mass index, hip-to-waist ratio and daily calorie intake. This will help determine the translatability of these studies.

## 7.5. Conclusions

In conclusion, this thesis begins to shed light on the roles of TET1 in adipose tissue. I have confirmed that *Tet1* gene deletion results in a level of protection against obesity, which is associated with decreased food intake and increased leptin sensitivity, but the mechanism for this appears not to be a primary effect of *Tet1* deletion in adipose tissue. Further work should investigate the role of TET1 in central control of food intake. I also report an unusual 5hmC profile in adipose tissue, which appears to differ in BAT and changes in WAT in response to cold exposure. This should be confirmed in studies with a higher number of replicates. Although TET1 is an unlikely therapeutic target, identification of TET1-mediated changes in obesity could reveal downstream molecules or pathways that offer potential therapeutic intervention.

# References


1. *Obesity: preventing and managing the global epidemic. Report of a WHO consultation.* World Health Organ Tech Rep Ser, 2000. **894**: p. i-xii, 1-253.
2. Organisation, W.H. *10 facts on obesity*. 2014 13/07/2015]; Available from: http://www.who.int/features/factfiles/obesity/en/.
3. Guh, D.P., et al., *The incidence of co-morbidities related to obesity and overweight: A systematic review and meta-analysis.* BMC Public Health, 2009. **9**(1): p. 88.
4. Organisation, W.H. *Obesity and overweight fact sheet*. 2015 13/07/2015]; Available from: http://www.who.int/mediacentre/factsheets/fs311/en/.
5. Science, G.O.f., *Reducing obesity: future choices*, in *Research and analysis*, www.gov.uk, Editor. 2007, UK Government: www.gov.uk.
6. van Dam, R.M., et al., *Dietary patterns and risk for type 2 diabetes mellitus in U.S. men.* Ann Intern Med, 2002. **136**(3): p. 201-9.
7. Schulze, M.B., et al., *Dietary patterns and changes in body weight in women.* Obesity (Silver Spring), 2006. **14**(8): p. 1444-53.
8. Neel, J.V., *Diabetes mellitus: a "thrifty" genotype rendered detrimental by "progress"?* Am J Hum Genet, 1962. **14**: p. 353-62.
9. Prentice, A.M., P. Rayco-Solon, and S.E. Moore, *Insights from the developing world: thrifty genotypes and thrifty phenotypes.* Proc Nutr Soc, 2005. **64**(2): p. 153-61.
10. Lazar, M.A., *How obesity causes diabetes: not a tall tale.* Science, 2005. **307**(5708): p. 373-5.
11. Considine, R.V., et al., *Evidence against either a premature stop codon or the absence of obese gene mRNA in human obesity.* Journal of Clinical Investigation, 1995. **95**(6): p. 2986-2988.
12. Friedman, J.M., R.L. Leibel, and N. Bahary, *Molecular mapping of obesity genes.* Mammalian Genome, 1991. **1**(3): p. 130-144.
13. Farooqi, I.S., et al., *Effects of Recombinant Leptin Therapy in a Child with Congenital Leptin Deficiency.* New England Journal of Medicine, 1999. **341**(12): p. 879-884.
14. Farooqi, I.S., *EJE Prize 2012: Obesity: from genes to behaviour.* Eur J Endocrinol, 2014. **171**(5): p. R191-5.
15. Elks, C.E., et al., *Variability in the heritability of body mass index: a systematic review and meta-regression.* Front Endocrinol (Lausanne), 2012. **3**: p. 29.
16. Maes, H.H., M.C. Neale, and L.J. Eaves, *Genetic and environmental factors in relative body weight and human adiposity.* Behav Genet, 1997. **27**(4): p. 325-51.
17. Friedman, J., *The long road to leptin.* The Journal of Clinical Investigation, 2016. **126**(12): p. 4727-4734.
18. Frayling TM, T.N., Weedon MN, Zeggini E, Freathy RM, Lindgren CM, Perry JR, Elliott KS, Lango H, Rayner NW, Shields B, Harries LW, Barrett JC, Ellard S, Groves CJ, Knight B, Patch AM, Ness AR, Ebrahim S, Lawlor DA, Ring SM, Ben-Shlomo Y, Jarvelin MR, Sovio U, Bennett AJ, Melzer D, Ferrucci L, Loos RJ, Barroso I, Wareham NJ, Karpe F, Owen KR, Cardon LR, Walker M, Hitman GA, Palmer CN, Doney AS, Morris AD, Smith GD, Hattersley AT, McCarthy MI., *A common variant in the FTO gene is associated with body mass index and predisposes to childhood and adult obesity.* Science, 2007. **316**(5826): p. 889-94.
19. Thorleifsson G, W.G., Gudbjartsson DF, Steinthorsdottir V, Sulem P, Helgadottir A, Styrkarsdottir U, Gretarsdottir S, Thorlacius S, Jonsdottir I, Jonsdottir T, Olafsdottir EJ, Olafsdottir GH, Jonsson T, Jonsson F, Borch-Johnsen K, Hansen T, Andersen G, Jorgensen T, Lauritzen T, Aben KK, Verbeek AL, Roeleveld N, Kampman E, Yanek LR, Becker LC, Tryggvadottir L, Rafnar T, Becker DM, Gulcher J, Kiemeney LA, Pedersen O, Kong A, Thorsteinsdottir U, Stefansson K., *Genome-wide association yields new sequence variants at seven loci that associate with measures of obesity.* Nat Genet, 2009. **41**(1): p. 18-24.

20. Willer CJ, S.E., Loos RJ, Li S, Lindgren CM, Heid IM, Berndt SI, Elliott AL, Jackson AU, Lamina C, Lettre G, Lim N, Lyon HN, McCarroll SA, Papadakis K, Qi L, Randall JC, Roccasecca RM, Sanna S, Scheet P, Weedon MN, Wheeler E, Zhao JH, Jacobs LC,Hirschhorn JN *et al.*, *Six new loci associated with body mass index highlight a neuronal influence on body weight regulation.* Nat Genet, 2009. **41**(1): p. 25-34.
21. Meyre, D., et al., *Variants of ENPP1 are associated with childhood and adult obesity and increase the risk of glucose intolerance and type 2 diabetes.* Nat Genet, 2005. **37**(8): p. 863-7.
22. Groves, C.J., et al., *Significant linkage of BMI to chromosome 10p in the U.K. population and evaluation of GAD2 as a positional candidate.* Diabetes, 2006. **55**(6): p. 1884-9.
23. Herbert, A., et al., *A common genetic variant is associated with adult and childhood obesity.* Science, 2006. **312**(5771): p. 279-83.
24. Wang, J., et al., *Study of eight GWAS-identified common variants for association with obesity-related indices in Chinese children at puberty.* Int J Obes (Lond), 2012. **36**(4): p. 542-7.
25. Kilpelainen, T.O., et al., *Obesity-susceptibility loci have a limited influence on birth weight: a meta-analysis of up to 28,219 individuals.* Am J Clin Nutr, 2011. **93**(4): p. 851-60.
26. Ng, M.C., et al., *Implication of genetic variants near NEGR1, SEC16B, TMEM18, ETV5/DGKG, GNPDA2, LIN7C/BDNF, MTCH2, BCDIN3D/FAIM2, SH2B1, FTO, MC4R, and KCTD15 with obesity and type 2 diabetes in 7705 Chinese.* J Clin Endocrinol Metab, 2010. **95**(5): p. 2418-25.
27. Loos, R.J., et al., *Common variants near MC4R are associated with fat mass, weight and risk of obesity.* Nat Genet, 2008. **40**(6): p. 768-75.
28. Wen, W., et al., *Meta-analysis identifies common variants associated with body mass index in east Asians.* Nat Genet, 2012. **44**(3): p. 307-11.
29. Frayling, T.M., et al., *A Common Variant in the FTO Gene Is Associated with Body Mass Index and Predisposes to Childhood and Adult Obesity.* Science (New York, N.Y.), 2007. **316**(5826): p. 889-894.
30. Weedon, M.N., et al., *No evidence of association of ENPP1 variants with type 2 diabetes or obesity in a study of 8,089 U.K. Caucasians.* Diabetes, 2006. **55**(11): p. 3175-9.
31. Swarbrick, M.M., et al., *Lack of Support for the Association between GAD2 Polymorphisms and Severe Human Obesity.* PLoS Biology, 2005. **3**(9): p. e315.
32. Kalderon, B., et al., *Fatty acid cycling in the fasting rat.* Am J Physiol Endocrinol Metab, 2000. **279**(1): p. E221-7.
33. Crabtree, B. and E.A. Newsholme, *The activities of lipases and carnitine palmitoyltransferase in muscles from vertebrates and invertebrates.* Biochem J, 1972. **130**(3): p. 697-705.
34. Large, V., et al., *Decreased expression and function of adipocyte hormone-sensitive lipase in subcutaneous fat cells of obese subjects.* J Lipid Res, 1999. **40**(11): p. 2059-66.
35. Lehr, S., S. Hartwig, and H. Sell, *Adipokines: a treasure trove for the discovery of biomarkers for metabolic disorders.* Proteomics Clin Appl, 2012. **6**(1-2): p. 91-101.
36. Trayhurn, P. and J.H. Beattie, *Physiological role of adipose tissue: white adipose tissue as an endocrine and secretory organ.* Proceedings of the Nutrition Society, 2001. **60**(3): p. 329-339.
37. Smiechowska, J., et al., *Adipokines in patients with cancer anorexia and cachexia.* J Investig Med, 2010. **58**(3): p. 554-9.
38. Alipoor, E., et al., *The relationship of serum adipokines with malnutrition inflammation score in haemodialysis.* Eur J Clin Invest, 2017. **47**(8): p. 545-554.
39. Chan, J.L. and C.S. Mantzoros, *Role of leptin in energy-deprivation states: normal human physiology and clinical implications for hypothalamic amenorrhoea and anorexia nervosa.* Lancet, 2005. **366**(9479): p. 74-85.
40. Licinio, J., et al., *Synchronicity of frequently sampled, 24-h concentrations of circulating leptin, luteinizing hormone, and estradiol in healthy women.* Proc Natl Acad Sci U S A, 1998. **95**(5): p. 2541-6.

41. Kopp, W., et al., *Low leptin levels predict amenorrhea in underweight and eating disordered females.* Mol Psychiatry, 1997. **2**(4): p. 335-40.
42. Audi, L., et al., *Leptin in relation to resumption of menses in women with anorexia nervosa.* Mol Psychiatry, 1998. **3**(6): p. 544-7.
43. Smith, R.E. and B.A. Horwitz, *Brown fat and thermogenesis.* Physiological Reviews, 1969. **49**(2): p. 330-425.
44. Foster, D.O. and M.L. Frydman, *Nonshivering thermogenesis in the rat. II. Measurements of blood flow with microspheres point to brown adipose tissue as the dominant site of the calorigenesis induced by noradrenaline.* Canadian Journal of Physiology and Pharmacology, 1978. **56**(1): p. 110-122.
45. Heaton, J.M., *The distribution of brown adipose tissue in the human.* J Anat, 1972. **112**(Pt 1): p. 35-9.
46. Nedergaard, J., T. Bengtsson, and B. Cannon, *Unexpected evidence for active brown adipose tissue in adult humans.* Am J Physiol Endocrinol Metab, 2007. **293**(2): p. E444-52.
47. van Marken Lichtenbelt, W.D., et al., *Cold-activated brown adipose tissue in healthy men.* N Engl J Med, 2009. **360**(15): p. 1500-8.
48. Cypess, A.M., et al., *Anatomical localization, gene expression profiling and functional characterization of adult human neck brown fat.* Nat Med, 2013. **19**(5): p. 635-9.
49. Virtanen, K.A., et al., *Functional brown adipose tissue in healthy adults.* N Engl J Med, 2009. **360**(15): p. 1518-25.
50. Cypess, A.M., et al., *Identification and importance of brown adipose tissue in adult humans.* N Engl J Med, 2009. **360**(15): p. 1509-17.
51. Orava, J., et al., *Different metabolic responses of human brown adipose tissue to activation by cold and insulin.* Cell Metab, 2011. **14**(2): p. 272-9.
52. Nedergaard, J., D. Ricquier, and L.P. Kozak, *Uncoupling proteins: current status and therapeutic prospects*, in *EMBO Rep*. 2005: England. p. 917-21.
53. Brondani, L.A., et al., *The role of the uncoupling protein 1 (UCP1) on the development of obesity and type 2 diabetes mellitus.* Arq Bras Endocrinol Metabol, 2012. **56**(4): p. 215-25.
54. Oelkrug, R., E.T. Polymeropoulos, and M. Jastroch, *Brown adipose tissue: physiological function and evolutionary significance.* J Comp Physiol B, 2015. **185**(6): p. 587-606.
55. Perkins, A.C., et al., *Prevalence and pattern of brown adipose tissue distribution of 18F-FDG in patients undergoing PET-CT in a subtropical climatic zone.* Nucl Med Commun, 2013. **34**(2): p. 168-74.
56. Au-Yong, I.T., et al., *Brown adipose tissue and seasonal variation in humans.* Diabetes, 2009. **58**(11): p. 2583-7.
57. Gerngross, C., et al., *Active Brown Fat During 18F-FDG PET/CT Imaging Defines a Patient Group with Characteristic Traits and an Increased Probability of Brown Fat Redetection.* J Nucl Med, 2017. **58**(7): p. 1104-1110.
58. Pfannenberg, C., et al., *Impact of age on the relationships of brown adipose tissue with sex and adiposity in humans.* Diabetes, 2010. **59**(7): p. 1789-93.
59. Yoneshiro, T., et al., *Age-related decrease in cold-activated brown adipose tissue and accumulation of body fat in healthy humans.* Obesity (Silver Spring), 2011. **19**(9): p. 1755-60.
60. Kolditz, C.I. and D. Langin, *Adipose tissue lipolysis.* Curr Opin Clin Nutr Metab Care, 2010. **13**(4): p. 377-81.
61. Morrison, S.F. and C.J. Madden, *Central Nervous System Regulation of Brown Adipose Tissue.* Comprehensive Physiology, 2014. **4**(4): p. 1677-1713.
62. Barbatelli, G., et al., *The emergence of cold-induced brown adipocytes in mouse white fat depots is determined predominantly by white to brown adipocyte transdifferentiation.* Am J Physiol Endocrinol Metab, 2010. **298**(6): p. E1244-53.
63. Petrovic, N., et al., *Chronic peroxisome proliferator-activated receptor gamma (PPARgamma) activation of epididymally derived white adipocyte cultures reveals a population of*

*thermogenically competent, UCP1-containing adipocytes molecularly distinct from classic brown adipocytes.* J Biol Chem, 2010. **285**(10): p. 7153-64.
64. Wilson-Fritch, L., et al., *Mitochondrial remodeling in adipose tissue associated with obesity and treatment with rosiglitazone.* J Clin Invest, 2004. **114**(9): p. 1281-9.
65. Sell, H., et al., *Peroxisome proliferator-activated receptor gamma agonism increases the capacity for sympathetically mediated thermogenesis in lean and ob/ob mice.* Endocrinology, 2004. **145**(8): p. 3925-34.
66. Vernochet, C., et al., *C/EBPalpha and the corepressors CtBP1 and CtBP2 regulate repression of select visceral white adipose genes during induction of the brown phenotype in white adipocytes by peroxisome proliferator-activated receptor gamma agonists.* Mol Cell Biol, 2009. **29**(17): p. 4714-28.
67. Tai, T.A., et al., *Activation of the nuclear receptor peroxisome proliferator-activated receptor gamma promotes brown adipocyte differentiation.* J Biol Chem, 1996. **271**(47): p. 29909-14.
68. Viswakarma, N., et al., *Transcriptional regulation of Cidea, mitochondrial cell death-inducing DNA fragmentation factor alpha-like effector A, in mouse liver by peroxisome proliferator-activated receptor alpha and gamma.* J Biol Chem, 2007. **282**(25): p. 18613-24.
69. Ohno, H., et al., *PPARgamma agonists induce a white-to-brown fat conversion through stabilization of PRDM16 protein.* Cell Metab, 2012. **15**(3): p. 395-404.
70. Bordicchia, M., et al., *Cardiac natriuretic peptides act via p38 MAPK to induce the brown fat thermogenic program in mouse and human adipocytes.* J Clin Invest, 2012. **122**(3): p. 1022-36.
71. Li, G., et al., *Induction of uncoupling protein 1 by central interleukin-6 gene delivery is dependent on sympathetic innervation of brown adipose tissue and underlies one mechanism of body weight reduction in rats.* Neuroscience, 2002. **115**(3): p. 879-89.
72. Roberts, L.D., et al., *beta-Aminoisobutyric acid induces browning of white fat and hepatic beta-oxidation and is inversely correlated with cardiometabolic risk factors.* Cell Metab, 2014. **19**(1): p. 96-108.
73. Poher, A.L., et al., *Brown adipose tissue activity as a target for the treatment of obesity/insulin resistance.* Front Physiol, 2015. **6**: p. 4.
74. Lee, P., et al., *Irisin and FGF21 are cold-induced endocrine activators of brown fat function in humans.* Cell Metab, 2014. **19**(2): p. 302-9.
75. Bostrom, P., et al., *A PGC1-alpha-dependent myokine that drives brown-fat-like development of white fat and thermogenesis.* Nature, 2012. **481**(7382): p. 463-8.
76. Handschin, C. and B.M. Spiegelman, *The role of exercise and PGC1α in inflammation and chronic disease.* Nature, 2008. **454**(7203): p. 463-469.
77. Saito, M., et al., *High incidence of metabolically active brown adipose tissue in healthy adult humans: effects of cold exposure and adiposity.* Diabetes, 2009. **58**(7): p. 1526-31.
78. McDonald, R.B. and B.A. Horwitz, *Brown adipose tissue thermogenesis during aging and senescence.* J Bioenerg Biomembr, 1999. **31**(5): p. 507-16.
79. Osellame, L.D., T.S. Blacker, and M.R. Duchen, *Cellular and molecular mechanisms of mitochondrial function.* Best Pract Res Clin Endocrinol Metab, 2012. **26**(6): p. 711-23.
80. Ouellet, V., et al., *Brown adipose tissue oxidative metabolism contributes to energy expenditure during acute cold exposure in humans.* The Journal of Clinical Investigation, 2012. **122**(2): p. 545-552.
81. Blondin, D.P., et al., *Increased Brown Adipose Tissue Oxidative Capacity in Cold-Acclimated Humans.* The Journal of Clinical Endocrinology and Metabolism, 2014. **99**(3): p. E438-E446.
82. Weir, G., et al., *Substantial Metabolic Activity of Human Brown Adipose Tissue during Warm Conditions and Cold-Induced Lipolysis of Local Triglycerides.* Cell Metab, 2018. **27**(6): p. 1348-1355.e4.
83. Rothwell, N.J. and M.J. Stock, *A role for brown adipose tissue in diet-induced thermogenesis.* Nature, 1979. **281**(5726): p. 31-5.

84. Hill, J.O., *Can a small-changes approach help address the obesity epidemic? A report of the Joint Task Force of the American Society for Nutrition, Institute of Food Technologists, and International Food Information Council.* Am J Clin Nutr, 2009. **89**(2): p. 477-84.
85. Seale, P., et al., *Prdm16 determines the thermogenic program of subcutaneous white adipose tissue in mice.* J Clin Invest, 2011. **121**(1): p. 96-105.
86. Kopecky, J., et al., *Reduction of dietary obesity in aP2-Ucp transgenic mice: physiology and adipose tissue distribution.* Am J Physiol, 1996. **270**(5 Pt 1): p. E768-75.
87. Scime, A., et al., *Rb and p107 regulate preadipocyte differentiation into white versus brown fat through repression of PGC-1alpha.* Cell Metab, 2005. **2**(5): p. 283-95.
88. Chiang, S.H., et al., *The protein kinase IKKepsilon regulates energy balance in obese mice.* Cell, 2009. **138**(5): p. 961-75.
89. Feldmann, H.M., et al., *UCP1 ablation induces obesity and abolishes diet-induced thermogenesis in mice exempt from thermal stress by living at thermoneutrality.* Cell Metab, 2009. **9**(2): p. 203-9.
90. Lowell, B.B., et al., *Development of obesity in transgenic mice after genetic ablation of brown adipose tissue.* Nature, 1993. **366**(6457): p. 740-2.
91. Wang, Q., et al., *Brown Adipose Tissue Activation Is Inversely Related to Central Obesity and Metabolic Parameters in Adult Human.* PLoS ONE, 2015. **10**(4): p. e0123795.
92. Peirce, V. and A. Vidal-Puig, *Regulation of glucose homoeostasis by brown adipose tissue.* Lancet Diabetes Endocrinol, 2013. **1**(4): p. 353-60.
93. Lee, P., et al., *Temperature-acclimated brown adipose tissue modulates insulin sensitivity in humans.* Diabetes, 2014. **63**(11): p. 3686-98.
94. Bartelt, A., et al., *Brown adipose tissue activity controls triglyceride clearance.* Nat Med, 2011. **17**(2): p. 200-5.
95. Khedoe, P.P.S.J., et al., *Brown adipose tissue takes up plasma triglycerides mostly after lipolysis.* Journal of Lipid Research, 2015. **56**(1): p. 51-59.
96. Berbee, J.F., et al., *Brown fat activation reduces hypercholesterolaemia and protects from atherosclerosis development.* Nat Commun, 2015. **6**: p. 6356.
97. Lorenzo, F.D., et al., *Central cooling effects in patients with hypercholesterolaemia.* Clinical Science, 1998. **95**(2): p. 213.
98. Su, A.I., et al., *Large-scale analysis of the human and mouse transcriptomes*, in *Proc Natl Acad Sci U S A*. 2002. p. 4465-70.
99. Wu, J., et al., *Beige adipocytes are a distinct type of thermogenic fat cell in mouse and human.* Cell, 2012. **150**(2): p. 366-76.
100. Cohen, P., et al., *Ablation of PRDM16 and beige adipose causes metabolic dysfunction and a subcutaneous to visceral fat switch.* Cell, 2014. **156**(1-2): p. 304-16.
101. Bartesaghi, S., et al., *Thermogenic activity of UCP1 in human white fat-derived beige adipocytes.* Mol Endocrinol, 2015. **29**(1): p. 130-9.
102. Vitali, A., et al., *The adipose organ of obesity-prone C57BL/6J mice is composed of mixed white and brown adipocytes.* J Lipid Res, 2012. **53**(4): p. 619-29.
103. Fazeli, P.K., et al., *Marrow Fat and Bone—New Perspectives.* The Journal of Clinical Endocrinology and Metabolism, 2013. **98**(3): p. 935-945.
104. Custer, R.P., *Studies on the structure and function of bone marrow part I. .* J Lab Clin Med, 1932. **17**: p. 951-60.
105. Custer, R.P., *Studies on the structure and function of bone marrow part II. .* J Lab Clin Med, 1932. **17**: p. 960-62.
106. Newlin, H.E. and C.M. McCay, *Bone marrow for fat storage in rabbits.* Arch Biochem, 1948. **17**(1): p. 125-8.
107. Piney, A., *The anatomy of the bone marrow. .* Br Med J, 1922. **2**: p. 792-95.
108. Zhang, Y., et al., *Positional cloning of the mouse obese gene and its human homologue.* Nature, 1994. **372**(6505): p. 425-432.

109. Krings, A., et al., *Bone marrow fat has brown adipose tissue characteristics, which are attenuated with aging and diabetes.* Bone, 2012. **50**(2): p. 546-52.
110. Scheller, E.L. and C.J. Rosen, *What's the matter with MAT? Marrow adipose tissue, metabolism, and skeletal health.* Annals of the New York Academy of Sciences, 2014. **1311**(1): p. 14-30.
111. Tavassoli, M., D.N. Houchin, and P. Jacobs, *Fatty acid composition of adipose cells in red and yellow marrow: A possible determinant of haematopoietic potential.* Scand J Haematol, 1977. **18**(1): p. 47-53.
112. Griffith, J.F., et al., *A study of bone marrow and subcutaneous fatty acid composition in subjects of varying bone mineral density.* Bone, 2009. **44**(6): p. 1092-6.
113. Liu, L.F., et al., *Characterization of age-related gene expression profiling in bone marrow and epididymal adipocytes.* BMC Genomics, 2011. **12**: p. 212.
114. Bathija, A., S. Davis, and S. Trubowitz, *Bone marrow adipose tissue: response to acute starvation.* Am J Hematol, 1979. **6**(3): p. 191-8.
115. Tavassoli, M., *Differential response of bone marrow and extramedullary adipose cells to starvation.* Experientia, 1974. **30**(4): p. 424-5.
116. Devlin, M.J., et al., *Caloric restriction leads to high marrow adiposity and low bone mass in growing mice.* J Bone Miner Res, 2010. **25**(9): p. 2078-88.
117. Bredella, M.A., et al., *Increased bone marrow fat in anorexia nervosa.* J Clin Endocrinol Metab, 2009. **94**(6): p. 2129-36.
118. Ecklund, K., et al., *Bone marrow changes in adolescent girls with anorexia nervosa.* J Bone Miner Res, 2010. **25**(2): p. 298-304.
119. Fazeli, P.K., et al., *Marrow fat and preadipocyte factor-1 levels decrease with recovery in women with anorexia nervosa.* J Bone Miner Res, 2012. **27**(9): p. 1864-71.
120. Berry, R., E. Jeffery, and M.S. Rodeheffer, *Weighing in on adipocyte precursors.* Cell Metab, 2014. **19**(1): p. 8-20.
121. Spalding, K.L., et al., *Dynamics of fat cell turnover in humans.* Nature, 2008. **453**(7196): p. 783-7.
122. Rozman, C., et al., *Age-related variations of fat tissue fraction in normal human bone marrow depend both on size and number of adipocytes: a stereological study.* Exp Hematol, 1989. **17**(1): p. 34-7.
123. Cawthorn, W.P., et al., *Bone marrow adipose tissue is an endocrine organ that contributes to increased circulating adiponectin during caloric restriction.* Cell metabolism, 2014. **20**(2): p. 368-375.
124. Cawthorn, W.P., et al., *Expansion of Bone Marrow Adipose Tissue During Caloric Restriction Is Associated With Increased Circulating Glucocorticoids and Not With Hypoleptinemia.* Endocrinology, 2016. **157**(2): p. 508-21.
125. Devlin, M.J., *Why does starvation make bones fat?* Am J Hum Biol, 2011. **23**(5): p. 577-85.
126. Di Iorgi, N., et al., *Reciprocal relation between marrow adiposity and the amount of bone in the axial and appendicular skeleton of young adults.* J Clin Endocrinol Metab, 2008. **93**(6): p. 2281-6.
127. Justesen, J., et al., *Adipocyte tissue volume in bone marrow is increased with aging and in patients with osteoporosis.* Biogerontology, 2001. **2**(3): p. 165-171.
128. Shen, W., et al., *MRI-measured bone marrow adipose tissue is inversely related to DXA-measured bone mineral in Caucasian women.* Osteoporos Int, 2007. **18**(5): p. 641-7.
129. Wang, Q.A., et al., *Tracking adipogenesis during white adipose tissue development, expansion and regeneration.* Nat Med, 2013. **19**(10): p. 1338-44.
130. Scheller, E.L., et al., *Region-specific variation in the properties of skeletal adipocytes reveals regulated and constitutive marrow adipose tissues.* Nature Communications, 2015. **6**: p. 7808.

131. Kricun, M.E., *Red-yellow marrow conversion: its effect on the location of some solitary bone lesions.* Skeletal Radiol, 1985. **14**(1): p. 10-9.
132. Symonds, M.E., et al., *Endocrine and nutritional regulation of fetal adipose tissue development.* J Endocrinol, 2003. **179**(3): p. 293-9.
133. Emery, J.L. and G.F. Follett, *REGRESSION OF BONE-MARROW HAEMOPOIESIS FROM THE TERMINAL DIGITS IN THE FOETUS AND INFANT.* Br J Haematol, 1964. **10**: p. 485-9.
134. Gesta, S., Y.H. Tseng, and C.R. Kahn, *Developmental origin of fat: tracking obesity to its source.* Cell, 2007. **131**(2): p. 242-56.
135. Tang, W., et al., *White fat progenitor cells reside in the adipose vasculature.* Science, 2008. **322**(5901): p. 583-6.
136. Rodeheffer, M.S., K. Birsoy, and J.M. Friedman, *Identification of white adipocyte progenitor cells in vivo.* Cell, 2008. **135**(2): p. 240-9.
137. Timmons, J.A., et al., *Myogenic gene expression signature establishes that brown and white adipocytes originate from distinct cell lineages.* Proc Natl Acad Sci U S A, 2007. **104**(11): p. 4401-6.
138. Seale, P., et al., *PRDM16 controls a brown fat/skeletal muscle switch.* Nature, 2008. **454**(7207): p. 961-7.
139. Muruganandan, S., A.A. Roman, and C.J. Sinal, *Adipocyte differentiation of bone marrow-derived mesenchymal stem cells: cross talk with the osteoblastogenic program.* Cell Mol Life Sci, 2009. **66**(2): p. 236-53.
140. Suchacki, K.J., W.P. Cawthorn, and C.J. Rosen, *Bone marrow adipose tissue: formation, function and regulation.* Curr Opin Pharmacol, 2016. **28**: p. 50-6.
141. Zhou, B.O., et al., *Leptin-receptor-expressing mesenchymal stromal cells represent the main source of bone formed by adult bone marrow.* Cell Stem Cell, 2014. **15**(2): p. 154-68.
142. Yue, R., et al., *Leptin Receptor Promotes Adipogenesis and Reduces Osteogenesis by Regulating Mesenchymal Stromal Cells in Adult Bone Marrow.* Cell Stem Cell, 2016. **18**(6): p. 782-96.
143. Ambrosi, T.H., et al., *Adipocyte Accumulation in the Bone Marrow during Obesity and Aging Impairs Stem Cell-Based Hematopoietic and Bone Regeneration.* Cell Stem Cell, 2017.
144. Weatherill, A.R., et al., *Saturated and polyunsaturated fatty acids reciprocally modulate dendritic cell functions mediated through TLR4.* J Immunol, 2005. **174**(9): p. 5390-7.
145. Turer, A.T. and P.E. Scherer, *Adiponectin: mechanistic insights and clinical implications.* Diabetologia, 2012. **55**(9): p. 2319-26.
146. Arita, Y., et al., *Paradoxical decrease of an adipose-specific protein, adiponectin, in obesity.* Biochem Biophys Res Commun, 1999. **257**(1): p. 79-83.
147. Dalamaga, M., K.N. Diakopoulos, and C.S. Mantzoros, *The role of adiponectin in cancer: a review of current evidence.* Endocr Rev, 2012. **33**(4): p. 547-94.
148. Cawthorn, W.P., et al., *Bone marrow adipose tissue is an endocrine organ that contributes to increased circulating adiponectin during caloric restriction.* Cell Metab, 2014. **20**(2): p. 368-75.
149. Sulston, R.J. and W.P. Cawthorn, *Bone marrow adipose tissue as an endocrine organ: close to the bone?* Horm Mol Biol Clin Investig, 2016. **28**(1): p. 21-38.
150. Corre, J., et al., *Human bone marrow adipocytes support complete myeloid and lymphoid differentiation from human CD34 cells.* Br J Haematol, 2004. **127**(3): p. 344-7.
151. Laharrague, P., et al., *High expression of leptin by human bone marrow adipocytes in primary culture.* Faseb j, 1998. **12**(9): p. 747-52.
152. Laharrague, P., et al., *Regulation by cytokines of leptin expression in human bone marrow adipocytes.* Horm Metab Res, 2000. **32**(10): p. 381-5.
153. Belaid-Choucair, Z., et al., *Human bone marrow adipocytes block granulopoiesis through neuropilin-1-induced granulocyte colony-stimulating factor inhibition.* Stem Cells, 2008. **26**(6): p. 1556-64.

154. Uchihashi, K., et al., *Organotypic culture of human bone marrow adipose tissue.* Pathol Int, 2010. **60**(4): p. 259-67.
155. Montague, C.T., et al., *Congenital leptin deficiency is associated with severe early-onset obesity in humans.* Nature, 1997. **387**(6636): p. 903-8.
156. Rosenbaum, M. and R.L. Leibel, *20 years of leptin: role of leptin in energy homeostasis in humans.* J Endocrinol, 2014. **223**(1): p. T83-96.
157. Devlin, M.J., et al., *Caloric restriction leads to high marrow adiposity and low bone mass in growing mice.* Journal of Bone and Mineral Research, 2010. **25**(9): p. 2078-2088.
158. Bredella, M.A., et al., *Determinants of Bone Microarchitecture and Mechanical Properties in Obese Men.* The Journal of Clinical Endocrinology & Metabolism, 2012. **97**(11): p. 4115-4122.
159. Bredella, M.A., et al., *Vertebral Bone Marrow Fat Is Positively Associated With Visceral Fat and Inversely Associated With IGF-1 in Obese Women.* Obesity, 2011. **19**(1): p. 49-53.
160. Doucette, C.R., et al., *A High Fat Diet Increases Bone Marrow Adipose Tissue (MAT) But Does Not Alter Trabecular or Cortical Bone Mass in C57BL/6J Mice.* Journal of Cellular Physiology, 2015. **230**(9): p. 2032-2037.
161. Halade, G.V., et al., *High fat diet-induced animal model of age-associated obesity and osteoporosis.* J Nutr Biochem, 2010. **21**(12): p. 1162-9.
162. Shu, L., et al., *High-fat diet causes bone loss in young mice by promoting osteoclastogenesis through alteration of the bone marrow environment.* Calcif Tissue Int, 2015. **96**(4): p. 313-23.
163. Styner, M., et al., *Bone marrow fat accumulation accelerated by high fat diet is suppressed by exercise.* Bone, 2014. **64**: p. 39-46.
164. Martin, L.M. and L.R. McCabe, *Type I diabetic bone phenotype is location but not gender dependent.* Histochemistry and Cell Biology, 2007. **128**(2): p. 125-133.
165. Slade, J.M., et al., *Human bone marrow adiposity is linked with serum lipid levels not T1-diabetes.* Journal of Diabetes and its Complications, 2012. **26**(1): p. 1-9.
166. Baum, T., et al., *Does vertebral bone marrow fat content correlate with abdominal adipose tissue, lumbar spine bone mineral density, and blood biomarkers in women with type 2 diabetes mellitus?* Journal of Magnetic Resonance Imaging, 2012. **35**(1): p. 117-124.
167. Hamrick, M.W., et al., *Leptin Treatment Induces Loss of Bone Marrow Adipocytes and Increases Bone Formation in Leptin-Deficient ob/ob Mice.* Journal of Bone and Mineral Research, 2005. **20**(6): p. 994-1001.
168. Schwartz, A.V., *Marrow Fat and Bone: Review of Clinical Findings.* Frontiers in Endocrinology, 2015. **6**: p. 40.
169. Vande Berg, B.C., et al., *Fat conversion of femoral marrow in glucocorticoid-treated patients: A cross-sectional and longitudinal study with magnetic resonance imaging.* Arthritis & Rheumatism, 1999. **42**(7): p. 1405-1411.
170. Wei, W., et al., *Fibroblast growth factor 21 promotes bone loss by potentiating the effects of peroxisome proliferator-activated receptor γ.* Proceedings of the National Academy of Sciences, 2012. **109**(8): p. 3143-3148.
171. Iwaniec, U.T. and R.T. Turner, *Failure to generate bone marrow adipocytes does not protect mice from ovariectomy-induced osteopenia.* Bone, 2013. **53**(1): p. 145-53.
172. Syed, F.A., et al., *Effects of estrogen therapy on bone marrow adipocytes in postmenopausal osteoporotic women.* Osteoporosis International, 2008. **19**(9): p. 1323-1330.
173. Scheller, E.L., et al., *Marrow Adipose Tissue: Trimming the Fat.* Trends Endocrinol Metab, 2016. **27**(6): p. 392-403.
174. Yeung, D.K., et al., *Osteoporosis is associated with increased marrow fat content and decreased marrow fat unsaturation: a proton MR spectroscopy study.* J Magn Reson Imaging, 2005. **22**(2): p. 279-85.
175. Griffith, J.F., et al., *Vertebral bone mineral density, marrow perfusion, and fat content in healthy men and men with osteoporosis: dynamic contrast-enhanced MR imaging and MR spectroscopy.* Radiology, 2005. **236**(3): p. 945-51.

176. Kajkenova, O., et al., *Increased adipogenesis and myelopoiesis in the bone marrow of SAMP6, a murine model of defective osteoblastogenesis and low turnover osteopenia.* J Bone Miner Res, 1997. **12**(11): p. 1772-9.
177. Kurabayashi, T., et al., *Effects of a beta 3 adrenergic receptor agonist on bone and bone marrow adipocytes in the tibia and lumbar spine of the ovariectomized rat.* Calcif Tissue Int, 2001. **68**(4): p. 248-54.
178. Li, G.W., et al., *The temporal characterization of marrow lipids and adipocytes in a rabbit model of glucocorticoid-induced osteoporosis.* Skeletal Radiol, 2013. **42**(9): p. 1235-44.
179. Abdallah, B.M. and M. Kassem, *New factors controlling the balance between osteoblastogenesis and adipogenesis.* Bone, 2012. **50**(2): p. 540-5.
180. Nuttall, M.E., et al., *Adipocytes and the regulation of bone remodeling: a balancing act.* Calcif Tissue Int, 2014. **94**(1): p. 78-87.
181. Sadie-Van Gijsen, H., et al., *The interrelationship between bone and fat: from cellular see-saw to endocrine reciprocity.* Cell Mol Life Sci, 2013. **70**(13): p. 2331-49.
182. Muruganandan, S., A.A. Roman, and C.J. Sinal, *Role of chemerin/CMKLR1 signaling in adipogenesis and osteoblastogenesis of bone marrow stem cells.* J Bone Miner Res, 2010. **25**(2): p. 222-34.
183. Taipaleenmaki, H., et al., *Wnt signalling mediates the cross-talk between bone marrow derived pre-adipocytic and pre-osteoblastic cell populations.* Exp Cell Res, 2011. **317**(6): p. 745-56.
184. Elias, C.F., et al., *Leptin differentially regulates NPY and POMC neurons projecting to the lateral hypothalamic area.* Neuron, 1999. **23**(4): p. 775-86.
185. Fekete, C., et al., *alpha-Melanocyte-stimulating hormone is contained in nerve terminals innervating thyrotropin-releasing hormone-synthesizing neurons in the hypothalamic paraventricular nucleus and prevents fasting-induced suppression of prothyrotropin-releasing hormone gene expression.* J Neurosci, 2000. **20**(4): p. 1550-8.
186. Pelleymounter, M.A., et al., *Effects of the obese gene product on body weight regulation in ob/ob mice.* Science, 1995. **269**(5223): p. 540-3.
187. Halaas, J.L., et al., *Weight-reducing effects of the plasma protein encoded by the obese gene.* Science, 1995. **269**(5223): p. 543-6.
188. Comninos, A.N., C.N. Jayasena, and W.S. Dhillo, *The relationship between gut and adipose hormones, and reproduction.* Hum Reprod Update, 2014. **20**(2): p. 153-74.
189. Zhao, J., et al., *Leptin receptor expression increases in placenta, but not hypothalamus, during gestation in Mus musculus and Myotis lucifugus.* Placenta, 2004. **25**(8-9): p. 712-22.
190. Anifandis, G., et al., *Estradiol and leptin as conditional prognostic IVF markers.* Reproduction, 2005. **129**(4): p. 531-4.
191. Matkovic, V., et al., *Leptin is inversely related to age at menarche in human females.* J Clin Endocrinol Metab, 1997. **82**(10): p. 3239-45.
192. Zhang, W., et al., *Adenovirus-mediated leptin expression normalises hypertension associated with diet-induced obesity.* J Neuroendocrinol, 2010. **22**(3): p. 175-80.
193. Knight, W.D., et al., *Short-term physiological hyperleptinemia decreases arterial blood pressure.* Regul Pept, 2009. **154**(1-3): p. 60-8.
194. Ducy, P., et al., *Leptin inhibits bone formation through a hypothalamic relay: a central control of bone mass.* Cell, 2000. **100**(2): p. 197-207.
195. Dam, J. and R. Jockers, *Hunting for the functions of short leptin receptor isoforms().* Molecular Metabolism, 2013. **2**(4): p. 327-328.
196. Hummel, K.P., M.M. Dickie, and D.L. Coleman, *Diabetes, a New Mutafton in the Mouse.* Science, 1966. **153**(3740): p. 1127.
197. Funahashi, T., I. Shimomura, and Y. Matsuzawa, *Adipocytokines*, in *Encyclopedia of Endocrine Diseases*, L. Martini, Editor. 2004, Elsevier: New York. p. 41-44.

198. Burguera, B., et al., *The long form of the leptin receptor (OB-Rb) is widely expressed in the human brain.* Neuroendocrinology, 2000. **71**(3): p. 187-95.
199. Fruhbeck, G., *Intracellular signalling pathways activated by leptin.* Biochem J, 2006. **393**(Pt 1): p. 7-20.
200. Lee, G.H., et al., *Abnormal splicing of the leptin receptor in diabetic mice.* Nature, 1996. **379**(6566): p. 632-5.
201. Uotani, S., et al., *Functional properties of leptin receptor isoforms: internalization and degradation of leptin and ligand-induced receptor downregulation.* Diabetes, 1999. **48**(2): p. 279-86.
202. Muoio, D.M. and G. Lynis Dohm, *Peripheral metabolic actions of leptin.* Best Pract Res Clin Endocrinol Metab, 2002. **16**(4): p. 653-66.
203. Gorska, E., et al., *Leptin receptors.* European Journal of Medical Research, 2010. **15**(Suppl 2): p. 50-54.
204. Chan, J.L., et al., *Regulation of circulating soluble leptin receptor levels by gender, adiposity, sex steroids, and leptin: observational and interventional studies in humans.* Diabetes, 2002. **51**(7): p. 2105-12.
205. Kabir, M., et al., *Negative regulation of leptin by chronic high-glycemic index starch diet.* Metabolism, 2000. **49**(6): p. 764-9.
206. Romon, M., et al., *Leptin response to carbohydrate or fat meal and association with subsequent satiety and energy intake.* Am J Physiol, 1999. **277**(5 Pt 1): p. E855-61.
207. Maffei, M., et al., *Leptin levels in human and rodent: Measurement of plasma leptin and ob RNA in obese and weight-reduced subjects.* Nature Medicine, 1995. **1**: p. 1155.
208. Considine, R.V., et al., *Serum immunoreactive-leptin concentrations in normal-weight and obese humans.* N Engl J Med, 1996. **334**(5): p. 292-5.
209. Lonnqvist, F., et al., *Overexpression of the obese (ob) gene in adipose tissue of human obese subjects.* Nat Med, 1995. **1**(9): p. 950-3.
210. Ahima, R.S., et al., *Role of leptin in the neuroendocrine response to fasting.* Nature, 1996. **382**(6588): p. 250-2.
211. Sinha, M.K., et al., *Nocturnal rise of leptin in lean, obese, and non-insulin-dependent diabetes mellitus subjects.* J Clin Invest, 1996. **97**(5): p. 1344-7.
212. Schoeller, D.A., et al., *Entrainment of the diurnal rhythm of plasma leptin to meal timing.* J Clin Invest, 1997. **100**(7): p. 1882-7.
213. Otsuka, R., et al., *Perceived psychological stress and serum leptin concentrations in Japanese men.* Obesity (Silver Spring), 2006. **14**(10): p. 1832-8.
214. Hickey, M.S., et al., *Gender-dependent effects of exercise training on serum leptin levels in humans.* Am J Physiol, 1997. **272**(4 Pt 1): p. E562-6.
215. Murakami, T., M. Iida, and K. Shima, *Dexamethasone regulates obese expression in isolated rat adipocytes.* Biochem Biophys Res Commun, 1995. **214**(3): p. 1260-7.
216. De Vos, P., et al., *Induction of ob gene expression by corticosteroids is accompanied by body weight loss and reduced food intake.* J Biol Chem, 1995. **270**(27): p. 15958-61.
217. Cizza, G., et al., *Plasma leptin levels do not change in patients with Cushing's disease shortly after correction of hypercortisolism.* J Clin Endocrinol Metab, 1997. **82**(8): p. 2747-50.
218. Ahima, R.S. and J.S. Flier, *Leptin.* Annu Rev Physiol, 2000. **62**: p. 413-37.
219. Scriba, D., et al., *Catecholamines suppress leptin release from in vitro differentiated subcutaneous human adipocytes in primary culture via beta1- and beta2-adrenergic receptors.* Eur J Endocrinol, 2000. **143**(3): p. 439-45.
220. Igel, M., et al., *Long-term and rapid regulation of ob mRNA levels in adipose tissue from normal (Sprague Dawley rats) and obese (db/db mice, fa/fa rats) rodents.* Diabetologia, 1996. **39**(7): p. 758-65.

221. MacDougald, O.A., et al., *Regulated expression of the obese gene product (leptin) in white adipose tissue and 3T3-L1 adipocytes.* Proceedings of the National Academy of Sciences of the United States of America, 1995. **92**(20): p. 9034-9037.
222. Slieker, L.J., et al., *Regulation of expression of ob mRNA and protein by glucocorticoids and cAMP.* J Biol Chem, 1996. **271**(10): p. 5301-4.
223. Malmstrom, R., et al., *Insulin increases plasma leptin concentrations in normal subjects and patients with NIDDM.* Diabetologia, 1996. **39**(8): p. 993-6.
224. Kolaczynski, J.W., et al., *Acute and chronic effects of insulin on leptin production in humans: Studies in vivo and in vitro.* Diabetes, 1996. **45**(5): p. 699-701.
225. Dagogo-Jack, S., et al., *Plasma leptin and insulin relationships in obese and nonobese humans.* Diabetes, 1996. **45**(5): p. 695-8.
226. Vidal, H., et al., *The expression of ob gene is not acutely regulated by insulin and fasting in human abdominal subcutaneous adipose tissue.* J Clin Invest, 1996. **98**(2): p. 251-5.
227. Rayner, D.V. and P. Trayhurn, *Regulation of leptin production: sympathetic nervous system interactions.* J Mol Med (Berl), 2001. **79**(1): p. 8-20.
228. Hardie, L.J., et al., *Circulating leptin levels are modulated by fasting, cold exposure and insulin administration in lean but not Zucker (fa/fa) rats as measured by ELISA.* Biochem Biophys Res Commun, 1996. **223**(3): p. 660-5.
229. Ricci, M.R., S.K. Fried, and K.D. Mittleman, *Acute cold exposure decreases plasma leptin in women.* Metabolism, 2000. **49**(4): p. 421-3.
230. Vallerand, A.L., F. Perusse, and L.J. Bukowiecki, *Stimulatory effects of cold exposure and cold acclimation on glucose uptake in rat peripheral tissues.* Am J Physiol, 1990. **259**(5 Pt 2): p. R1043-9.
231. Trayhurn, P., J.S. Duncan, and D.V. Rayner, *Acute cold-induced suppression of ob (obese) gene expression in white adipose tissue of mice: mediation by the sympathetic system.* Biochemical Journal, 1995. **311**(Pt 3): p. 729-733.
232. Mantzoros, C.S., et al., *Activation of beta(3) adrenergic receptors suppresses leptin expression and mediates a leptin-independent inhibition of food intake in mice.* Diabetes, 1996. **45**(7): p. 909-14.
233. Swoap, S.J. and D. Weinshenker, *Norepinephrine controls both torpor initiation and emergence via distinct mechanisms in the mouse.* PLoS One, 2008. **3**(12): p. e4038.
234. Yang, G., et al., *Modulation of direct leptin signaling by soluble leptin receptor.* Mol Endocrinol, 2004. **18**(6): p. 1354-62.
235. Yannakoulia, M., et al., *Body fat mass and macronutrient intake in relation to circulating soluble leptin receptor, free leptin index, adiponectin, and resistin concentrations in healthy humans.* J Clin Endocrinol Metab, 2003. **88**(4): p. 1730-6.
236. Misra, M., et al., *Hormonal and body composition predictors of soluble leptin receptor, leptin, and free leptin index in adolescent girls with anorexia nervosa and controls and relation to insulin sensitivity.* J Clin Endocrinol Metab, 2004. **89**(7): p. 3486-95.
237. Wabitsch, M., et al., *Biologically inactive leptin and early-onset extreme obesity.* N Engl J Med, 2015. **372**(1): p. 48-54.
238. Masuo, K., et al., *Leptin-receptor polymorphisms relate to obesity through blunted leptin-mediated sympathetic nerve activation in a Caucasian male population.* Hypertens Res, 2008. **31**(6): p. 1093-100.
239. Farooqi, I.S., et al., *Effects of recombinant leptin therapy in a child with congenital leptin deficiency.* N Engl J Med, 1999. **341**(12): p. 879-84.
240. Friedman, J., *The long road to leptin.* J Clin Invest, 2016. **126**(12): p. 4727-4734.
241. Sahu, A., *Resistance to the satiety action of leptin following chronic central leptin infusion is associated with the development of leptin resistance in neuropeptide Y neurones.* J Neuroendocrinol, 2002. **14**(10): p. 796-804.

242. Munzberg, H., et al., *Leptin receptor action and mechanisms of leptin resistance.* Cell Mol Life Sci, 2005. **62**(6): p. 642-52.
243. El-Haschimi, K., et al., *Two defects contribute to hypothalamic leptin resistance in mice with diet-induced obesity.* J Clin Invest, 2000. **105**(12): p. 1827-32.
244. Bouret, S.G. and R.B. Simerly, *Developmental programming of hypothalamic feeding circuits.* Clin Genet, 2006. **70**(4): p. 295-301.
245. Farooqi, I.S. and S. O'Rahilly, *Monogenic obesity in humans.* Annu Rev Med, 2005. **56**: p. 443-58.
246. Considine, R.V., et al., *The hypothalamic leptin receptor in humans: identification of incidental sequence polymorphisms and absence of the db/db mouse and fa/fa rat mutations.* Diabetes, 1996. **45**(7): p. 992-4.
247. Munzberg, H., J.S. Flier, and C. Bjorbaek, *Region-specific leptin resistance within the hypothalamus of diet-induced obese mice.* Endocrinology, 2004. **145**(11): p. 4880-9.
248. Caro, J.F., et al., *Decreased cerebrospinal-fluid/serum leptin ratio in obesity: a possible mechanism for leptin resistance.* Lancet, 1996. **348**(9021): p. 159-61.
249. Veyrat-Durebex, C., et al., *Improved leptin sensitivity as a potential candidate responsible for the spontaneous food restriction of the Lou/C rat.* PLoS One, 2013. **8**(9): p. e73452.
250. Kaszubska, W., et al., *Protein tyrosine phosphatase 1B negatively regulates leptin signaling in a hypothalamic cell line.* Mol Cell Endocrinol, 2002. **195**(1-2): p. 109-18.
251. Dupont, C., D.R. Armant, and C.A. Brenner, *Epigenetics: definition, mechanisms and clinical perspective.* Semin Reprod Med, 2009. **27**(5): p. 351-7.
252. Ledford, H., *Language: Disputed definitions*, in *Nature*. 2008: England. p. 1023-8.
253. Berger, S.L., et al., *An operational definition of epigenetics.* Genes Dev, 2009. **23**(7): p. 781-3.
254. Jablonka, E. and G. Raz, *Transgenerational epigenetic inheritance: prevalence, mechanisms, and implications for the study of heredity and evolution.* Q Rev Biol, 2009. **84**(2): p. 131-76.
255. Costa, S. and P. Shaw, *'Open minded' cells: how cells can change fate.* Trends in Cell Biology, 2007. **17**(3): p. 101-106.
256. Banno, K., et al., *Epimutation and cancer: a new carcinogenic mechanism of Lynch syndrome (Review).* Int J Oncol, 2012. **41**(3): p. 793-7.
257. Novak, K., *Epigenetics changes in cancer cells*, in *MedGenMed*. 2004: United States. p. 17.
258. Rothbart, S.B. and B.D. Strahl, *Interpreting the language of histone and DNA modifications.* Biochim Biophys Acta, 2014. **1839**(8): p. 627-43.
259. Kornberg, R.D. and Y. Lorch, *Twenty-five years of the nucleosome, fundamental particle of the eukaryote chromosome.* Cell, 1999. **98**(3): p. 285-94.
260. Luger, K. and J.C. Hansen, *Nucleosome and chromatin fiber dynamics.* Curr Opin Struct Biol, 2005. **15**(2): p. 188-96.
261. Burgess, R.J. and Z. Zhang, *Histone chaperones in nucleosome assembly and human disease.* Nat Struct Mol Biol, 2013. **20**(1): p. 14-22.
262. Avvakumov, N., A. Nourani, and J. Cote, *Histone chaperones: modulators of chromatin marks.* Mol Cell, 2011. **41**(5): p. 502-14.
263. Talbert, P.B. and S. Henikoff, *Histone variants--ancient wrap artists of the epigenome.* Nat Rev Mol Cell Biol, 2010. **11**(4): p. 264-75.
264. Narlikar, G.J., R. Sundaramoorthy, and T. Owen-Hughes, *Mechanisms and functions of ATP-dependent chromatin-remodeling enzymes.* Cell, 2013. **154**(3): p. 490-503.
265. Kouzarides, T., *Chromatin modifications and their function.* Cell, 2007. **128**(4): p. 693-705.
266. Kohli, R.M. and Y. Zhang, *TET enzymes, TDG and the dynamics of DNA demethylation.* Nature, 2013. **502**(7472): p. 472-9.
267. Klose, R.J. and A.P. Bird, *Genomic DNA methylation: the mark and its mediators.* Trends Biochem Sci, 2006. **31**(2): p. 89-97.
268. Greer, E.L. and Y. Shi, *Histone methylation: a dynamic mark in health, disease and inheritance.* Nat Rev Genet, 2012. **13**(5): p. 343-57.

269. Bannister, A.J., et al., *Selective recognition of methylated lysine 9 on histone H3 by the HP1 chromo domain.* Nature, 2001. **410**(6824): p. 120-4.
270. Strahl, B.D. and C.D. Allis, *The language of covalent histone modifications.* Nature, 2000. **403**(6765): p. 41-5.
271. Krogan, N.J., et al., *The Paf1 complex is required for histone H3 methylation by COMPASS and Dot1p: linking transcriptional elongation to histone methylation.* Mol Cell, 2003. **11**(3): p. 721-9.
272. Bernstein, B.E., et al., *Genomic maps and comparative analysis of histone modifications in human and mouse.* Cell, 2005. **120**(2): p. 169-81.
273. Ng, H.H., et al., *Targeted recruitment of Set1 histone methylase by elongating Pol II provides a localized mark and memory of recent transcriptional activity.* Mol Cell, 2003. **11**(3): p. 709-19.
274. Cao, R., et al., *Role of histone H3 lysine 27 methylation in Polycomb-group silencing.* Science, 2002. **298**(5595): p. 1039-43.
275. Lachner, M., et al., *Methylation of histone H3 lysine 9 creates a binding site for HP1 proteins.* Nature, 2001. **410**(6824): p. 116-20.
276. Schotta, G., et al., *A silencing pathway to induce H3-K9 and H4-K20 trimethylation at constitutive heterochromatin.* Genes Dev, 2004. **18**(11): p. 1251-62.
277. Kourmouli, N., et al., *Heterochromatin and tri-methylated lysine 20 of histone H4 in animals.* J Cell Sci, 2004. **117**(Pt 12): p. 2491-501.
278. Turner, B.M., *Histone acetylation and an epigenetic code.* Bioessays, 2000. **22**(9): p. 836-45.
279. Shogren-Knaak, M., et al., *Histone H4-K16 acetylation controls chromatin structure and protein interactions.* Science, 2006. **311**(5762): p. 844-7.
280. Bird, A., *DNA methylation patterns and epigenetic memory.* Genes Dev, 2002. **16**(1): p. 6-21.
281. Choy, M.K., et al., *Genome-wide conserved consensus transcription factor binding motifs are hyper-methylated.* BMC Genomics, 2010. **11**: p. 519.
282. Defossez PA, S.I., *Biological functions of methyl-CpG-binding proteins.* Prog Mol Bio Trans Sci, 2011. **101**: p. 377-98.
283. Lander, E.S., et al., *Initial sequencing and analysis of the human genome.* Nature, 2001. **409**(6822): p. 860-921.
284. Bird, A.P., *CpG-rich islands and the function of DNA methylation.* Nature, 1986. **321**(6067): p. 209-13.
285. Saxonov, S., P. Berg, and D.L. Brutlag, *A genome-wide analysis of CpG dinucleotides in the human genome distinguishes two distinct classes of promoters.* Proc Natl Acad Sci U S A, 2006. **103**(5): p. 1412-7.
286. Illingworth, R.S., et al., *Orphan CpG islands identify numerous conserved promoters in the mammalian genome.* PLoS Genet, 2010. **6**(9): p. e1001134.
287. Dean, W., F. Santos, and W. Reik, *Epigenetic reprogramming in early mammalian development and following somatic nuclear transfer.* Semin Cell Dev Biol, 2003. **14**(1): p. 93-100.
288. Valinluck, V. and L.C. Sowers, *Endogenous cytosine damage products alter the site selectivity of human DNA maintenance methyltransferase DNMT1.* Cancer Res, 2007. **67**(3): p. 946-50.
289. Tahiliani, M., et al., *Conversion of 5-methylcytosine to 5-hydroxymethylcytosine in mammalian DNA by MLL partner TET1.* Science, 2009. **324**(5929): p. 930-5.
290. Ji, D., et al., *Effects of Tet-induced oxidation products of 5-methylcytosine on Dnmt1- and DNMT3a-mediated cytosine methylation.* Mol Biosyst, 2014. **10**(7): p. 1749-52.
291. Bird, A., *The dinucleotide CG as a genomic signalling module.* J Mol Biol, 2011. **409**(1): p. 47-53.
292. Mellen, M., et al., *MeCP2 binds to 5hmC enriched within active genes and accessible chromatin in the nervous system.* Cell, 2012. **151**(7): p. 1417-30.

293. Song, C.X., et al., *Selective chemical labeling reveals the genome-wide distribution of 5-hydroxymethylcytosine.* Nat Biotechnol, 2011. **29**(1): p. 68-72.
294. Ito, S., et al., *Tet proteins can convert 5-methylcytosine to 5-formylcytosine and 5-carboxylcytosine.* Science, 2011. **333**(6047): p. 1300-3.
295. Thomson, J.P. and R.R. Meehan, *The application of genome-wide 5-hydroxymethylcytosine studies in cancer research.* Epigenomics, 2017. **9**(1): p. 77-91.
296. Wyatt, G.R. and S.S. Cohen, *A new pyrimidine base from bacteriophage nucleic acids.* Nature, 1952. **170**(4338): p. 1072-3.
297. Wyatt, G.R. and S.S. Cohen, *The bases of the nucleic acids of some bacterial and animal viruses: the occurrence of 5-hydroxymethylcytosine.* Biochem J, 1953. **55**(5): p. 774-82.
298. Kriaucionis, S. and N. Heintz, *The nuclear DNA base 5-hydroxymethylcytosine is present in Purkinje neurons and the brain.* Science, 2009. **324**(5929): p. 929-30.
299. Tahiliani M, K.K., Shen Y, Pastor WA, Bandukwala H, Brudno Y, Agarwal S, Iyer LM, Liu DR, Aravind L, Rao A., *Conversion of 5-methylcytosine to 5-hydroxymethylcytosine in mammalian DNA by MLL partner TET1.* Science, 2009. **324**: p. 5929.
300. Globisch, D., et al., *Tissue distribution of 5-hydroxymethylcytosine and search for active demethylation intermediates.* PLoS One, 2010. **5**(12): p. e15367.
301. Kubiura, M., et al., *Chromosome-wide regulation of euchromatin-specific 5mC to 5hmC conversion in mouse ES cells and female human somatic cells.* Chromosome Res, 2012. **20**(7): p. 837-48.
302. Nestor, C.E., et al., *Tissue type is a major modifier of the 5-hydroxymethylcytosine content of human genes.* Genome Res, 2012. **22**(3): p. 467-77.
303. Szulwach, K.E., et al., *Integrating 5-hydroxymethylcytosine into the epigenomic landscape of human embryonic stem cells.* PLoS Genet, 2011. **7**(6): p. e1002154.
304. Tan, L., et al., *Genome-wide comparison of DNA hydroxymethylation in mouse embryonic stem cells and neural progenitor cells by a new comparative hMeDIP-seq method.* Nucleic Acids Res, 2013. **41**(7): p. e84.
305. Pastor, W.A., et al., *Genome-wide mapping of 5-hydroxymethylcytosine in embryonic stem cells.* Nature, 2011. **473**(7347): p. 394-7.
306. Williams K, C.J., Pedersen MT, Johansen JV, Cloos PA, Rappsilber J, Helin K., *TET1 and hydroxymethylcytosine in transcription and DNA methylation fidelity.* Nature, 2011. **473**(7347): p. 343-8.
307. Wu H, D.A.A., Ito S, Xia K, Wang Z, Cui K, Zhao K, Sun YE, Zhang Y., *Dual functions of Tet1 in transcriptional regulation in mouse embryonic stem cells.* Nature, 2011. **473**(7347): p. 389-93.
308. Thomson, J.P., et al., *Loss of Tet1-Associated 5-Hydroxymethylcytosine Is Concomitant with Aberrant Promoter Hypermethylation in Liver Cancer.* Cancer Res, 2016. **76**(10): p. 3097-108.
309. Thomson, J.P., et al., *Non-genotoxic carcinogen exposure induces defined changes in the 5-hydroxymethylome.* Genome Biology, 2012. **13**(10): p. R93.
310. Song, C.-X. and C. He, *Balance of DNA methylation and demethylation in cancer development.* Genome Biology, 2012. **13**(10): p. 173.
311. Yu, Z., et al., *The protein that binds to DNA base J in trypanosomatids has features of a thymidine hydroxylase.* Nucleic Acids Res, 2007. **35**(7): p. 2107-15.
312. Cliffe, L.J., et al., *JBP1 and JBP2 are two distinct thymidine hydroxylases involved in J biosynthesis in genomic DNA of African trypanosomes.* Nucleic Acids Res, 2009. **37**(5): p. 1452-62.
313. Ono, R., et al., *LCX, leukemia-associated protein with a CXXC domain, is fused to MLL in acute myeloid leukemia with trilineage dysplasia having t(10;11)(q22;q23).* Cancer Res, 2002. **62**(14): p. 4075-80.

314. He YF, L.B., Li Z, Liu P, Wang Y, Tang Q, Ding J, Jia Y, Chen Z, Li L, Sun Y, Li X, Dai Q, Song CX, Zhang K, He C, Xu GL., *Tet-mediated formation of 5-carboxylcytosine and its excision by TDG in mammalian DNA.* Science, 2011. **333**(6047): p. 1303-7.
315. Huang, Y., et al., *Distinct roles of the methylcytosine oxidases Tet1 and Tet2 in mouse embryonic stem cells.* Proc Natl Acad Sci U S A, 2014. **111**(4): p. 1361-6.
316. Ito S, D.A.A., Taranova OV, Hong K, Sowers LC, Zhang Y, *Role of Tet proteins in 5mC to 5hmC conversion, ES-cell self-renewal and inner cell mass specification.* Nature, 2010. **466**(7310): p. 1129-33.
317. Lorsbach RB, M.J., Mathew S, Raimondi SC, Mukatira ST, Downing JR, *TET1, a member of a novel protein family, is fused to MLL in acute myeloid leukemia containing the t(10;11)(q22;q23).* Leukemia, 2003. **17**(3): p. 637-41.
318. Nestor CE, O.R., Reddington J, Sproul D, Reinhardt D, Dunican D, Katz E, Dixon JM, Harrison DJ, Meehan RR., *Tissue type is a major modifier of the 5-hydroxymethylcytosine content of human genes.* Genome Res, 2012. **22**(3): p. 467-77.
319. Kriaucionis S, H.N., *The nuclear DNA base 5-hydroxymethylcytosine is present in Purkinje neurons and the brain.* Science, 2009. **324**(5929): p. 929-30.
320. Wu Y, G.Z., Liu Y, Tang B, Wang Y, Yang L, Du J, Zhang Y., *Oct4 and the small molecule inhibitor, SC1, regulates Tet2 expression in mouse embryonic stem cells.* Mol Biol Rep, 2013. **40**(4): p. 2897-906.
321. Zhao Z, C.L., Dawlaty MM, Pan F, Weeks O, Zhou Y, Cao Z, Shi H, Wang J, Lin L, Chen S, Yuan W, Qin Z, Ni H, Nimer SD, Yang FC, Jaenisch R, Jin P, Xu M., *Combined Loss of Tet1 and Tet2 Promotes B Cell, but Not Myeloid Malignancies, in Mice.* Cell Rep, 2015. **13**(8): p. 1692-704.
322. Shen L, I.A., He J, Liu Y, Lu F, Zhang Y., *Tet3 and DNA replication mediate demethylation of both the maternal and paternal genomes in mouse zygotes.* Cell Stem Cell, 2014. **15**(4): p. 459-70.
323. Hu, L., et al., *Structural insight into substrate preference for TET-mediated oxidation.* Nature, 2015. **527**(7576): p. 118-22.
324. Jin, S.G., et al., *Tet3 Reads 5-Carboxylcytosine through Its CXXC Domain and Is a Potential Guardian against Neurodegeneration.* Cell Rep, 2016. **14**(3): p. 493-505.
325. Williams, K., et al., *TET1 and hydroxymethylcytosine in transcription and DNA methylation fidelity.* Nature, 2011. **473**(7347): p. 343-8.
326. Dawlaty, M.M., et al., *Tet1 is dispensable for maintaining pluripotency and its loss is compatible with embryonic and postnatal development.* Cell Stem Cell, 2011. **9**(2): p. 166-75.
327. Zhao, X.Y., et al., *iPS cells produce viable mice through tetraploid complementation.* Nature, 2009. **461**(7260): p. 86-90.
328. Dawlaty MM, G.K., Powell BE, Hu YC, Markoulaki S, Cheng AW, Gao Q, Kim J, Choi SW, Page DC, Jaenisch R., *Tet1 is dispensable for maintaining pluripotency and its loss is compatible with embryonic and postnatal development.* Cell Stem Cell, 2011. **9**(2): p. 166-75.
329. Kang, J., et al., *Simultaneous deletion of the methylcytosine oxidases Tet1 and Tet3 increases transcriptome variability in early embryogenesis.* Proc Natl Acad Sci U S A, 2015. **112**(31): p. E4236-45.
330. Yamaguchi, S., et al., *Tet1 controls meiosis by regulating meiotic gene expression.* Nature, 2012. **492**(7429): p. 443-7.
331. Yamaguchi, S., et al., *Role of Tet1 in erasure of genomic imprinting.* Nature, 2013. **504**(7480): p. 460-4.
332. Kumar, D., et al., *Tet1 Oxidase Regulates Neuronal Gene Transcription, Active DNA Hydroxy-methylation, Object Location Memory, and Threat Recognition Memory.* Neuroepigenetics, 2015. **4**: p. 12-27.
333. Xin, Y.J., et al., *Tet1-mediated DNA demethylation regulates neuronal cell death induced by oxidative stress.* Sci Rep, 2015. **5**: p. 7645.

334. Ko, M., et al., *Ten-Eleven-Translocation 2 (TET2) negatively regulates homeostasis and differentiation of hematopoietic stem cells in mice.* Proc Natl Acad Sci U S A, 2011. **108**(35): p. 14566-71.
335. Li, Z., et al., *Deletion of Tet2 in mice leads to dysregulated hematopoietic stem cells and subsequent development of myeloid malignancies.* Blood, 2011. **118**(17): p. 4509-18.
336. Quivoron, C., et al., *TET2 inactivation results in pleiotropic hematopoietic abnormalities in mouse and is a recurrent event during human lymphomagenesis.* Cancer Cell, 2011. **20**(1): p. 25-38.
337. Moran-Crusio, K., et al., *Tet2 loss leads to increased hematopoietic stem cell self-renewal and myeloid transformation.* Cancer Cell, 2011. **20**(1): p. 11-24.
338. Dawlaty, M.M., et al., *Combined deficiency of Tet1 and Tet2 causes epigenetic abnormalities but is compatible with postnatal development.* Developmental cell, 2013. **24**(3): p. 310-323.
339. Gu, T.P., et al., *The role of Tet3 DNA dioxygenase in epigenetic reprogramming by oocytes.* Nature, 2011. **477**(7366): p. 606-10.
340. Dawlaty, M.M., et al., *Loss of Tet enzymes compromises proper differentiation of embryonic stem cells.* Developmental cell, 2014. **29**(1): p. 102-111.
341. Tan, L. and Y.G. Shi, *Tet family proteins and 5-hydroxymethylcytosine in development and disease.* Development, 2012. **139**(11): p. 1895-902.
342. Hales, C.N. and D.J.P. Barker, *Type 2 (non-insulin-dependent) diabetes mellitus: the thrifty phenotype hypothesis.* Diabetologia, 1992. **35**(7): p. 595-601.
343. Stoger, R., *The thrifty epigenotype: an acquired and heritable predisposition for obesity and diabetes?* Bioessays, 2008. **30**(2): p. 156-66.
344. Ravelli, G.P., Z.A. Stein, and M.W. Susser, *Obesity in young men after famine exposure in utero and early infancy.* N Engl J Med, 1976. **295**(7): p. 349-53.
345. Tobi, E.W., et al., *Early gestation as the critical time-window for changes in the prenatal environment to affect the adult human blood methylome.* Int J Epidemiol, 2015. **44**(4): p. 1211-23.
346. Xiao, M., et al., *Inhibition of alpha-KG-dependent histone and DNA demethylases by fumarate and succinate that are accumulated in mutations of FH and SDH tumor suppressors.* Genes Dev, 2012. **26**(12): p. 1326-38.
347. Carey, B.W., et al., *Intracellular alpha-ketoglutarate maintains the pluripotency of embryonic stem cells.* Nature, 2015. **518**(7539): p. 413-6.
348. Wang, Y., et al., *WT1 recruits TET2 to regulate its target gene expression and suppress leukemia cell proliferation.* Molecular cell, 2015. **57**(4): p. 662-673.
349. Ward, P.S., et al., *The common feature of leukemia-associated IDH1 and IDH2 mutations is a neomorphic enzymatic activity that converts α-ketoglutarate to 2-hydroxyglutarate.* Cancer cell, 2010. **17**(3): p. 225-234.
350. Capper, D., et al., *Monoclonal antibody specific for IDH1 R132H mutation.* Acta Neuropathol, 2009. **118**(5): p. 599-601.
351. Lu, C., et al., *IDH mutation impairs histone demethylation and results in a block to cell differentiation.* Nature, 2012. **483**(7390): p. 474-8.
352. Moussaieff, A., et al., *Glycolysis-mediated changes in acetyl-CoA and histone acetylation control the early differentiation of embryonic stem cells.* Cell Metab, 2015. **21**(3): p. 392-402.
353. Wellen, K.E., et al., *ATP-citrate lyase links cellular metabolism to histone acetylation.* Science, 2009. **324**(5930): p. 1076-80.
354. Inagaki, T., J. Sakai, and S. Kajimura, *Transcriptional and epigenetic control of brown and beige adipose cell fate and function.* Nat Rev Mol Cell Biol, 2016. **17**(8): p. 480-95.
355. Mittelman, S.D., et al., *Extreme insulin resistance of the central adipose depot in vivo.* Diabetes, 2002. **51**(3): p. 755-61.
356. Smith, U.L.F., et al., *Regional differences and effect of weight reduction on human fat cell metabolism.* European Journal of Clinical Investigation, 1979. **9**(5): p. 327-332.

357. Tsushima, Y., et al., *Uric acid secretion from adipose tissue and its increase in obesity.* J Biol Chem, 2013. **288**(38): p. 27138-49.
358. Cummins, T.D., et al., *Metabolic remodeling of white adipose tissue in obesity.* American Journal of Physiology - Endocrinology and Metabolism, 2014. **307**(3): p. E262-E277.
359. Nagao, H., et al., *Increased Dynamics of Tricarboxylic Acid Cycle and Glutamate Synthesis in Obese Adipose Tissue: IN VIVO METABOLIC TURNOVER ANALYSIS.* J Biol Chem, 2017. **292**(11): p. 4469-4483.
360. Jufvas A, S.S., Lundqvist K, Amin R, Vener AV, Strålfors P., *Global differences in specific histone H3 methylation are associated with overweight and type 2 diabetes.* Clin Epigenetics, 2013. **5**(1): p. 15.
361. van Dijk, S.J., et al., *Epigenetics and human obesity.* International Journal Of Obesity, 2014. **39**: p. 85.
362. Zhang, F.F., et al., *White blood cell global methylation and IL-6 promoter methylation in association with diet and lifestyle risk factors in a cancer-free population.* Epigenetics, 2012. **7**(6): p. 606-14.
363. Gomes, M.V., et al., *Age-related changes in the global DNA methylation profile of leukocytes are linked to nutrition but are not associated with the MTHFR C677T genotype or to functional capacities.* PLoS One, 2012. **7**(12): p. e52570.
364. Pearce, M.S., et al., *Global LINE-1 DNA methylation is associated with blood glycaemic and lipid profiles.* Int J Epidemiol, 2012. **41**(1): p. 210-7.
365. Ulrich, C.M., et al., *Metabolic, hormonal and immunological associations with global DNA methylation among postmenopausal women.* Epigenetics, 2012. **7**(9): p. 1020-8.
366. Figueiredo, J.C., et al., *Global DNA hypomethylation (LINE-1) in the normal colon and lifestyle characteristics and dietary and genetic factors.* Cancer Epidemiol Biomarkers Prev, 2009. **18**(4): p. 1041-9.
367. Jintaridth, P., et al., *Hypomethylation of Alu elements in post-menopausal women with osteoporosis.* PLoS One, 2013. **8**(8): p. e70386.
368. Piyathilake, C.J., et al., *A lower degree of PBMC L1 methylation is associated with excess body weight and higher HOMA-IR in the presence of lower concentrations of plasma folate.* PLoS One, 2013. **8**(1): p. e54544.
369. Kim, M., et al., *DNA methylation as a biomarker for cardiovascular disease risk.* PLoS One, 2010. **5**(3): p. e9692.
370. Cash, H.L., et al., *Cardiovascular disease risk factors and DNA methylation at the LINE-1 repeat region in peripheral blood from Samoan Islanders.* Epigenetics, 2011. **6**(10): p. 1257-64.
371. Nomura, Y., et al., *Global methylation in the placenta and umbilical cord blood from pregnancies with maternal gestational diabetes, preeclampsia, and obesity.* Reprod Sci, 2014. **21**(1): p. 131-7.
372. Hermsdorff, H.H., et al., *TNF-alpha promoter methylation in peripheral white blood cells: relationship with circulating TNFalpha, truncal fat and n-6 PUFA intake in young women.* Cytokine, 2013. **64**(1): p. 265-71.
373. Barres, R., et al., *Weight loss after gastric bypass surgery in human obesity remodels promoter methylation.* Cell Rep, 2013. **3**(4): p. 1020-7.
374. Obermann-Borst, S.A., et al., *Duration of breastfeeding and gender are associated with methylation of the LEPTIN gene in very young children.* Pediatr Res, 2013. **74**(3): p. 344-9.
375. Kuehnen, P., et al., *An Alu element-associated hypermethylation variant of the POMC gene is associated with childhood obesity.* PLoS Genet, 2012. **8**(3): p. e1002543.
376. Milagro, F.I., et al., *CLOCK, PER2 and BMAL1 DNA methylation: association with obesity and metabolic syndrome characteristics and monounsaturated fat intake.* Chronobiol Int, 2012. **29**(9): p. 1180-94.

377. Drake, A.J., et al., *An unbalanced maternal diet in pregnancy associates with offspring epigenetic changes in genes controlling glucocorticoid action and foetal growth.* Clin Endocrinol (Oxf), 2012. **77**(6): p. 808-15.
378. Huang, R.C., et al., *DNA methylation of the IGF2/H19 imprinting control region and adiposity distribution in young adults.* Clin Epigenetics, 2012. **4**(1): p. 21.
379. Xu, X., et al., *A genome-wide methylation study on obesity: differential variability and differential methylation.* Epigenetics, 2013. **8**(5): p. 522-33.
380. Wang, X., et al., *Obesity related methylation changes in DNA of peripheral blood leukocytes.* BMC Medicine, 2010. **8**: p. 87-87.
381. Almen, M.S., et al., *Genome wide analysis reveals association of a FTO gene variant with epigenetic changes.* Genomics, 2012. **99**(3): p. 132-7.
382. Dubois-Chevalier, J., et al., *A dynamic CTCF chromatin binding landscape promotes DNA hydroxymethylation and transcriptional induction of adipocyte differentiation.* Nucleic Acids Res, 2014. **42**(17): p. 10943-59.
383. Fujiki K, S.A., Kano F, Sato R, Shirahige K, Murata M., *PPARc-induced PARylation promotes local DNA demethylation by production of 5-hydroxymethylcytosine.* Nat Commun, 2013. **4**: p. 2262.
384. Choi I, K.R., Lim HW, Kaestner KH, Won KJ., *5-hydroxymethylcytosine represses the activity of enhancers in embryonic stem cells: a new epigenetic signature for gene regulation.* BMC Genomics, 2014. **15**: p. 670.
385. Wiehle L, R.G., Musch T, Dawlaty MM, Jaenisch R, Lyko F, Breiling A., *Tet1 and Tet2 Protect DNA Methylation Canyons against Hypermethylation.* Mol Cell Biol, 2015. **36**(3): p. 452-61.
386. Sayeed SK, Z.J., Sathyanarayana BK, Golla JP, Vinson C., *C/EBPβ (CEBPB) protein binding to the C/EBP|CRE DNA 8-mer TTGC|GTCA is inhibited by 5hmC and enhanced by 5mC, 5fC, and 5caC in the CG dinucleotide.* Biochim Biophys Acta, 2015. **1849**(6): p. 583-9.
387. ED., R., *The transcriptional basis of adipocyte development.* Prostaglandins Leukot Essent Fatty Acids. , 2005. **73**(1): p. 31-4.
388. Ross SR, G.R., Greenstein A, Platt KA, Shyu HL, Mellovitz B, Spiegelman BM., *A fat-specific enhancer is the primary determinant of gene expression for adipocyte P2 in vivo.* Proc Natl Acad Sci U S A, 1990. **87**(24): p. 9590-4.
389. Tontonoz P, H.E., Graves RA, Budavari AI, Spiegelman BM., *mPPAR gamma 2: tissue-specific regulator of an adipocyte enhancer.* Genes Dev, 1994. **8**(10): p. 1224-34.
390. Rajakumari, S., et al., *EBF2 determines and maintains brown adipocyte identity.* Cell Metab, 2013. **17**(4): p. 562-74.
391. Ohno, H., et al., *EHMT1 controls brown adipose cell fate and thermogenesis through the PRDM16 complex.* Nature, 2013. **504**(7478): p. 163-7.
392. Seale, P., et al., *Transcriptional control of brown fat determination by PRDM16.* Cell Metab, 2007. **6**(1): p. 38-54.
393. Kajimura, S., et al., *Initiation of myoblast/brown fat switch through a PRDM16-C/EBP-β transcriptional complex.* Nature, 2009. **460**(7259): p. 1154-1158.
394. Hondares, E., et al., *Peroxisome proliferator-activated receptor alpha (PPARalpha) induces PPARgamma coactivator 1alpha (PGC-1alpha) gene expression and contributes to thermogenic activation of brown fat: involvement of PRDM16.* J Biol Chem, 2011. **286**(50): p. 43112-22.
395. Wang, W., et al., *Ebf2 is a selective marker of brown and beige adipogenic precursor cells.* Proc Natl Acad Sci U S A, 2014. **111**(40): p. 14466-71.
396. Harms, M.J., et al., *PRDM16 binds MED1 and controls chromatin architecture to determine a brown fat transcriptional program.* Genes & Development, 2015. **29**(3): p. 298-307.
397. Whyte, W.A., et al., *Master transcription factors and mediator establish super-enhancers at key cell identity genes.* Cell, 2013. **153**(2): p. 307-19.

398. Iida, S., et al., *PRDM16 enhances nuclear receptor-dependent transcription of the brown fat-specific Ucp1 gene through interactions with Mediator subunit MED1.* Genes & Development, 2015. **29**(3): p. 308-321.
399. Emmett, M.J., et al., *Histone deacetylase 3 prepares brown adipose tissue for acute thermogenic challenge.* Nature, 2017. **546**(7659): p. 544-548.
400. Ferrari, A., et al., *HDAC3 is a molecular brake of the metabolic switch supporting white adipose tissue browning.* Nat Commun, 2017. **8**(1): p. 93.
401. Li, F., et al., *Histone Deacetylase 1 (HDAC1) Negatively Regulates Thermogenic Program in Brown Adipocytes via Coordinated Regulation of Histone H3 Lysine 27 (H3K27) Deacetylation and Methylation.* J Biol Chem, 2016. **291**(9): p. 4523-36.
402. Brunmeir, R., et al., *Comparative Transcriptomic and Epigenomic Analyses Reveal New Regulators of Murine Brown Adipogenesis.* PLoS Genet, 2016. **12**(12): p. e1006474.
403. Abe, Y., et al., *JMJD1A is a signal-sensing scaffold that regulates acute chromatin dynamics via SWI/SNF association for thermogenesis.* Nat Commun, 2015. **6**: p. 7052.
404. Duteil, D., et al., *Lsd1 Ablation Triggers Metabolic Reprogramming of Brown Adipose Tissue.* Cell Rep, 2016. **17**(4): p. 1008-1021.
405. Shapira, S.N., et al., *EBF2 transcriptionally regulates brown adipogenesis via the histone reader DPF3 and the BAF chromatin remodeling complex.* Genes Dev, 2017. **31**(7): p. 660-673.
406. Truett GE, H.P., Mynatt RL, Truett AA, Walker JA, Warman ML., *Preparation of PCR-quality mouse genomic DNA with hot sodium hydroxide and tris (HotSHOT).* Biotechniques, 2000. **29**(1): p. 52, 54.
407. Weir, J.B., *New methods for calculating metabolic rate with special reference to protein metabolism.* J Physiol, 1949. **109**(1-2): p. 1-9.
408. Lee, M.-J., R.T. Pickering, and V. Puri, *Prolonged efficiency of siRNA-mediated gene silencing in primary cultures of human preadipocytes and adipocytes.* Obesity (Silver Spring, Md.), 2014. **22**(4): p. 1064-1069.
409. Hiller, K., et al., *MetaboliteDetector: comprehensive analysis tool for targeted and nontargeted GC/MS based metabolome analysis.* Anal Chem, 2009. **81**(9): p. 3429-39.
410. Dubois-Chevalier J, O.F., Dehondt H1, Firmin FF1, Gheeraert C1, Staels B1, Lefebvre P2, Eeckhoute J2., *A dynamic CTCF chromatin binding landscape promotes DNA hydroxymethylation and transcriptional induction of adipocyte differentiation.* Nucleic Acids Res, 2014. **42**(17): p. 10943-59.
411. Song, Y., M. Ailenberg, and M. Silverman, *Human munc13 Is a Diacylglycerol Receptor that Induces Apoptosis and May Contribute to Renal Cell Injury in Hyperglycemia.* Molecular Biology of the Cell, 1999. **10**(5): p. 1609-1619.
412. Nguyen, M., et al., *Caenorhabditis elegans mutants resistant to inhibitors of acetylcholinesterase.* Genetics, 1995. **140**(2): p. 527-35.
413. Trégouet, D.-A., et al., *G/T Substitution in Intron 1 of the UNC13B Gene Is Associated With Increased Risk of Nephropathy in Patients With Type 1 Diabetes.* Diabetes, 2008. **57**(10): p. 2843-2850.
414. Chevalier, S., et al., *The greater contribution of gluconeogenesis to glucose production in obesity is related to increased whole-body protein catabolism.* Diabetes, 2006. **55**(3): p. 675-81.
415. Golay, A., et al., *Study on lipid metabolism in obesity diabetes.* Metabolism, 1984. **33**(2): p. 111-6.
416. Vernia, S., et al., *An alternative splicing program promotes adipose tissue thermogenesis.* Elife, 2016. **5**.
417. Resnyk, C.W., et al., *RNA-Seq Analysis of Abdominal Fat in Genetically Fat and Lean Chickens Highlights a Divergence in Expression of Genes Controlling Adiposity, Hemostasis, and Lipid Metabolism.* PLoS One, 2015. **10**(10): p. e0139549.

418. Mardinoglu, A., et al., *Defining the human adipose tissue proteome to reveal metabolic alterations in obesity.* J Proteome Res, 2014. **13**(11): p. 5106-19.
419. Yoon, J.C., et al., *Peroxisome proliferator-activated receptor gamma target gene encoding a novel angiopoietin-related protein associated with adipose differentiation.* Mol Cell Biol, 2000. **20**(14): p. 5343-9.
420. Fujiki, K., et al., *PPARgamma-induced PARylation promotes local DNA demethylation by production of 5-hydroxymethylcytosine.* Nat Commun, 2013. **4**: p. 2262.
421. Gonzalez-Muniesa, P., et al., *Fatty acids and hypoxia stimulate the expression and secretion of the adipokine ANGPTL4 (angiopoietin-like protein 4/ fasting-induced adipose factor) by human adipocytes.* J Nutrigenet Nutrigenomics, 2011. **4**(3): p. 146-53.
422. Lehmann, M., et al., *ARTD1-induced poly-ADP-ribose formation enhances PPARgamma ligand binding and co-factor exchange.* Nucleic Acids Res, 2015. **43**(1): p. 129-42.
423. Erener, S., et al., *Poly(ADP-ribose)polymerase-1 (PARP1) controls adipogenic gene expression and adipocyte function.* Mol Endocrinol, 2012. **26**(1): p. 79-86.
424. Duggan, G.E., et al., *Differentiating short- and long-term effects of diet in the obese mouse using (1) H-nuclear magnetic resonance metabolomics.* Diabetes Obes Metab, 2011. **13**(9): p. 859-62.
425. Xie, B., M.J. Waters, and H.J. Schirra, *Investigating Potential Mechanisms of Obesity by Metabolomics.* Journal of Biomedicine and Biotechnology, 2012. **2012**: p. 805683.
426. Tschöp, M.H., et al., *A guide to analysis of mouse energy metabolism.* Nature methods, 2011. **9**(1): p. 57-63.
427. Melzner, I., et al., *Leptin gene expression in human preadipocytes is switched on by maturation-induced demethylation of distinct CpGs in its proximal promoter.* J Biol Chem, 2002. **277**(47): p. 45420-7.
428. Noer, A., et al., *Stable CpG Hypomethylation of Adipogenic Promoters in Freshly Isolated, Cultured, and Differentiated Mesenchymal Stem Cells from Adipose Tissue.* Molecular Biology of the Cell, 2006. **17**(8): p. 3543-3556.
429. Stoger, R., *In vivo methylation patterns of the leptin promoter in human and mouse.* Epigenetics, 2006. **1**(4): p. 155-62.
430. Farooqi, I.S., et al., *Partial leptin deficiency and human adiposity.* Nature, 2001. **414**(6859): p. 34-5.
431. Ravussin, E., et al., *Relatively low plasma leptin concentrations precede weight gain in Pima Indians.* Nat Med, 1997. **3**(2): p. 238-40.
432. Marchi, M., et al., *Human leptin tissue distribution, but not weight loss-dependent change in expression, is associated with methylation of its promoter.* Epigenetics, 2011. **6**(10): p. 1198-206.
433. Yokomori, N., M. Tawata, and T. Onaya, *DNA demethylation modulates mouse leptin promoter activity during the differentiation of 3T3-L1 cells.* Diabetologia, 2002. **45**(1): p. 140-8.
434. Pan, H., J. Guo, and Z. Su, *Advances in understanding the interrelations between leptin resistance and obesity.* Physiol Behav, 2014. **130**: p. 157-69.
435. Garcia-Cardona, M.C., et al., *DNA methylation of leptin and adiponectin promoters in children is reduced by the combined presence of obesity and insulin resistance.* Int J Obes (Lond), 2014. **38**(11): p. 1457-65.
436. Shen, W., et al., *Epigenetic modification of the leptin promoter in diet-induced obese mice and the effects of N-3 polyunsaturated fatty acids.* Sci Rep, 2014. **4**: p. 5282.
437. Milagro, F.I., et al., *High fat diet-induced obesity modifies the methylation pattern of leptin promoter in rats.* J Physiol Biochem, 2009. **65**(1): p. 1-9.
438. Cordero, P., et al., *Leptin and TNF-alpha promoter methylation levels measured by MSP could predict the response to a low-calorie diet.* J Physiol Biochem, 2011. **67**(3): p. 463-70.

439. Fan, C., et al., *The Regulation of Leptin, Leptin Receptor and Pro-opiomelanocortin Expression by N-3 PUFAs in Diet-Induced Obese Mice Is Not Related to the Methylation of Their Promoters.* Nutr Metab (Lond), 2011. **8**(1): p. 31.
440. Okada, Y., et al., *Diet-induced up-regulation of gene expression in adipocytes without changes in DNA methylation.* Kobe J Med Sci, 2009. **54**(5): p. E241-9.
441. Nuffer, W., J.M. Trujillo, and J. Megyeri, *A Comparison of New Pharmacological Agents for the Treatment of Obesity.* Ann Pharmacother, 2016. **50**(5): p. 376-88.
442. Wadden, T.A., et al., *Weight loss with naltrexone SR/bupropion SR combination therapy as an adjunct to behavior modification: the COR-BMOD trial.* Obesity (Silver Spring), 2011. **19**(1): p. 110-20.
443. Greenway, F.L., et al., *Comparison of combined bupropion and naltrexone therapy for obesity with monotherapy and placebo.* J Clin Endocrinol Metab, 2009. **94**(12): p. 4898-906.
444. Greenway, F.L., et al., *Rational design of a combination medication for the treatment of obesity.* Obesity (Silver Spring), 2009. **17**(1): p. 30-9.
445. Johnstone, R.W., *Histone-deacetylase inhibitors: novel drugs for the treatment of cancer.* Nat Rev Drug Discov, 2002. **1**(4): p. 287-99.
446. McManus, K.J. and M.J. Hendzel, *Quantitative Analysis of CBP- and P300-Induced Histone Acetylations In Vivo Using Native Chromatin.* Molecular and Cellular Biology, 2003. **23**(21): p. 7611-7627.
447. Eyal, S., et al., *The activity of antiepileptic drugs as histone deacetylase inhibitors.* Epilepsia, 2004. **45**(7): p. 737-44.
448. Ko, M., et al., *TET proteins and 5-methylcytosine oxidation in hematological cancers.* Immunol Rev, 2015. **263**(1): p. 6-21.
449. Ito, S., et al., *Role of Tet proteins in 5mC to 5hmC conversion, ES-cell self-renewal and inner cell mass specification.* Nature, 2010. **466**(7310): p. 1129-33.
450. Marks, P., et al., *Histone deacetylases and cancer: causes and therapies.* Nat Rev Cancer, 2001. **1**(3): p. 194-202.
451. de Ruijter, A.J., et al., *Histone deacetylases (HDACs): characterization of the classical HDAC family.* Biochem J, 2003. **370**(Pt 3): p. 737-49.
452. Jo, J., et al., *Hypertrophy and/or Hyperplasia: Dynamics of Adipose Tissue Growth.* PLoS Comput Biol, 2009. **5**(3): p. e1000324.
453. Ehrlund, A., et al., *Transcriptional Dynamics During Human Adipogenesis and Its Link to Adipose Morphology and Distribution.* Diabetes, 2017. **66**(1): p. 218-230.
454. Ito, A., et al., *Role of MAPK phosphatase-1 in the induction of monocyte chemoattractant protein-1 during the course of adipocyte hypertrophy.* J Biol Chem, 2007. **282**(35): p. 25445-52.
455. Minchin, J.E., et al., *Plexin D1 determines body fat distribution by regulating the type V collagen microenvironment in visceral adipose tissue.* Proc Natl Acad Sci U S A, 2015. **112**(14): p. 4363-8.
456. Sugii, S., et al., *PPARgamma activation in adipocytes is sufficient for systemic insulin sensitization.* Proc Natl Acad Sci U S A, 2009. **106**(52): p. 22504-9.
457. Guerra, C., et al., *Emergence of brown adipocytes in white fat in mice is under genetic control. Effects on body weight and adiposity.* J Clin Invest, 1998. **102**(2): p. 412-20.
458. Qiang, L., et al., *Brown remodeling of white adipose tissue by SirT1-dependent deacetylation of Ppargamma.* Cell, 2012. **150**(3): p. 620-32.
459. Wu, J., H. Jun, and J.R. McDermott, *Formation and activation of thermogenic fat.* Trends in genetics : TIG, 2015. **31**(5): p. 232-238.
460. Nicholls, D.G. and R.M. Locke, *Thermogenic mechanisms in brown fat.* Physiological Reviews, 1984. **64**(1): p. 1-64.
461. Muller, M.D., et al., *Effect of cold acclimatization on exercise economy in the cold.* Eur J Appl Physiol, 2012. **112**(2): p. 795-800.

462. Makinen, T.M., et al., *Seasonal changes in thermal responses of urban residents to cold exposure.* Comp Biochem Physiol A Mol Integr Physiol, 2004. **139**(2): p. 229-38.
463. Nishimura, T., et al., *Seasonal variation of non-shivering thermogenesis (NST) during mild cold exposure.* J Physiol Anthropol, 2015. **34**: p. 11.
464. Depocas, F., J.S. Hart, and O. Heroux, *Cold acclimation and the electromyogram of unanesthetized rats.* J Appl Physiol, 1956. **9**(3): p. 404-8.
465. Davis, T.R., et al., *Regulation of shivering and non-shivering heat production during acclimation of rats.* Am J Physiol, 1960. **198**: p. 471-5.
466. Bauwens, J.D., et al., *Cold tolerance, cold-induced hyperphagia, and nonshivering thermogenesis are normal in α1-AMPK−/− mice.* American Journal of Physiology-Regulatory, Integrative and Comparative Physiology, 2011. **301**(2): p. R473-R483.
467. Yoo, H.s., et al., *Intermittent Cold Exposure Enhances Fat Accumulation in Mice.* PLOS ONE, 2014. **9**(5): p. e96432.
468. Shore, A.M., et al., *Cold-Induced Changes in Gene Expression in Brown Adipose Tissue, White Adipose Tissue and Liver.* PLoS ONE, 2013. **8**(7): p. e68933.
469. Lee, Y.-H., et al., *Metabolic heterogeneity of activated beige/brite adipocytes in inguinal adipose tissue.* Scientific Reports, 2017. **7**: p. 39794.
470. Cannon, B. and J. Nedergaard, *Brown adipose tissue: function and physiological significance.* Physiol Rev, 2004. **84**(1): p. 277-359.
471. Kajimura, S., B.M. Spiegelman, and P. Seale, *Brown and Beige Fat: Physiological Roles beyond Heat Generation.* Cell Metab, 2015. **22**(4): p. 546-59.
472. Mottillo, E.P., et al., *Coupling of lipolysis and de novo lipogenesis in brown, beige, and white adipose tissues during chronic beta3-adrenergic receptor activation.* J Lipid Res, 2014. **55**(11): p. 2276-86.
473. Trayhurn, P., *Fatty acid synthesis in mouse brown adipose tissue. The influence of environmental temperature on the proportion of whole-body fatty acid synthesis in brown adipose tissue and the liver.* Biochim Biophys Acta, 1981. **664**(3): p. 549-60.
474. Yu, X.X., et al., *Cold elicits the simultaneous induction of fatty acid synthesis and beta-oxidation in murine brown adipose tissue: prediction from differential gene expression and confirmation in vivo.* Faseb j, 2002. **16**(2): p. 155-68.
475. Watanabe, M., et al., *Synchronized changes in transcript levels of genes activating cold exposure-induced thermogenesis in brown adipose tissue of experimental animals.* Biochim Biophys Acta, 2008. **1777**(1): p. 104-12.
476. Daikoku, T., et al., *Specific elevation of transcript levels of particular protein subtypes induced in brown adipose tissue by cold exposure.* Biochim Biophys Acta, 2000. **1457**(3): p. 263-72.
477. Lu, X., et al., *The early metabolomic response of adipose tissue during acute cold exposure in mice.* Sci Rep, 2017. **7**(1): p. 3455.
478. Labbe, S.M., et al., *mTORC1 is Required for Brown Adipose Tissue Recruitment and Metabolic Adaptation to Cold.* Sci Rep, 2016. **6**: p. 37223.
479. Hiroshima, Y., et al., *Effects of cold exposure on metabolites in brown adipose tissue of rats.* Mol Genet Metab Rep, 2018. **15**: p. 36-42.
480. Nagao, H., et al., *Increased Dynamics of Tricarboxylic Acid Cycle and Glutamate Synthesis in Obese Adipose Tissue: IN VIVO METABOLIC TURNOVER ANALYSIS.* The Journal of Biological Chemistry, 2017. **292**(11): p. 4469-4483.
481. Nilsson, R., et al., *Estimation of flux ratios without uptake or release data: application to serine and methionine metabolism.* Metabolic engineering, 2017. **43**(Pt B): p. 137-146.
482. Mattaini, K.R., M.R. Sullivan, and M.G. Vander Heiden, *The importance of serine metabolism in cancer.* J Cell Biol, 2016. **214**(3): p. 249-57.
483. Cavuoto, P. and M.F. Fenech, *A review of methionine dependency and the role of methionine restriction in cancer growth control and life-span extension.* Cancer Treat Rev, 2012. **38**(6): p. 726-36.

484. Meyer, K.D., et al., *Comprehensive analysis of mRNA methylation reveals enrichment in 3' UTRs and near stop codons.* Cell, 2012. **149**(7): p. 1635-46.
485. Chi, P., C.D. Allis, and G.G. Wang, *Covalent histone modifications--miswritten, misinterpreted and mis-erased in human cancers.* Nat Rev Cancer, 2010. **10**(7): p. 457-69.
486. Locasale, J.W., *The consequences of enhanced cell-autonomous glucose metabolism.* Trends Endocrinol Metab, 2012. **23**(11): p. 545-51.
487. Vallerand, A.L., F. Perusse, and L.J. Bukowiecki, *Stimulatory effects of cold exposure and cold acclimation on glucose uptake in rat peripheral tissues.* American Journal of Physiology-Regulatory, Integrative and Comparative Physiology, 1990. **259**(5): p. R1043-R1049.
488. Thomson, J.P., et al., *Comparative analysis of affinity-based 5-hydroxymethylation enrichment techniques.* Nucleic Acids Research, 2013. **41**(22): p. e206-e206.
489. Thomson, J.P., et al., *DNA immunoprecipitation semiconductor sequencing (DIP-SC-seq) as a rapid method to generate genome wide epigenetic signatures.* Sci Rep, 2015. **5**: p. 9778.
490. Taylor, S.E.B., et al., *Genome-wide mapping of DNA hydroxymethylation in osteoarthritic chondrocytes.* Arthritis & rheumatology (Hoboken, N.J.), 2015. **67**(8): p. 2129-2140.
491. Papin, C., et al., *Combinatorial DNA methylation codes at repetitive elements.* Genome Res, 2017. **27**(6): p. 934-946.
492. Matarese, F., E. Carrillo-de Santa Pau, and H.G. Stunnenberg, *5-Hydroxymethylcytosine: a new kid on the epigenetic block?* Molecular Systems Biology, 2011. **7**: p. 562-562.
493. Uribe-Lewis, S., et al., *5-hydroxymethylcytosine marks promoters in colon that resist DNA hypermethylation in cancer.* Genome Biology, 2015. **16**(1): p. 69.
494. Esteve Rafols, M., *Adipose tissue: cell heterogeneity and functional diversity.* Endocrinol Nutr, 2014. **61**(2): p. 100-12.
495. Niimura, Y., *Evolutionary dynamics of olfactory receptor genes in chordates: interaction between environments and genomic contents.* Hum Genomics, 2009. **4**(2): p. 107-18.
496. Ramage, Lynne E., et al., *Glucocorticoids Acutely Increase Brown Adipose Tissue Activity in Humans, Revealing Species-Specific Differences in UCP-1 Regulation.* Cell Metabolism, 2016. **24**(1): p. 130-141.
497. Macari, M., M.J. Dauncey, and D.L. Ingram, *Changes in food intake in response to alterations in the ambient temperature: modifications by previous thermal and nutritional experience.* Pflugers Arch, 1983. **396**(3): p. 231-7.
498. Brobeck, J.R., *Food Intake as a Mechanism of Temperature Regulation.* The Yale Journal of Biology and Medicine, 1948. **20**(6): p. 545-552.
499. Langeveld, M., et al., *Mild cold effects on hunger, food intake, satiety and skin temperature in humans.* Endocrine Connections, 2016. **5**(2): p. 65-73.
500. Jespersen, N.Z., et al., *A classical brown adipose tissue mRNA signature partly overlaps with brite in the supraclavicular region of adult humans.* Cell Metab, 2013. **17**(5): p. 798-805.
501. Shinoda, K., et al., *Genetic and functional characterization of clonally derived adult human brown adipocytes.* Nat Med, 2015. **21**(4): p. 389-94.
502. Wu, H., et al., *Dual functions of Tet1 in transcriptional regulation in mouse embryonic stem cells.* Nature, 2011. **473**(7347): p. 389-93.
503. Wu, Y., et al., *Oct4 and the small molecule inhibitor, SC1, regulates Tet2 expression in mouse embryonic stem cells.* Mol Biol Rep, 2013. **40**(4): p. 2897-906.
504. Shen, L., et al., *Tet3 and DNA replication mediate demethylation of both the maternal and paternal genomes in mouse zygotes.* Cell Stem Cell, 2014. **15**(4): p. 459-471.
505. Winquist, E., et al., *Phase II trial of DNA methyltransferase 1 inhibition with the antisense oligonucleotide MG98 in patients with metastatic renal carcinoma: a National Cancer Institute of Canada Clinical Trials Group investigational new drug study.* Invest New Drugs, 2006. **24**(2): p. 159-67.
506. Wyce, A., et al., *BET inhibition silences expression of MYCN and BCL2 and induces cytotoxicity in neuroblastoma tumor models.* PLoS One, 2013. **8**(8): p. e72967.

507. Santer, F.R., et al., *Inhibition of the acetyltransferases p300 and CBP reveals a targetable function for p300 in the survival and invasion pathways of prostate cancer cell lines.* Mol Cancer Ther, 2011. **10**(9): p. 1644-55.
508. Miranda, T.B., et al., *DZNep is a global histone methylation inhibitor that reactivates developmental genes not silenced by DNA methylation.* Mol Cancer Ther, 2009. **8**(6): p. 1579-88.
509. Wang, F., B. Zhong, and Z. Zhao, *ACY 1215, a histone deacetylase 6 inhibitor, inhibits cancer cell growth in melanoma.ACY 1215, a histone deacetylase 6 inhibitor, inhibits cancer cell growth in melanoma.* J Biol Regul Homeost Agents, 2018. **32**(4): p. 851-858.
510. Richon, V.M., *Cancer biology: mechanism of antitumour action of vorinostat (suberoylanilide hydroxamic acid), a novel histone deacetylase inhibitor.* British Journal of Cancer, 2006. **95**(Suppl 1): p. S2-S6.